UNIVERSITY OF SOUTHAMPTON

The effect of large-scale interannual variations in the Gulf of Guinea

by

Ibrahim Muhammed

Thesis for the degree of Doctor of Philosophy

Faculty of Natural and Environmental Sciences
School of Ocean and Earth Science

October 2011

UNIVERSITY OF SOUTHAMPTON

The effect of large-scale interannual variations in the Gulf of Guinea

Abstract

Faculty of Natural and Environmental Sciences

School of Ocean and Earth Science

Doctor of Philosophy

by Ibrahim Muhammed

The Gulf of Guinea is an important region of tropical Atlantic variability, and embedded within it are the Atlantic Niño and the seasonal tropical instability waves. Although, the dynamics of this region are accepted to modulate the monsoon system by the scientific community, it is still debated what controls temperatures and the exact coupling mechanism with the atmosphere. Here, I present the results of temperature advection, variability of the Equatorial Undercurrent (EUC) in relation to atmospheric forcing, influence of Gulf of Guinea sea surface temperature (SST) to rainfall variability over West Africa and the Sahel, spatio-temporal variability of non-seasonal ocean-atmosphere processes and the coupling of winds and SST. The central aim is to understand how anomalous currents advect temperatures, and how anomalous oceanic temperatures respond to the atmosphere to cause coupled variability.

In order to understand the enigmatic influence of temperature advection by tropical instability waves (TIW), I examined the influence of anomalous currents and temperatures associated with the waves. Results show that TIWs advect temperatures zonally and warm the Gulf of Guinea during the boreal summer, and at the central equatorial Atlantic, they advect temperatures to the north. The EUC, represented by salinity maximum is investigated from four regions to cover the northern, central and southern branches of the current. West of the Gulf of Guinea, anomalous northward currents associated with TIWs destabilise the vertical positioning of the EUC core during the boreal summer. In the Gulf of Guinea, where bathymetry, river discharge and winds vary seasonally, vertical fluctuations are apparent every three months and the shallowing of the EUC affects the upper layer temperatures.

The Gulf of Guinea SST correlates well with variability of rainfall over West Africa and the Sahel, where cold (warm) temperatures in 2005 (2007) explained the causes of drought (flooding) that occurred in those years respectively. Strongest intraseasonal SST variability is observed at the Guinea Dome and the Gulf of Guinea region and both occur due to seasonally varying northeasterlies and southeasterlies. However, north of 18°N, zonal tropospheric winds associated with Madden-Julian Oscillation appear to alter the changes on surface winds. This connection between surface and atmospheric winds explains the inability of the winds to covary interannually with SST at the TIWs frontal zones. Investigations presented in this thesis increase our understanding of tropical Atlantic variability and results therein are useful as background conditions for coupled ocean-atmosphere models.

Contents

List of Figures

List of Tables

Declaration of Authorship

I, IBRAHIM MUHAMMED, declare that this thesis titled, 'THE EFFECT OF LARGE-SCALE INTERANNUAL VARIATIONS IN THE GULF OF GUINEA' and the work presented in the thesis are both my own, and have been generated by me as the result of my own original research. I confirm that:

- this work was done wholly or mainly while in candidature for a research degree at this University;
- where any part of this thesis has previously been submitted for a degree or any other qualification at this University or any other institution, this has been clearly stated;
- where I have consulted the published work of others, this is always clearly attributed;
- where I have quoted from the work of others, the source is always given. With the exception of such quotations, this thesis is entirely my own work;
- I have acknowledged all main sources of help;
- where the thesis is based on work done by myself jointly with others, I have made clear exactly what was done by others and what I have contributed myself;
- none of this work has been published before submission.

Signed: _____

Date: _____

Acknowledgements

This work is sponsored by the Petroleum Technology Development Fund (PTDF) of Nigeria, and I am very grateful.

I am sincerely grateful to my supervisors, Dr Graham Quartly and Dr Peter Challenor for their inspirations, encouragement and for continually showing an immense optimism and unswerving faith in my abilities. They uplifted my morale throughout the research period by maintaining an open door policy that I can bump into their offices any time my thoughts go sway.

I am indebted to my panel chair, Prof Ian S. Robinson for his insight and unreserved guidance to see the PhD train reaches the destination. I am particularly thankful to Dr Adrian P. Martin, whose advises during the panel meetings and even during his busy schedules has helped in shaping the direction of this thesis.

I am grateful to Prof. Harry Bryden for all the help, and to Drs Jeremy Grist, Adrian New and Antonio Caltabiano for their invaluable advises.

I am indebted to late Abba Modibbo Umar (may Allah forgive your shortcomings), Nafiu Baba Ahmed and Barr. Kabir Mohammed. My great appreciation goes to Alh. Tijjani Ahmed Galadima, Hajiya Rabiah Umar and the rest of PTDF staff for all their helps. Many thanks to my uncle Dr Gidado Muhammed and my cousin Alh. Buba Kembu for their assistances.

My sincere thanks to Dr Richenda Hoseago-Stokes for her warm-heartedness, and Drs Paolo Cipollini, Valborg Byfield, Helen Snaith and Andrew Shaw for their help whenever I approach them. Thanks to Dr Graham Quartly for showing me, *'other things in the UK outside the research'!*

I m grateful to the unsung heroes. First and foremost is the external examiner of this thesis who had to read this thesis in a bulk and grab the ideas I put forward line by line in a shortest possible time. Second, my internal examiner who also has to go through various processes including the thesis to make sure I see this day. Thanks to the staff of the National Oceanography Library (NOL), Information Technology Group (ITG) and Health and Safety/Facilities/Cafeteria who has always been there whenever I needed them. I am particularly grateful to Mr Stephen Haywood for his hospitality and help.

My earnest gratitude to Drs Bernard Bourlès and Guillaume Charria, without whose kind assistance I won′t have known what it means to be an oceanographer in the field! I can′t forget the pleasurable company of Fabrice Roubaud, Noreddine Khatir and the rest of the officers and cruise participants of RV Antea during PIRATA FR18 mission. I′m equally thankful to the French Institute for Research and Development (IRD) for funding the cruise entirely. Thanks to Guillaume Charria and Karine Amato for their hospitality in Toulouse. *Je suis tes reconnaissant* (I'm very grateful)!

Claire Best at the International Office, you′re the best! Thank you! Mr Ian Richards and Jane Weatherby have showed me a way to escape when research gets touch. Thank you for your hospitality at Callington and for showing me around the amazing landscape!

I am equally thankful to my colleagues, friends and office mates, Murtala Mohammed Ahmed, Auwal Muhammed Bibi, Anna kaczmarska, Aurelié Persechino, Catriona Menzies, Khairul Nizam Mohamed, Turki Al-raddadi, Mounir Leukora, Aldo Aquino-Cruiz, Sudipta Sarkar, Anastasia Charalampopoulou, and a lot of others, especially at the PGCOM, without whose friendship life during PhD wouldn′t have been fun.

I am obliged to my wife Aisha, who understood the PhD and who has been with me during the darkest hours of our child′s sickness. Her love and support has been a thrust to a stronger commitment toward getting this thesis done, and I′m grateful. To my son Sagir, though now is your second birthday, I hope when you read this in the future you will forgive my absence when you needed me most.

I am heartily grateful to my parents, late Muhammed Usman and Khadija Muhammed for their love, kindness and guidance to life.

Dedication

All gratitude be to Allah, the beneficent, the merciful, who started it all by the first word *read (Q96:1)*, and taught me by the *pen (Q96:4)*, what *I knew not (Q96:5)* about *ocean properties (Q55:19)*.

I dedicate this work to my parents, Late Muhammed Usman & Khadiza Muhammed.

To my extended family

Abbreviations

AABW	**A**ntarctic **B**ottom **W**ater
AAIW	**A**ntarctic **I**ntermediate **W**ater
AATSR	**A**dvanced **A**long-**T**rack **S**canning **R**adiometer
ABF	**A**ngola-**B**enguela **F**ront
ABL	**A**tmospheric **B**oundary **L**ayer
AC	**A**ngola **C**urrent
ACC	**A**ntarctic **C**ircumpolar **C**urrent
ADCP	**A**coustic **D**oppler **C**urrent **P**rofiler
AEJ	**A**frican **E**asterly **J**ets
AEW	**A**frican **E**asterly **W**aves
AMM	**A**tlantic **M**eridional **M**ode
AMMI	**A**tlantic **M**eridional **M**ode **I**ndex
Argo	global system of drifting and profiling sub-surface oceanographic floats
Argos	a CNES/NASA/NOAA Doppler-based satellite system that locate and transmit remote data such as Argo and drifter floats
ATLAS	**A**utonomous **T**emperature **L**ine **A**cquisition **S**ystem
AVHRR	**A**dvanced **V**ery **H**igh **R**esolution **R**adiometer
AVISO	**A**rchivage, **V**alidation et **I**nterprétation des données des **S**atellites **O**céanographiques
BC	**B**razil **C**urrent
BN	**B**enguela **N**iño
BNI	**B**enguela **N**iño **I**ndex

CC	**C**anary **C**urrent
CEOF	**C**omplex **E**OF
CHEOF	**C**omplex **H**ilbert **E**OF
CHPC	**C**omplex **H**ilbert **P**rincipal **C**omponent
CNES	**C**entre **N**ational d'**E**tudes **S**patiales (French Space Agency)
COADS	**C**ombined **O**cean **A**tmosphere **D**ata **S**et
COI	**C**one **o**f **I**nfluence
CPC	**C**omplex **P**rincipal **C**omponent
CPC	**C**limate **P**rediction **C**entre
CPSD	**C**ross **P**ower **S**pectral **D**ensity
cSEC	**c**entral **S**outh **E**quatorial **C**urrent
CSIRO	**C**ommonwealth **S**cientific and **I**ndustrial **R**esearch **O**rganization
CTD	**C**onductivity **T**emperature **D**epth
CWT	**C**ontinuous **W**avelet **T**ransform
DINEOF	**D**ata **I**NterpolationEmpirical **O**rthogonal **F**unction
DJF	**D**ecember **J**anuary **F**ebruary
DUACS	**D**ata **U**nification **A**nd **C**ombination **S**ystem
DWBC	**D**eep **W**estern **B**oundary **C**urrent
ECMWF	**E**uropean **C**entre for **M**edium-range **W**eather **F**orecasts
EIC	**E**quatorial **I**ntermediate **C**urrent
EKE	**E**ddy **K**inetic **E**nergy
EKW	**E**quatorial **K**elvin **W**ave
ENSO	**E**l **N**iño-**S**outhern **O**scillation
Envisat	**E**nvironmental **s**atellite, a major polar platform of ESA's EOS
EO	**E**arth **O**bservation (typically refers only to satellite observations)
EOF	**E**mpirical **O**rthogonal **F**unction
EOS	**E**arth **O**bservation **S**ystem
ERS-1,2	**E**uropean **R**emote **S**ensing satellite series
ESA	**E**uropean **S**pace **A**gency
EUC	**E**quatorial **Under**current
FAO	**F**ood and **A**griculture **O**rganisation

FLAME	**F**amily of **L**inked **A**tlantic **M**odel **E**xperiments
FOCAL	programme **F**rançais **O**cean-**C**limat en **A**t**l**antique equatorial
Geosat	Department of Defence (USA) satellite altimetry mission
GC	**G**uinea **C**urrent
GCM	**G**eneral **C**irculation **M**odel
GCUC	**G**abon-**C**ongo **U**nder**c**urrent
GD	**G**uinea **D**ome
GFO	**G**eosat **f**ollow-**o**n mission
GODAE	**G**lobal **O**cean **D**ata **A**ssimilation **E**xperiment
GoG	**G**ulf of **G**uinea
GOGI	**G**ulf **o**f **G**uinea SST **I**ndex
GPCP	**G**lobal **P**recipitation **C**limatology **P**roject
GPS	**G**lobal **P**ositioning **S**ystem
GUC	**G**uinea **U**nder**c**urrent
HDF	**H**ierarchical **D**ata **F**ormat
IFREMER	**I**nstitut **F**rançais de **R**echerche pour l'**E**xploitation de la **MER** translated as **F**rench **R**esearch **I**nstitute for **E**xploitation of the **S**ea
IRD	**I**nstitut de **R**echerche pour le **D**evelopement
ITCZ	**I**nter-**T**ropical **C**onvergence **Z**one
IUC	**I**vorian **U**nder**c**urrent
JJA	**June** **J**uly **A**ugust
LME	**L**arge **M**arine **E**cosystem
LADCP	**L**owered **A**coustic **D**oppler **C**urrent **P**rofiler
MABL	**M**arine **A**tmospheric **B**oundary **L**ayer
MAM	**M**arch **A**pril **M**ay
MEI	**M**ultivariate **E**NSO **I**ndex
MSI	**M**editerranean **S**ST **I**ndex
MJO	**M**adden-**J**ulian **O**scillation
MLD	**M**ixed **L**ayer **D**epth
MSLA	**M**aps of **S**ea **L**evel **A**nomaly

MSLP	**M**ean **S**ea **L**evel **P**ressure
NADW	**N**orth **A**tlantic **D**eep **W**ater
NASA	**N**ational **A**eronautics and **S**pace **A**dministration (US space agency)
NASDA	**NA**tional **S**pace **D**evelopment **A**gency (Japan space agency) (now known as JAXA)
NBC	**N**orth **B**razil **C**urrent
NBUC	**N**orth **B**razil **U**nder**c**urrent
NCAR	**N**ational **C**entre for **A**tmospheric **R**esearch
NCEP	**N**ational **C**enter for **E**nvironmental **P**rediction
NDVI	**N**ormalised **D**ifference **V**egetation **I**ndex
NEC	**N**orth **E**quatorial **C**urrent
NECC	**N**orth **E**quatorial **C**ounter **C**urrent
NEUC	**N**orth **E**quatorial **U**ndercurrent
NetCDF	**Net**work **C**ommon **D**ata **F**ormat
NOAA	**N**ational **O**ceanographic and **A**tmospheric **A**dministration
nSEC	**n**orthern **S**outh **E**quatorial **C**urrent
OI	**O**ptimal **I**nterpolation
OISST	**O**ptimal **I**nterpolation **S**ea **S**urface **T**emperature
PC	**P**rincipal **C**omponent
PCA	**P**rincipal **C**omponents **A**nalysis
PDO	**P**acific **D**ecadal **O**scillation
PIRATA	**P**red**I**ction **R**esearch moored-**A**rray in the **T**ropical **A**tlantic
Poseidon	Radar altimeter (CNES)
PSD	**P**ower **S**pectral **D**ensity
PSDn	**P**hysical **S**ciences **D**ivision a branch of NOAA
QBO	**Q**uasi-**B**iennial **O**scillation
QuikScat	Satellite with a dedicated scatterometer mission (NASA)
SACW	**S**outh **A**tlantic **C**entral **W**ater
SEC	**S**outh **E**quatorial **C**urrent
SEQUAL	**S**easonal **EQU**atorial **A**t**L**antic **r**esponse program

SEUC	**S**outh **E**quatorial **U**ndercurrent
SLP	**S**ea **L**evel **P**ressure
SO	**S**outhern **O**scillation
SOI	**S**outhern **O**scillation **I**ndex
SON	**S**eptember **O**ctober **N**ovember
sSEC	**s**outhern **S**outh **E**quatorial **C**urrent
SSH	**S**ea **S**urface **H**eight
SSHA	**S**ea **S**urface **H**eight **A**nomaly
SSM/I	**S**pecial **S**ensor **M**icrowave/**I**maging
SSSA	**S**ea **S**urface **S**lope **A**nomaly
SST	**S**ea **S**urface **T**emperature
STD	**S**Tandard **D**eviation
SVD	**S**ingular **V**alue **D**ecomposition
SSALTO	**S**egment **S**ol multimissions d'**ALT**imétrie, d'**O**rbitographie et de localisation précise
TAV	**T**ropical **A**tlantic **V**ariability
TEJ	**T**ropical **E**asterly **J**ets
THC	**T**hermo**h**aline **C**irculation
TIW	**T**ropical **I**nstability **W**ave
TIV	**T**ropical **I**nstability **V**ortices
TMI	**T**RMM **M**icrowave **I**mager
TOPEX	**Top**ographic **Ex**periment: radar altimeter (NASA)
TOPEX/Poseidon	Altimeter mission (NASA/CNES)
TRMM	**T**ropical **R**ainfall **M**easuring **M**ission
T-S diagram	**T**emperature-**S**alinity diagram
UNESCO	**U**nited **N**ations **E**ducational, **S**cientific and **C**ultural **O**rganization
WAM	**W**est **A**frican **M**onsoon
WES	**W**ind **E**vaporation **S**ST, an ocean-atmosphere feedback mechanism
WBC	**W**estern **B**oundary **C**urrent

WMO	**W**orld **M**eteorological **O**rganisation
WTC	**W**avelet **T**ransform **C**oherence
XBT	e**X**pendable **B**athy **T**hermographs
XWT	Cross **W**avelet **T**ransform
2D-FFT	Two **-** **D**imensional **F**ast **F**ourier **T**ransform

CHAPTER 1

General Introduction

1.1 Introduction

The Gulf of Guinea is an important region in the tropical Atlantic by virtue of its geographical position with a closed boundary to the east and north and an open South Atlantic Ocean to the south. It provides the main oceanic connection between the South Atlantic Ocean and the southeast trade winds with the climate of West Africa and the Sahel. This facilitates the impact of oceanic forcings onto the land via the atmosphere as a result of temperature gradient between ocean and land. The oceans and atmosphere also responds to each other in a fundamentally different manner. While the oceans respond to atmospheric temperatures, humidity, solar heat flux, wind and aerosols, the atmosphere only responds to ocean surface temperature field. These coupled interactions control heat and water vapor fluxes at the ocean-atmosphere interface that consequentially affects the climate.

The current system in the Gulf of Guinea comprises surface currents such as

South Equatorial Currents (westward), Guinea Current (eastward) and the Angola Current (southward). The eastward undercurrents are the Equatorial Undercurrent (EUC) and the southward current is Gabon-Congo Undercurrent, while the westward undercurrent is the Guinea Undercurrent (GUC) (Figure 1.1). The Antarctic Intermediate Water (AAIW) also crosses the region towards the north at approximately 630m depth. These currents are driven by the global thermohaline circulation (THC), Ekman pumping velocity and by changes in local water properties due to influx of fresh water (Chang et al., 2006)

In response to the strengthening of the southeasterly trade winds, a cold tongue develops at the southeastern part of tropical Atlantic during the boreal summer. The cold tongue is a band of conspicuous cold surface waters that emerges in the southeastern tropical Atlantic and Pacific that extends across the equator having a width of about 1000km. The cold tongue is fully developed in July of each year in the Atlantic (Figure 1.2) and it is associated with tropical instability waves (Xie and Carton, 2004).

Tropical instability waves (TIWs) are perturbations in the SST fronts characterised by undulations in the north and south sea surface temperature (SST) fronts marking the cold tongue (Legeckis, 1977; Weisberg and Weingartner, 1988). They produce SST variations on the order of 1-2°C, have periods of 20-40 days, wavelengths of 1000-2000km, phase speeds of around 0.5m/s and propagate westward (Contreras, 2002; Legeckis, 1977; Qiao and Weisberg, 1995; Weisberg and Weingartner, 1988). These waves are unique in the Pacific and Atlantic oceans and do not occur in the Indian Ocean. They are known to develop as a result of shear instability of equatorial current system (Philander and Pacanowski, 1986), and can influence the state of the tropical climate by modifying the mixed layer (An, 2008; Jochum and Murtugudde, 2004; Seo et al., 2006). The waves are best observed from satellite sea surface temperature. However, they have also been documented from satellite chlorophyll and mooring measurements in both oceans. Associated with these waves are tropical instability vortices (TIVs), which are a train of westward propagating cyclones (Willett et al., 2006). These waves are associated with El Niño Southern Oscillation

(ENSO) (Yu and Liu, 2003) and can influence Rossby Waves (Lawrence and Angell, 2000). Both TIWs and TIVs are important elements of ocean heat budget and ocean-atmosphere coupling and therefore can modulate climate.

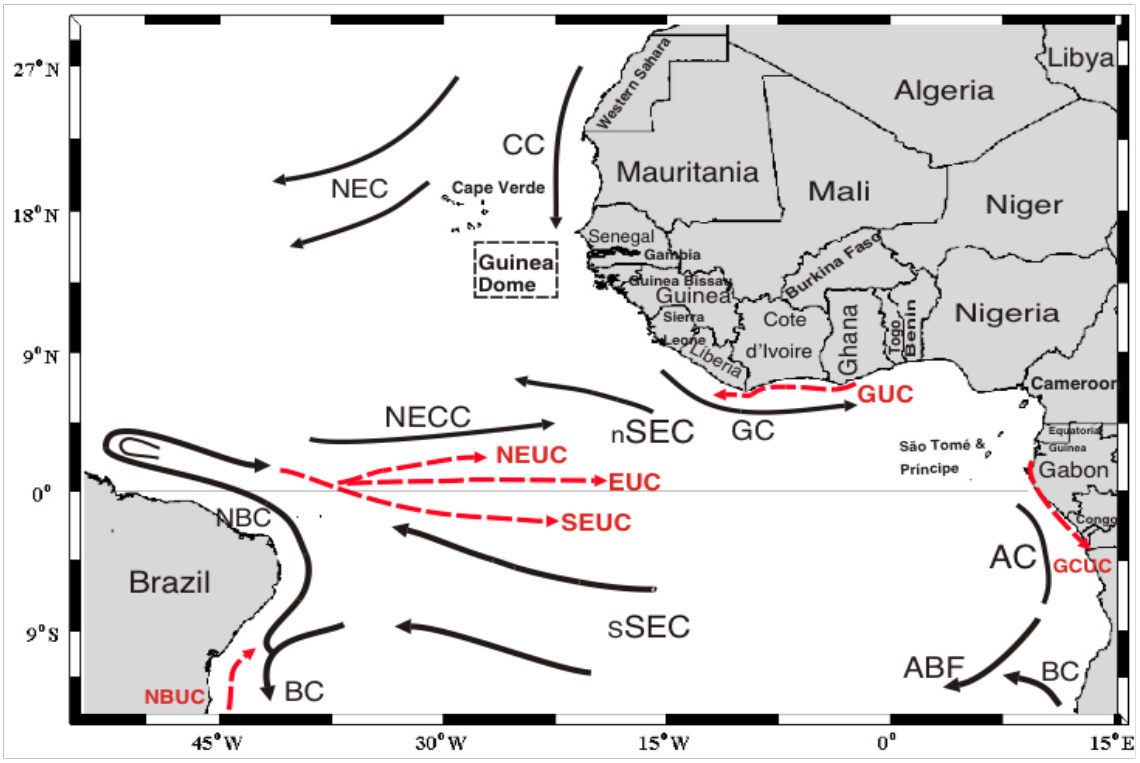

Figure 1.1. *A schematic representation of the major current system in the tropical Atlantic. The currents illustrated are in thick lines, subsurface currents are dashed red: The surface currents are the North Equatorial Current (NEC), Canary Current (CC), North Equatorial Counter current (NECC), northern South Equatorial Current (nSEC), Guinea Current (GC), North Brazil Current (NBC), Brazil Current (BC), southern South Equatorial Current (sSEC), Angola Current (AC), Benguela Current (BC) and the Angola Benguela front (ABF). The undercurrents are the North Brazil Undercurrent (NBUC), North Equatorial Undercurrent (NEUC), Equatorial Undercurrent (EUC), South Equatorial Undercurrent (SEUC), Guinea Undercurrent (GUC) and Gabon-Congo Undercurrent (GCUC). The shading of NBC is shown around 52° W, 3° N. These currents are modified from Schouten et al. (2005). The Guinea Dome region, countries, Islands and their boundaries in the region are also illustrated.*

The wind-driven Ekman layer varies seasonally, and tropical instability waves (TIWs) appear in June after the cold tongue develops north of the equator. The low-frequency coupling of the ocean and atmosphere at the SST frontal region of TIWs can influence interannual variations in the atmosphere (Wu and Bowman, 2007a,b). Equatorial Kelvin waves bring sub-thermocline waters to the

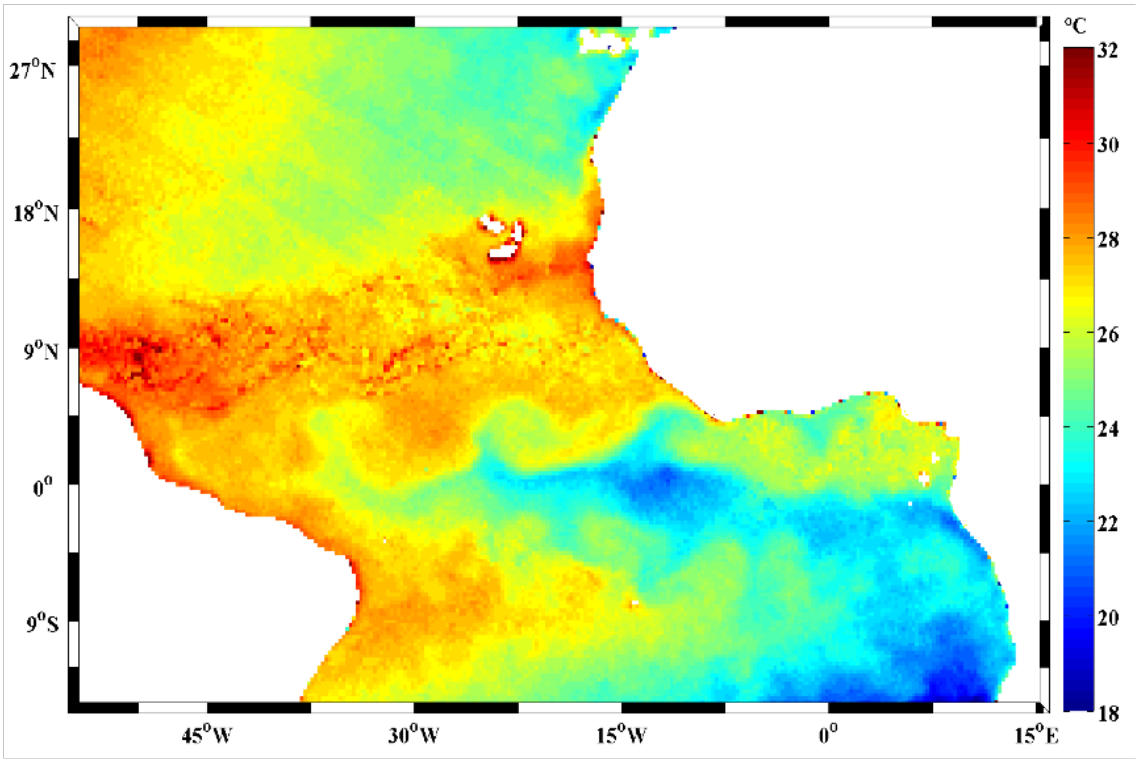

Figure 1.2. *A snapshot of sea surface temperature of the study area from 3-day (2-4 July 2009) averaged TMI SST data. The cold tongue spreads from the southeast around 12°E/15°S into the centre of the basin with temperatures less than 22°C. Tropical instability waves (TIWs) show stronger signatures north of the equator between 0-6°N than the south.*

near surface, where the thermocline is already shallow. At the same time, freshening from river runoff and upwelling changes the density structure considerably.

The Atlantic Niño, also called the equatorial mode, is located in the Gulf of Guinea. It is a phenomenon analogous to the Pacific El Niño, characterised by irregular episodes of anomalous warming during the boreal summer (Chang et al., 2006). The Atlantic Niño is an active determinant of tropical Atlantic climate variability through ocean-atmosphere fluxes as well as the regions connection to the Pacific El Niño. It intensifies atmospheric convection near the equator and keeps the rain band from advancing into the Sahel while increasing rainfall at the Gulf of Guinea (Giannini et al., 2003). The Atlantic Niño is weaker than the Pacific El Niño. While the Atlantic Niño occurs every summer, the Pacific counterpart occurs only once or twice in a decade and in December. Quite recently, Okumura and Xie (2006) discovered a phenomenon similar to the

Atlantic Niño but only exist in November-December months called the Atlantic Niño II.

The atmospheric circulation of the region is influence by southeast and northeast trade winds that converge at the Intertropical Convergence Zone (ITCZ). The southeast trade winds are a part of the large-scale monsoon circulation that drive precipitation over West Africa and the southern Sahel. Rainfall is important to the societies of this region both in terms of health and livelihoods. This justifies significantly the economic and scientific interest in understanding the climate variability of these areas and the knowledge of which could essentially lead to prediction of specific climate parameters.

In a nutshell, this thesis examines the role of SST, currents and winds against the backdrop of bathymetry and topography to answer long-standing questions that affect the West African climate.

1.2 Thesis aim and objectives

This thesis aims at investigating ocean circulation within the Gulf of Guinea and its possible effect on atmospheric circulation that consequentially affect land. The objectives are broken down into five: 1) To investigate the scales of contribution of TIWs to horizontal temperature advection and study whether they warm the Gulf of Guinea region. 2) To examine the connection between the shallowing of the EUC and the local winds in modulating oceanic circulation of the region. 3) To find out whether Gulf of Guinea SST has any influence on West African and Sahel rainfall anomalies and consider possible remote forcing from adjacent oceans and seas. 4) To study the scales and propagation characteristics of oceanic and atmospheric processes. 5) To investigate ocean-atmosphere coupling and high frequency variability.

1.3 Motivation

The motivations of this thesis are the driving questions that still remain unanswered. It is known that horizontal temperature advection plays a fundamental role in the equatorial heat transport (Deser et al., 2010; DeWitt and Schneider, 1999). It is also known that horizontal temperature advection at the SST fronts of TIWs is so large (Jochum and Murtugudde, 2006), that ocean simulations that fail to model them are unable to address tropical intraseasonal variability and other extreme events because their forecast capability would be reduced (Deser et al., 2006; Jochum et al., 2007; Lin et al., 2006). This thesis addresses the questions:

What are the scales of contributions of TIWs to horizontal temperature advection?

Do the TIWs warm the Gulf of Guinea region?

The depth of the tropical thermocline can vary seasonally from approximately 10-60m in the Gulf of Guinea (McGlade et al., 2002). The EUC shallows in the east and flows both north and south to feed the Guinea and Garbon-Congo undercurrents respectively. Precipitation is generally much larger than evaporation and strong but short-lived winds occur occasionally (Allersma and Tilmans, 1993). This thesis will examine:

Is the EUC shallowing in the Gulf of Guinea linked to the strengthening of the seasonal winds?

Does the EUC vary seasonally at any of its branches?

The Gulf of Guinea SST controls the moisture convergence of the monsoons (Fontaine et al., 2003), and due to its annual cycle, it determines rainfall variability over West Africa (Okumura and Xie, 2004). The forcing mechanism responsible for a wetter Sahel is, however, not connected to warming in the Gulf of Guinea (Cook and Vizy, 2006) . The general circulation models have difficulty

explaining the dry conditions of the Sahel (Vizy and Cook, 2001). This thesis tackles two of these points:

Is there any influence of the Gulf of Guinea SST on West Africa and Sahel rainfall anomalies?

Is there any remote forcing that controls the moisture convergence over West Africa and the Sahel rather than the Gulf of Guinea SST?

The ocean-atmosphere interaction in the tropical Atlantic is a complex one. It comprises of seasonal winds from opposite directions, asymmetric ITCZ, cold tongue complex, projected continents of Africa and South America and northward positioning of a thermal equator. The location of the strongest SST signature of TIW′s only north of the equator adds to this complexity. The surface currents of TIW's ocean fronts produce a relative motion between the ocean and the atmosphere, acting to change the surface stress, thus affecting the atmosphere as well as feeding back to the ocean (Cornillon and Park, 2001; Kelly et al., 2001). The SST frontal zones of these waves are areas with the strongest wind stress divergence at a mesoscale level (Chelton et al., 2004). The related questions addressed herein are:

What are the scales and propagation characteristics of non-seasonal variability?

Are non-seasonal variability in the tropical Atlantic a part of the TIWs?

Are 5-20day oscillations in the tropical Atlantic related to the TIWs?

1.4 Thesis Structure

This thesis comprises of eight chapters, with the major contributions to science discussed in four major chapters (**chapters 4-8**). To the extent possible, each chapter is documented independently as a self-contained unit without the need to refer to other chapters. The structure of the thesis is as follows:

In Chapter 1, a general overview to set the work in context is highlighted and the aim and objectives and motivation of the thesis are briefly outlined.

In Chapter 2, the scientific background knowledge of the region, which includes the physical setting, oceanic and atmospheric circulation as well as climate indices of the region is discussed.

In Chapter 3, the types of data used, quality control procedures applied, spatial and temporal resolutions, applications and sources of data are discussed.

In Chapter 4, the contribution of horizontal temperature advection by ocean currents is examined. The relative contribution of each term of horizontal advection is presented, and their anomalies due to mean or anomalous currents due to TIWs is studied and fully documented.

In Chapter 5, the seasonal variability of the equatorial undercurrent and its connection with seasonal winds is studied. Density variations due to shallowing of salty equatorial undercurrent, freshwater input from rivers, shallow bathymetry and seasonal winds are investigated. The possible impact of current anomalies due to these dynamics to offshore oil installations is discussed.

In Chapter 6, the impact of sea surface temperature on rainfall and its connection with other large-scale climate indices is described. Potential findings on the influence of SST to coastal flooding and the extent of such impact into the Sahel are highlighted.

In Chapter 7, the spatial and temporal variability of oceanic and atmospheric signals are investigated and their propagating characteristics are determined based on complex signal analysis. Their potential impacts on climate are discussed.

In Chapter 8, the ocean-atmosphere interaction processes are examined in their broader spatial and temporal context, and important characteristics of

variability are quantified based on their scales of interaction. The leading hypotheses for the variability are discussed and examined in the light of new insights into the scales of variability.

In Chapter 9, conclusions of the thesis are drawn by highlighting the main findings and their significance, as well as proffering suggestions on future work.

Processing, All data processing has been done in MatLab, except for the interpolation of satellite data for which windows command is used. The interpolation was done with the help of DInEOF tool provided by (Alvera-Azcárate et al., 2005), which is available at their homepage. Wavelet analysis software has been provided by A. Grinsted, which is available . Some maps were produced using *M_Map*, which is available to download online at http://www.eos.ubc.ca/ rich/map.html.

CHAPTER 2

Overview

2.1 Introduction

The oceanic and atmospheric dynamics in the Gulf of Guinea are fully connected with those in the tropical Atlantic as well as large-scale processes. The shape of the bathymetry modulates the current systems, and the undulating orographic features affect the wind system and precipitation over land. The meridional shifting of the ITCZ, the monsoon dynamics and the local climates related to rainfall are interwoven. In order to fully understand the nature of this region, each system is treated individually considering their relative contributions to climate. This chapter provides background information of oceanic heat budget. The study area is highlighted by focusing on bathymetry and topography, the local climate system, ocean circulation pattern, atmospheric circulation pattern and the climate indices based in the region and beyond.

2.2 Heat budget of the ocean

The knowledge of heat budget in the oceans is fundamental to our understanding of the climate system. The ocean′s role in the climate system is paramount due to its capacity to store large amounts of heat. Approximately 3.5m of near-surface water column contains as much heat as the entire atmospheric column (Deser et al., 2010). This heat is transported by currents across the oceans thereby regulating the heat budget. Air-sea interaction processes on localised surface temperatures then act to maintain or vary local or regional climates through convective processes.

The oceanic heat content is the major source of energy needed to drive atmospheric circulation. Changes in the upper ocean heat content are due to an imbalance of input and output of heat at the surface. This adjusts the density structure of the ocean at the near surface. The total flux of energy into and out of the global ocean must be equal to zero, otherwise the ocean as a whole will either heat up or cold down. The sum of heat energy in and out of a volume of water is the heat budget (Stewart, 2004).

Sea surface temperature is influenced by both oceanic and atmospheric processes at various temporal and spatial scales. On the atmospheric side, air temperature, wind speed, cloudiness and humidity are the dominant factors regulating heat exchange at the sea surface (Deser et al., 2010). The major terms of the upper-ocean mixed layer heat budget are:

$$\frac{\delta T}{\delta t} = \frac{Q_{net}}{\rho CpH} + (\vec{U}_{geo} + \vec{U}_{ek}).\vec{\nabla}T + \frac{(W_e + W_{ek})(T - T_b)}{H}, \tag{2.1}$$

where Q_{net} is the net surface energy flux, ρ is the density of sea water, Cp is the specific heat capacity of sea water, H is the mixed layer depth, $\vec{U}_{geo}$ is the geostrophic current velocity, $\vec{U}_{ek}$ is the Ekman current velocity, $\vec{\nabla}T$ is the spatial gradient operator, W_e is the vertical entrainment rate, W_{ek} is the Ekman pumping velocity, T is the mixed layer temperature and T_b is the temperature of

the water depth that is entrained into the mixed layer. Surface heat flux (Q_{net}) is defined as:

$$Q_{net} = Q_{sh} + Q_{lh} + Q_{sw} + Q_{lw}, \tag{2.2}$$

where Q_{sh} is the sensible heat flux, $Q_{lh}$is the latent heat flux, $Q_{sw}$is the downward solar radiative flux minus the portion that penetrates through the mixed layer, and Q_{lw} is the longwave radiative flux. The turbulent energy flux (Q_{sh} + Q_{lh}) is linearly proportional to the wind speed and the air-sea temperature or humidity difference (Deser et al., 2010). This is based on the bulk parametisation coefficients at a threshold of 10m-height and wind speed above 5ms^{-1} (Liu et al., 1979; Smith, 1988). The radiative fluxes (Q_{sw} + Q_{lw}) are functions of air temperature, humidity and cloudiness. Ekman and geostrophic currents contribute to the mixed layer heat budget through horizontal advection, whereas entrainment and Ekman pumping alter the SST through vertical advection (Deser et al., 2010). Details of heat budget terms for the sea surface can be found in Stewart (2004).

2.3 Bathymetry and Topography

The bathymetry of the region show both narrow and deep continental shelves (figure 2.1a). In the Gulf of Guinea it is quite narrow, and shelf widths are 20-25km along the coast from Côte d′Ivoire to Cameroon, and around the Niger Delta where it has a width of 50-56km (Allersma and Tilmans, 1993).The continental shelf off Sierra Leone - Guinea is the largest in West Africa, especially off Guinea-Bissau covering approximately 53,000 km^2 and up to 150km wide. The shallow continental shelf is extended to Islands of São Tomé and Príncipe, Cape Verde and Canary (figure 1.1). The Mid-Atlantic Ridge is closer to the African continent at about ±8 degrees of latitude.

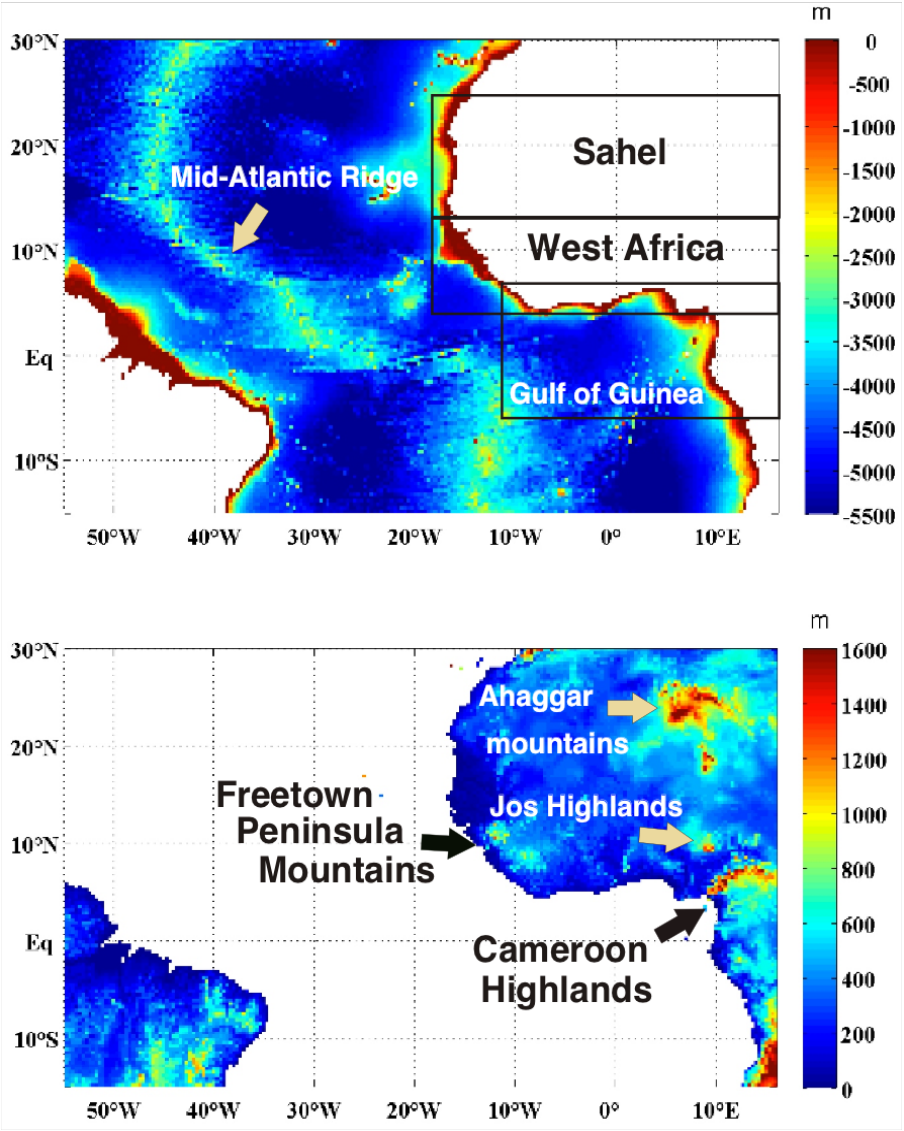

Figure 2.1. *The bathymetry and topography of the study area. a) The bathymetry showing continental shelf. The boxes represent the Gulf of Guinea region (7° S-7° N, 10° W-14° E), the West African climate boundary (3-12° N, 18° W-16° E) and the Sahel region (12-25° N, 18° W-16° E). b) The topography of West Africa and the Sahel showing mountain reliefs. Data used is Etop02v2.*

The boxes shown (figure 2.1a) represent areas that are particularly considered in this study. The southernmost box is the Gulf of Guinea area (7°S-7°N , 10°W-14°E), the middle is the West African climate boundary (3-12°N, 18°W-16°E) which has distinct rainfall characteristics compared to the area north of it, and the northernmost box is the Sahel region (12-25°N, 18°W-16°E).

The topography of West Africa and the Sahel (figure 2.1b) features mountain ranges. These are Freetown Peninsula Mountains, Ahaggar Mountains, Jos Highlands and Cameroon Highlands. These rise to various heights above sea level. Ahaggar rises to 1550m, Cameroon Highlands to 1450m, Freetown Peninsula Mountains to 1200m and Jos Highlands to 110m. Data used are Etop02v2 gridded bathymetry and topography.

2.4 Climate

2.4.1 Wind regimes

The wind systems of the tropical Atlantic Ocean are mainly a combination of southeasterly and northeasterly winds that vary at a seasonal time scale. Wind vectors derived from QuikScat scatterometer data (figure 2.2) show the convergence zone during boreal winter and summer. The southeasterlies are the West African Monsoon (WAM) wind system that conveys moisture over the continent (figure 2.2). The strengthening of WAM is associated with the annual migration of Intertropical Convergence Zone (ITCZ). This leads to a strong dynamic response in the ocean during boreal spring, that affects currents and heat transport. The cross-equatorial flow at the western boundary accelerates, leading to i) an intensification of the North Brazil Current (NBC figure 1.1) and a growing extension of its retroflection, ii) the North Equatorial Countercurrent (NECC) develops at the western boundary part carrying retroflected NBC into the interior (eastward), iii) Ekman transport from the tropics and subtropics reaches its seasonal maximum and the excess upper ocean waters are stored in the NECC ridge at 3-5°N (Schott et al., 2003). At this point, the Equatorial Undercurrent accelerates eastward.

2.4.2 The Intertropical Convergence Zone

The Intertropical Convergence Zone (ITCZ) is the band where the southeasterly and northeasterly winds converge. This climatic band shifts between 5°S and 12°N asymmetrically, and this shifting depends on the seasonal variations of wind and sea surface temperature gradient. The sea surface temperature influences the ITCZ through fluctuations in the meridional tropical Atlantic SST gradient. Such changes shift the ITCZ to the warmer hemisphere, affecting rainfall in the colder hemisphere (Nobre and Shukla, 1996). Generally, when the ITCZ is south of the equator during the boreal winter (figure 2.2) there is abundant rainfall over South America especially at the Amazon. During the boreal summer, the ITCZ shifts northward, taking moisture-laden winds northward and heavy rains over West Africa and the southern Sahel.

It has been suggested that an anomalously warm tropical north Atlantic has contributed to the Amazon drought in 2005 (Marengo, 2006). The ITCZ is characterized by a low-pressure trough, maximum precipitation and maximum in regional SST distribution (Schott et al., 2003). The reason for this behaviour of the ITCZ is due to complex interactions of SST, convection and surface winds. It was emphasized (Mitchell and Wallace, 1992) that the second harmonic of the semi-annual cycle in the pattern of ITCZ dominates seasonal variability, and that this behaviour lies in the atmosphere-ocean system. This is through the variations of insolation in the presence of north-south asymmetry of the distribution of land masses around the equator, particularly at the eastern boundary where the winds are stronger. The seasonal pattern of the ITCZ varies from year to year, and this accounts for the tropical Atlantic variability. A strong link exists between anomalies in the ITCZ position and the anomalies in SST within the tropical Atlantic basin (Giannini et al., 2003).

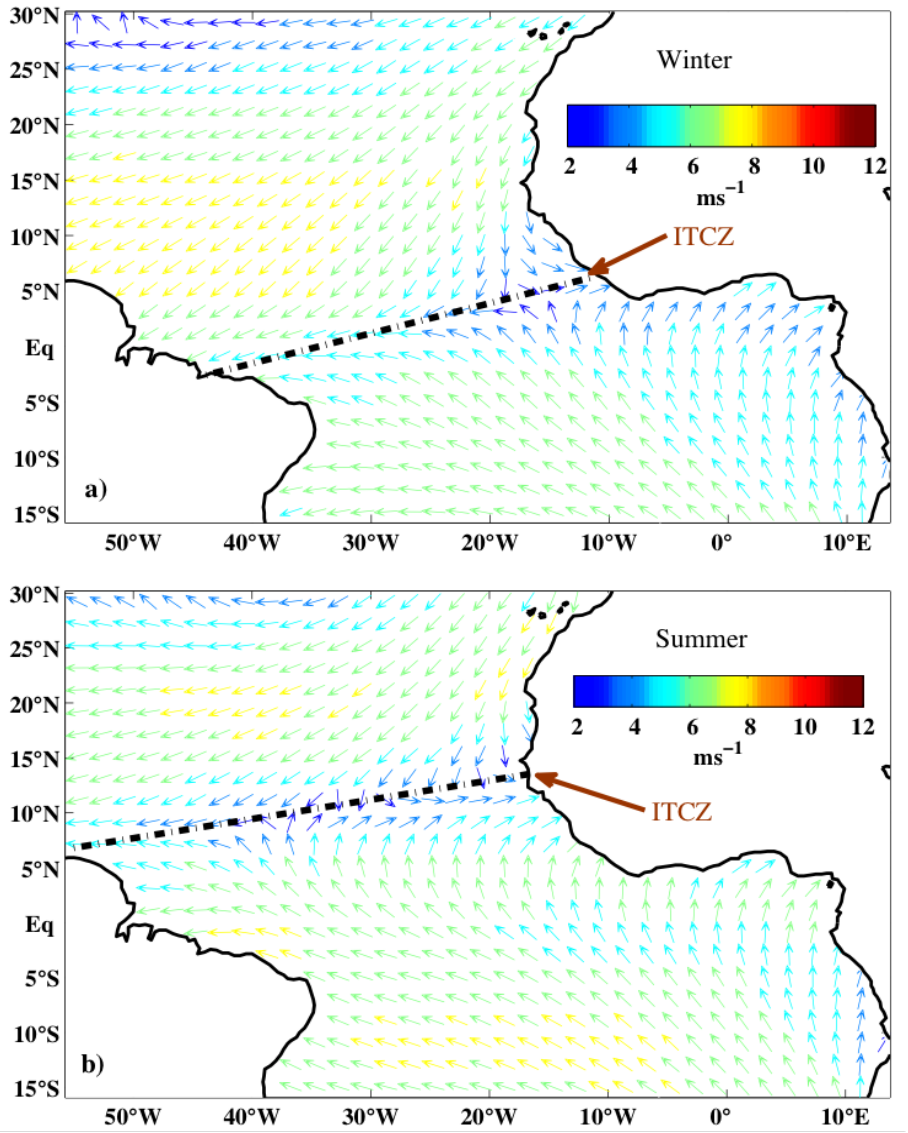

Figure 2.2. *The wind speed and direction vectors are shown, a) boreal winter, b) boreal summer. The mean position of the marine ITCZ is shown for each season. The data are from QuikScat scatterometer 10-metre winds for 2009.*

2.4.3 The West African Monsoon

Monsoon systems are the seasonal changes of atmospheric circulation and precipitation associated with differential heating of land, ocean and atmosphere. The West African Monsoon (WAM) is characterized by the combination of different thermal and dynamical factors that contribute to the intensity, location and duration of the seasonal rainfall (Chauvin et al., 2010). In the past, the

variability of WAM has been investigated at interannual time scales and in relation to global SSTs (Fontaine and Janicot, 1996; Giannini et al., 2003). The WAM is inhibited by ENSO (Folland et al., 1986), connected with the meridional march of ITCZ (Janicot, 1992) and with the Mediterranean SST through the Sahel (Rowell, 2003)

Intense rainfall appears over the Gulf of Guinea from April, moves to the latitude of about $10°N$, and then retreats back to the south mid-SeptemberOctober, mirroring the seasonal march of the ITCZ. There are two maxima: May-June and October-November. The May-June maximum is associated with the warming of the east Atlantic SST and meridional SST gradient (Gu and Adler, 2004). The October-November maximum does not extend beyond the coast of the gulf. In the eastern Gulf of Guinea, however, the monsoon climate leads to one long rainy period (Allersma and Tilmans, 1993). Cameroon has the highest rainfall with about 11,000mm per year, and this is due to orographic effects of the imposing volcano and the perpendicular orientation of the coast to the main convection coming from the sea. An average rainfall of 1500mm per year is recorded at the tropical rainforests of Côte d′Ivoire, Ghana and Benin (see figure 1.1 for countries in the region).

2.5 Ocean Circulation

The interest in understanding ocean current systems around the Gulf of Guinea and their interaction with atmospheric fields permits me to investigate their sources as well as their control mechanisms. These currents are a part of the global thermohaline circulation and originate from other major current systems from both hemispheres, which are then modulated, in addition by wind stress. These are important as they transport heat and salt to other regions and also couple with the atmosphere to drive heat and moisture. I attempt to investigate these currents from the existing literature as a prelude to knowing their interactions with other current systems and with the atmosphere. The currents in

the tropical Atlantic are made up of both surface and sub-surface currents that originate mostly from the south. Those that affect the region most are located within the latitude band of $\pm 10^{\circ}$ (Figure 1.1), and are additionally highlighted in the next subsections.

The Western Boundary Current (WBC) in the equatorial Atlantic comprises the Deep Western Boundary Current (DWBC) at a depth of between 1300-2000m and the North Brazil Current (NBC) (Eden and Dengler, 2008; Fischer and Schott, 1997). The DWBC is a major component of the global thermohaline circulation as well as inter-hemispheric water mass exchange balancing the temperature and salinity between the northern and the southern parts of the Atlantic. It comprises the oxygen rich, warm and saline North Atlantic Deep Water (NADW) between 1200m to 4000m flowing southward and the near bottom flow of Antarctic Bottom Water (AABW) carrying water mass into the northern hemisphere (Rhein et al., 1995). Below 4000m, all of the Atlantic Ocean is occupied by AABW formed in the eastern south Pacific, then spreading from the Antarctic Circumpolar Current (ACC) and penetrating both east and west of the Mid-Atlantic Ridge to the north (Tomczak and Godfrey, 2003).

The Antarctic Intermediate Waters (AAIW) occurs as a result of water mass conversion in the Southern Ocean. It flows northward at the southern basin along the Brazilian coast and in the same northward direction as the North Brazil Undercurrent (NBUC). A comprehensive survey was conducted between Oct 1990 and November 1992 to determine the fate of water masses at the western tropical Atlantic using various instrumentation (Rhein et al., 1995). Instruments used include the lowered-ADCP (LADCP), Expendable BathyThermographs (XBTs), vessel mounted Acoustic Doppler Current Profiler (ADCP), Pegasus and Conductivity Temperature Depth (CTD). The NBUC shows a subsurface core at about 200m depth with velocities of up to $0.9\mathrm{m}s^{-1}$, resulting in strong transports with more than 22Sv in the upper 1000m in the latitude range of 5°S-10°N (Stramma et al., 1995). NBUC continues its northward flow and sheds its water to three main currents that flows eastward, namely, the South

Equatorial Undercurrent (SEUC), the Equatorial Undercurrent (EUC) as well as the North Equatorial Undercurrent (NEUC) (Siedler et al., 2001).

The surface South Equatorial Current (SEC) splits into two branches around 8°S near the coast of Brazil, forming the southward flowing Brazil Current (BC) and the northward flowing NBC (Schouten et al., 2005; Stramma et al., 1995). The NBC extends to the north, forming the Guyana Current. In this study, I am only concerned with the NBC and its retroflection around 5°N due its influence on the equatorial dynamics. The NBUC is also important for its contribution to the subsurface eastward flow around the equator.

The NBC continues to flow northward and then retroflects around 4°N and feeds the eastward flowing North Equatorial Countercurrent (NECC). The retroflection depends on the season (Schouten et al., 2005) and contributes to the flow of NECC in addition to the NEC (North Equatorial Current) (Siedler et al., 2001). At the equator, the Equatorial Undercurrent (EUC) usually overlies the EIC (Equatorial Intermediate Current - a westward flowing current) bounded by eastward currents, NEUC at 4°N and the SEUC at 3-4°S. Vertical and lateral flows of the EIC is quite varying especially on seasonal basis.

The NEUC and the SEUC do not have a clear distinguishable separation with the NECC and the EUC respectively. Detailed analysis of water mass characteristics by various authors e.g. Schott et al. (2003) and Stramma et al. (1995) show that the EUC, the SEUC and the NEUC derive their sources from the NBUC. The NEUC had some contributions from the northern hemisphere and is seasonally dependent.

Strong zonal currents characterize the near surface circulation in the equatorial Atlantic. The EUC is the strongest and on either north or south of it is the SEC, with speeds exceeding $1 \mathrm{m} s^{-1}$ (Kelly et al., 1995). The opposite moving currents produce shears, which may produce barotropic instabilities in the equatorial flow. Instability waves have been observed around the equator and it is widely believed that they occur as a result of barotropic instability between SEC and NECC.

The Gulf of Guinea is characterized by both eastward and westward currents and undercurrents of various magnitudes. The eastward flowing Guinea Current flows along the West African coast at approximately 3°N. It has two main sources, the North Equatorial Counter Current (NECC) and the Canary Current. Beneath the Guinea Current is the westward flowing Guinea Undercurrent (GUC), which was previously called the Ivorian Undercurrent (IUC).

In a study of Sea Surface Slope Anomaly (SSSA) along the Atlantic equator (Provost et al., 2004) the magnitude of both zonal and meridional local wind components was found to increase at the beginning of May. Almost immediately, the westward surface flow intensifies and the EUC core deepens from about 60m to reach 100m depth in mid-September. After a brief intermediate state where the EUC core velocity weakens, it intensifies again but ends up only slightly faster in the fall than in the spring. The June to December period of strong winds also corresponds to a deepening of the thermocline. The depth of the thermocline fluctuates between 40-80m depth, depending on the region and season.

Biweekly oscillations of variability were observed (Bunge et al., 2007) from ADCP measurements at 10°W and 23°W along the equator which were present exclusively on the meridional component. This showed a clear upward phase propagation and downward energy radiation, suggesting a first mode mixed Rossby-gravity (Yanai) wave. Yanai waves propagates eastwards even though their wave crests and troughs are westward. Observations from all the oceans indicate that the waves have a preferential period and wavelength of around 25 days and 1000 km respectively (Kelly et al., 1995).

2.6 Atmospheric Circulation

Atmospheric circulation refers to large-scale movement of air that, together with small-scale ocean circulation distributes thermal energy on the earth′s surface. The major form of large-scale circulation that affects the climate of the tropical

Atlantic is the El Niño Southern Oscillation (ENSO). The Pacific SST anomalies are connected with the Atlantic anomalies (Colberg et al., 2004; Hu and Huang, 2007), but the Pacific anomalies come earlier. This shows a connection between the two oceans via heat and moisture fluxes. The ENSO has also been found to modulate rainfall over West Africa (Janicot et al., 2001; Rowell, 2001) remotely. With the monsoon occurring in boreal summer and ENSO in late autumn, Joly and Voldoire (2010) suggested that either the developing phase of ENSO or the decay of some long-lasting La Niña might explain the reason for the ENSO influence on the monsoon.

The Quasi-biennial Oscillation (QBO) is the quasi-periodic oscillation of the equatorial winds. This occurs within the tropical stratosphere above the equator with a mean period of 28-29 months and has been observed since the 1950s from climatological records. The alternating winds develop from the top of the lower troposphere and descend downwards at about 1km per month. These oscillations modulate monsoonal precipitation. A number of authors have suggested that the QBO is an integral part of the ENSO having an oscillatory behaviour that represents amplification and deamplification of the annual cycle (Gutzler and Harrison, 1987).

Another important large-scale variability associated with the climate of the region is the Madden-Julian-Oscillation (MJO). The MJO is the dominant mode of global intraseasonal variability in the tropics (Madden and Julian, 1994). It is characterized by the eastward propagation of regions of enhanced and suppressed tropical rainfall, primarily over the Indian and Pacific regions. However, the exact mechanism behind the eastward and northward propagation of the MJO convective anomalies is still open to debate. This mode has remote influence on West African monsoon region by modulating winds, precipitation and African Easterly Wave (AEW) activity (Matthews, 2004).

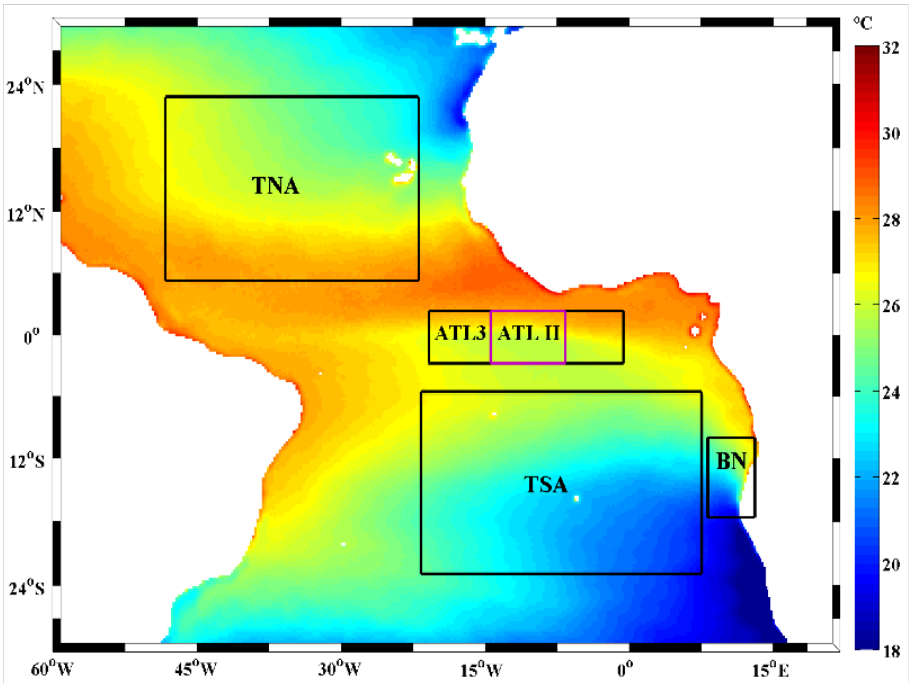

Figure 2.3. *Locations of boxes representing regional climate indices of the tropical Atlantic. These include the Atlantic Meridional Mode Index (AMMI=TNA-TSA), Atlantic Niño (ATL3), Atlantic Niño II (ATL II) and Benguela Niño (BN). Respective time series of these are shown in figure 2.4. The background colour is the annual mean sea surface temperature for 2009 from TMI SST data.*

2.7 Climate Indices

The equatorial Atlantic Ocean is characterised by four major variability modes. These include the Atlantic Meridional Mode Index (AMMI), the Atlantic Niño, the Atlantic Niño II and the Benguela Niño. All these lie within the tropical band bounded by the tropics of Capricorn and Cancer as shown in figure 2.3. The region is also influenced by large-scale ENSO dynamics and the tropospheric forcings of Quasi-Biennial Oscillation (QBO).

2.7.1 Atlantic Meridional Mode Index

The Atlantic Meridional Mode Index (AMMI) is the SST anomalies of (5-15°N, 50-20°W) - (5-15°S, 20°W-10°E) (see figure 2.3). The AMMI is connected with

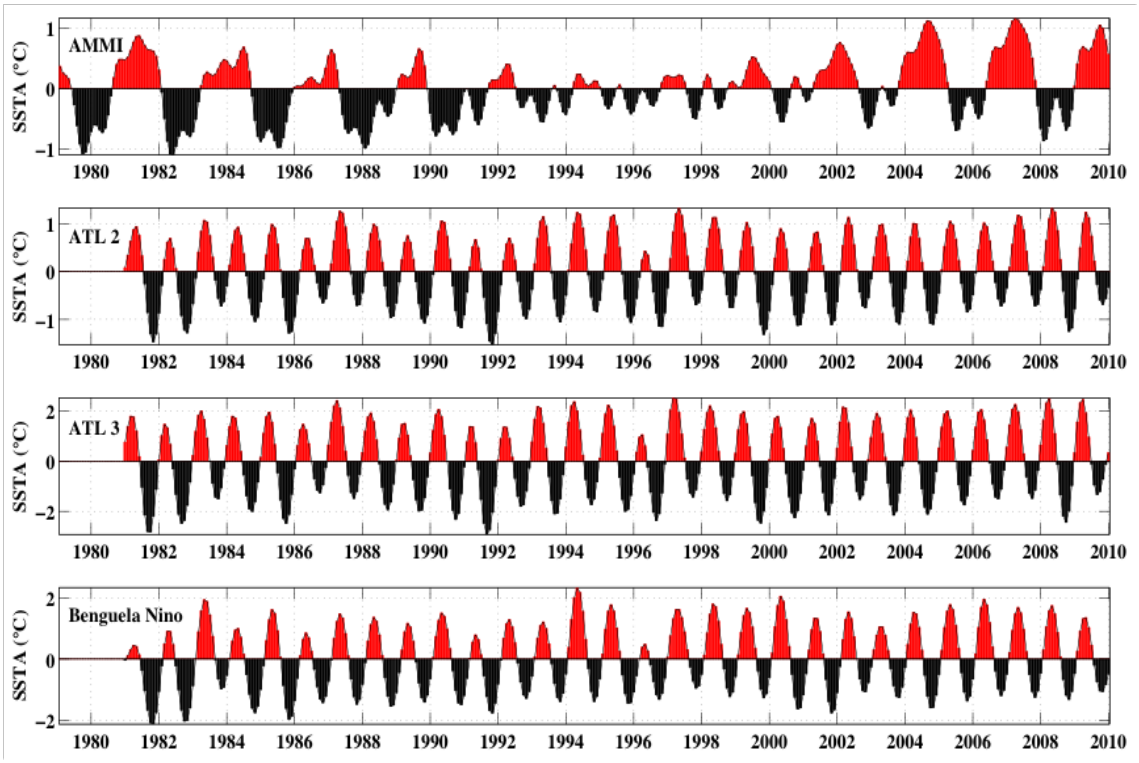

Figure 2.4. *Monthly time series of regional climate indices of the tropical Atlantic produced from SST anomalies bounded by the regions shown in figure 2.3. These include the Atlantic Meridional Mode Index (AMMI)[5-15° N, 50-20° W]-[5-15° S, 20° W-10° E], Atlantic Niño (ATL3) [20° W-0°, 3° S-3° N], Atlantic Niño II (ATL II)[5-15° W, 3° S-3° N] and Benguela Niño (BN)[8° E-14° E, 10° S-20° S]. The data are from NOAA Climate Prediction Centre.*

the large-scale atmospheric wind patterns and the seasonal migration of the ITCZ. It involves a positive feedback between surface winds, evaporation and SST, the so-called Wind-Evaporation-SST-feedback (WES-feedback) (Vimont and Kossin, 2007), and its dynamics are connected with the Atlantic hurricane tracks (Vimont and Kossin, 2007; Xie et al., 2005). The positive mode means warmer north, and more rainfall over West Africa and southern Sahel, and the reverse is the case in south and over South America. The AMMI index is shown in figure 2.4.

2.7.2 The Atlantic Niño

The Atlantic Niño is similar to that of the Pacic but weaker in amplitude and spatial scale. It comprises of warm SST, relaxed trade winds and shifts in convection during summer (Merle, 1980). The index is created from SST anomalies at (20°W-0°, 3°S-3°N). The Atlantic Niño is similar to the Pacific Niño but occurs the following year, suggesting that they are connected (Bakun, 1996). The Atlantic Niño is situated in the Gulf of Guinea, a region where warmer SSTs increases the potential of rainfall in West Africa through convection. Its variability is shown as an index (AMMI) in Figure 2.4.

2.7.3 The Atlantic Niño II

The Atlantic Niño II is an equatorial mode similar to the Atlantic Niño but occurs only in November-December period. It was found to be statistically independent from both the Pacific and Atlantic Niño (Okumura and Xie, 2006), with characteristics that have previously being ignored. The Atlantic Niño II is defined as the SST anomalies in the equatorial Atlantic centred at (5-15°W, 3°S-3°N). This mode affects rainfall at interannual scale in the coastal area of Congo-Angola during the early raining season of the next March-April period (Okumura and Xie, 2006).

2.7.4 The Benguela Niño

The Benguela Niño is an intermittent, acute and extremely warm event near the border between the southward flowing Angola Current and Benguela upwelling system off southwestern Africa (Shannon et al., 1986). Analogous to the Pacific, the warm phase is called Benguela Niño and the cold phase Benguela Niña. The Benguela Niño Index is generated from SST anomalies in the region bounded by (8°E-14°E, 10°S-20°S). Although, it occurred only a few times (1934, 1949, 1963,

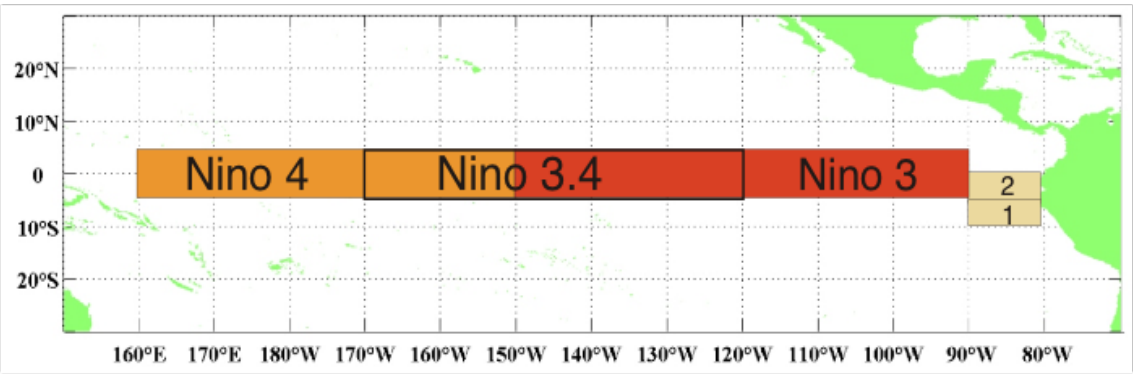

Figure 2.5. *Regions used to calculate Pacific El Niño indices that include Niño 1+2, 3, 3.4 and 4.*

1984 and 1995), it can drastically affect fisheries (Gammelsrød et al., 1998) and induce significant rainfall anomalies (Rouault et al., 2003a).

2.8 Large-scale global climate indices

The El Niño Southern Oscillation (ENSO) is the most important coupled ocean-atmosphere phenomenon that affects the global climate at interannual time scales. ENSO is the general name that encompasses both the warm ENSO phase (El Niño) and the cold phase (La Niña). The ENSO is studied from SST anomalies in the Pacific Ocean and also from atmospheric measurements to determine climate variability. Pacific ENSO indices that are calculated from SST anomalies include Niño1+2, Niño3, Niño3.4 and Niño4 and covers the regions shown in figure 2.5. These indices are shown from 30-year time series in figure 2.6.

Other ENSO indices that are important to the large-scale global climate are the Southern Oscillation Index (SOI) and the Multivariate ENSO Index (MEI). These indices are shown in figure 2.7. Southern Oscillation (SO) is the atmospheric component of El Niño, which is an oscillation of surface air pressure between tropical eastern and the western Pacific Ocean waters. The SOI is the normalised monthly-mean sea level pressure difference between Tahiti and Darwin. The SOI usually corresponds very well with the SST-based ENSO indices.

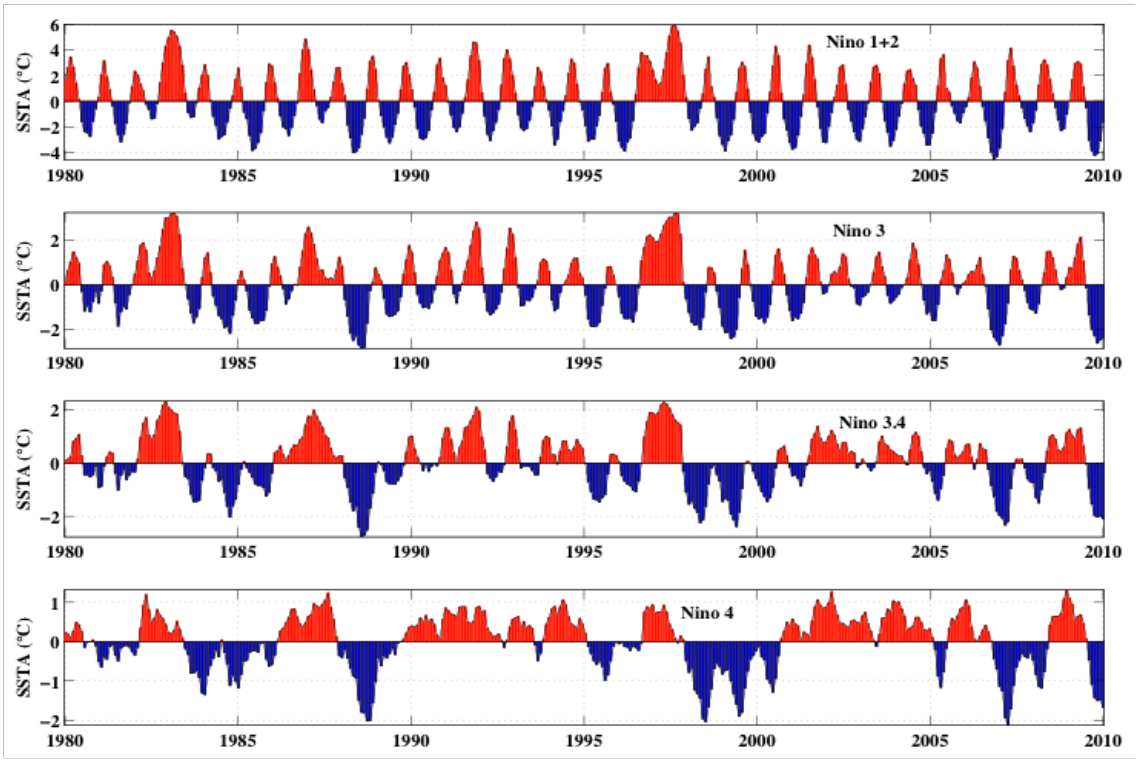

Figure 2.6. *time series of Pacific El Niño Southern Oscillation indices from NOAA Climate Prediction Centre. These were produced from area averages based on optimally interpolated SST (OISST) data. These SST anomaly indices include Niño1+2 (90° W - 80° W, 10° S - 0°), Niño3 (150° W - 90° W, 5° S - 5° N), Niño3.4 (170° W - 120° W, 5° S - 5° N), and Niño4 (160° E - 150° W, 5° S - 5° N).*

The MEI index is also used to monitor ENSO, and calculated from six main observed variables in the Pacific Ocean. These include sea-level pressure (SLP), zonal (U) and meridional (V) components of the surface wind, sea surface temperature (SST), surface air temperature (A) and total cloudiness fraction of the sky (C). The MEI can be understood as a weighted average of the main ENSO features.

The Quasi-Biennial Oscillation (QBO) is a periodic oscillation of equatorial zonal winds between easterlies and westerlies in the tropical troposphere (10-50km heights) with a mean period of 28-29 months. A strong teleconnection between ENSO and QBO has been recent studied (Garfinkel and Hartmann, 2010). This shows an indirect impact of the QBO to the climate through ENSO. The QBO (figure 2.7) is calculated from the NCEP/NCAR Reanalysis data based on

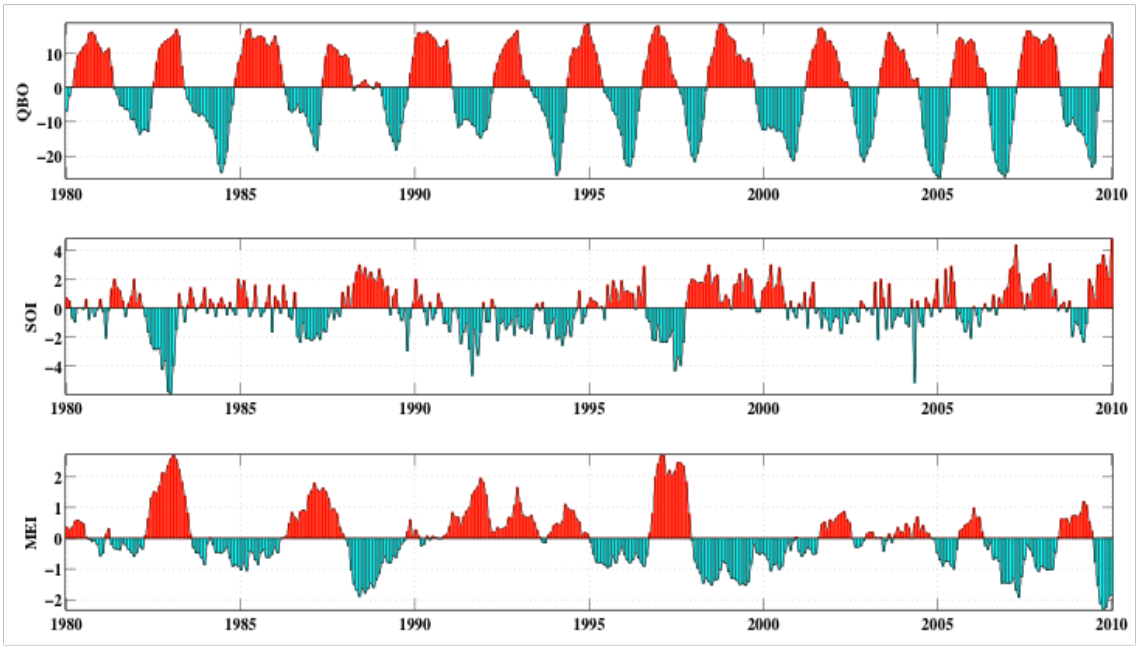

Figure 2.7. *time series of global-scale climate indices that are connected with the tropical Atlantic variability. These are the Quasi-Biennial Oscillation (QBO), the Southern Oscillation Index (SOI) and the Multivariate ENSO Index (MEI). Data are from NOAA Climate Prediction Centre and calculated at Physical Sciences Division (PSDn).*

zonally averaged 30mb zonal wind at the equator.

CHAPTER 3

Data

3.1 Introduction

In this thesis, various data sets are employed comprising different variables at spatial and temporal resolutions. Large fractions of the work uses satellite data due to its inherent advantage of synoptic coverage of the study area as well as a consistent repeat cycles (Challenor et al., 2004). The quality control procedures and interpolation scheme I applied and source of each data is shown. Data sets used include satellite, *In situ* and reanalysis products tailored to specific questions that the thesis aimed to answer, and these are:

1. **Satellite data, which include:**
   (a) Tropical Rainfall Measuring Mission (TRMM) radar precipitation,
   (b) TRMM Microwave Imager (TMI) sea surface temperature,
   (c) QuikScat scatterometer winds
   (d) Altimeter Sea Surface Height Anomaly (SSHA) and its derived geostrophic velocity anomalies.

2. ***In situ* data, which include:**

   (a) Argo profiles

   (b) Drifters

   (c) Prediction Research moored Array in the Tropical Atlantic (PIRATA) moorings.

3. **NCEP/NCAR reanalysis v1 daily products, which include:**

   (a) Atmospheric temperatures

   (b) Atmospheric winds

4. Other data used are the ETOP02v2 bathymetry and relief data.

3.2 Satellite Data

3.2.1 Tropical Rainfall Measuring Mission (TRMM) radar precipitation

The TRMM precipitation radar (PR) is the first space borne rain radar and the only instrument that measures vertical distribution of rain. It can achieve quantitative rainfall estimates both over ocean and land. The PR footprint is 0.25° x 0.25° horizontal resolution. Prior to February 2000, the PR data cover the span of (40°S-40°N, 180°W-180°E). After and including February 2000, the data cover (50°S-50°N, 180°W-180°E). The data are gridded to 0.25° x 0.25° horizontal resolution and the temporal resolution of 3-hourly is averaged to daily to give a complete spatial coverage. Daily averaged 3B42 version 6 is used in this study. The period considered is 12 years (1998-2009) to allow for analysis of interannual variability.

These data incorporate different satellite products including the TRMM Microwave Imager (TMI) and the TRMM precipitation radar to calibrate infrared

precipitation estimates from geostationary satellites (Maloney et al., 2008) These data has a daily temporal resolution and a spatial grid of 0.25° x 0.25°. Although, these data have been found to correlate very well (r=0.9) with rain gauge data at a monthly time period, Nicholson et al. (2003) found a moderately positive bias on daily data.

The TRMM products were specifically validated (Nicholson et al., 2003) over West Africa and a very small overall bias (4%) was observed in the daily datasets. This bias is insignificant in the tropical region where precipitation is always large. Correlations (r) between the satellite products and the gauges on a monthly scale are also shown to be very good (approximately 0.9). These data can be accessed at the NASA′s Goddard Earth Sciences Data and Information Services Centre and detailed documentation is available at the NASA GFSC website.

3.2.2 TRMM Microwave Imager (TMI) SST

The Sea Surface Temperature (SST) data used for this study are provided by the Tropical Rainfall Measuring Mission (TRMM) Microwave Image (TMI) on board TRMM satellite (Chelton et al., 2000). This TRMM radiometer provides uninterrupted record of SST signatures on a global coverage of 40°S-40°N, at a pixel resolution of 0.25° x 0.25° daily and measuring through clouds except rain-clouds. The choice of TMI SST in this thesis is due to its inherent advantage over Infrared sensors, which are affected by clouds. While infra red sensors, such as the Advanced Very High Resolution Radiometer (AVHRR) or Advanced Along-Track Scanning Radiometer (AATSR) has the advantage of having higher spatial resolution and ability to resolve small-scale features at the coast, it is generally not very good in the tropical regions where cloud cover is always prominent. Although, the microwave instrument cannot resolve small-scale features at the coasts and has coarser spatial resolution, it is very useful in addressing mesoscale variability such as tropical instability waves which are central to investigations in this thesis. Details of inherent advantages of using microwave

instruments for measuring the oceans and sea ice are found in Mitchelson-Jacob (1996); Robinson (2010).

In addition to SST retrievals, worth mentioning are other geophysical parameters can also be obtained from the TMI data, though not used in this study. These include Atmospheric Water Vapour, Cloud Liquid Water, Rain Rate, 10-meter Surface Wind Speed using 11 GHz (Z) and 10-meter Surface Wind Speed using 37 GHz (W). These data and the detailed documentations are available at the Remote Sensing Systems website.

3.2.3 QuikScat winds

Wind data are from the SeaWinds scatterometer onboard the QuikScat satellite that provides estimates of the wind at 10m above water surface. Scatterometer winds are affected by rain where by it becomes difficult to differentiate signals from actual winds and those of rain. However, scatterometer processing uses contemporaneous radiometer measurements for rain flagging. Therefore, Remote Sensing Systems used four microwave radiometers (F13 SSMI, F14 SSMI, F15 SSMI and TMI) to determine if rain is present at the location of QuikScat observation and that allowed proper flagging of scatterometer observations. The daily level 3 gridded ocean wind vector data has a pixel resolution of 0.25° x 0.25°. The data are further averaged to 3-daily before analysis. The three daily averages also tend to have gaps between satellite tracks, and I retrieved these through interpolation procedure described in section 3.3. The gap filling was systematically done and there is no error whatsoever that can affect the results.

QuikScat is in a sun-synchronous orbit an altitude of 803km and a period of 101 minutes. It has a 0600 ascending equator-crossing time, and the scatterometer swath has an overall width of 1800km with no nadir gap. Daily data exist from 19 July 1999 to 19 November 2009, marking the period of existence of the mission. These data are obtainable from NASA′s Jet Propulsion Laboratory at the website.

3.2.4 Altimeter Sea Surface Height (SSH) and geostrophic velocity

The altimeter products are the global near-real time multi-mission satellite products. Satellite altimeter products from all available missions that include Jason-1, Envisat, GFO, ERS-1, ERS-2 and Topex/Poseidon data of various timescales are re-gridded to daily products. These data include the Maps of Sea Level Anomaly (MSLA) Sea Surface Height (SSH) and geostrophic velocity anomalies. Both data are processed to a Mercator grid of 0.3° x 0.3° spatial resolution. Altimeter geostrophic velocities at the equator are not valid due to the breakdown of geostrophy. However, it can be calculated to ±1 degree latitude to still give correct results (Picaut et al., 1989). The data has been re-gridded to 1° x 1° Cartesian grid to allow easy comparison with other satellite products used in this thesis. The data are produced by SSALTO/DUACS and distributed by AVISO, and can be accessed at their website.

3.3 Filling gaps in data

The TMI SST has a gap between 17-19 September 2000, 14-16 August 2001 and also gaps created due to the inability of the sensor to penetrate through raining clouds. This is a major problem from the microwave satellite temperature data that results in the disappearance of patterns (Quartly et al., 2006). In this thesis, analysis is done mostly based on 3-daily averages and that has taken care of the aforementioned gaps in 2000 and 2001. However, a few gaps still exist due to the effect of raining clouds and that is handled through an optimal interpolation scheme.

This interpolation is also applied to the QuikScat wind vector products, which still have gaps after averaging of 3-day passes.

A part of this thesis employs the use of Singular Value Decomposition (SVD) to describe modes of variability from the data sets. However, computing the covariance matrix from missing data is not easily carried out especially for large datasets. These missing data have to be filled before performing SVD calculations (Houseago-Stokes and Challenor, 2004).

Furthermore, gaps in datasets could also lead to biased results from climatology prepared from these data. It is imperative, therefore to fill in the gaps with objective interpolation methods so as to achieve the desired accuracy, as consecutive adding of images with gaps could not essentially give a statistically coherent result. Hence, all data used in this thesis are clear of gaps.

3.3.1 Method of filling gaps in data

The SST data interpolation was done using Data Interpolation Empirical Orthogonal Functions (DInEOF) (Alvera-Azcárate et al., 2005). It is parameter-free, that is all necessary parameters are derived internally from the existing data, and it is an EOF-based method for reconstruction of missing data.

The DInEOF method works in this way: the input data is stored with spatial and temporal averages subtracted *apriori*. Missing data are set to zero, to guarantee that they are unbiased with the training data. With this first guess, an SVD is computed. Missing data are then replaced with the EOF obtained. With a new value for the EOF, the SVD is run again recursively, and each time a new EOF is also produced throughout the time.

The optimal number of EOFs retained for the reconstruction is determined by cross-validation (a number of points typically 1% of the initial data) are set aside and considered as missing. After each estimation, the error between these initial points and their reconstruction is calculated, so the optimal number of EOFs minimizing this error can be determined. Along with the reconstructed data, local error fields reflecting the accuracy of the reconstruction can also

be generated. Lanczos strategy was employed to enhance computational speed (Alvera-Azcárate et al., 2005).

After interpolating a complete dataset using DInEOF, the product was not used directly in order to maximize statistical accuracy. Instead, the original data set with missing records and the interpolated data set are used to produce a reconstructed data set by filling only the gaps in the original data products. An example of a 3-day averaged reconstructed TMI SST data is shown in figure 3.1.

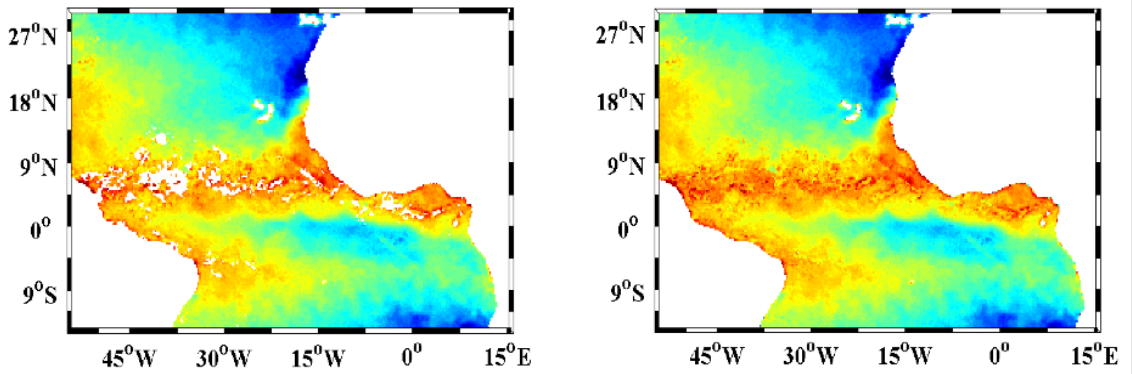

Figure 3.1. *An example of a 3-day averaged new TMI SST data: Left panel is the original data; right panel is the final product.*

3.4 In Situ data

3.4.1 Argo data

Argo floats are freely drifting arrays of global ocean observing system that measure temperature and salinity in the upper 2000m of the water column. Over 3000 floats have been launched and are actively sampling the global ocean with an unprecedented 10-day standard sampling per profile giving salinity and temperature data. Each float is capable of collecting more than 100 samples, and data are made freely available to scientific community via the US GODAE website and various other distributors online. Each profiler floats at 1000m depth for 10 days before diving down to 2000m from where it samples the ocean to the surface. Data is then relayed to satellite through an antenna. Monitoring of

float position is made possible by the Argos system, and each float is identified by World Meteorological Centre (WMO) assigned number.

Other parameters are also deducted from Argo floats such as current velocity due to shift in position determined by Argos system. An alternative system to Argos has already been tested using Global Positioning Syste (GPS) and data communication using the Iridium and Orbcomm satellites. This allows more detailed data proles to be transmitted with a shorter period at the surface and even two-way communication. Some Argo floats are specifically tailored to sample the ocean and provide other data such as oxygen and nitrate by adding additional sensors. These floats can also be designed to sample the ocean less or above the standard 10-day sampling.

The Argo profiles used are processed by French operational oceanography centre, Coriolis and distributed by US Global Ocean Data Assimilation Experiment (GODAE). Floats were considered based on their length of profiling time, spatial coverage and quality of data. The profiles used are as identified by World Meteorological Organization (WMO) IDs are 1900652, 1900663, 1900550, 1900543 each with a 10-day cycle. The floats were launched at different times, but profiles taken were at exact timing to allow covariability studies.

3.4.2 Drifter data

One of the current data used for this study is derived from satellite-tracked surface drifting buoy observations gridded at 1° x 1° horizontal resolution (Lumpkin and Garraffo, 2005). It is a product of Drifting Buoy Data Assembly Centre at National Oceanic and Atmospheric Administration (NOAA). It consists of monthly climatological fields of near-surface temperature (0.5m) and zonal and meridional currents as a collection of available data sampling the global ocean with time scale spanning from 1979-2009.

To derive the fields contained in the climatology, the time-mean, annual and semi-annual components of total temperature and velocity were combined and

integrated to yield monthly averages. The results were further smoothed using an Optimal Interpolation method described by Cuny et al. (2002). The interpolated data covers the global ocean at 73°S-85°N,180°W-180°E. In comparison of this methodology to other modern data sets of the tropical Atlantic observations, many features of the near surface circulation which were not resolved by traditional ship-drift-based climatologies (e.g. Near Global Ocean Currents Climatology of the National Centre for Atmospheric Research, NCAR) or by FOCAL/SEQUAL (Programme Français Ocean-Climat en Atlantique Equatorial/Seasonal Equatorial Atlantic Response Program) drifter trajectories (Lumpkin and Garraffo, 2005) became apparent.

3.4.3 PIRATA data

The PredIction Research moored-Array in the Tropical Atlantic (PIRATA) is a tripartite programme between USA, France and Brazil that was established to study the ocean-atmosphere system in the tropical Atlantic (Bourlès et al., 2006). The programme involves data collection from moorings established across the whole tropical region. Data collection ranges from surface to 500m depth, depending on the sensor and variable required to be sampled. These include temperature, salinity, currents and surface water partial pressure of Carbon Dioxide (pCO2). Other parameters such as dynamic height and heat content can also be determined from the observed data. Instruments on these moorings also collect meteorological variables simultaneously. These include zonal and meridional wind vectors, wind speed, wind direction, air temperature, longwave radiation, shortwave radiation, sea level pressure, rain and relative humidity. Sampling is at high temporal resolution of 10 minutes, allowing the possibility of identifying fast changing incidences and diurnal cycle.

Data from a mooring at 0°N/23°W is used in this study to supplement Argo profile data in the region. This mooring is equipped with ADCP instrument to collect zonal and meridional currents from surface to 120m depth. Temperature and salinity from the same mooring and depth are also used. The 10-minute

data are averaged to 10-day to correspond with the temporal resolution of Argo profiles. These data are obtainable from the Tropical Atmosphere Ocean (TAO) portal of National Oceanic and Atmospheric Administration of USA. The accuracies of various observed parameters and their units are shown in table 3.1.

Table 3.1. *Accuracies of observed datasets and their units*

S/N	Parameter	Accuracy	Unit
1	TMI SST	0.5	$^{\circ}C$
2	AATSR SST	0.3	k
3	AVHRR SST	0.5	k
4	Argo temperature	0.005	$^{\circ}C$
5	Drifter temperature	0.05	$^{\circ}C$
6	Drifter currents	± 1	cms^{-1}
7	PIRATA temperature	0.01	$^{\circ}C$
8	PIRATA Salinity	0.003	psu
9	TRMM precipitation	0.7	mm/day
10	QuikScat winds	2	m/s
11	QuikScat direction	20	degrees
12	MSLA SSHA	3	cm

3.5 Reanalysis data

The daily air temperature and zonal/meridional wind vectors for the atmospheric column are NCEP/NCAR reanalysis v1 products. These data are on 2.5° x 2.5° global grids of 17 pressure levels from 1000 to 10hPa (Kalnay et al., 1996). Sea level pressure products are also from the same source. The data are based on observed and forecast systems using state-of-the-art data assimilation techniques. These data supplement TMI SST data in the analysis of buoyancy difference along the atmospheric air-column due to mesoscale variability.

3.6 Bathymetry and topography data

The bathymetry and topography data used in this thesis is the Smith & Sandwell 2-minute gridded global relief data (ETOP02v2) provided by the National Geophysical Data Centre, National Oceanic and Atmospheric Administration (NOAA). This gridded data is derived from 1978 SEASAT satellite radar altimetry of the sea surface. These data and further details are obtainable at the NGDC centre.

CHAPTER 4

Temperature advection

4.1 Introduction

The role of the equatorial Atlantic in the tropical heat budget remains an unresolved question due to the complexities associated with the cold tongue, tropical instability waves (TIWs) and the southeast monsoon winds. Sea Surface Temperature (SST) in this region is largely controlled by upper ocean dynamics, which include advection via large-scale circulation, coastal and equatorial upwelling as well as contributions from equatorial waves. At high frequencies, SST variability has been characterised into two components: the diurnal cycle associated with daytime warming and night time cooling as well as fluctuations with time scales of 20-40 days associated with seasonal TIWs (Garzoli, 1987; Wainer et al., 2003).

At the beginning of the boreal summer, there is an intensification of the cold tongue, which straddles the equator with temperatures of about 23°C at the centre of the core. The northern edge of the cold tongue is characterised by strong SST anomalies characterised by the cusp-shaped TIW signatures (Chelton et al., 2000) between 2-4°N with SST in the range of 25-27°C. These SST

signatures occur mostly within the latitude range because the waves are stronger to the north. This is also a region of strongest wind stress divergence, and hence Ekman pumping and forms the boundary between the westward South Equatorial Current (SEC) and the eastward North Equatorial Countercurrent (Richardson and Reverdin, 1987). North of 4°N the SST can reach 30°C, marking the position of the Atlantic thermal equator.

A thorough understanding of the processes governing heat budget requires investigation of SST evolution through time and its roles to local surface heat flux, freshwater flux, turbulent heat flux and advection. Hence, understanding the importance of currents in the distribution of temperature is vital to the climate both in terms of heat and moisture fluxes and the carbon sink. In a similar vein, SST variability in the equatorial Atlantic cold tongue region (25°W-15°E, 12°S-4°N) has been found to correlate well with rainfall anomalies in both the surrounding regions of Brazil and West Africa (Chang et al., 2006; Xie and Carton, 2004). Therefore, a good understanding of SST variability could lead to the prediction of rainfall.

The equatorial Atlantic SST is characterised by two modes of interannual variability: one is the equatorial mode similar to the Pacific El Niño Southern Oscillation (ENSO) and the other is the dipole mode, also called the Atlantic interhemispheric SST gradient (Servain et al., 2003; Wainer et al., 2003; Wang and Weisberg, 2001). The dipole mode of the equatorial Atlantic may be explained through inter-play between two feedbacks of opposite sign. The positive one is based on wind induced heat fluxes and changes in SST anomalies that control the southern cold basin and the northern warm basin. The negative phase involves oceanic anomalous advection that goes from north to south (Chang et al., 1997). The meridional mode, a north-south mode of variability in the tropical Atlantic, is sensitive to the anomalous cross equatorial SST gradient (CESG), especially in February-April when the ITCZ is at its southernmost position and the climatological CESG is weak (Carton et al., 1996; Seager et al., 2001). The meridional positioning of the ITCZ is sensitive to CESG anomalies.

The wind-induced changes in evaporation and SST due to anomalous trade winds is organised into a wind-evaporation-SST feedback (WES). The cross-equatorial WES feedback works as follows: Consider the presence of an anomalous cross equatorial SST gradient (CESG) that causes southward pressure gradient due to hydrostatic adjustment (Lindzen and Nigam, 1987). This generates anomalous cross-equatorial winds that turn to the west in the southern hemisphere and east in the northern hemisphere due to the Coriolis force. The anomalous south-westerly (south-easterly) winds dampen (enhance) the north-easterly (south-easterly) background trade winds over the northern (southern) side of the equator. This leads to a decrease (increase) in latent heat flux release from the ocean to the atmosphere, leading to a local warming (cooling) in the northern (southern) part region, hence amplifying the initial anomaly in equatorial SST. The WES feedback mechanism manifests itself as a positive (negative) feedback in a region where mean background trade winds are easterlies (westerlies) (Mahajan et al., 2009). On a decadal time-scale, the WES feedback is counteracted by advection caused by meridional ocean currents (Chang et al., 1997) and by the poleward advection due to Ekman pumping (Xie, 1999).

The ocean′s role in the SST gradient of WES is not clear. At interannual timescales, Seager et al. (2001) suggested that the ocean creates a damping effect on the emerging large-scale SST anomalies by horizontal advection due to mean Ekman flow. In Chang et al. (1997) model, the CESG feedback is limited by cross-equatorial advection by the northward flowing North Brazil Current, which helps switch the phase of the coupled oscillation, therefore setting the timescale of reversal.

In a study of heat and moisture fluxes in the equatorial Atlantic, Yu et al. (2011) observed a positive correlation between SST and a proxy depth of the thermocline (20°C isotherm). A high correlation was found to occur between 3-10°N that is associated with vertical advection induced by the Ekman pumping velocity. This is because the upward Ekman pumping due to divergence raises the thermocline water to the mixed layer and cools the SST.

Temperature advection is highly relevant and plays a fundamental role in the equatorial heat transport while latent heat loss has greater impact at the subtropics (DeWitt and Schneider, 1999) Assessing the advective tendencies of current anomalies is also important to the general circulation models without which their forecast capability is reduced and they would not be able to address tropical intraseasonal variability and other extreme events (Deser et al., 2006; Jochum et al., 2007; Lin et al., 2006). The contribution of advection in the heat budget has prompted the need to better understand the mechanisms by which oceanic dynamics are reflected by near-surface currents. The goal of this chapter therefore, is to quantify the role of horizontal temperature advection in setting the distribution of equatorial Atlantic temperature. The contributions of mean and anomalous temperature advection in the zonal and meridional direction that may have an impact on the cross-equatorial SST gradient are examined. This was previously not possible due to lack of observed currents. Because of the eastward anomalous cross-equatorial winds of the WES-feedback mechanism north of the equator, I hypothesis that meridional temperature advection would be greater than the zonal component in transporting heat across the basin due to Ekman flow. In the boundary layer, the Gulf of Guinea SST controls the moisture convergence over West Africa monsoons (Fontaine et al., 2003). However, the effect of currents in determining SST anomalies in this region is not clear. I therefore, also hypotheses that temperature advection of tropical instability waves does warm the Gulf of Guinea region.

The most recent and up-to-date climatological velocity and SST data with improved spatial resolution of 1° latitude x 1° longitude and monthly temporal resolution is used in this chapter. The accuracy of the near surface (0.5m) current using these drifters is $\pm 1 cms^{-1}$ in a 10 ms^{-1} wind (Falco and Zambianchi, 2011; Pazan and Niiler, 2001). These were produced from 30 years (1979-2009) of drifter data, and were able to highlight small scale features at the near-surface which was not achievable previously even from the comprehensive joint SEQUAL and Programme Français Océan-Climat en Atlantique Equatorial (FOCAL) programs of 19831985 (Lumpkin and Garzoli, 2005). The drifter data is

supplemented with daily multi-satellite near real-time altimeter derived geostrophic currents for three years (2007-2009). The data is of high resolution (0.3° x 0.3° grid) and can provide a view of higher frequency advective tendencies. Daily gridded data are only made available as near-real time products. Tropical Rainfall Measuring Mission (TRMM Microwave Imager - TMI) SST with spatial resolution of 0.25° x 0.25° are used in conjunction with the altimeter data for the analysis. For consistency, both the velocity and TMI SST data were linearly interpolated to 1°x1° grid and averaged to 3-day before additional calculation. Details of these data and the quality control applied are discussed in chapter 3.

This chapter is organised as follows: Section 4.2) Seasonal variability of SST and surface currents, 4.3) temperature advection, 4.4) results, 4.5) discussion, and 4.6) summary.

4.2 Seasonal variability of SST and surface currents

Oceanographic conditions in the equatorial Atlantic during the summer are characterised by quasi-equatorial upwelling driven by persistent southeast trade winds. The seasonal variability of mean equatorial Atlantic SST is shown in figure 4.1 with the associated standard deviations (std). The warmest part of the basin is in the Gulf of Guinea (10°W-14°E, 7°S-7°N) region during the March-April-May (MAM) period with ∼30°C maximum that is associated with the boreal spring. Highly variable SST (std $>$ 0.6) occur at the cold tongue region during MAM and that corresponds to the period when southeast trade winds begin to advance. The cold tongue usually starts to develop in the Atlantic around mid May, and disappears in November. The maximum std signal is seen in the Gulf of Guinea and south during JJA months. Regions of enhanced std greater than 0.4 represent areas of dominant spatial modes of variability in the equatorial Atlantic (Huang et al., 2004).

The current velocity structure of the equatorial Atlantic is a complex one, being characterised by strong surface currents and undercurrents that lead to the

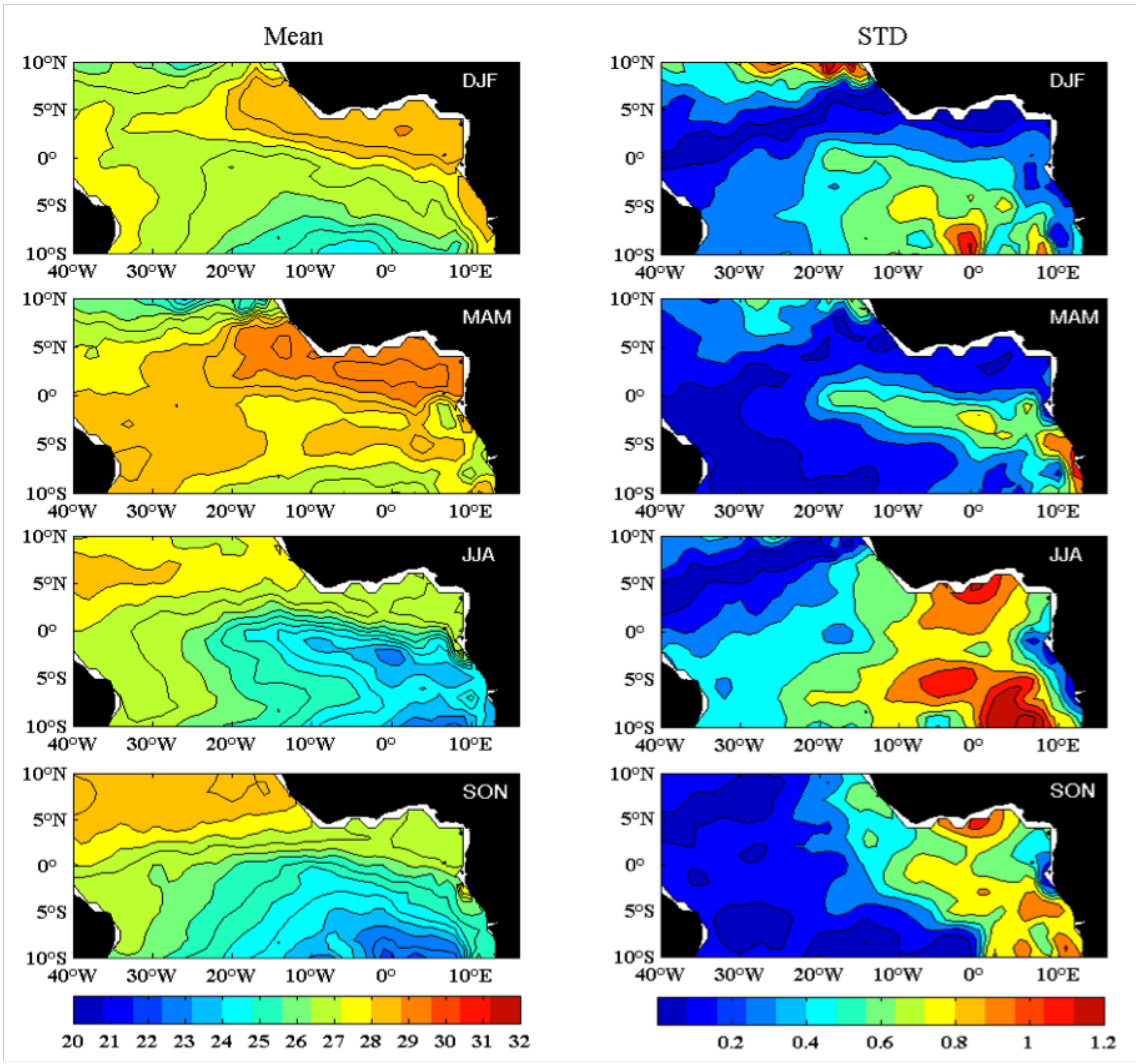

Figure 4.1. *Seasonal SST variability from drifters. Left panel (mean), right panel (standard deviation). Contour interval is 1°C for mean SST and 0.15 for std SST. Units are in °C.*

generation of barotropic and baroclinic instabilities. The consequences are the generation of TIWs that straddle the equator, leading to a net increase in thermodynamic processes at the air-sea interface as well as temperature advection. The strongest surface current is the SEC, reaching up to ∼3°N, with a typical speed of 60cm/s at the centre of the basin, and can reach up to 100cm/s (Kelly et al., 1995).

Surface circulation (figure 4.2) shows weak flows in DJF, implying less impact of seasonal winds and wave activity. The Guinea Current (3-5°N, 8°W-0°E) reveals a stronger velocity of ∼50cm/s and maintains strong flows throughout the

year with maximum in JJA (∼65cm/s). The SEC also shows strong velocities in both MAM and JJA periods, with the latter having over 60cm/s. Significantly low velocities of ∼10cm/s are seen north of 5°N in both DJF and MAM, as well as south of 7°S for all the seasons. Interestingly, the existence of the eastward-flowing North Equatorial Countercurrent (NECC) is seen very clearly in the JJA season between 3-10°N. The NECC is considered to have a boundary between 3-10°N (Bischof et al., 2004), and is important in the seasonal circulation due to its influence on the generation of TIWs. The NECC is stronger and more visible during the boreal summer but barely seen in other seasons. The SON season shows weaker flows generally, except the Guinea Current and South Equatorial Current (SEC) that showed significant values in the eastern part of the basin.

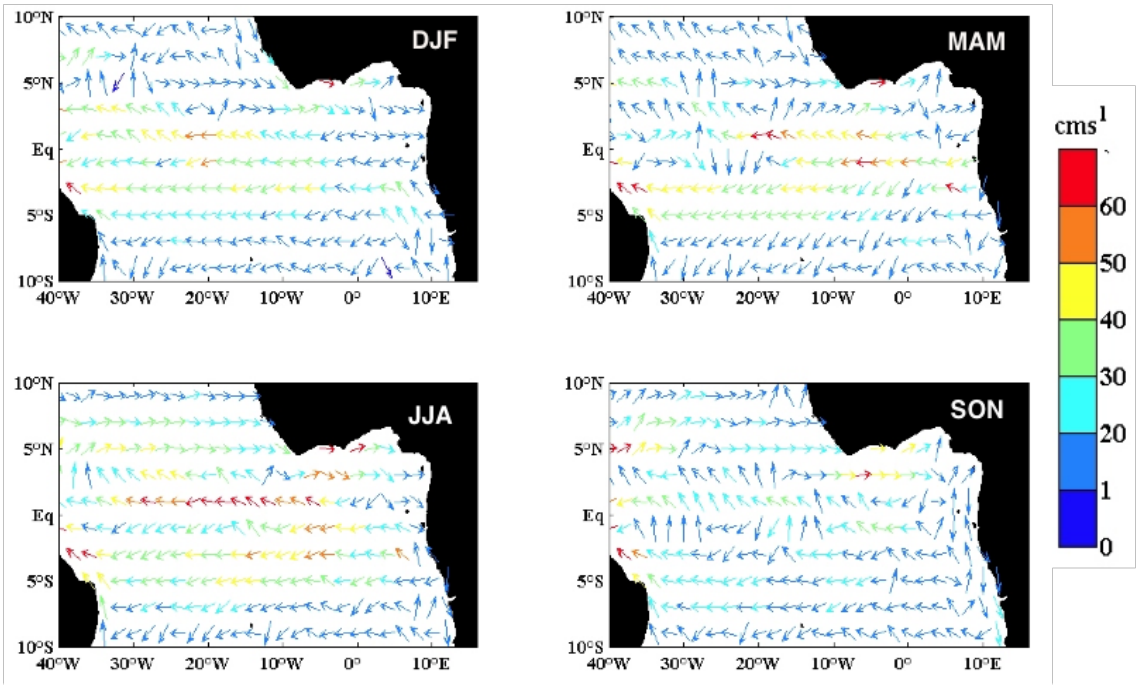

Figure 4.2. *Seasonal variability of surface currents from drifters (long term mean).*

Drifter and satellite data are used to describe the spatial and temporal evolution of SST due to surface currents in the equatorial Atlantic region. Temperature advection by surface and near-surface currents are characterised to determine their contributions to SST variability at both highly variable north equatorial Atlantic region and the less variable south. Two boxes (A and B) are chosen

north of the equator to determine the relative contributions of temperature advection from both drifter climatological mean data and high temporal and spatial resolution TMI SST and altimeter (MSLA) geostrophic currents. Another box (C) is chosen south of the equator, utilising only drifter data to characterise dynamics in a less variable region. The drifter measures currents and temperatures at approximately 0.5m depths while satellite SST is skin temperature.

4.3 Method

Understanding the contribution and effect of advection on the scale of the heat budget requires the availability of ocean current data. I use highly accurate monthly drifter climatology data of SST and zonal and meridional velocities to build up a framework under which advective tendencies of temperature as well as other oceanographic features are interpreted and discussed. The contribution of temperature advection in the equatorial heat budget from much higher temporal and spatial resolution satellite data is also studied. The spatially averaged time series were taken from three boxes shown in figure 4.3, with box A (6-8°N, 18-34°W) for the high-resolution satellite data, and boxes B (3-5°N, 18-34°W) and C (10-12°S, 18-34°W) for the drifter climatology.

The northernmost boxes A and B were intended to focus on the location of the NECC which has been found to exist between 3-10°N from other studies, e.g. (3-10° Richardson and McKee, 1984), (3-9°N Garzoli and Richardson, 1989) and (3-10°N Fonseca et al., 2004). The presence of NECC is important because current shear between it and the westward flowing NEC (7-20°N) as well as between NEC and EUC (2°S-2°N, 80-100m depth) results in the generation of TIWs, which are important aspects of anomaly circulation in the region. The third box C is considered for the analysis in a region not influenced by the waves.

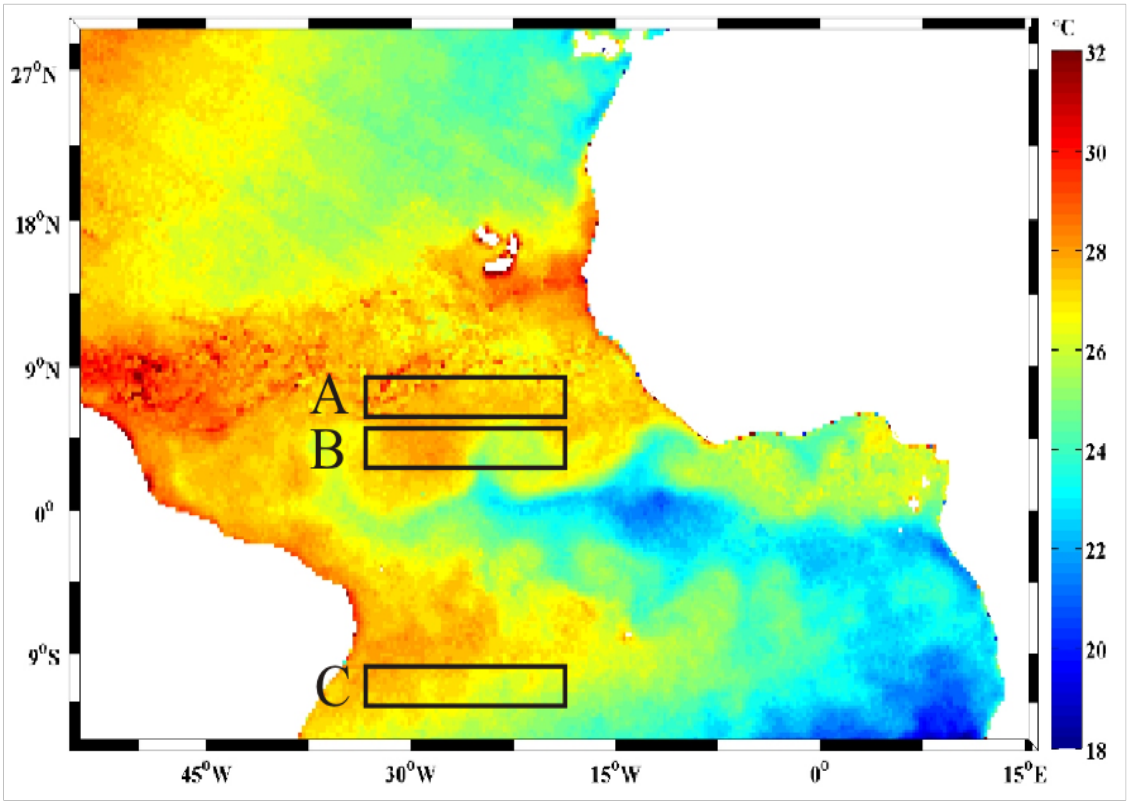

Figure 4.3. *A snapshot of TMI SST averaged over three days, 3-5 July 2009. The cold tongue is fully matured and TIWs are seen on the northern and southern edges of the tongue. Box A (6-8° N, 18-34° W) is considered for analysis of altimeter geostrophic currents and TMI SST data while boxes B (3-5° N, 18-34° W) and C (10-12° S, 18-34° W) were considered for analysis of drifter current and drifter SST data. Boxes A and B were chosen so that advection changes related to anomalous currents due to TIWs can be observed, while box C was chosen because the area is not influenced by the seasonal TIWs.*

The horizontal temperature advection has been used to study individual directional contributions of currents to temperature gradients with the aim of evaluating the impact of these currents to local climate (Foltz et al., 2003; Lee et al., 2004). The temperature advection equation is given by

$$-\vartheta \nabla T = \left(-u\frac{dT}{dx} - v\frac{dT}{dy} - w\frac{dT}{dz} \right) \tag{4.1}$$

where

ϑ =velocity vector with directional elements u,v, and z, in the zonal (x), meridional (y) and vertical (z) respectively, and ∇ is the gradient operator. The terms on the right are zonal, meridional and vertical temperature advection components respectively. For the purpose of this work, and due to absence of vertical velocity data, I consider only the first two terms

$$-\vartheta\nabla T = \left(-u\frac{dT}{dx} - v\frac{dT}{dy}\right)$$

for zonal and meridional temperature advection components.

To calculate temperature advection, I applied equation 4.1 by considering the boxes shown in figure 4.3, with the aim of evaluating the time evolution of advective tendencies in the region. Time series of temperature advection from each box were then created and analysed. Finally, spatial advective tendencies over the equatorial Atlantic basin are calculated and presented. Box B is analysed first because it is directly on a region where TIWs are strongest, and then the results of C and A are presented.

4.4 Results

4.4.1 Analysis from drifter data 1: Box B

The zonal velocity (figure 4.4a) remains eastward from May and peaking in August with about 22cm/s due to the presence of NECC, while the meridional component is weaker with ∼3cm/s southward in the same month. The NECC is strong and visible during the boreal summer and spring but disappears by late winter. From mid-May to November, the flows change direction, becoming stronger eastward and southward. However, the reverse is the case in November when both zonal and meridional velocities account only for about 3cm/s, leading to a minimal flow.

The SST anomalies based on the overall average (figure 4.4b) began to increase at the beginning of the boreal summer, cooling from May as the cold tongue develops but returning to a peak in November. This signifies the seasonal cycle of SST in the equatorial Atlantic sub-domain. Surface flows close to the equator are highly influenced by seasonal winds as a major driving force since the Coriolis force diminishes at the equator. The southeast trade winds must have excited the surface of the ocean remotely and raised surface currents at the southwestern flank of the South Equatorial Current (SEC) but at earlier time, as the winds were stronger in the south in March. The strengthening of northeasterly trade winds when the ITCZ is retreating southward might have enhanced the North Equatorial Currents through surface stress in August-September (figure 4.4a).

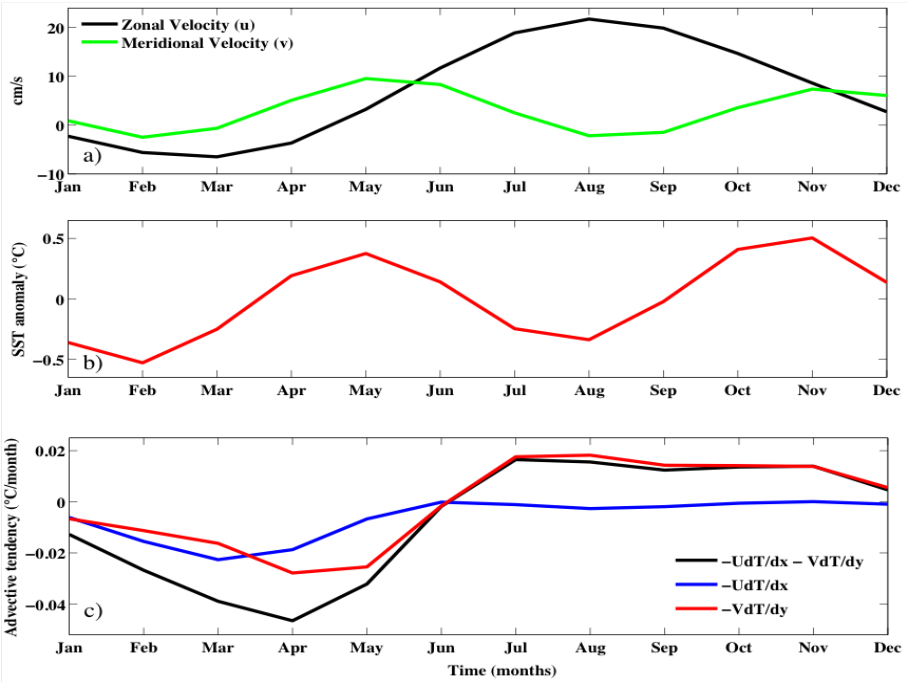

Figure 4.4. *Box B (shown in figure 4.3) indicating mean monthly, a) zonal and meridional velocities b) Spatially averaged SST anomaly from drifter and c) horizontal temperature advection tendencies and its zonal and meridional components.*

The SST anomalies (figure 4.4b) show the seasonal cycle of SST in the region with higher values in May, which subsequently drop as the strength of the cold tongue reaches its northernmost position in July/August. The temperature

advection time series (figure 4.4c) show the horizontal advection (black) having a considerable cooling effect with ∼-0.05°C/month in the boreal spring but warming from May. Warming tendencies reach maximum in July/August with ∼0.02°C/month, and this continues until November, possibly influenced by the high SST observed in figure 4.4b. The main contributor of advection is the meridional component with values closer to that of horizontal temperature advection, while the zonal component is much smaller from mid-May to end of the year. This implies that from June-December, the influence of zonal currents in transporting heat within the chosen box is quite minimal.

Since this analysis is in a region of significant anomalous circulation due to tropical instability waves and their vortices, it is important to decompose the advection term into mean and anomaly components to see the magnitude of contribution of each to temperature advection. I decompose both U and dT to their mean and anomaly components to examine their relative importance to circulation. For ease of nomenclature, $\frac{dT}{dx}$ is written dT. This should provide a quantitative representation of the contributions of mean and anomaly components of the variable pairs.

$U = \bar{U} + U'$,

where $\bar{U}$ is the mean seasonal cycle of zonal velocities and U' from the mean seasonal cycle of zonal velocities and

$dT = \bar{dT} + dT'$,

where $\bar{dT}$ is the mean seasonal cycle of temperatures and dT' from the mean seasonal cycle of temperatures.

$$UdT = \bar{U}\bar{dT} + \bar{U}dT' + U'\bar{dT} + U'dT', \tag{4.2}$$

The anomaly component of zonal advection (figure 4.5a) corresponds to the total horizontal advection term UdT. That means the advection of anomalous temperatures due to current anomalies $U'dT'$ relate to the zonal advection UdT,

but entails relatively more cooling than warming throughout the year. Anomalous circulation in this region are associated with the oscillatory behaviour of the waves due to anomalous currents and temperatures. This demonstrates that the TIWs are the major contributors to advection in the region. Advection of mean (anomalous) temperatures due to anomalous (mean) currents $\bar{U}dT'$ lead to warming (cooling) from January-June.

Contrasting $U'd\bar{T}$ with $\bar{U}dT'$ shows a striking out of phase relationship between the two, with almost the same magnitude of alternating warming/cooling tendencies during the first and second halves of the year. These phenomena are due to changes of surface currents caused by prevailing southeasterly and northeasterly winds in the Atlantic.

A similar calculation was done for the meridional component (figure 4.5b), in which the mean and anomalous components are contrasted in each case to reveal their individual contributions to advection. This is expressed as follows:

$$VdT = \bar{V}d\bar{T} + \bar{V}dT' + V'd\bar{T} + V'dT', \tag{4.3}$$

The seasonal cycles of both the meridional advection term (VdT) and the anomaly component ($V'dT'$) exhibit a similar pattern but with a reversed magnitude around mid-June. Before this period, the meridional advection term reveals a significant cooling effect due to the strengthening of the cold tongue in April-May, where cold waters are advected northward. The anomaly component ($V'dT'$) maintained a warming effect until April and by mid-June, involved with advection of cold waters toward the end of the year. The mean temperatures due to anomalous meridional currents ($V'd\bar{T}$) and the anomalous temperatures due to the mean meridional currents ($\bar{V}dT'$) remained out of phase prior to June, but however came in to phase when the NECC forms in June and remained so until the end of year. It is clear, that $V'd\bar{T}$ is the least contributor to meridional temperature advection, with peak values in the range of ± 0.2°C/month throughout the year.

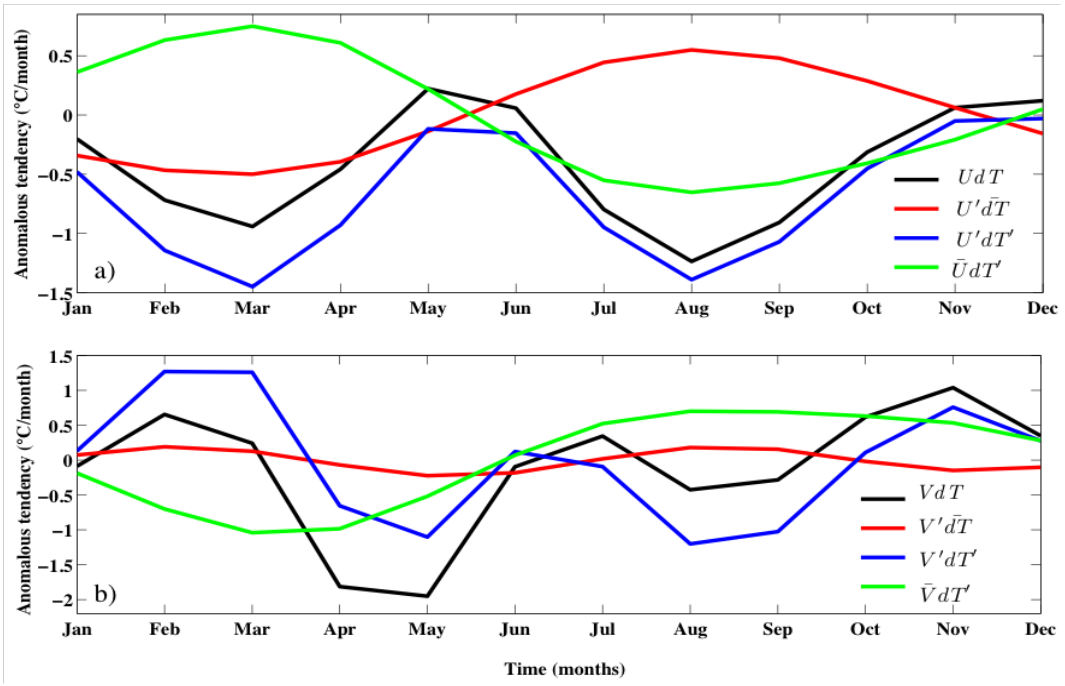

Figure 4.5. *Box B (shown in figure 3.3) decomposition of temperature advection terms a) zonal and b) meridional.*

Prior to June, each of the decomposed terms of advection for the zonal component (figure 4.5a) is out of phase with the corresponding terms in the meridional direction (figure 4.5b). However, the cooling and warming effects are in phase between June until December. Generally, the warming tendency is exhibited in the later half of the year by meridional advection due to the impact of tropical instability waves.

4.4.2 Analysis from drifter data 2: Box C

The zonal and meridional velocities shown in figure 4.6a exhibit westward and southward flows respectively, with a considerable degree of change in magnitude from June to December. Earlier from April to May, the zonal currents were weaker but became stronger as they are perturbed by the southeast trade winds with westward velocities increasing from 5cm/s in May to 10cm/s from August-December. This is reflected in the cooling of the SST shown in figure 4.6b as the southerly winds strengthen. The region bounded by this box is influenced

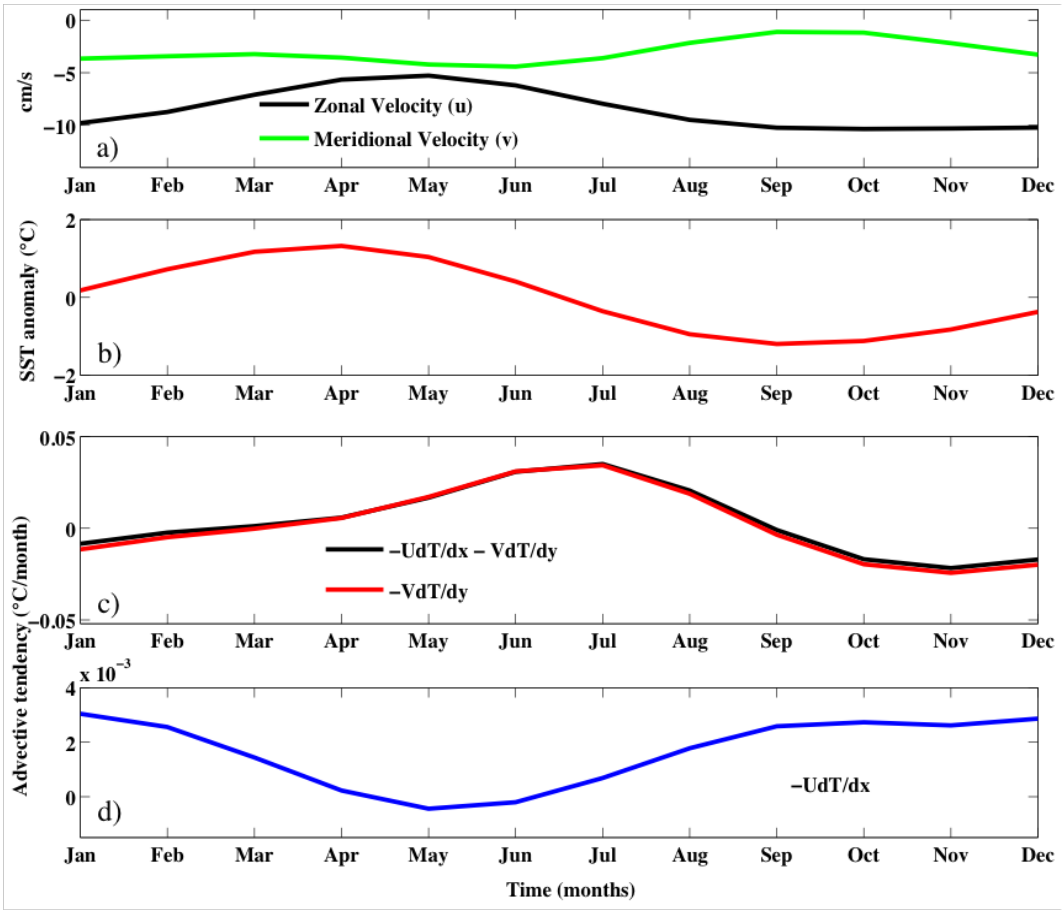

Figure 4.6. *Box C (shown in figure 4.3) indicating mean monthly, a) zonal and meridional velocities b) Spatially averaged SST anomaly from drifter, c) horizontal temperature advection tendencies and its meridional components, and d) zonal temperature advection tendencies.*

by both westward South Equatorial Current (SEC) and the southward Brazil Current (BC). There is a net increase in warming due to horizontal advection (figure 4.6c) from May to August and peaking in July. Meridional advection is almost as strong as the total advection term, having ∼0.04°/month (warming) maximum in July and -0.03°C/month (cooling) in November. The contribution from zonal advection (figure 4.6d) is however negligible and is about a tenth of the meridional component exhibiting sustained warming almost throughout the year.

The advection term for box C is now decomposed into mean and anomaly components, to highlight the magnitude of the contribution of each to temperature advection. Figure 4.7a shows the decomposition of zonal advection, with the

total term UdT showing a reduced warming effect from March-May. This is attributable to the strengthening of the southeasterly monsoonal winds heading equatorward and cooling temperatures on its path. Interestingly, UdT has not compensated with negative values and maintained warming throughout the year with a peak of 1.5°C/month.

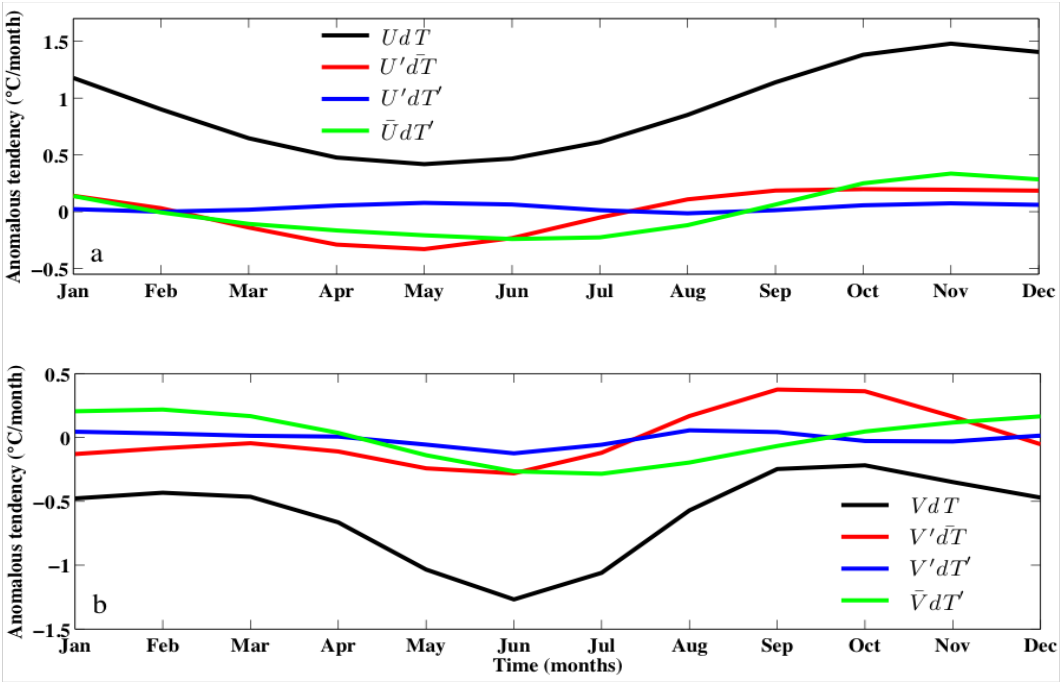

Figure 4.7. *Box C (shown in figure 4.3) decomposition of temperature advection terms a) zonal b) and meridional.*

The anomaly component $U'dT'$ maintained a fairly constant signature throughout the year exhibiting the least contribution to warming/cooling tendencies. Advection of mean temperatures due to anomalous currents $U'd\bar{T}$ and advection of anomalous temperatures due to mean currents $\bar{U}dT'$ maintained a fairly similar signature throughout the year with the total advection term UdT except the difference in magnitude. The large difference in magnitude indicates that advection of mean temperatures due to mean currents $\bar{U}d\bar{T}$ play an important role in the circulation pattern at box C.

The meridional component VdT is also decomposed into the mean and anomaly components as shown in figure 3.7b. The total term VdT reveals a cooling effect throughout the year with highly significant values and peaks with 1.3°C/month

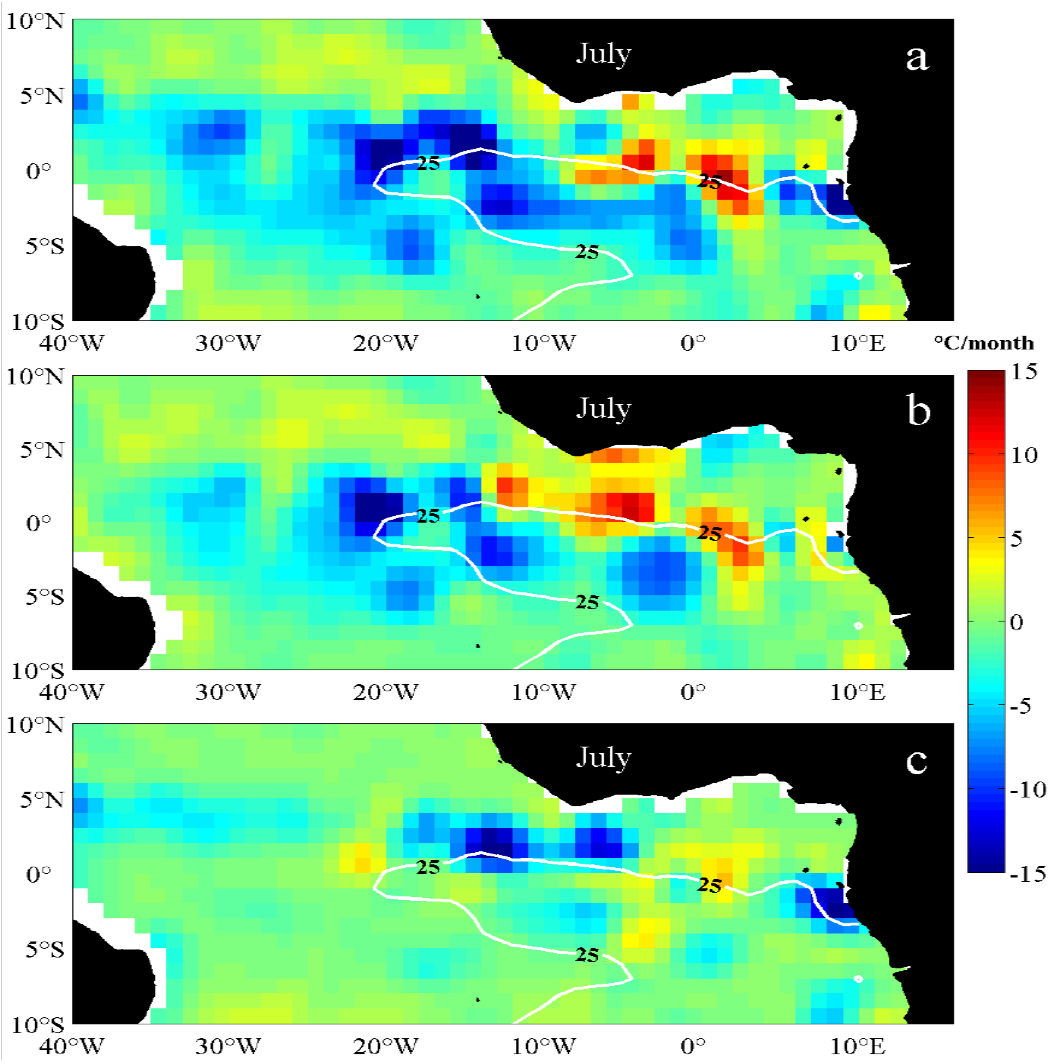

Figure 4.8. *Spatial patterns of SST advection for the month of July from the drifter climatology. a)* $-u\frac{dT}{dx} - v\frac{dT}{dy}$*, b)* $-u\frac{dT}{dx}$ *and c)* $-v\frac{dT}{dy}$*. The contour line is a 25°C isotherm which delineates the cold tongue from the surrounding waters. Temperature data smoothed by a Gaussian filter.*

in June. Advection of mean temperatures by meridional current anomalies $V'd\bar{T}$ shows a substantial cooling effect prior to June and warming afterwards until November. The anomaly component $V'dT'$ is the least contributor to the warming/cooling effects of advection term VdT.

4.4.3 Analysis from drifter data 3: spatial

This analysis is supplemented by the basin-scale spatial advection shown in figure 4.8. With the resolution of 1°x1°, the surface drifter data of SST and velocity highlights regions of strong and weak warming/cooling tendencies. The month of July was chosen because it is the period of maximum anomaly circulation due to the presence of TIW and its vortices in the equatorial Atlantic. The overlaid contour is the 25°C isotherm from the SST data, indicating the boundary of the Atlantic cold tongue with the surrounding waters in July.

The horizontal advection term (figure 4.8a) shows distinct characteristics of warming (positive) and cooling (negative) mesoscale features with values of the order of ±12 °C/month within the latitudinal band of ±3 degrees from the equator. These meso-scale patterns explain the impact of near-surface currents (∼0.5m depth) on advection of temperatures across the basin. The larger peaks seen in the zonal advection than in the meridional component are due to the presence of TIWs and their vortices that help advect temperatures eastward. This can be observed from figure 4.5, where zonal advection is almost as large as the horizontal advection. These are strongest north of the equator between 1-5°N than to the south. Strong wind stress divergence occur at the northern flank and that brings about accelerated zonal currents. The minima (maxima) of features observed from the spatial plot (figure 4.8) are due to the interaction of currents and waves in the distributions of cold (warm) SSTs. Enhanced warming seen in the Gulf of Guinea (10°W-14°E, 7°S-7°N) is related to the TIWs. The impact of these waves on near-surface circulation is important because they lift and suppress the thermocline, and by so doing transfers heat into the mixed layer.

4.4.4 Analysis from geostrophic currents and satellite SST: Box A

The advection analysis is taken further hereby using satellite in addition to drifter data with higher resolution data at both temporal (3-daily) and spatial scales ($\frac{1}{3}x\frac{1}{3}$ for currents and $\frac{1}{4}x\frac{1}{4}$ for SST). Altimeter-derived surface geostrophic velocities and TMI SST are used to study temperature advection to allow subseasonal and seasonal scales to be studied at interannual time scale. Because of the diminishing of the Coriolis force at the equator, I consider a region far from it. This analysis covers the period 2007 to 2009 with data averaged to monthly.

The altimeter-derived geostrophic current anomalies (figure 4.9a) show that the zonal velocity increases due to the emergence of NECC from May of each year. However, despite having similar magnitude of peaks of ∼+12cm/s around August of each year, there is a variation between the years in terms of westward flows. The years 2007, 2008 and 2009 are characterised by maximum westward flows in February, June and August respectively, signifying an interannual variability of circulation at the chosen box A. In April 2009, the westward zonal currents peak with ∼18cm/s but with less magnitude in the preceding years. The meridional currents are weaker with not more than ±3cm/s at peak periods throughout the years. The SST shows a weak seasonal signal with significantly lower value during March-April-May 2009 (figure 4.9b).

Horizontal advection anomaly (figure 4.9c) shows a significant amount of cooling during the boreal spring of 2007 with values of ∼-0.1°C/month. The zonal component contributes minimally to the total advection compared with the meridional component. For the period of observation, a strong warming tendency is only present in spring of 2008 with values of 0.14°C/month. The year 2009 recorded a considerable cooling in June and it peaks with a value of -0.14°C/month. During the boreal winter, the ITCZ is approximately parallel with the equator and is located at ∼5°N. At this period, the region of box A (6-8°N) is characterised by weak winds and strong SST that allow significant warming in winter

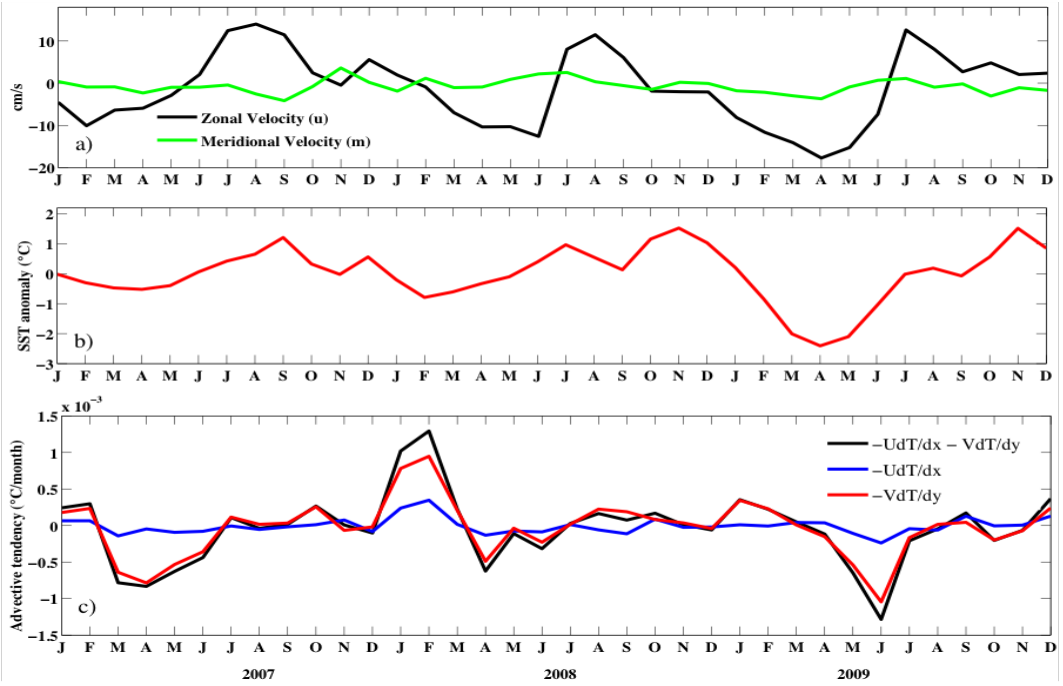

Figure 4.9. *Box A (shown in figure 4.3) indicating mean monthly, a) Zonal and meridional velocity anomalies from altimeter-derived geostrophic currents b) TMI SST anomaly using monthly mean data. The currents ($\frac{1}{3}$ degree resolution) were interpolated to the same grid as the SST (0.25° x 0.25° resolution) and c) advective temperature tendencies calculated from the box.*

of 2008. The ITCZ is a band of weak winds charaterised by strong warming and overcast. On the contrary, cold upwelled waters associated with the strengthening of the cold tongue during the early boreal summer creates low SST and this is reflected in strong cooling observed during spring times of 2007 and 2009, with 2008 showing very low cooling values.

The anomaly component of zonal advection $U'dT'$ (figures 4.10a) is nearly as large as the zonal advection term. Advection of anomalous temperatures due to mean currents shows a weaker contribution with an e-folding scale of ∼-0.005°C/month compared with the anomaly component that peaks with -0.4°C/month. The advection of mean temperatures due to current anomalies $U'd\bar{T}$ shows some noticeable peaks of warming in June-July-August of all the years, with significant cooling in April-May of 2008 and 2009.

In figure 4.10b, the meridional advection component shows strong warming in

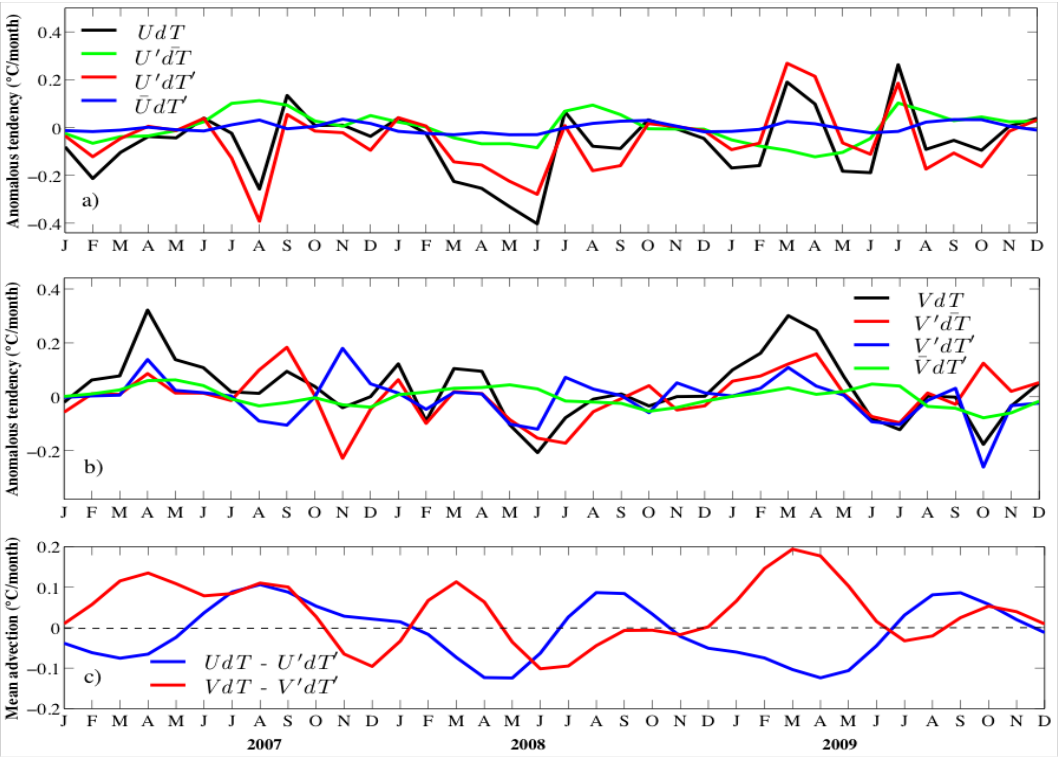

Figure 4.10. *Box A (shown in figure 4.3): decomposition of temperature advection terms from altimeter-derived geostrophic currents and TMI SST a) zonal component b) meridional component c) total directional contributions minus anomalous advection.*

the spring of 2007 and 2009, and significant cooling in July 2008 and October 2009. Fluctuations in warming/cooling tendencies are less in 2008. In general, each component is a strong contributor to warm/cooling observed in the plots but the contribution of advection due to mean currents $\bar{V}dT'$ is lowest.

Although, all other components contribute toward the fluctuating warming/-cooling of zonal advection (figure 4.10a), the anomaly component shows an interesting result, as it alternates its values rather than aligning to the pattern of the main advection UdT between June and December of each year. It signifies a considerable amount of cooling during those periods and subsequently affects the zonal advection term. That means temperature advection resulting from anomalous currents/SSTs is very important during those times. Total directional advection minus anomalous advection of temperatures is shown in Figure 4.10c.

This highlights the nature of temperature advection in the absence of its anomalous contribution that are mostly due to the presence of seasonal tropical instability waves. The zonal component shows a seasonal cycle with positive peaks in August-September and negative peaks in March-April each year arising from the contributions of all the components except the anomaly. A similar scenario is observed for the meridional component, but with a clear interannual variability. Anomalous temperature advection is therefore important in controlling the heat transport in the area.

4.5 Discussion

The drifter measures currents and temperatures at approximately 0.5m depths while satellite SST is skin temperature. Comparing the spatially averaged currents and temperatures of the drifter box to that of satellite shows great difference between the two data sets. The altimeter geostrophic currents and drifter data represented by boxes A and B respectively (see figures 4.3, 4.4, 4.9) show that drifter velocity components are two times greater than altimetry. However, TMI SST anomaly is four times greater in magnitude than the drifter SST. By implication, the zonal and meridional advective components of drifter data (figure 4.4) are much greater than those of altimeter/TMI SST (figure 4.9). This also applies to the decomposed advective terms of drifter (figure 4.5) and altimeter/TMI SST (figure 4.10). While the drifter data is based on long-term climatological mean, it still demonstrates the ability to show small-scale variability as well as long term anomalous circulation based on observed near-surface currents and SSTs. The drifter data contains both Ekman and geostrophic components of velocity, while Altimeter comprises only geostrophic currents. The main purpose of this investigation is to assess the contribution of current anomalies in transporting heat, rather than comparing the data sets that differ in spatial resolution and pre-processing technqiues.

Contrasting the zonal and meridional advection of temperatures at box B shows that the meridional component is larger, and zonal component is almost zero from June to end of year (figure 4.4). A similar result is obtained from the altimeter currents and TMI SST data (figure 4.9) with meridional advection closely matching the total advection. This has validated my hypothesis that the contribution of the meridional advective component is greater than that of the zonal component in transporting heat across the basin. Even though, as expected the meridional component is larger for both A and B boxes, the zonal component also contributes substantially in these areas where zonal current anomalies are large. Jochum and Murtugudde (2006) studied from a coupled ocean-atmosphere model, that the zonal temperature advection is as strong as the meridional component. However, in my own case that involves two different observational data, the meridional component is found to be stronger. It is important to stress that analysis from model simulations entails averaging over depth (h) and each depth layer comprise horizontal dimension such as what is considered in this chapter. It is important to stress that horizontal temperature advection from one single layer is not to be compared with advection computed from various averaged layers because each layer is independent of another.

In areas where zonal currents anomalies are weak, for example box C (figure 4.6c), the zonal temperature advection is weaker. This area is highly controlled by mean advection rather than other anomalies because there is no current shear counteracting the SEC. Because the C box is located within the South Equatorial Current and Brazil Current, both currents could have substantial impact on temperature advected either north-south or east-west. The southward flowing Brazil Current (BC) (figure 4.6a) is much weaker than the westward flowing South Equatorial Current. As such, the cold upwelled austral autumn/winter waters driven to the west within SEC influences the major cooling effect observed from both zonal and meridional advection shown in figure 4.7. Therefore, the influence of the BC in transporting warmer waters from north to south is negligible. Besides, the region is influenced only by southeasterlies, unlike A and B that are influenced by both southeasterlies and northeasterlies. The region is

also not affected by strong current anomalies that are related to TIWs compared with A and B. This further suggests the importance of boxes A and B and the surrounding area to future investigations whose results could be important for the general circulation models.

The influence of NECC on the equatorial Atlantic circulation is quite large, especially in the regions of A and B as shown in figure 4.4a. The zonal component is stronger and doubles the meridional component throughout the period of existence of NECC. The NECC is short-lived but dominates seasonal variability of the region (Bourlès et al., 1999). This demonstrates that any anomaly of NECC could substantially affect the circulation pattern in its domain and even beyond. There is no doubt, therefore to see the changing structure of advection components in figure 4.5a, where anomalous advection $U'dT'$ seems to warm the region with values close to the zonal advection UdT. More interestingly, the anomalous advection pattern of the meridional component $V'dT'$ cools the region from January to June, but when the NECC forms in June, the cooling is exceptionally high, and values went below the meridional advection term VdT. This calls for a future investigation of the circulation associated with NECC variability. Although, this chapter has concentrated on the temperature advection pattern, it is important to follow a full study of the advection from high-resolution numerical ocean models and consider various depth levels to characterise NECC and other currents associated with its variability in the tropical Atlantic.

The spatial pattern of temperature advection (figure 4.8) highlights strong warming in the Gulf of Guinea due to advection $-u\frac{dT}{dx} - v\frac{dT}{dy}$. This is contributed mainly by the zonal advection $-u\frac{dT}{dx}$. Analysis for other months (not shown), were smaller in magnitude, most likely due to July being a month of high anomalous flow. This is additionally verified from the satellite data analysis, especially figure 4.10c where anomalous advection is demonstrated to have a major impact in controlling heat transport in the area. If these anomalies are related to the TIWs that pick up a strong signal in June and weakens in November, then their contribution to advection of heat is large and important to the tropical Atlantic circulation. For example, Marin et al. (2009) observed that SSTs in the eastern

tropical Atlantic were stronger in June 2006 than in June 2005 with over 1°C difference, which they attributed to intense southeasterly trade winds in 2005 that led to substantial cooling of SSTs. Strong winds at the SST frontal zones enhance wind stress over the ocean that leads to secondary circulation (Small et al., 2008). Because strong winds in July are southeasterlies, then Ekman flow is enhanced leading to stronger zonal circulation and in this case eastward flow. Therefore, warm SSTs at the TIW zones are transported eastward into the Gulf of Guinea by anomalous currents that were once initiated by the SST threshold of ∼26-29°C. I have therefore validated my earlier hypothesis that the TIWs warm the Gulf of Guinea SST during the boreal summer. This also, in addition confirmed the studies by Jochum and Murtugudde (2006) that the most significant anomalous circulation is the TIWs whose oscillatory temperature advection is significantly larger than that of other times when they do not exist.

Looking at the bigger picture, ocean-atmosphere processes in the tropical Atlantic falls within the realm of the Wind-Evaporation-SST (WES) feedback mechanism, the inclusively ocean-atmosphere activities due to tropical instability waves demonstrates a uniquely interesting process. The WES feedback determines the amount of latent heat release from the ocean to atmosphere through the modification of anomalous trade winds on both sides of the equator. However, local contributions of ocean-atmosphere processes are linked to the WES mode and these vary due to certain non-linearities in the system, such as the SST threshold that would determine deep convection in the atmosphere and the wind speed over SST front that enhances drag over the ocean. For example, at the SST frontal zones of TIWs, strong divergence occurs (Small et al., 2008) due to wind speed response to the SST threshold (∼26-29°C) that increases wind stress over the region. Wind stress in the Atlantic is enhanced (diminished) over warm (cold) SST (Hashizume et al., 2001) patches of TIWs. These waves oscillate between the warm/cold patches due to the presence of Ekman divergence and TIW vortices leading to strong vertical entrainment. As a result, the atmosphere heats up the outside patches and this heat is transferred into the thermocline via the patch (Jochum and Murtugudde, 2006).

Jochum and Murtugudde (2006) attributed the major cause of zonal temperature advection to the thinning of the mixed layer as a result of TIW cyclones. While these waves increases heat transfer from surface to the depth of the thermocline, my results here suggested that horizontal advection due to their dynamics is a major contributor to heat transport in the region. The surface/near-surface temperature advection calculated suggests that their variability would impact changes in WES mode through oceanic feedback. For example, satellite calculations show significant interannual variations of warming/cooling tendencies for the three years (2007-2009). At decadal timescales, Chang et al. (1997) proposed an oscillatory process in which WES feedback is counteracted by temperature advection due to meridional currents, and by poleward advection due to Ekman pumping (Xie, 1999). These studies imply that the WES feedback mechanism can be affected at periods shorter than the proposed decadal time put forward by these authors, so long as the oceanic feedback is put into consideration. Additionally, decomposing the advective terms into their mean and anomalous components realistically identifies the damping mechanisms for stress fields that creates secondary circulation and accelerates zonal heat transport.

4.6 Summary

Temperature advection was calculated from satellite and drifter data sets. Meridional temperature advection is larger in the central equatorial Atlantic than the zonal component. However, the zonal component is larger in the east and that causes significant warming of the Gulf of Guinea region. This warming only occur during the boreal summer when the TIWs are well established. Advection due to anomalous currents by anomalous temperatures are larger for both data sets compared to their mean contributions. This is due to the influence of tropical instability waves that occur during the boreal summer and spring in the region. However, in a region not influenced by the TIWs south of the equator,

temperature advection by anomalous currents/temperatures do not show significant contribution to the main advection term. This is essentially due to weak anomalous flow and temperatures in the region.

While this chapter addresses the contributions of temperature advection in the tropical Atlantic, it is worthwhile looking at the subsurface circulation variability to highlight its connection with surface dynamics. The strengthening (weakening) of the trade winds and TIWs that lead to a shoaling (suppressing) of the thermocline are better understood from subsurface circulation and this is addressed in chapter 5.

CHAPTER 5

Water properties

5.1 Introduction

The ocean mixed layer is characterised by having the same properties throughout the layer with gradient properties at the bottom of the layer. The ability of the mixed layer to communicate with the atmosphere makes it important for ocean circulation and understanding its variability is crucial for climate studies. Atmospheric fluxes of heat, momentum and fresh water at the air-sea interface drive vertical mixing that generates the mixed layer, and this layer varies with time due to changes in atmospheric forcing (Dong et al., 2008). The thickness of the mixed layer indicates the amount of heat and moisture that directly interact with the atmosphere.

Freshwater fluxes due to excess rainfall lower salinity and have potential impact on mixed layer stratification. Under light wind conditions when the thermocline is deep, excess freshwater at the ocean surface creates a low-salinity layer

thereby inhibiting vertical convection and mixing. This also applies to high upwelling regions such as the coasts and the cold tongue regions. Conversely, excess evaporation due to solar incidence lowers sea surface temperature and enhances convection (Carton, 1991).

The closed northward boundary of the Gulf of Guinea may result in seasonal wind variability that directly affects ocean-atmosphere forcings. Equatorial Kelvin waves bring sub-thermocline waters to the near surface, where the thermocline was already shallow. At the same time, freshening from river runoff and upwelling changes the density structure of the mixed layer considerably.

The subtropical cells (STCs) are shallow overturning circulations confined to the upper 500m (Schott et al., 2003). The Atlantic STCs connect the subtropical subduction regions of both hemispheres to the eastern equatorial upwelling regimes by poleward surface flows and equatorward thermocline flows(e.g. Houghton, 1991; Liu et al., 1994; Malanotte-Rizzoli et al., 2000; McCreary Jr and Lu, 1994). Their existence implies that any measure of STC strength must be defined poleward of the tropical cell (TC) convergences, that is, closer to the dynamical intersection between the tropics and subtropics (near 8-10°N) (Schott et al., 2003). The primary function of the STCs is to provide cool subsurface water that is required to maintain the tropical thermocline (Hormann and Brandt, 2007). It was hypothesised (Schott et al., 2004) that STC variability could be related to decadal modulation of El Nio Southern Oscillation (ENSO) and may affect Atlantic equatorial SST. The EUC is the main branch of the STC that seems to terminate near the eastern boundary (Schott et al., 2004). It is therefore, important to study the variability of the EUC properties as it can affect ocean-atmosphere circulation through upwelling.

Various authors (Hazeleger et al., 2003; Philander and Pacanowski, 1986) have examined from a variety of model studies the seasonal cycle of the equatorial Atlantic, and has been generally accepted to be characterized by two maxima: the major one during northern summer/autumn and another during northern winter/spring. The sea surface temperature anomalies in the eastern tropical

Atlantic during the boreal summer are well correlated with rainfall variability (Chang et al., 2006; Giannini et al., 2003; Kushnir et al., 2006; Xie and Carton, 2004). These correlations suggests a potential for predictability of rainfall (Hormann and Brandt, 2007). The SST can vary based on many conditions, such as due to wind-induced, currents having contact with shallow bathymetry and change in density due to different water properties.

The objective of this chapter is to characterise the core depth of the equatorial undercurrent (EUC) to observe changes at sub-seasonal to annual time scales at four different chosen locations in the region: with EUC along the equator and its off-equatorial branches, the north and south equatorial undercurrents (NEUC and SEUC) respectively. The impact of wind forcing and its influence on the core depth of the EUC and the resulting consequence to local oceanic and atmospheric circulation is further examined.

This chapter employs four datasets, namely: Argo floats, PredIction Research moored-Array in the Tropical Atlantic (PIRATA) mooring, Sea Surface Height (SSH) from altimetry and QuikScat wind data.

This chapter is organised as follows: 5.2) Methods 5.3) Results, 5.4) Discussion, 5.5 Summary.

5.2 Methods

5.2.1 EUC core depth

The EUC is a water mass and it can be identified with its unique characteristics. This is possible with the use of Argo profiles and PIRATA mooring data sets. Argo float data having 10-day cycles were chosen at four locations shown in figure 5.1. The number of cycles chosen represents the same sampling period for each float. This corresponds to a period of 2 years spanning August 2006 to July 2008. This is the longest period that any four floats relatively provide up

to two years data in the region as of this period of investigation. The purpose of this choice lies on the advantage of calculating covariability of NEUC, EUC and SEUC simultaneously. PIRATA mooring data that allows a simultaneous investigation of temperature, salinity and currents is used. The data used covers the period of May 2005 to June 2006, and that supplements investigations conducted using Argo data.

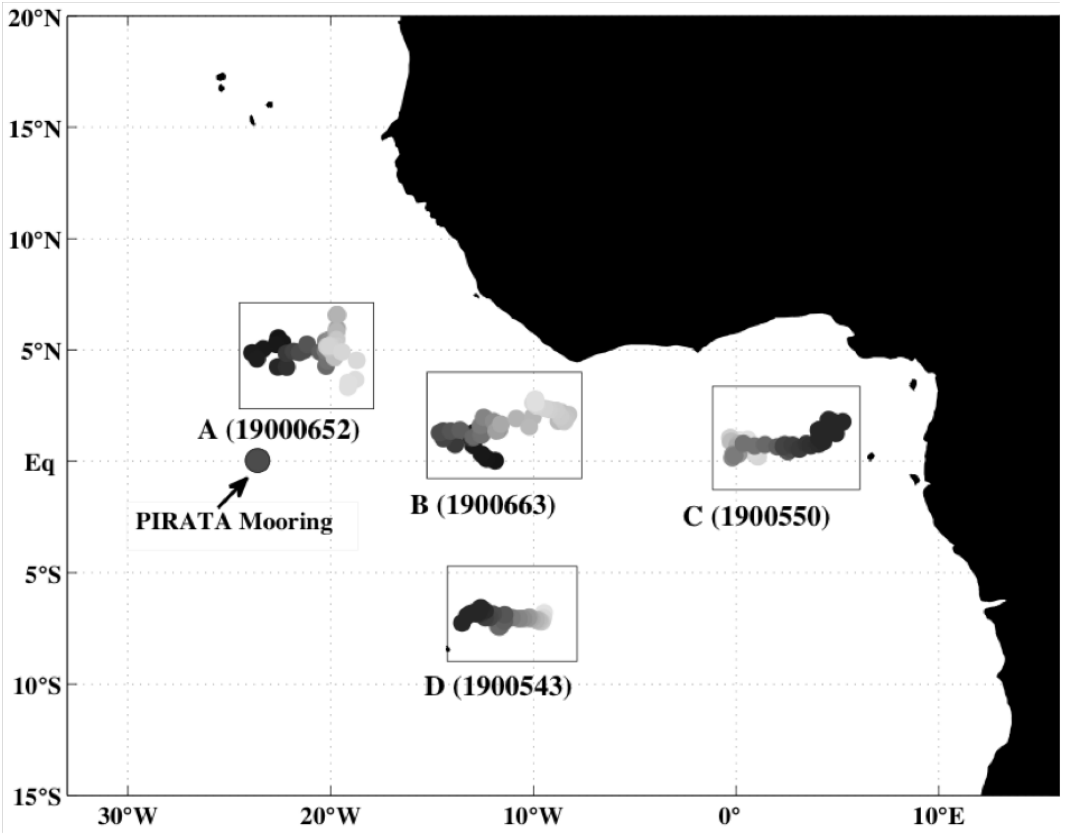

Figure 5.1. *Argo float trajectories at the chosen locations. The floats are A (3-7° N,18-24° W), B (0-4° N,7-15° w), C (0-3° N,1° W-7° E) and D (6.5-7.5° S, 9-14° W). Cycles chosen represent the period of 28 July 2006 to 8 August 2008 for each float. Trajectories start from the dark circles and end in the light grey. Argo identification number for each float is shown. PIRATA mooring located at 0° N/23° W is shown by an arrow.*

The EUC core depth is calculated as salinity maximum, while Antarctic Intermediate Water (AAIW) is calculated as salinity minimum. During computations, pressure is converted to depth using the standard UNESCO algorithm for seawater properties (Gill, 1982; Jackett and Mcdougall, 1995).

The EUC core depth is compared with wind anomalies as well as Ekman pumping velocity. To estimate surface wind stress, τ, for each scatterometer 10-m wind vector, the bulk formula based on Smith (1988) is used.

$$\tau = \tau_{x,y} = \rho C_d W_{u,v},$$

where g, u and v are scatterometer wind speed, zonal component and meridional wind components respectively. ρ is the density of surface air equal to $1.225 \text{kg} m^{-3}$. C_d is the drag coefficient. The magnitude of the stress at the ocean surface can be calculated from the square of the wind speed at 10m above sea surface (W):

$$|\tau| = \rho C_d W^2,$$

There have been many estimates of C_d. I have selected the one published and recommended by Smith (1988), which has been chosen by the World Ocean Circulation Experiment (WOCE) community. Details can be found in Piolle and Bentamy (2002).

5.2.2 Water mass properties

Water mass properties are calculated based on initial knowledge of their properties. Profiles of Argo temperature and salinity are used to calculated Temperature-Salinity (T-S) diagram. The diagram shows the relationship between temperature and salinity. Isopleths of constant density are also drawn on the diagram as useful additional information in identifying water masses and their distribution characteristics. Mean and seasonal variability of the water masses are then determined, and their variability explained.

5.2.3 Vertical stability

To determine variability of water at the float locations, I calculated potential temperature (θ) and density (σ) at the water column. To investigate the static stability of the water column, the Brunt-Väisälä frequency (BVF) is calculated at the Argo float sites for all profiles (Millard et al., 1990). This calculation is based on the UNESCO standard seawater library (Gill, 1982; Jackett and Mcdougall, 1995). The BVF is one of the most important descriptors of oceanic vertical structures. It relates to oceanic internal gravity wave properties and provides useful explanation on oceanic stability. That is the frequency at which a vertically displaced parcel of water will oscillate within a statistically stable environment (Okamoto et al., 2010). In the ocean, where density is not a linear function of temperature, it is given by

$$N = \sqrt{-\frac{g}{\rho}\frac{d\rho}{dz}},$$

where g is the acceleration due to gravity, ρ is the density of sea water and z is depth. Higher values of BVF indicate stronger stratification in the water column.

5.2.4 Spectral analysis

Sea surface height data from altimetry, and QuickScat scatterometer wind data were averaged within each box of float sampling to form a time series contemporaneous with the floats. The interrelationships between these temporal time series are analysed using spectral and coherence techniques based on Fourier, that allow the changes to be decomposed and studied as a function of frequency. Coherence analysis considers discrete signals and identifies patterns of relationships, while cross power spectral density show energy of correlation at each frequency. The phase relationship identifies the direction of relationship between the two signals.

The coherence function finds the magnitude squared coherence estimate of the input signals x and y using Welch′s averaged, modified periodogram method. The magnitude squared coherence estimate is a function of frequency with values between 0 and 1 that indicates how well x correlates to y at each frequency. The cross power spectral density (CPSD) is the distribution of power per unit frequency and it works also using Welch′s averaged, modified periodogram method. Details are found in appendix A.

5.3 Results

5.3.1 Temporal variability of the core depth of EUC

The time-depth salinity profiles at the four Argo locations are shown (Figure 5.2). The core depth of the EUC, represented by salinity maximum is shown in white lines. Seasonal variability of the EUC is observed at all float locations, with varying magnitudes of salinity. Low frequency variability in the tropical Atlantic that dominates the mixed layer is primarily induced by fluctuations of wind. Therefore, suppressing and lifting of the thermocline is heavily influenced by the seasonal winds. The magnitudes of influence also depend on location and time of the year.

The NEUC (A) shows strong seasonality and follows closely the shoaling of the mixed layer during winter/spring of 2007 and 2008. As previously noted by Okumura and Xie (2006), the equatorial region slowly warms up until March after the cold tongue reaches its maximum in July-August. This decreases the density of the mixed layer, and hence raises the thermocline. The core depth however deepens when tropical instability waves (TIWs) mix the thermocline around August. The zig-zag nature of the core depth during June-July-August is due to an increase in meridional flow that are associated with the instability waves. Maximum salinity is observed from winter-summer of 2007, which is not

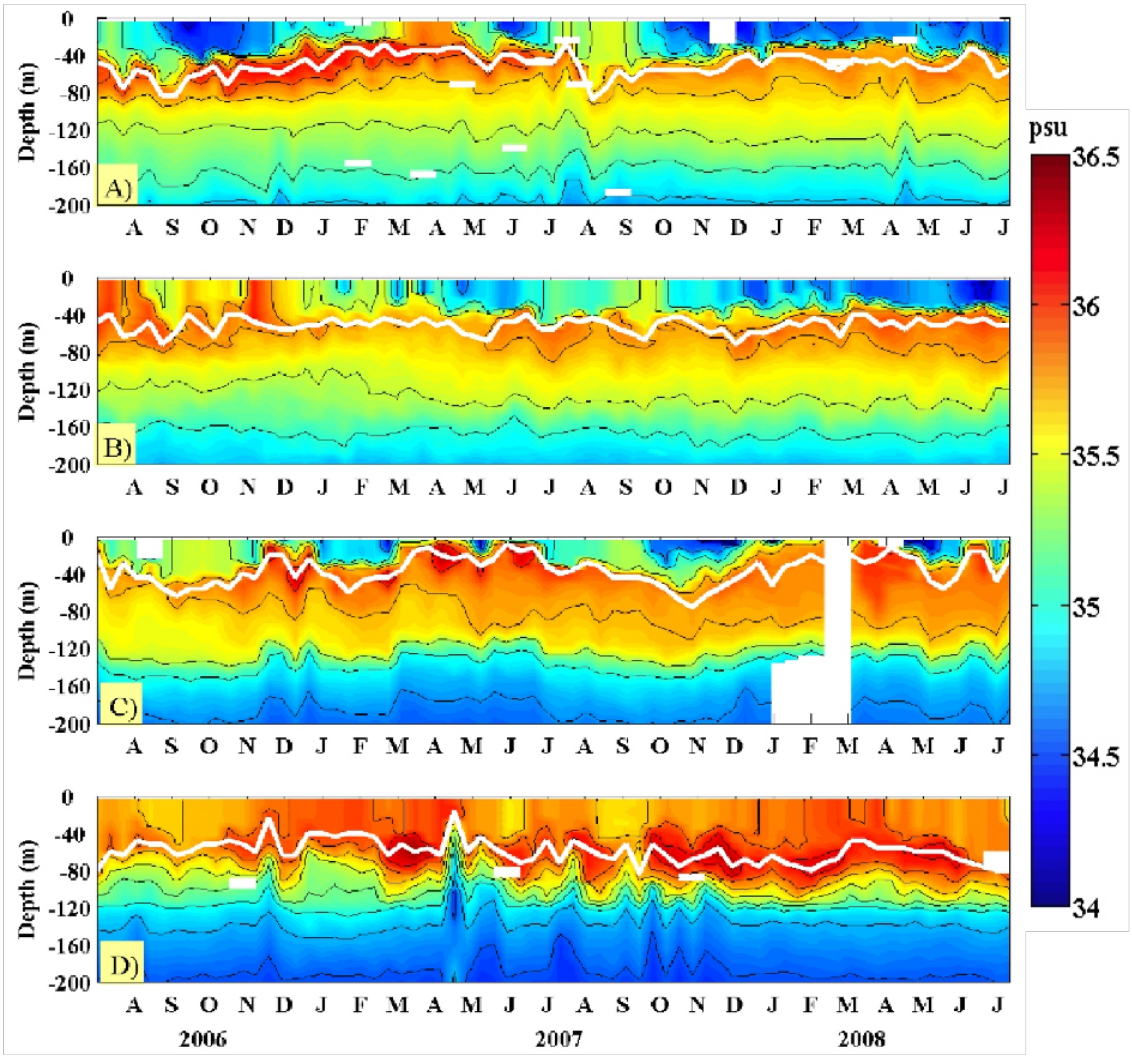

Figure 5.2. *Time-depth salinity profiles at the four Argo locations (A, B, C, and D) shown in figure 5.1. The core depths of the EUC, represented by salinity maximum are shown as white contours.*

reflected in 2008, suggesting that the NEUC is stronger along 5°N, and weaker north or south of it (see trajectory positions in figure 5.1 -A).

The core depth of EUC at B shows strong near-surface signature of salinity during autumn and winter of 2006. This does not seem to be the case in 2007, indicating an interannual variability of the EUC. Strong mixing especially at the mixed layer due to the presence of TIWs can significantly reduce the magnitude of salinity at the EUC, and the acceleration of meridional currents during the presence of the waves could slow the EUC. The EUC at B predominantly maintained an average depth of ±60m, with salinity of ∼36.0.

The EUC slows when close to the coast, hence by contrast its variability at C will significantly differ from that at B. Shoaling of the thermocline is observed in winter/spring of both 2006 and 2007. In both seasons, the EUC almost reaches to the surface owing to its northward and southward retroflection as it reaches land boundaries of the Islands of São Tomé and Príncipe. Because of the large seasonal cycle of the easterly winds, the eastward zonal pressure gradient force that drives the EUC helps in setting up the EUC with strong seasonal cycle in the eastern tropical Atlantic as observed previously by Stramma and Schott (1999). However, this could not completely explain the seasonal variability of the EUC at the extreme end of the tropical Atlantic, in this case, C. Other factors mentioned, such as the shoaling of the thermocline and the influx of fresh water from two big rivers as well as increased rainfall may determine the primary cause of the seasonal variability at C. Excessive fresh water flow from August-November is responsible for the decrease in salinity in the already shallow EUC (Figure 5.2 - C).

The core at D (SEUC) is relatively neutral to seasonal variations compared to A, B or C. Weaker core implies stronger meridional flow, weaker zonal and strong mixing. That means the zonal EUC if perturbed by a meridional flow carrying fresh water can both be slowed and mixing enhanced of different water properties. The average depth of the SEUC is 65m, and interannual variability is observed when August-October of 2006 is contrasted with that of 2007. The protrusions observed in December 2006 and May 2007 (Figure 5.2 - D) are artefacts created by pressure error by the float as documented on Argo homepage.

5.3.2 Seasonal variability of water mass properties

As a next step, I look at the annual and seasonal mean temperature-salinity (T-S) properties of the four locations to possibly detect water mass properties and their variability using Argo float data. Variability in thermocline water formation is particularly relevant to ocean-atmosphere processes. Warming and cooling signals at the air-sea interface is communicated to the thermocline through

the mixed layer. The depth of the thermocline is determined by both vertical and lateral current shear and by density gradients. Here, I use density gradients derived from temperature and salinity profiles to aid in the identification of water masses and their properties. The mean annual T-S diagram (figure 5.3, table 5.1) shows water mass properties at the four locations. The two curves of salinity maximum and salinity minimum show the equatorial undercurrent (EUC) and the Antarctic Intermediate Water (AAIW) respectively. A significant difference is observed between the northern and the southern branches of EUC (NEUC-A) and (SEUC-D) respectively. Studying the variability of the EUC is the main focus of this section.

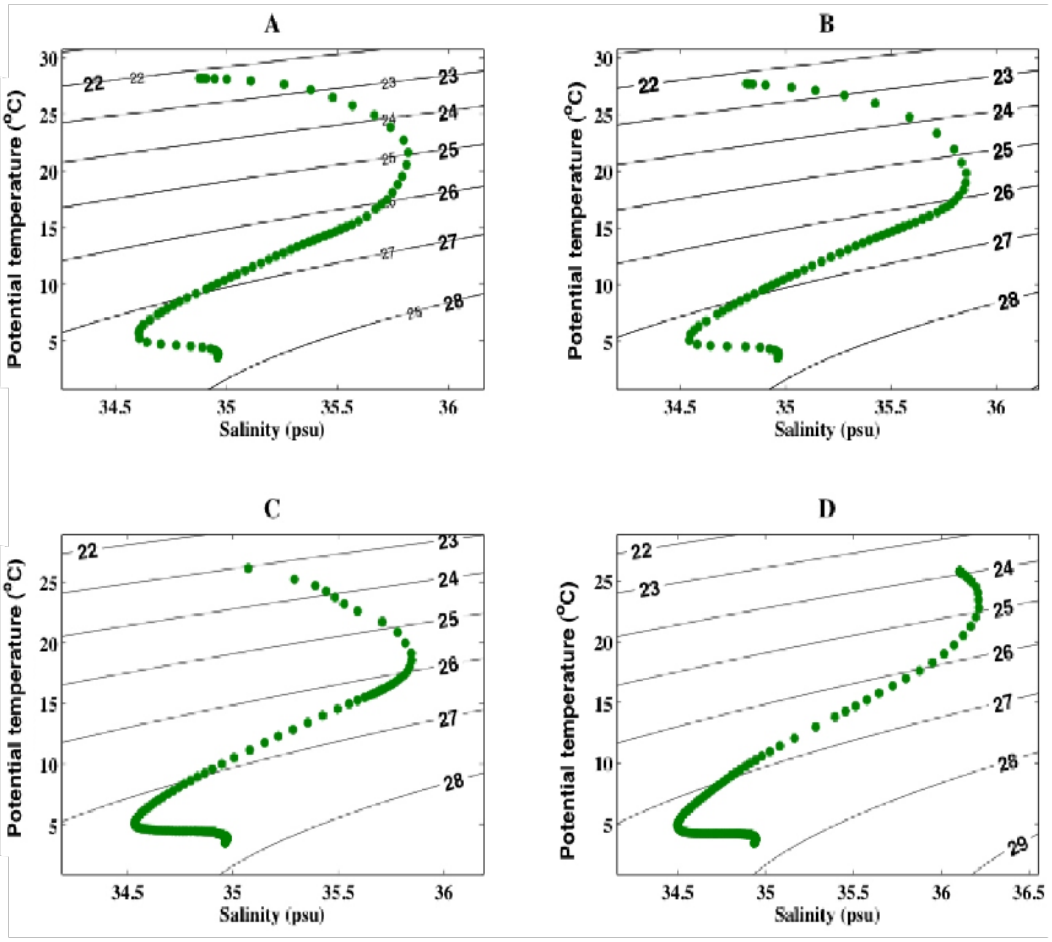

Figure 5.3. *Time-averaged temperature-salinity (T-S) for 2007 period showing mean positions of the EUC at each location. The T-S plots of A and D represents the Northern and the Southern EUC branches (NEUC and SEUC) respectively, while B and C represents the EUC along the equatorial waveguide.*

Seasonal fluctuations are observed at all stations (figure 5.4, table 5.2). There are two key factors for explaining this variability: 1) the influence of seasonal cold tongue upwelling that causes freshening by destabilising the salinity core, 2) the increase in wind divergence at the SST frontal zone of tropical instability waves. At station A, the properties of NEUC changes considerably in all seasons, with spring having a significant decrease in salinity from 36.1 to 35.7 psu. There is also a relative decrease in temperature compared to other reasons.

Table 5.1. *Mean water mass and current properties from T-S diagram*

Water mass	Temperature (°C)	Salinity (psu)	Density (kgm^{-3})
Antarctic Intermediate Water (AAIW)	5	34.6	27.3
Equatorial Undercurrent (EUC)	17	35.8	25.6
North Equatorial Undercurrent (NEUC)	21	35.7	25.0
South Equatorial Undercurrent (SEUC)	24	36.2	24.4

However, during boreal summer and autumn, salinity decreases due to fresh water flux that relatively increases density (Table 5.2). Little of this effect is observed in the South Equatorial Undercurrent (SEUC- position D), which recorded very little change in temperature and salinity (see figure 5.4 profile D). This demonstrates that variability of water properties at this location (D) differ from those along the equator or north, where tropical instability waves and an increase in meridional current (not shown) have potential impact on near surface circulation. Wave activity of the scale of TIWs is absent south of the equator, and the dominant processes that impacts on the SEUC are the southeast monsoon winds that creates strong divergence, and the south equatorial current.

Caveats similar to those observed in A apply also to the EUC (stations B and C), however, seasonal variability at C differ when contrasted with B. While both lie within the influence of the seasonally varying cold tongue and wind divergence due to SST signatures of TIWs, the C region is affected in addition by the influx of freshwater from river input. The inputs from Niger and Volta rivers would significantly affect the density structure of the water column and hence the EUC. As the EUC approaches the east toward its termination (C), shallow bathymetry supplements to its variability. The influence of cold tongue when its

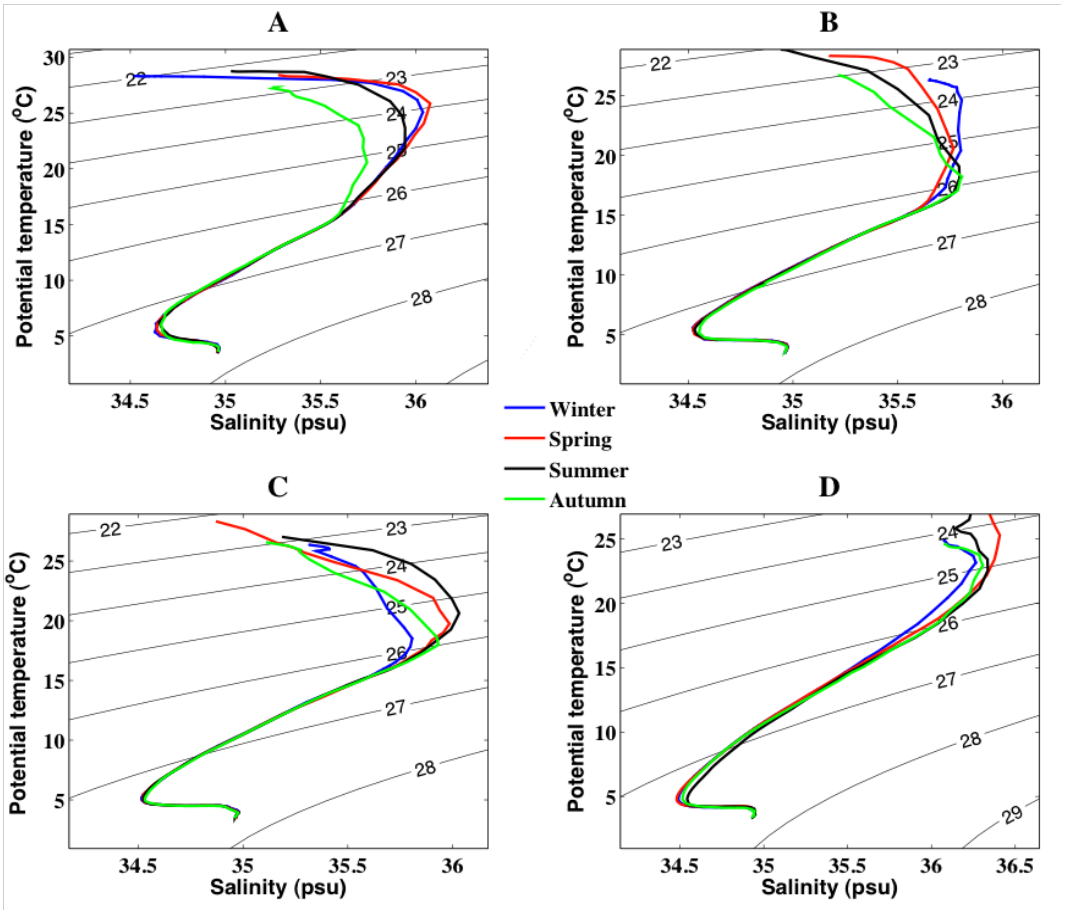

Figure 5.4. *Time-averaged seasonal temperature-salinity (T-S) for 2007 period showing mean positions of the EUC at each location. Winter (December-February), spring (MAM), summer (JJA) and autumn (SON). The T-S plots of A and D represents the Northern and the Southern EUC branches (NEUC and SEUC) respectively, while B and C represents the EUC.*

fully matured in autumn, surface cooling due to the strengthening of the south-east monsoon winds coupled with freshening from rivers results in colder and low saline EUC in autumn and winter (Figure 5.4 - C).

Table 5.2. *Seasonal density averages of the Equatorial Undercurrent T-S properties*

	A (kgm^{-3})	B (kgm^{-3})	C (kgm^{-3})	D (kgm^{-3})
Winter	24.2	24.0	25.8	24.9
Spring	23.8	25.2	25.6	24.3
Summer	24.4	25.7	25.5	24.9
Autumn	24.5	25.9	26.0	25.0

In spite of the similarity between the four regions of EUC, there are some differences between their density values that differ each season and at each location (Table 5.2). For example, the minimum values of the seasonally averaged densities are at isopycnals of: A (σ=23.8 - spring), B (σ=24.0 - winter), C (σ=25.5 - summer), D (σ=24.3 - spring) respectively. Interestingly, the influence of the cold tongue waters and divergence at the SST frontal zones of TIWs lowers the temperatures and increased the density at all stations in autumn (Table 5.2).

The AAIW, however is less influenced and maintained fairly the same structure with salinity ∼34.5 and temperature of 5°C, except in A, where it recorded salinity to 34.7. This explains a possible interaction of the AAIW and the North Atlantic Deep Water (NADW), which carries the highly saline but cold Mediterranean waters that flows southward between 1200 and 4000m. Fluctuations apparent in the seasonal variability of the AAIW at D are insignificant.

5.3.3 Potential temperature, density and buoyancy frequency

Temperature and density profiles (Figure 5.5) show strong variability due to vertical fluctuations of the thermocline. The core depth of the EUC follows approximately 27°C isotherm and 25 kgm^{-3} isopycnals. Variability in the vertical fluctuations of the thermocline is also reflected in the Brunt-Väisäläfrequency (BVF). Higher values of BVF indicate stronger stratification in the water column. The simultaneously low density and warmer water in winter and spring of 2008 results in relatively high BVF ($> 0.0015\ s^{-1}$) in the upper layer. This explains a stratified water column due to less turbulent activity. This is because the seasonal winds are weaker, and warming of the mixed-layer layer continues. This can have a vital impact on biological activity. A significant interannual variability is observed, considering that the high BVF is only observed in 2008 and not in preceding years. A suppressed thermocline observed in August 2007 might explain the effect of TIWs and/or wind burst.

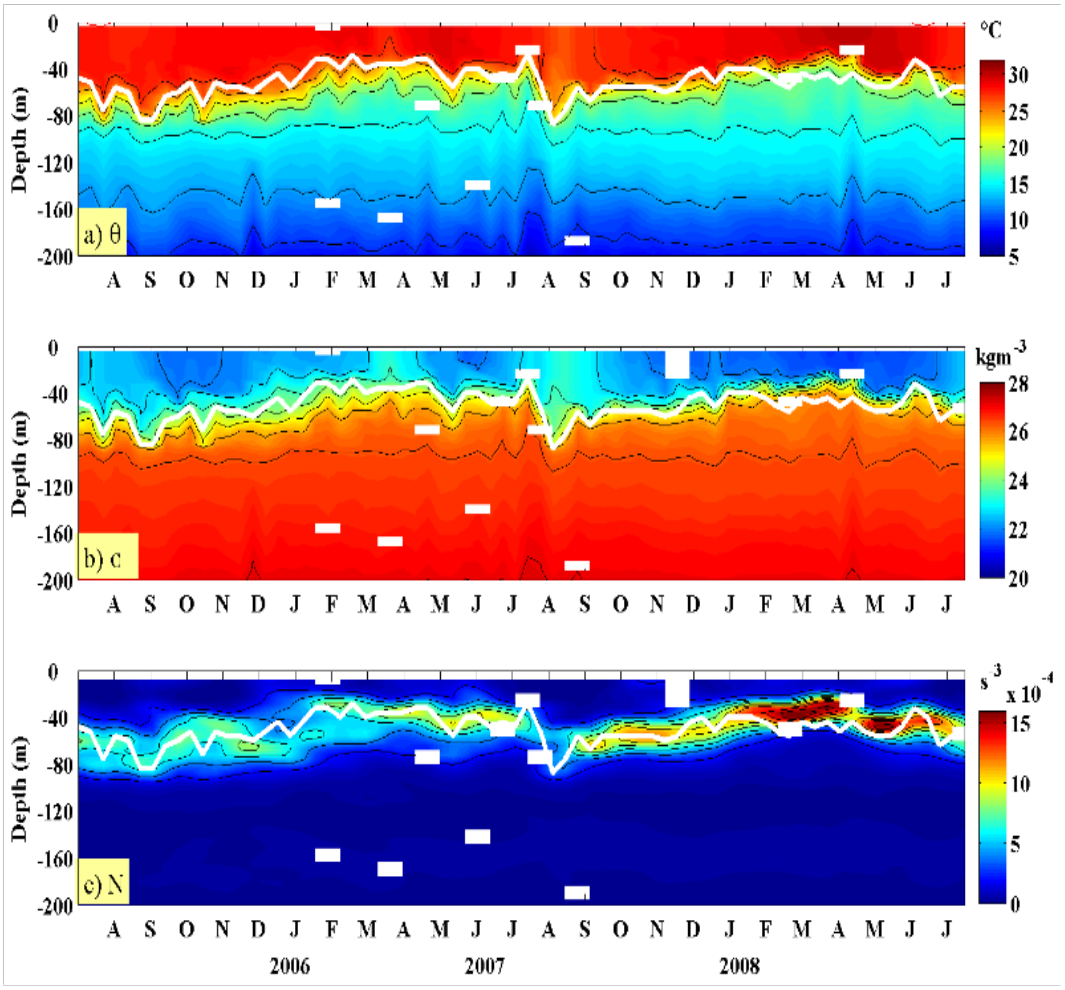

Figure 5.5. *Profiles of potential temperature ($\theta - °C$), density (σ- kgm^{-3}) and Brunt-Väisälä frequency (N-cycles/hr) for float A. The depth of salinity maximum (EUC core) are shown as white contours.*

The core depth of the EUC at position B shows weak seasonal changes (Figure 5.6) with high frequency (∼monthly) variability. However, the mixed layer indicates evidence of warming in spring of both 2007 and 2008, with corresponding low density along the water column. This is reflected in the BVF plot, showing stratified water column. Seasonal temperatures are well above 30°C at the near surface, giving rise to the development of a seasonal thermocline during the boreal summer of 2007 and 2008. Toward the end of summer, the southeasterly winds respond to these temperatures, which by means of vertical convection leads to mixed layer depth to gradually deepen and suppress the EUC. This continues until the end of boreal winter by completely eroding the seasonal thermocline and finally homogenising the water column.

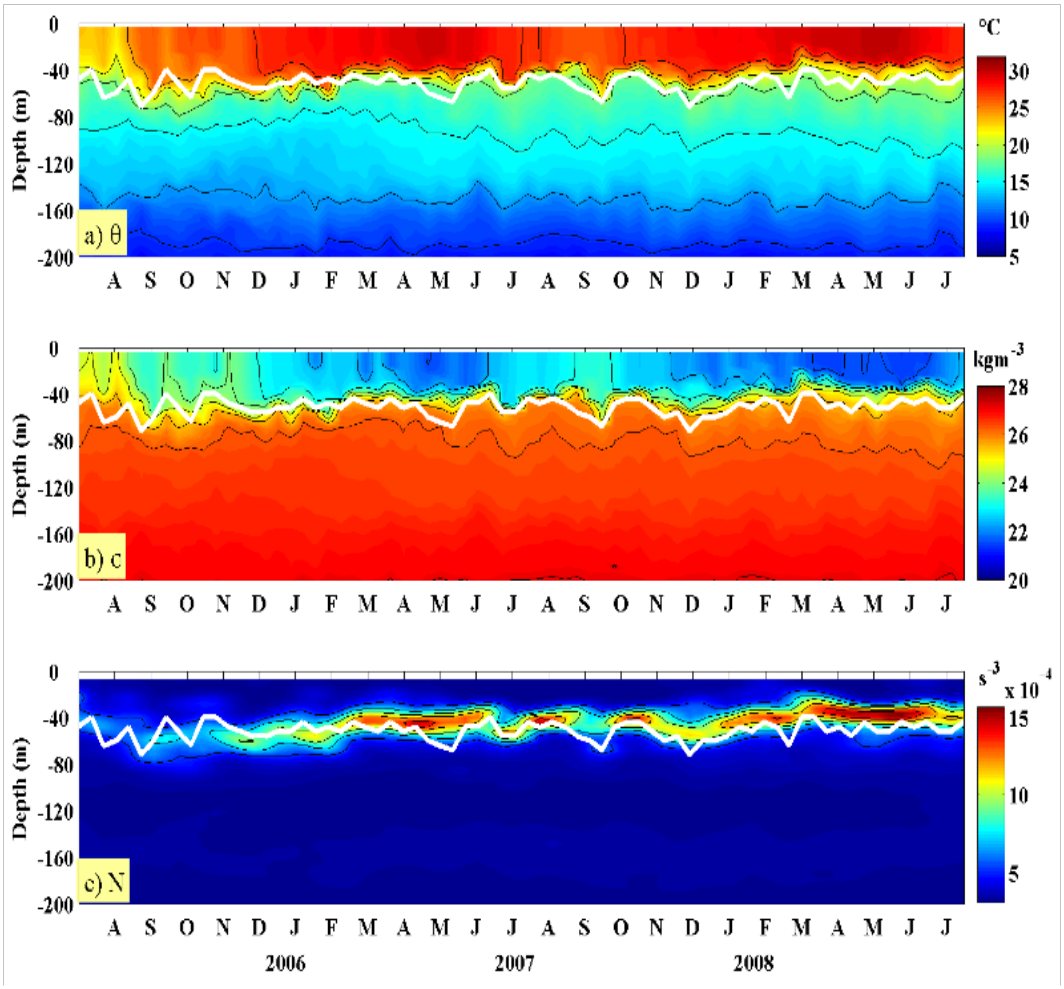

Figure 5.6. *Profiles of potential temperature ($\theta - °C$), density (σ- kgm^{-3}) and Brunt-Väisälä frequency (N-cycles/hr) for float B. The depth of salinity maximum (EUC core) are shown as white contours.*

Strong seasonality is observed in C (Figure 5.7), with the EUC core fluctuating approximately every three months. These undulations of the core follows the isotherm of ∼20°C and an isopycnal of 25kgm^{-3}. Interestingly, warmer and less dense mixed layer are not restricted to spring compared to A and B. The BVF shows stratification and mixing of water column fluctuating between 5-45m depths, indicating a seasonal variability at the ocean-atmosphere interface. When the ITCZ is close to the equator in boreal winter, the top layer is stratified, and when it shifts north or south, seasonal winds accelerates and that facilitates mixing. This variable mixing scenario may aid in contributing to the speed of the underlying EUC, but to a minimal scale due to geostrophic breakdown at the equator. A rapid eastward weakening of the EUC after 4°W was

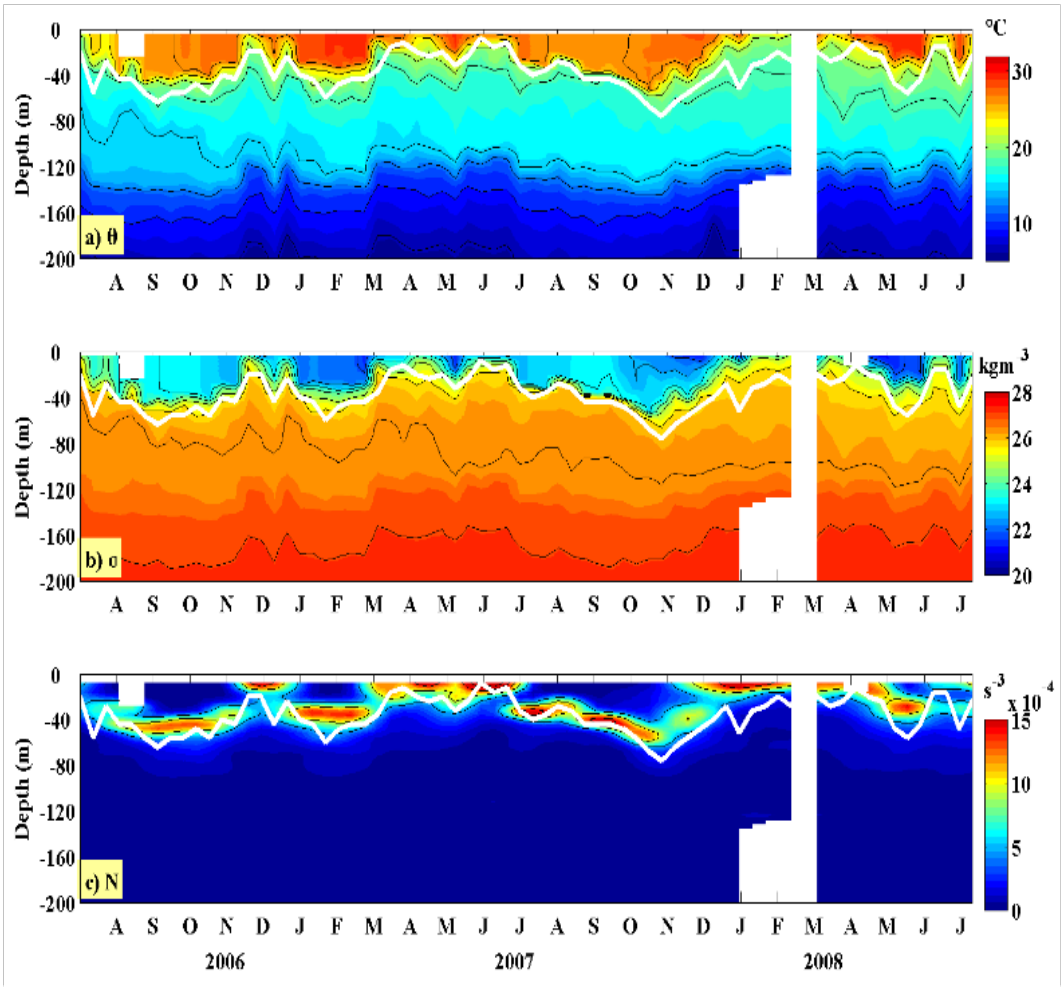

Figure 5.7. *Profiles of potential temperature ($\theta - °C$), density (σ -kgm^{-3}) and Brunt-Väisälä frequency (N-cycles/hr) for float C. The depth of salinity maximum (EUC core) are shown as white contours.*

observed by Hisard and Hénin (1987) to occur during summer and autumn than during winter and spring. This implies that the deeper penetration of the EUC into the Gulf of Guinea due to stratification allows the EUC to accelerate, and a reverse scenario occurs when the water column is mixed.

The float at D (Figure 5.8) shows warmer mixed layer during the first half of each year, and cooler the rest of the year that is attributable to the positioning of the ITCZ corresponding to the weakening of seasonal winds. The warming (cooling) is reflected in the low (high) density profiles that control the positing of the EUC core depth. Protrusions that appear in December 2006 and May 2007 are artefacts due to pressure error of the Argo float. The SEUC core in

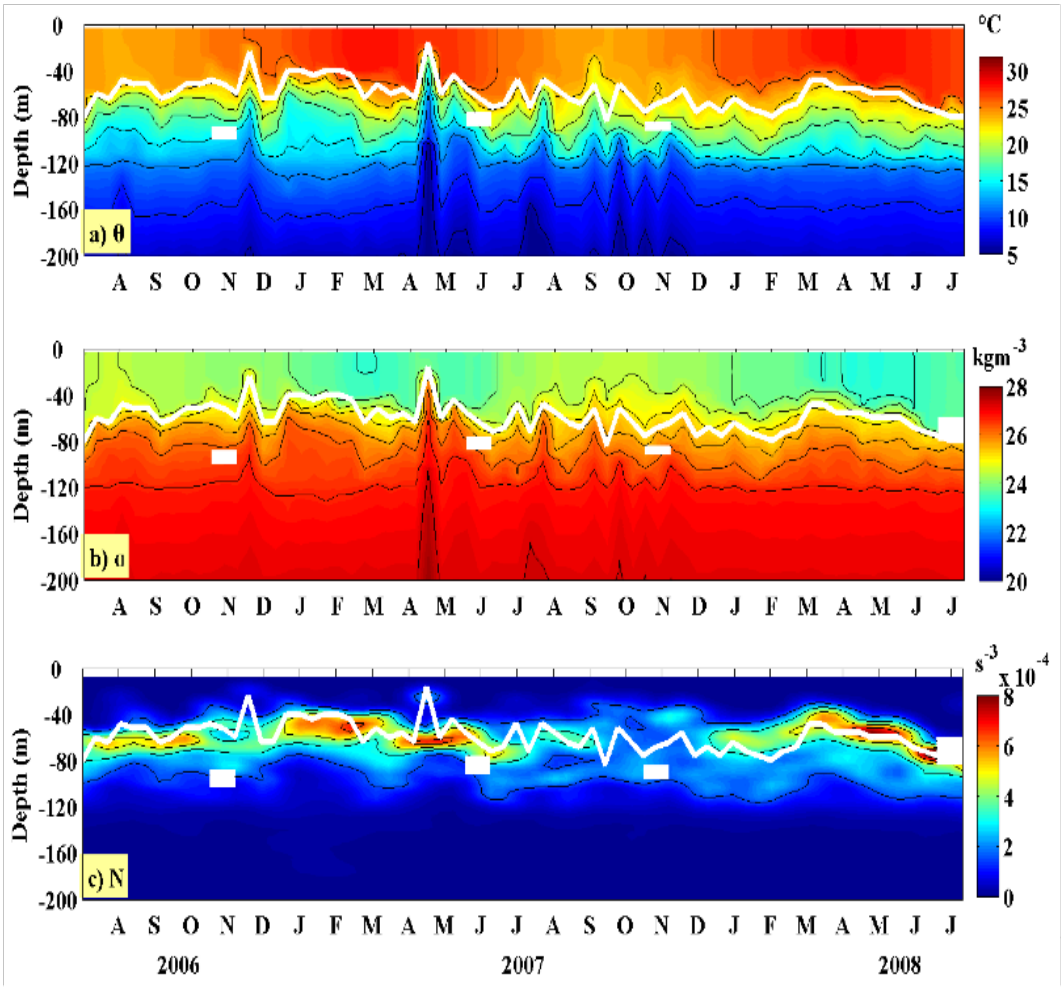

Figure 5.8. *Profiles of potential temperature ($\theta - °C$), density(σ -kgm^{-3}) and Brunt-Väisälä frequency (N-cycles/hr) for float D. The depth of salinity maximum (EUC core) are shown as white contours.*

this region did not show any seasonal variability, except high frequency variability appearing during the summer/autumn 2008 that suggests a response from the overlying mixed layer. The SEUC is less affected by the TIWs due to their weak nature south of the equator. At 7°S, mixed layer properties are influenced only by the southeast trade winds and the major surface current is the south equatorial current, and the strengthening and weakening of these result only on limited turbulence. Therefore, the SEUC maintains a regular depth of 40-80m. The BVF show strong mixing throughout the year except in boreal winter/spring. This mixing is attributable to wind stress of the monsoon. In the absence of the winds, stratification is observed. Stratification observed in winter/spring of both years is associated with weakening of the monsoon winds and

the zonal pressure gradient initiated from the western basin.

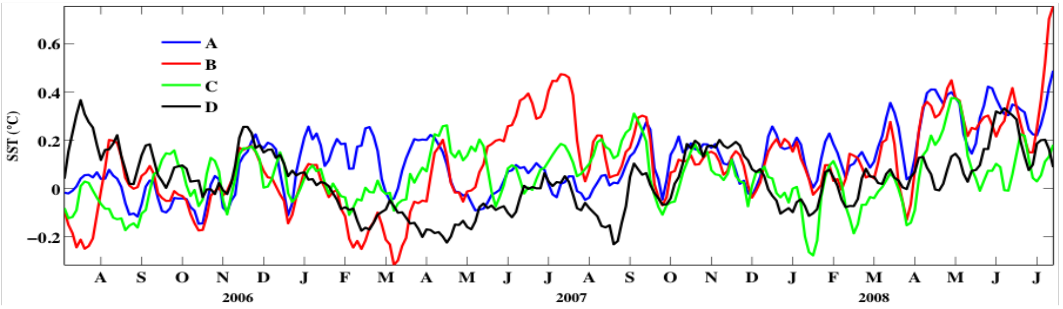

Figure 5.9. *Time series of detrended sea surface temperature anomalies at the boxes shown in Figure 5.1. The data is based on 3-day averaged TMI SST data corresponding to the period covered by the Argo floats.*

To help understand the link between the EUC and the mixed layer variability, it is paramount to assess the surface temperatures of the chosen boxes (Figure 5.1). These are shown in figure 5.9. While zonal and meridional temperature gradients of SST easily changes due to advection and evaporation, their time evolution explains the influx of heat in and out of the thermocline. Sea surface temperature anomalies at the NEUC (A) show warmer waters in winter/spring of all years and exceptionally in 2008. This explains the stratification observed from the Argo profiles (Figure 5.5c), indicating the impact of the surface temperatures at the ocean-atmosphere interface to the EUC. Strong SST anomaly in spring/summer of 2007 and 2008 shown at B also reflects on the stratification observed in the corresponding Argo plot (Figure 5.6c).

5.3.4 Seasonal variability of the EUC at 0°N/23°W

Seasonal variability of the EUC at a PIRATA mooring at 0°N/23°W is studied to advance earlier investigations. The mooring, fitted with temperature, salinity and ADCP sensors provides a contemporaneous investigation of time variability of water properties at that location. However, the only valid ADCP data for the mooring is between mid-2005 to mid-2006, and can give supplementary information even though time overlap is not possisble.

Strong mixing is observed from both temperature and salinity profiles during the summer of 2005 (figure 5.10a,b), which occurred due to the strengthening of the southeasterly winds. A corresponding circumstance is also observed in winter that explains the impact of northeasterly winds that strengthens while the Intertropical convergence zone already shifted southward.

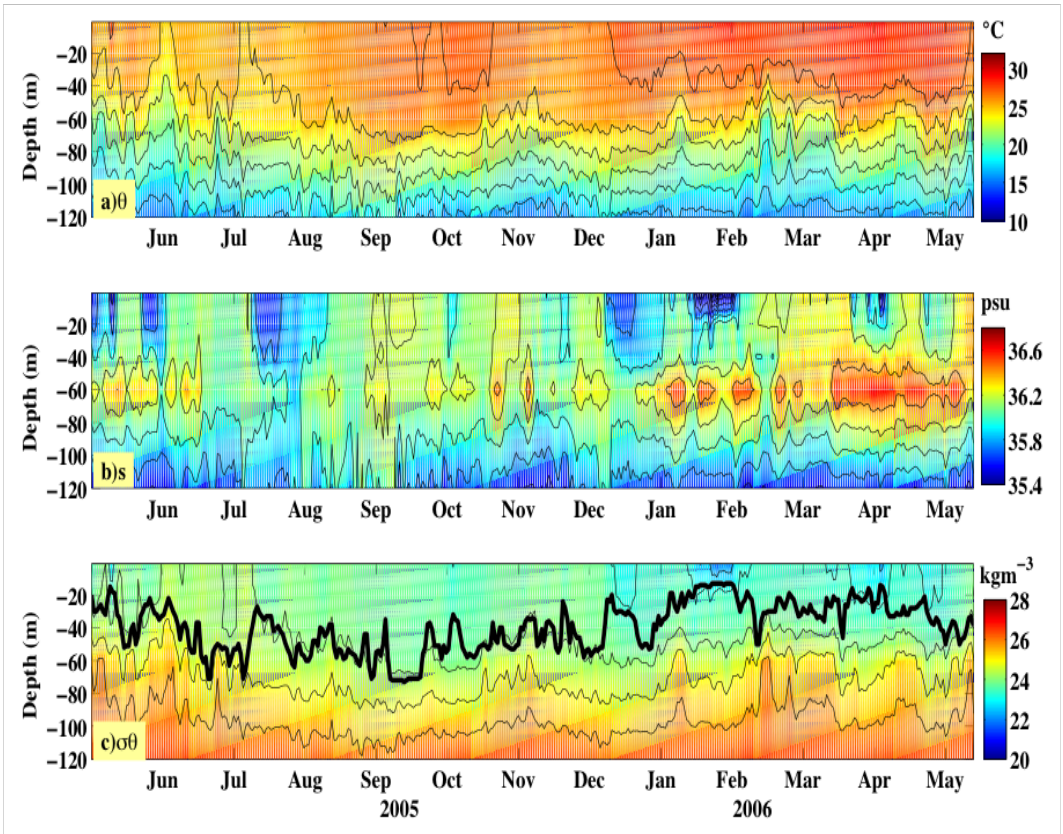

Figure 5.10. *Profiles of potential temperature (°C), salinity (psu) and density (kgm^{-3}) at a PIRATA mooring station located at 0°N/23°W. Mixed layer depth (MLD) at the station is represented by a black line on the density profile. The data ranges from 28 May 2005 to 14 June 2006.*

The core of the EUC (Figure 5.10b) maintains approximately the same positions throughout the period (mid-May 2005 to mid June 2006), with a depth of 60m. This is reproduced in Argo profile B shown in figure 5.6, but in contrast to Argo profile C shown in figure 5.7. In winter and spring, the EUC shows a remarkably high salinity of about 36.0 psu, which coincides with high temperatures in the mixed layer of ∼28°C. This further affirms what was observed earlier from

Argo float B, that when the ITCZ is close to the equator, SST peaks and stratification enhances. The consequence is the shallowing of the mixed layer depth (MLD) (figure 5.10c). This unique pattern along the equator suggests the presence of equatorial waves, particularly Kelvin waves.

PIRATA velocities are shown in figure 5.11, and no data areas are marked by empty (white spaces). At 0°N/23°W, the mixed layer is characterised by strong zonal flow with a marked difference in August 2005. An enhanced meridional velocity greater than $50 \text{cm} s^{-1}$ is also observed in August 2005 that is associated with the tropical instability waves. This enhances the shoaling of the EUC observed in the zonal velocity and the potential temperature (Figure 5.10).

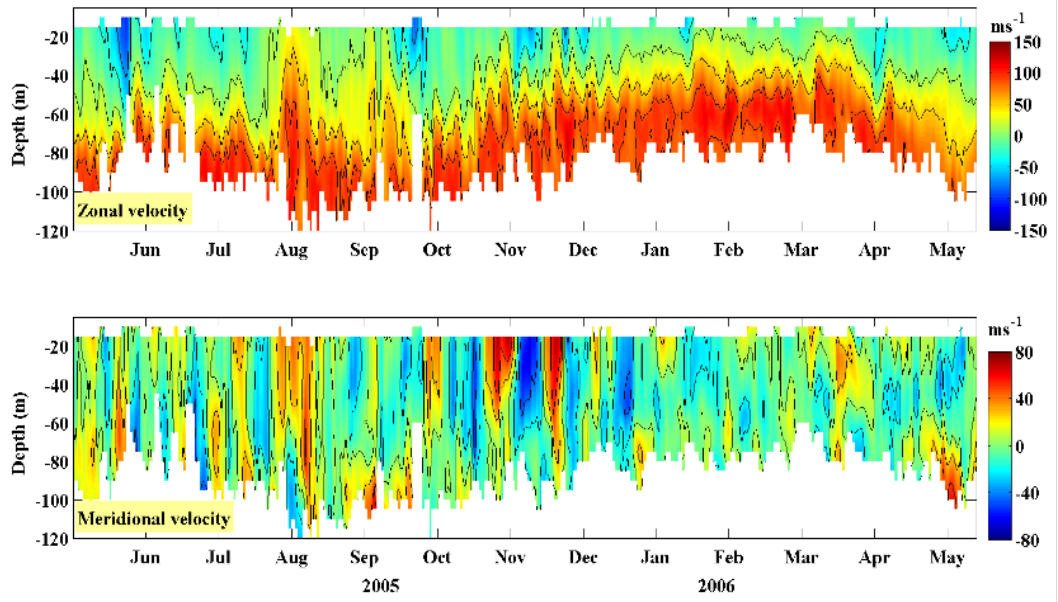

Figure 5.11. *Zonal and meridional velocity at a PIRATA mooring station located at 0° N/23° W. The data ranges from 28 May 2005 to 14 June 2006, corresponding to the temperature and salinity profiles in Figure 5.10. Note the difference in scale bars.*

The zonal currents (Figure 5.11) show remarkably strong eastward velocities of the EUC throughout, with maxima reaching up to 130cm/s. This is more than twice the magnitude observed in the meridional component. However, in August 2005 strong near-surface currents are observed in both zonal and meridional components. This is attributable to influx of the cold tongue (Figure 5.10) associated with the strengthening of the southeasterly monsoon winds that

bring a shear between the currents. These currents are associated with the tropical instability waves. The shallowing of the EUC during winter/spring of 2006 is attributable to the weakening of the trade winds that maintains the EUC depth. Fluctuations of meridional velocity are observed in November/December 2005 and that explain the restoration of the near-surface circulation when the North Equatorial Countercurrent ceases to exist in December. At this point, the stronger northward velocity typical of summer season is weakened by another stronger southward flow associated with strengthening of the northeast trade winds prior to winter.

5.3.5 Spectral analysis of the core depth of EUC and SSH

To assess the relation between the EUC core and the sea surface height variations, cross spectral analysis are carried out to investigate the relationship between the EUC core and the sea surface height (Figure 5.12). This is the first time this investigation is done in this region to my knowledge.

At all locations, the EUC core and the SSHA shows higher coherence at 364 day, having higher power (CPSD), indicating an annual cycle related to the cold tongue variability. That means the seasonal cycle of the cold tongue have a substantial effect on both the EUC and SSHA. The phases in A and B at these frequencies indicate SSHA as westward cyclones, while EUC as eastward flow. Strong coherence observed at 33-day, with weaker power and slightly westward SSHA cyclones. High coherence at sub-seasonal scales is also observed at floats A, B and C. Those at the periods of less than 40 days are associated with the seasonal tropical instability waves. This means that the waves could have a substantial impact on the variability of the EUC through temperature advection as studied in chapter 4. A clear distinguishable variability at sub-seasonal scale is absent at float D, and this is because the waves are weak south of the equator.

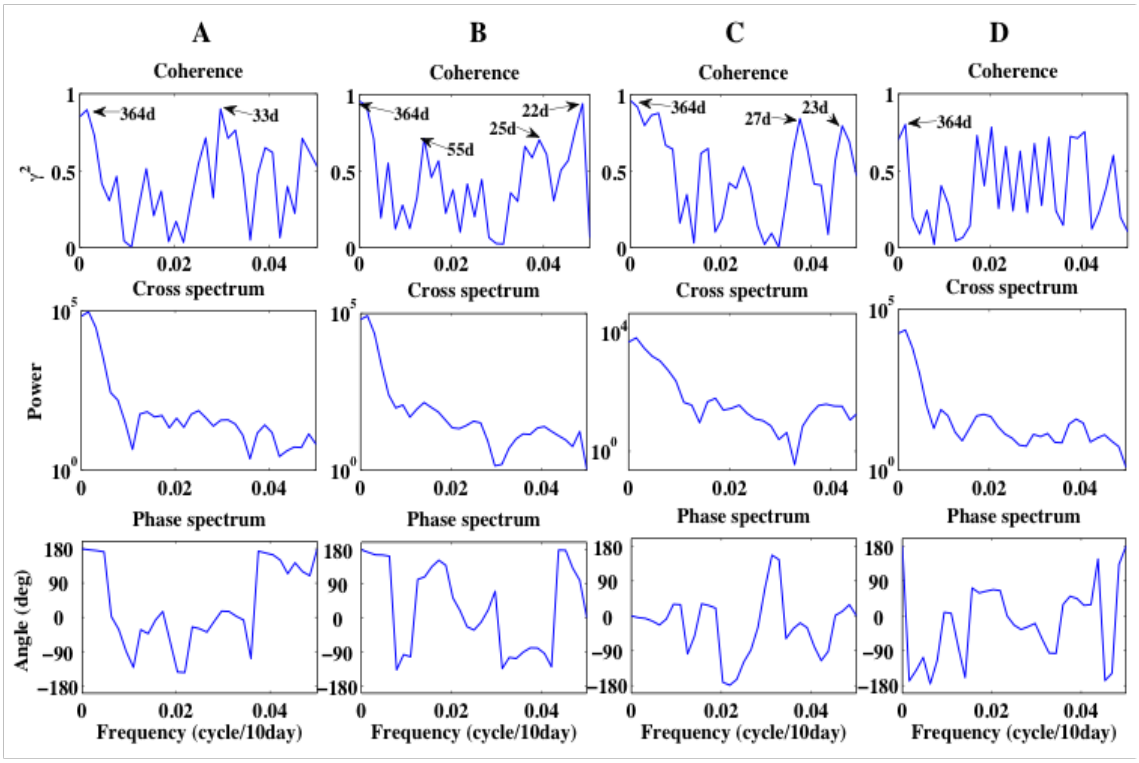

Figure 5.12. *Coherence squared amplitude, cross power spectral density (CPSD) and phase spectrum of the depth of salinity maximum of the EUC (EUC core) and sea surface height anomaly (SSHA). Data is for the period covered by Argo floats. Both coherence and CPSD are estimated via Welch periodogram using Hamming window.*

5.3.6 The core depth of the EUC and winds

Investigations on the influence of seasonal winds on the EUC core is advanced by studying its relationship to various wind components. This will aid in explanation of how the core is influenced by the overlying atmosphere. The oceanic response to winds is more closely related to wind stresses components than the winds themselves. I therefore, calculated wind speed, wind stresses, wind stress curl and Ekman pumping velocity from QuikScat scatterometer winds averaged at the four float locations.

Contrasting the core depth of the EUC, NEUC and SEUC (Figure 5.13) show remarkably similar signatures between floats A and B. However, float C show an apparent shallowing in all seasons with significant interannual variability that reflects in the Brunt-Väisälä frequency (Figure 5.7). This is reflected in high

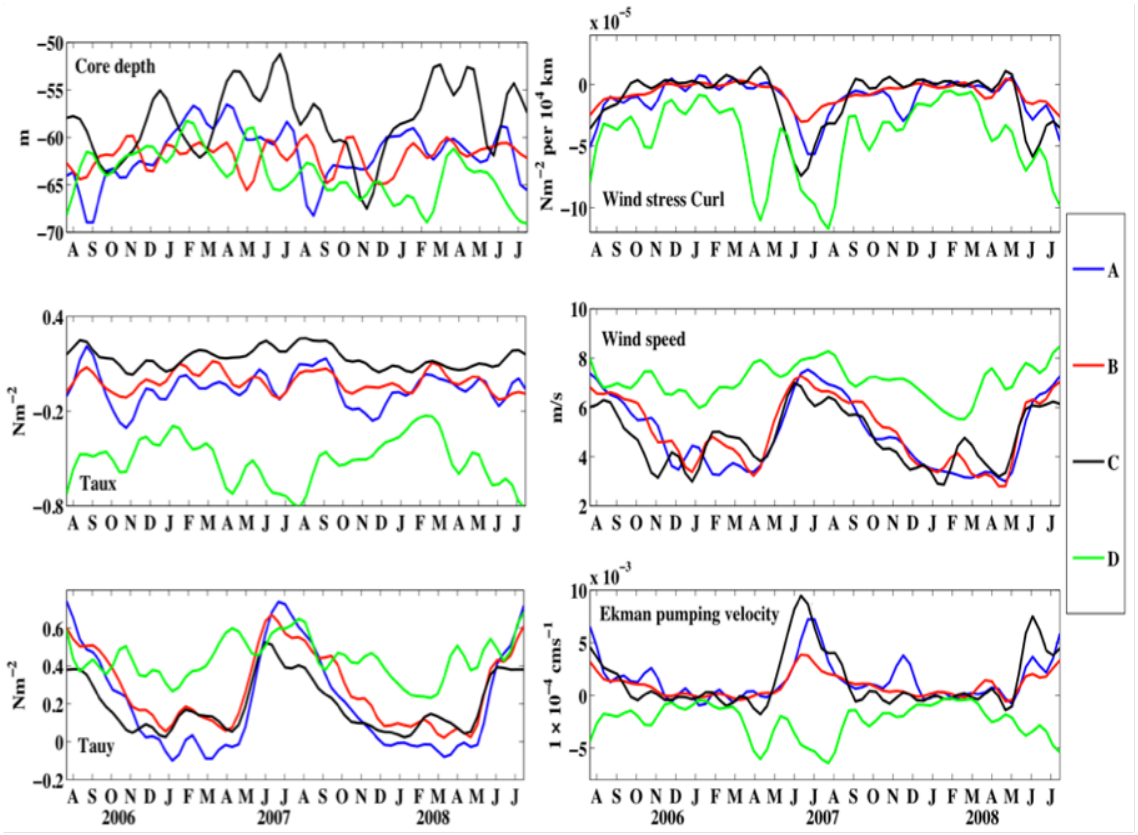

Figure 5.13. *Time-averaged core depth of the EUC at the four float locations and wind (see legend). Left panel represents the core depth, zonal and meridional wind stress fields (Taux and Tauy). Right panel represents wind stress curl, wind speed and Ekman pumping velocity. Due to the diminishing of the Coriolis close to the equator, Ekman pumping is calculated at ±1 degree latitude away from the equator. This is ok considering a small area average.*

zonal wind stress, Taux comparable to other floats. This suggests that, although the EUC become weaker along the zonal direction due to closeness to the continental boundary and shallow bathymetry, the zonal winds could still influence its variability. This is by helping to raise the thermocline through divergence and distributing the salty water at the near surface. The meridional component (Tauy) of C is comparatively weaker than other Tauy in the other regions. Earlier studies by Hormann and Brandt (2007) showed that the EUC become weaker along the zonal direction from west to east. During the boreal summer (JJA), meridional winds are generally stronger for A, B and C floats, and that result in strong divergence (weaker wind stress curl) and high Ekman pumping velocity due to shoaling of the thermocline.

5.4 Discussion

One clear implication of the variability of EUC is that it is influenced by the current and temperature anomalies along the equatorial pathway. However, its northern and southern branches, NEUC and SEUC do vary but according to the circulation patterns typical of those regions. For example, the NEUC is affected by both the SEC and the NECC. The NECC only appear in July and ceases to exist after November. Both SEUC and NEUC are equally important to the equatorial circulation. For example, Hormann and Brandt (2007) found out that both the EUC and SEUC do contribute to the equatorial upwelling east of 10°W. The EUC at B in particular exhibit strong signatures during the last half of 2006. This is in response to summer easterly wind acceleration that speeds up the south equatorial current (Richardson and McKee, 1984) and increases equatorial upwelling (Helber et al., 2007). This raises the thermocline as much as 30-40m (Houghton, 1983; Lamb and Peppler, 1992). The EUC maximum in spring of both 2007 and 2008 is induced by enhanced equatorial ventilation by extra tropical winds (Arhan et al., 2006), while fall maximum is attributable to westward winds and zonal pressure gradient along the equatorial band (Giarolla et al., 2005). Both NEUC and SEUC derives their sources from North Brazil Undercurrent (NBUC) (Bourlès et al., 1999) with other contributions from Guiana Undercurrent via retroflection of North Brazil Current and northern branch of South Equatorial Current (nSEC) (Stramma and Schott, 1999).

The variability of the EUC in the eastern tropical Atlantic is quite unique. Freshening from heavy rainfall, outputs of Volta and Niger rivers, shallow bathymetry, wind stress and its retroflection are complicated and that causes a change in density and stratification. In previous studies based on model outputs, Carton (1991) observed that seasonal changes in net fresh water flux do alter sea surface temperature by ±0.1°C, but the value is too small to significantly alter the exchange of heat across the ocean surface. However, the effects are larger in areas of river discharge and at the base of the mixed layer (Carton, 1991). This could however alter temperatures and heat in the gulf being a semi-closed region.

Generally, year-to-year variability occur at all Argo float sampling regions, and the EUC is found to outcrop due to weakening of the northeast and southeast winds. This is more prominent at float C, and that occurs in winter/spring period when the ITCZ is on average along the equator. This is in agreement with previous studies (Giarolla et al., 2005) where the EUC was found to shallow due to the weakening of the trade winds. It was explained by Philander and Pacanowski (1986) that, should the trade winds, which maintain the EUC experience weakening, an unbalanced pressure force would force to the EUC to shallow as a surface current.

5.5 Summary

In this chapter, water properties of the equatorial undercurrent and its branches at various locations have been studied while employing a suit of observed in situ and satellite data sets. At all locations, an annual cycle related to the cold tongue had significant coherence with sea surface height, indicating a direct relationship between the EUC and the surface dynamics. A summary of my findings is as follows:

I show that the equatorial undercurrent becomes shallower east of the basin in the Gulf of Guinea due to its proximity to land and shallow bathymetry. The strong shear between these currents and surface currents could enhance vertical turbulence and diffusion through the core. This surpasses stratification due to intense solar heating which by itself, supported by weakening of seasonal winds during winter and spring seasons. By implication, biological activities could be enhanced due to ease of penetration of oxygen down the core and nutrients reach the surface easily. Anomalies of this shear, especially between Guinea Current and the retroflecting northern branch of equatorial undercurrent could perturb circulation and create waves that impact the coastal regions.

I showed that the presence of year-to-year variability of the EUC at all Argo float locations, where the lifting(suppressing) of the thermocline is associated

with the strengthening (weakening) of the trade winds respectively. The seasonal variability of the EUC at its various branches is due to both the presence of waves and/or wind forcing of the trade winds.

Results from spectral analysis suggest that the driving force of the cold tongue that is the southeasterly winds has greater implication on the covariability of the EUC and the sea surface height anomaly. The annual cycle dominates the westward surface SSHA and the eastward EUC. This demonstrates that both are modulated by the changes in water properties associated with the cold tongue.

Temperature advection of tropical instability waves could aid in the variability of the NEUC and EUC, but that effect is absent at SEUC due to the weak signatures of the waves south of the equator (Figure 5.12). The waves warm SSTs east in the Gulf of Guinea through temperature advection anomalies as studied in chapter 4.

At 0°N/23°W (Figure 5.11), the mixed layer is characterised by strong zonal flow with a marked difference in August 2005. An enhanced meridional velocity greater than $50\text{cm}s^{-1}$ is also observed in August 2005 that is associated with the tropical instability waves. This has enhanced the shoaling of the EUC observed in the zonal velocity and the potential temperature (Figure 5.10).

I observed that the shoaling of the mixed layer depth (MLD) associated with weaker trade winds and positioning of the ITCZ close to the equator is observed from PIRATA mooring data. Mixing at the near-surface due to shear of zonal and meridional velocities helped maintain the EUC depth at ∼60m, but weakened in its zonal flow.

In the Gulf of Guinea, shallowing of the EUC does not depend solely on the trade winds, but on the bathymetry and freshwater fluxes from Rivers Niger and Volta that influences the density structure. Anomalous transport of the EUC therefore, will have consequential effects on coastal circulation and the tidal constituents. However, studying water properties and density variations especially in the Gulf of Guinea are improved when freshwater input is analysed, since

river runoff due to high rains could lead to anomalous circulation. Rainfall variability in the region is the focus of chapter 6.

CHAPTER 6

Impact of Sea Surface Temperature on rainfall

6.1 Introduction

The West Africa and Sahel regions experience fluctuations in rainfall that vary latitudinally, and these have been attributed to changes related to oceanic, atmospheric and orographic forcings. Long-term droughts have affected the region, with total amount of precipitation reducing at interannual and interdecadal scales during the second half of the 20th century (Benson and Clay, 1998; Nicholson, 1993; Nicholson and Palao, 1993). The unreliability of rainfall in these regions has a large impact on the continental hydrological cycle, water resources, economy, health as well as food security (Le Barbé et al., 2002). Research on rainfall variability has been the preoccupation of scientists for the last three decades in these regions.

The known mechanisms affecting rainfall over the two regions include forcing at: a) sub-seasonal scales e.g. equatorial waves, enhanced moisture supply, delay in the monsoon winds etc and b) seasonal to inter annual which includes Pacific El

Niño due to Pacific impact on Atlantic wind stress fields, Quasi-biennial Oscillation (QBO), Madden-Julian Oscillation (MJO), strengthening of low-level moisture convergence from westerly winds, weakening of north-easterly dry winds, influence of orography etc.

Several hypotheses have been put forward (Cook and Vizy, 2006; Grist and Nicholson, 2001) to explain the causes of rainfall anomalies in these regions, and whether local or global sea surface temperatures (SSTs) can modulate rainfall in both the Sahel and West Africa. I aim to understand the response of West Africa and Sahel rainfall with respect to particular SSTs from 12 years of observed data in the region and elsewhere for the purpose of predictability. I focus mainly on the influence of SST on sub-seasonal to interannual variability of rainfall in the region. The Gulf of Guinea SST is prioritized in this study due its inherent influence on the climate of West Africa and the Sahel. The motivation here is to build on previous studies by answering the following questions: *What are the scales of the impact of Gulf of Guinea SST over West Africa and Sahel rainfall? What are the scales of teleconnection between Pacific El Niño, Benguela Niño and Mediterranean SST with rainfall patterns over West Africa and the Sahel if any? Is there any connection between drought/flooding over West Africa and the Sahel regions and SST anomalies in the Gulf of Guinea?*

Various studies have been dedicated to rainfall variability in the region but mainly focusing on decadal variability from atmospheric models due to the paucity of observed data (e.g Fontaine et al. (2010); Jenkins (1997)). Others made use of a very few station data to corroborate their findings from numerical models, while some studies employed observations that covered a brief period (e.g. Biasutti et al. (2003); Gu and Adler (2004); Maloney and Shaman (2008)). This present analysis uses observational data only that spans a period of 12 years from 1998 to 2009. These data include Tropical Rainfall Measuring Mission (TRMM) precipitation radar (TRMM3B42 v6.1) data that covers land and ocean, TMI (TRMM Microwave Imager) SST data and QuikScat scatterometer winds. Each of these data has a spatial resolution of 0.25 by 0.25 degree and are daily data that are later averaged to suit various purposes. The quality control of these data has

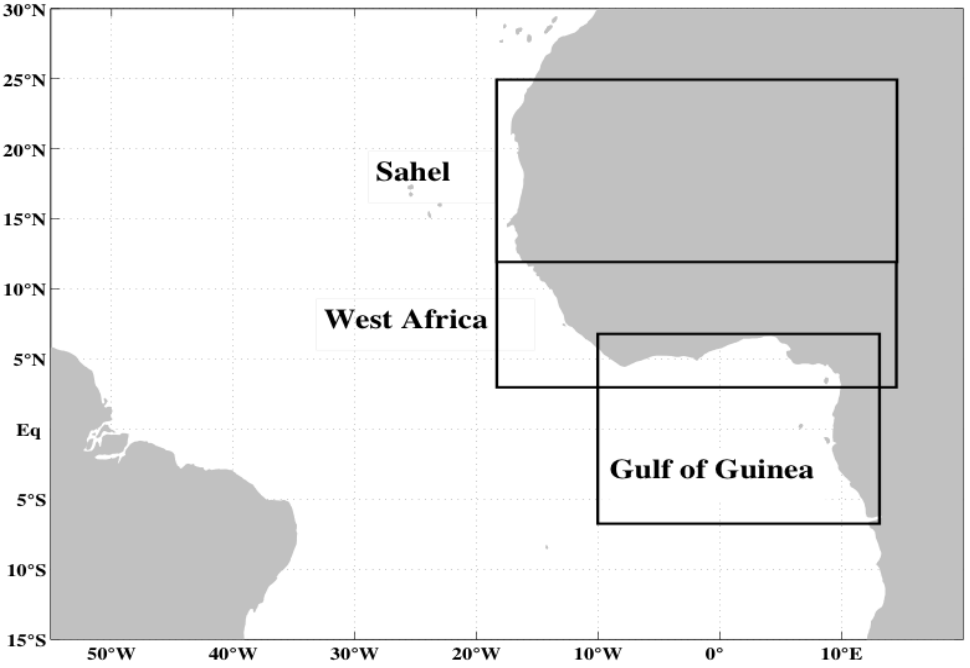

Figure 6.1. *The boxes shown represents areas under study on this chapter. The southernmost box is the Gulf of Guinea area (7° S-7° N, 10° W-14° E), the middle is the West African climate boundary (3-12° N, 18° W-16° E) which has distinct rainfall characteristics compared with areas north or south of it, and northernmost box is the Sahel region (12-25° N, 18° W-16° E)*

already been discussed in chapter three. Additionally, 2-minute gridded global relief data (Etop02v2) are used to show geographical features over land.

The plan here is to characterise West Africa and Sahel rainfall together and then separately, and correlate each with the known mechanisms mentioned above that are directly linked to SST forcing. Further to this, interannual variability of rainfall and SST will be analysed to study how they affect each other and their possible impact on local climate.

This chapter is organised as follows: 6.2) Methods 6.3) Results, 6.4) Discussion, 6.5 Summary.

6.1.1 The influence of orography on rainfall

Previous investigations on Sahel and West African rainfall using both numerical simulations and NCEP data have attributed local and large scale SST forcing to drought conditions in the region (Polo et al., 2008; Rowell, 2001, 2003; Vizy and Cook, 2001; Ward, 1998). Based on NASA′s GEOS-1 general circulation model, the role of orography in determining West African summer climate has been investigated (Semazzi and Sun, 1997). Results show that orography plays a major role in determining the climate of the Sahel as well as the region extending south across West Africa to the Guinea coast. Over the Sahel, moist air emanating from southwest region of Atlas-Ahaggar Orographic trough converges along a zonal axis with hot and dry northeast air, resulting in the strengthening of the ITCZ. The model shows a wetter Sahel in the presence of orography than in the absence of it. However, by subjecting the model to a particular year of drought (eg 1973), a weaker orography-induced rainfall dipole was observed, with drier conditions over the Guinea coast and wetter Sahel that was associated with the northward location of the ITCZ. Generally a permanent orography-induced rainfall dipole pattern over West Africa has been observed.

Even though most of West Africa and the Sahel are free of steep slopes, the Ahaggar Mountains (figure 6.2) could exert a significant control on atmospheric circulation and convection of the ITCZ (Sultan et al., 2003). In a similar study (Allersma and Tilmans, 1993), the Cameroon Highlands (figure 6.2) were found to have the highest rainfall record of up to 11,000 mm per year. This is attributable to orography, as the adjoining low areas do not receive even a half of that magnitude.

In this chapter, analysis is based mainly on SST anomalies in the Gulf of Guinea and rainfall over the West Africa and the Sahel (figure 6.1), with supplementary investigations to assess possible teleconnection with other SSTs such as the Pacific ENSO, Mediterranean SST and the Benguela Niño.

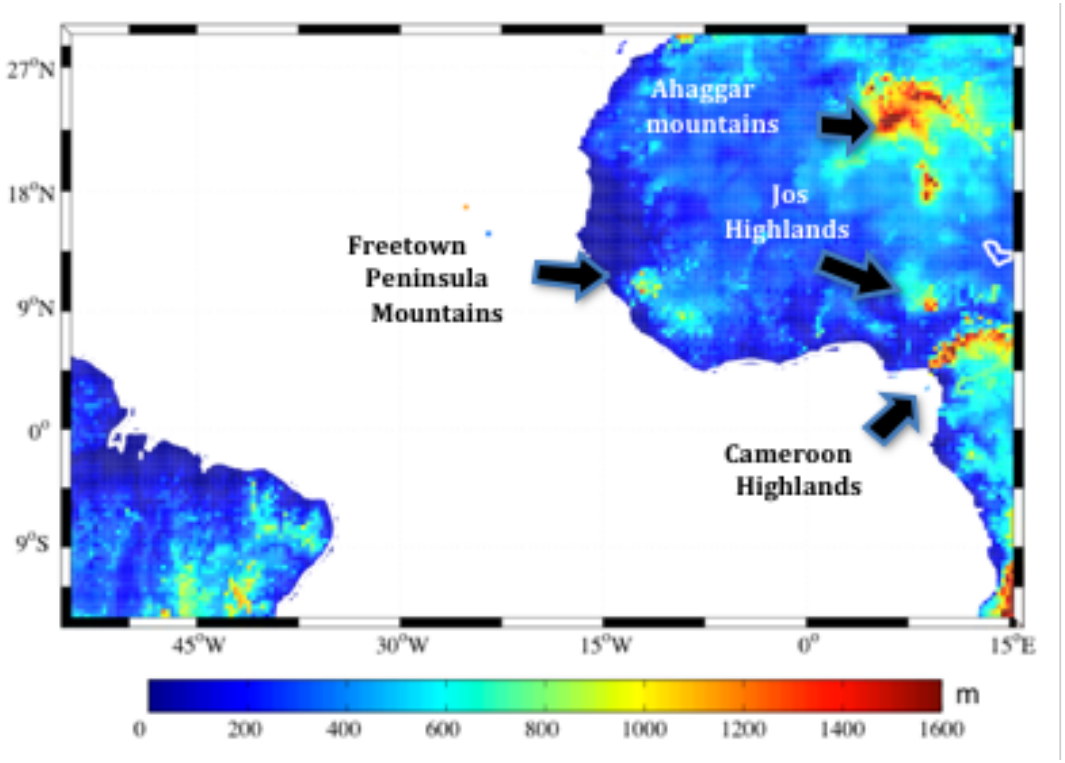

Figure 6.2. *Topographical map of the study area showing location of Orographic features. Contour interval is 200m. Data used is Etopo2v2.*

6.1.2 Gulf of Guinea SST and rainfall

The Gulf of Guinea SST is important in determining rainfall variability over West Africa (Okumura and Xie, 2004). The seasonal modification of the SST, especially through the cold tongue leads to an ocean-land temperature gradient, which then strengthens the West African Monsoon (WAM). In the boundary layer, the Gulf of Guinea controls the moisture convergence of the monsoons (Fontaine et al., 2003). Therefore, SST anomalies could lead to significant changes in West African rainfall.

The incidence of solar radiation during the boreal summer heats up the West African continent and creates a gradient of surface pressure. In the atmospheric boundary layer, the southerly winds are accelerated over the Gulf of Guinea due to a change in buoyancy (Okumura and Xie, 2004). This leads to equatorial cooling that favours the southerly monsoon winds, which accelerate and push the rain band around the Guinea coast into West Africa and the southern Sahel.

Although, the ocean influences rainfall over West Africa and the Sahel through heat fluxes, a clear mechanism on how this is done is not yet understood. Gu and Adler (2004) suggested that, despite the influence of eastern tropical Atlantic SST on seasonal rainfall over the Gulf of Guinea, any modification of rainfall within the inland are primarily due to many other factors rather than the monsoons. Giannini et al. (2003) showed that SST variability is instrumental in determining rainfall variability over the Sahel whereas land-atmosphere interaction acts to amply this through impacting on monsoon winds.

Seasonal variations in surface rainfall and its associated large-scale processes over the eastern tropical Atlantic and the West African region have been investigated (Gu and Adler, 2004). Results, based mainly on observed TRMM products such as SST, water vapour, cloud liquid water as well as NCEP-NCAR reanalysis, showed two different rain bands each being modulated by a different physical process. The seasonal cycle of the eastern tropical Atlantic was found to modulate convection by means of thermal forcing and SST-related meridional gradients. This however only has an impact on rainfall from the Guinea Coast extending to 10°N. North of 10°N, rainfall was found to be modulated within the ITCZ rain band by various processes. These include moist convection, African Easterly Jets (AEJs), Tropcial Easterly Jets (TEJs), Low-level westerly flows and African Easterly Waves (AEWs) during July-September months.

The interannual variability of rainfall over Africa has been examined. The year-to-year variability of the Atlantic cold tongue region are well correlated with West Africa and Sahel rainfall anomalies during JJAS months (Janowiak, 1988). From composites of rotated principal component analysis, wetter than normal conditions over West Africa (5-10°N) and drier than in the Sahel (north of 10°N) were found to be associated with positive SST anomalies in the south Atlantic. A reversed scenario occurs when SST anomalies are negative.

Studies from a model gave evidence that the increase in Sahel precipitation is not coming off the Guinea coast, but from the west (Cook and Vizy, 2006). A

similar study (Grist and Nicholson, 2001) indicated that in the years when the Sahel gains more rain, the low-level westerly winds are also stronger. This suggests that the forcing mechanism responsible for a wetter Sahel is not connected to warming in the Gulf of Guinea (Cook and Vizy, 2006). Whereas many studies that support this hypothesis are based on model simulations, and climatological records, I aim here to characterise and correlate simultaneously both West Africa and Sahel rainfall with SSTs at sub-seasonal to interannual time scales. Since atmospheric GCMs have difficulty in explaining the observed drying condition of the Sahel (Cook and Vizy, 2006), observational analysis is important to address some of these issues.

The dynamical response of rainfall over the southern Sahel has been studied (Vizy and Cook, 2001). Despite an increase of water vapour content in the southern Sahel due to a warm Gulf of Guinea SST anomaly, the Sahel rainfall was still low. This is because the low-level southerly monsoon convergence is weakened due to weak land-sea temperature gradient between the southern Sahel and the Guinea coast. Therefore, moisture convergence is reduced and there is an increase in vertical motion. Instead of the increase in rainfall being associated with an increase in low-level moisture convergence, a different scenario was observed. The decrease in rainfall relates to low-level subsidence over the Sahel. The northward low-level monsoon flow was found to have maximum velocities of about 4m/s, confined below 850hPa and penetrates far north from the Guinea coast (5°N) to ∼20°N (Cook and Vizy, 2006).

A dipole mode of rainfall variability has been observed between West Africa and the Sahel (Lamb and Peppler, 1992; Lough, 1986), having both dry and wet patterns. A wet (dry) Guinea coast is associated with warm (cold) Gulf of Guinea SST anomalies and a dry (wet) Sahel. The link between changes in SST in the Gulf of Guinea and rainfall across the region and the Sahel has been studied for the purpose of forecasting (Bah, 1987). The results showed that Sahel rainfall is dependent on Gulf of Guinea SST during the summer (wet) season. Positive SST anomalies correlate well with rainfall over the Gulf of Guinea and negatively correlate with Sahel rainfall.

The interannual variability of rainfall patterns across West Africa and the Sahel in relation to SST was investigated between 1950-1990 (Fontaine and Janicot, 1996). Analysis showed that, droughts over West Africa are due to a remote forcing of positive SST anomalies in the eastern Pacific and the Indian Ocean as well as negative SST anomalies in the Gulf of Guinea. In the same vein, floods over West Africa are associated with positive SST anomalies in the northern Atlantic. Sahel region was found to be highly sensitive to changes in remote (Pacific) and local (African and Indian) SSTs (Giannini et al., 2003). Positive SST trend in the tropical Indian Ocean was found to be the proximate cause of negative rain events over the Sahel between the 1960s and the 1980s.

The ITCZ is connected to the tropical convection scheme and displays a significant seasonal cycle in the tropical Atlantic. The rain band being the major signature of convection follows the seasonal march of the sun on the continents of the tropical Atlantic and reaches its northernmost (southernmost) position in July-September (December-February) (Biasutti et al., 2003; Mitchell and Wallace, 1992).

A significantly enhanced rainfall over the Sahel has been observed to accompany warmer SST and low Sea Level Pressure (SLP) in the Mediterranean Sea (Ward, 1994). Moisture convergence over the Sahel when the SSTs in the Mediterranean are warmer has been studied from AGCM simulations (Rowell, 2003). Although, not much is documented on the relationship of African rainfall with Mediterranean SST based on observed data, I attempt to investigate whether it correlates with rainfall over the Sahel and West Africa.

The analysis of Gu and Adler (2004) gave some interesting results based on the observed data but that covered only a short period from 1998-2003. Here I use similar data that cover 12 years to assess variability at interannual time scale.

6.2 Method

The methodology applied in this chapter vary with respect to analysis being conducted. Processing applied include both using data with seasonal cycle, as in the case of climate indices although not all and also spatial rainfall over land. Signal processing using Fourier is also employed and that is based on non-seasonaly anomaly data that is devoid of seasonal and long-term means.

6.3 Results

6.3.1 Mean and standard deviation

The long-term precipitation distribution is shown in figure 6.3a. Four regions stand out as having the largest mean rainfall: the north-eastern part of the Gulf of Guinea, the north-western Gulf of Guinea, the northern part of equatorial Atlantic and over south America. Areas with very low rainfall include the Atlantic Ocean south of 3°S, and also north of 15°N and the northern Sahel. In order to quantify the magnitude and spatial distribution of non-seasonal precipitation variability, the standard deviation (σ) of precipitation is computed and plotted (figure 6.3b). Areas with maximum precipitation variability are similar to those described in the mean figure (figure 6.3a), with precipitation standard deviation exceeding 1.8mm/day. The maximum standard deviation observed along the West African coastline corresponds to the Cameroon highlands in the north-eastern part of Gulf of Guinea, and the Freetown peninsula mountains around 12°W/7°N. Orographic forcing contributes to rainfall distribution over those regions during the boreal summer. Sultan et al. (2003) observed that the interaction of orography and atmospheric circulation might increase cyclonic vorticity in the heat low (a low pressure zone with hot air), which stimulates moisture convergence over the oceanic ITCZ at the western coast of West Africa.

The large signal observed in the middle of the Atlantic corresponds to a quasi-stationary ITCZ position that defines the convective scheme, which largely occurs during the boreal summer.

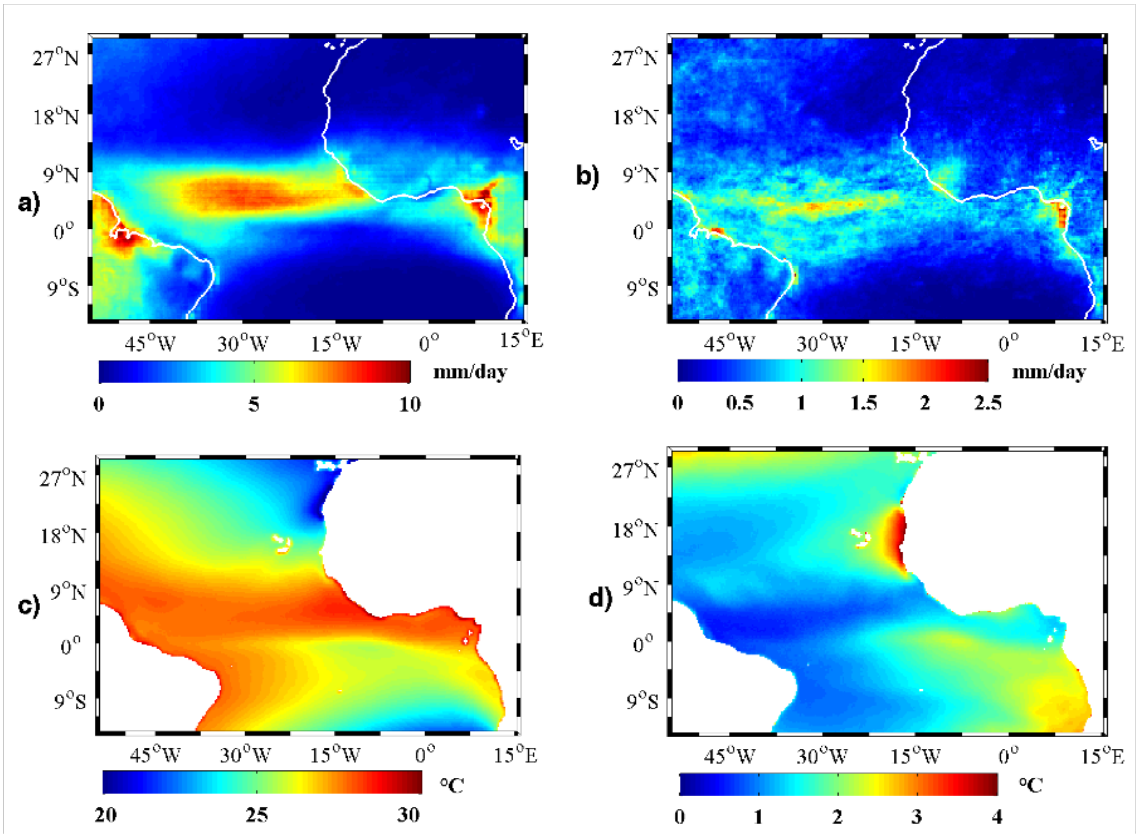

Figure 6.3. *Long-term precipitation and sea surface temperature (SST) distribution during 1998-2009 a) mean precipitation from TRMM radar, b) standard deviation of precipitation based on the same data. c) Mean SST from TMI, d) standard deviation of TMI SST.*

The distribution of sea surface temperatures across the region is also calculated from the long-term mean as shown in figure 6.3c. This shows the quasi-stationary position of the ITCZ as a band of maximum temperatures. Regions of high SST areas are seen north of the equator between 0-13°N and in a region around the Brazil coast. The long stretch of SST band north of the equator is centred at ∼5°N, indicating the position of the climatic thermal equator. Another important region is shown with cold temperatures below 20°C northwest of Africa. This is an important region because North Equatorial Current (NEC) originates from there and carries cold waters toward the equator. A slight signature of the seasonal cold tongue also appears along the equatorial upwelling

zone. Ares of high variability in the eastern tropical Atlantic is not similar to that of the west because the dynamics of both oceanic (e.g. TIWs, cold tongue) and atmospheric (e.g. southeast and northeast trade winds) are stronger and seasonally phase-locked in the east than the west.

6.3.2 Spatial distribution of rainfall

To characterise precipitation over West Africa and the Sahel, I use daily mean fields of TRMM 3B42 version 6 products for a period of 12 years (1998-2009) with the intent of finding interannual variability of precipitation rates over the land. The daily data are important because of its resolution in time and space (0.25 x 0.25 degree), which allows me to examine sub-seasonal changes of rainfall over land. However, due to individual storms that travel hundreds of kilometres per day in the tropics, these signals look spurious with very high/low frequency intervals. All the daily data are considered with values equal or above 1-mm rainfall. This threshold was chosen because it typically marks the precision of rainfall measurements and the resolution of many rainfall datasets (Paeth et al., 2010). Therefore, daily data has been averaged to either 3-daily or monthly before any analysis in this study.

The 3-daily averages are used to quantify precipitation estimates and these are shown in figures 6.4, 6.5 and 6.6. Due to spurious signals in the 3-daily means, negative values were removed and the data are subjected to a 2-d FIR smoothening filter to capture the necessary signals at their spatial scales. For correlation and coherence analysis, only monthly averages are used. Moreover, Ward (1998) provided evidence that the factors controlling rainfall variability at interannual time scale in this region differ during the wet and dry periods. Therefore, the averaged 3-day and monthly data provide the means of quantifying changes of rainfall at sub-seasonal periods.

Rather than considering the Sahel separately from West Africa, TRMM precipitation rate is decomposed to highlight space/time magnitude of occurrences at

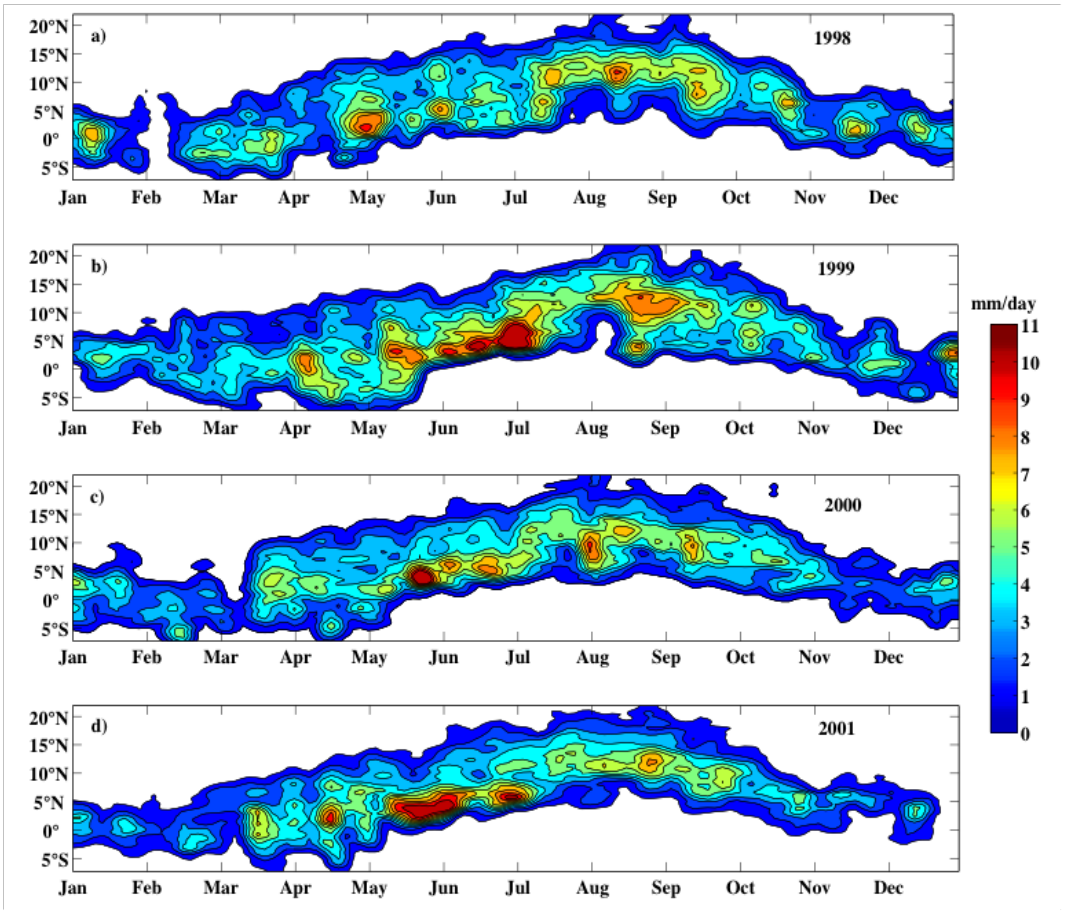

Figure 6.4. *Variability of zonally averaged rainfall over West Africa and the Sahel (18° W to 16° E) from TRMM Precipitation radar based on 3-day running mean. Precipitation estimates between 0 and 1 are not shown. Data were filtered by a 2-d FIR filter to remove spurious signals. Cotour interval is 1mm/day.*

interannual time scales. The Sahel here is defined as a region between 12-25°N and 18°W-16°E. Two peak rain rates each with magnitude of about 10mm/day manifest in April 1998 within the Guinea Coast and further north in August. As expected, rains of this magnitude only occur within the confines of West Africa, and do not extend into the western Sahel. A reduction in rain rate that is far less in magnitude compared to the following years occurred from June to early July.

A remarkable rainfall of magnitude of about 11mm/day is observed in June-July of 1999 (figure 6.4b). This is followed by a dry spell in early August and a sudden northward shift of the rain band measuring about 8mm/day and lasting for

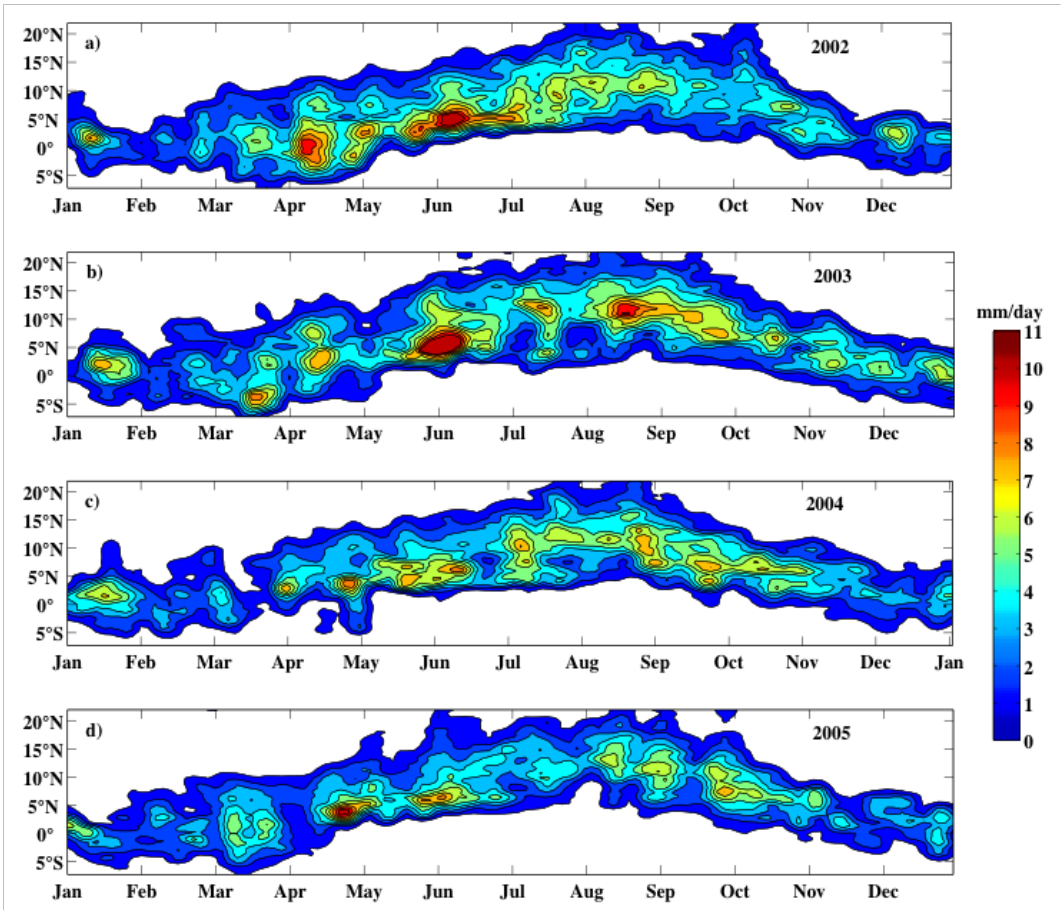

Figure 6.5. *Variability of zonally averaged rainfall over West Africa and the Sahel from TRMM precipitation radar. Cotour interval is 1mm/day. Data were filtered as in figure 6.4.*

2 weeks.

A distinctly dry spell with precipitation less than 1 mm/day is observed during the first 10-days of February 1998, extending from 7°S to 7°N. Although this occurs during the dry season, it is however exceptional compared with the results of the following years, which recorded between 3-4mm/day. The observed SST for the time period (figure 6.7) shows SST anomaly of the same magnitude when compared to the following years of 1999 to 2003. A similar observation is found in the Hovmöller plots and these will be shown later in the next section. If SST were below average, it would have been compelling to attribute this circumstance to cold SST damping in the Gulf of Guinea.

The year 2000 clearly highlights a weaker magnitude and spreading of rains,

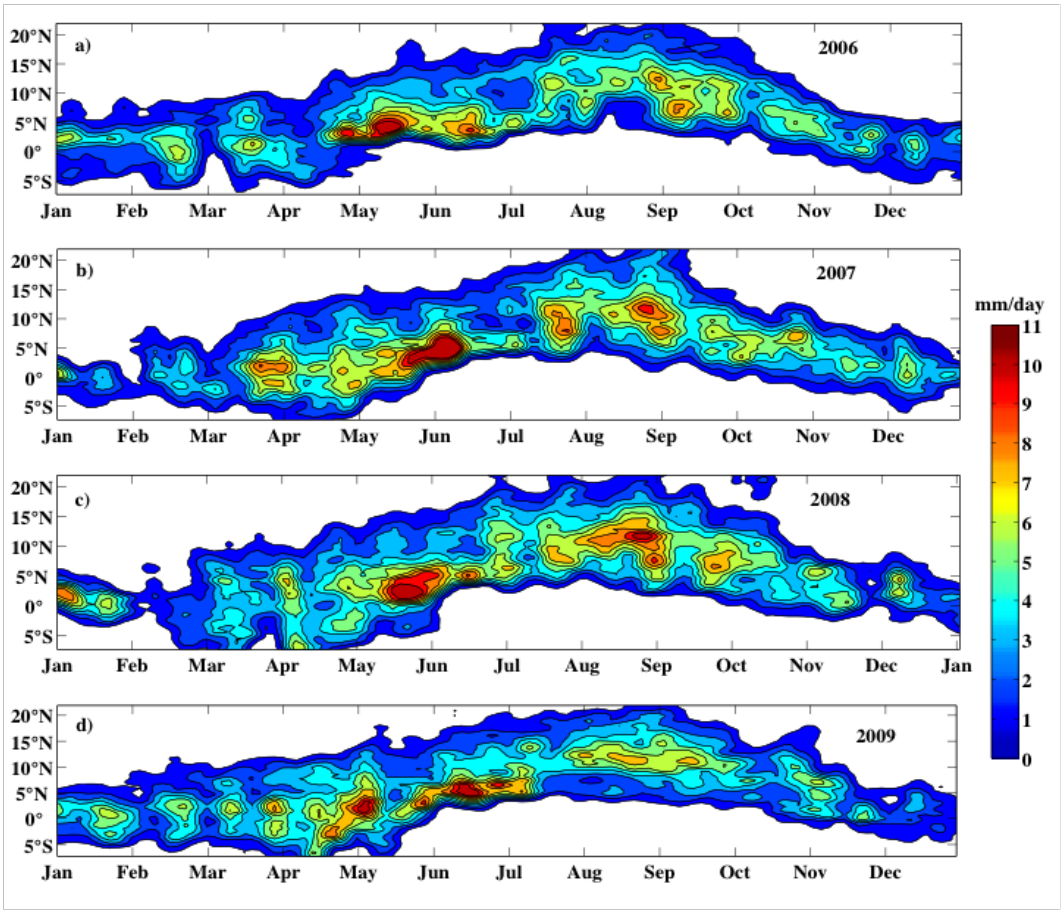

Figure 6.6. *Variability of zonally averaged rainfall over West Africa and the Sahel from TRMM precipitation radar. Cotour interval is 1mm/day. Data were filtered as in figure 6.4.*

with strong rains only lasting a week or two in May and July. Guinea coast experiences strong rainfall in May-June 2001 (figure 6.4d) as the summer monsoon strengthens and the ITCZ moved northward. A drop in rain magnitude is seen further north until another high magnitude appears at 11°N in August. This is the maximum northward position of the ITCZ that controls convection over the region.

In 2002, peak rain rates occurred only in the second quarter of the year (April-June), after which a reduced rainfall persisted until the end of the year. These rains remained within the realms of the Guinea coast as was previously noted by Gu and Adler (2004), and are concomitant with the Gulf of Guinea SST at the same time as far as the Guinea coast is concerned (figure 6.7). The low rainfall from July-December also corresponds with very low SST anomalies of less

than 1°C shown in figure 6.7. Contrary to the previous years (2001 and 2002), years 2003 and 2004 exhibit just an average rainfall in both the Guinea coast and north of it almost all the year. A strong weeklong rain pattern in April is observed in 2005 (figure 6.5d). A beak in rainfall is observed south of 3°N) between February and early April but returns from late April.

The peak rain pattern observed in year 2006 (figure 6.6a) seems to shift in time the year after. This time lag could have a possible impact on the local climate, especially since both patterns are on the same latitude. I will develop this idea by analysis of lagged correlation between rainfall and SSTs in the region. In late-August to early-September 2007, there is a peak in rainfall pattern that lasts about 1 month. This is repeated in the following year (2008) with almost the same phase at the same latitude of ∼5-12°N. In 2009, only a half of this magnitude is observed with rainfall of ∼6mm/day. This raises a question as to why this large difference occurs in such a small area. In the next section, I attempt to investigate whether SST, as one of the major mechanisms driving rainfall in this region is responsible for the observed interannual variability signature.

6.3.3 The seasonal cycle of SST and rainfall

Based on the description of rainfall shown in figures 6.4-6.6, it is possible to separate clearly the rainfall occurrences between the drier Sahel and West Africa. I have chosen the boundary at 12°N based on the observed magnitude of rainfall shown in figures 6.4-6.6 so as to characterise each region separately to further my analysis. Janicot (1992) has shown that distinguishing the region north and south of 10°N would give a better description of interannual variability of rainfall over the region. In addition, various studies have suggested a different mechanism of rainfall variability in the Sahel compared to West Africa. For example, the dipole years in which rainfall anomalies in West Africa and the Sahel (i.e. either either side of ∼10°N) differ in sign has been clearly described (Fontaine and Janicot, 1996; Janicot, 1992; Ward, 1998). Dipole and non-dipole years for the

last century have been classified (see table 4 of Ward, 1998). Each rainfall region chosen is studied in comparison with changes in SST in the Gulf of Guinea.

The seasonal cycle of SST in the Gulf of Guinea as seen from anomaly time series (figure 6.7a) shows high positive SST corresponding to the solar heating when the sun is directly overhead in spring. The intensification of the southeasterly monsoon winds at the beginning of the boreal summer lead to the formation of cold tongue and that reduces the SST the Gulf of Guinea region. The year-to-year variations are evident with 1998 having warmer SSTs in spring, and much colder from May to July. A clear contrast between 2001 and 2003 SST anomalies is observed. A dissimilarity of ∼1°C occurred throughout the year except April – May.

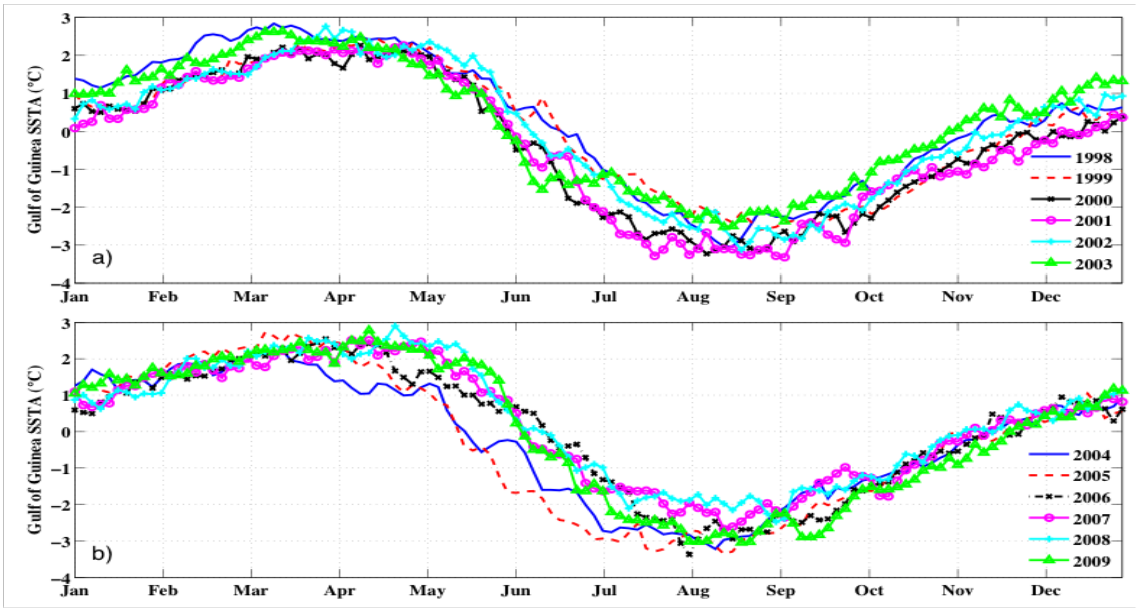

Figure 6.7. *The seasonal cycle of the Gulf of Guinea SST averaged between (7°S-7°N,10°W-14°E) for a) 1998-2003, b) 2004-2009.*

SST anomalies of e.g. 1998, 1999 and 2003 (figure 6.7a) are concurrent with rainfall anomalies (figure 6.9a) of the same years. An interesting peak of rainfall anomalies in 2007 (figure 6.9b) may perhaps be another feature to focus that is masked by the seasonal cycle. Hence, the climatological seasonal cycle is removed from the data to further my investigation on the impact of Gulf of Guinea SST on rainfall over land. Considering previous studies e.g. Bah (1987),

and the peak rainfall observed in 2007 in the Sahel that corresponds to the peak in rainfall over West Africa, then the year 2007 is a non-dipole year. This suggests that a non-dipole year is a year when Gulf of Guinea SST could modulate rainfall over the Sahel much more than the influence of other factors such as the AEJ.

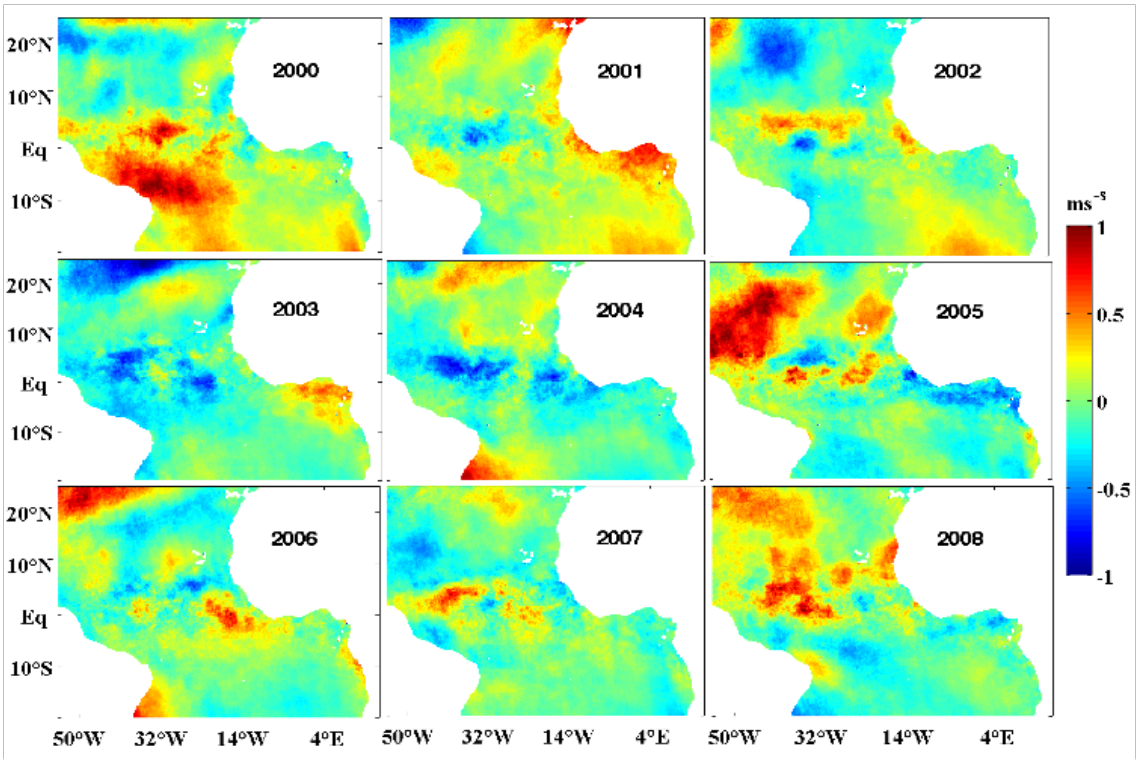

Figure 6.8. *Wind speed anomalies during June-July-August (JJA) months. The seasonal cycle has been removed based on the length of data (1998-2009).*

The influence of Gulf of Guinea SST to rainfall is further reflected in the rainfall anomalies averaged over West Africa (figure 6.9a). Higher SSTs in 2003 from June to December as against lower SSTs in 2001 (figure 6.7a) showed simultaneity in rainfall estimates (figure 6.9a).

Another important scenario in this analysis is the sensitivity of rainfall to SST changes on seasonal basis. The very low SST anomaly record in spring and summer of 2005 (figure 6.7b) is reflected in the West African rainfall anomaly time series (figure 6.9b). The SST anomaly recorded low from April-August while rainfall response is from May-September, presenting a lag of 1 month. Rainfall over West Africa showed positive anomaly in July of all the twelve years except

in 2005. The cooling effect in 2005 is attributable to the basin-wide strengthening winds (figure 6.8). This is coincident with West Africa and Sahel drought of 2005.

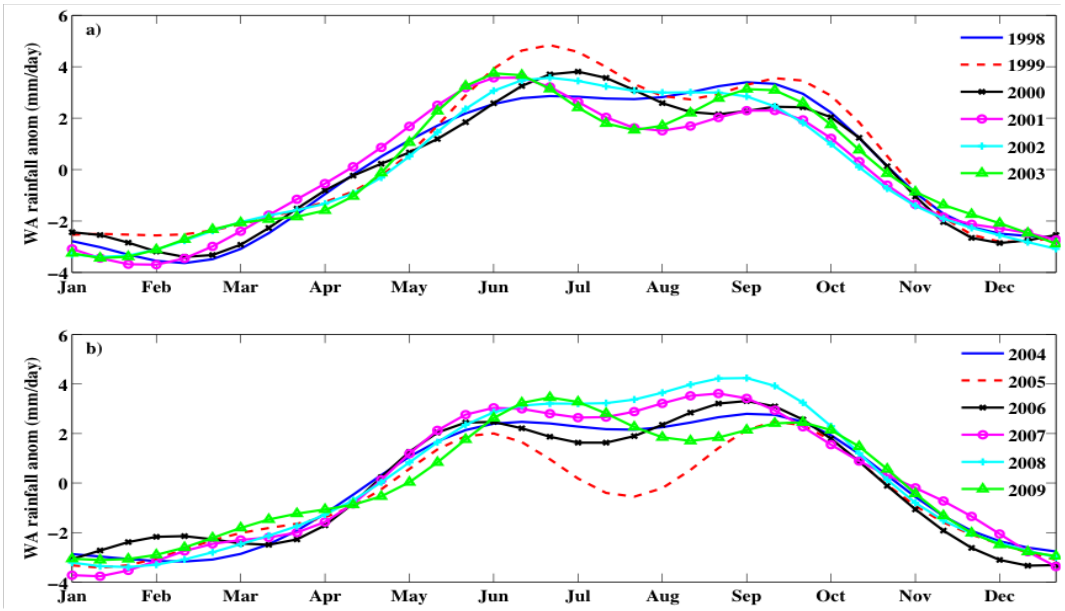

Figure 6.9. *The seasonal cycle of rainfall over West Africa averaged between [3° N-12° N, 10° W-16° E) for a) 1998-2003, b) 2004-2009.*

In figure 6.16, SST anomalies in the Gulf of Guinea are largely negative during the boreal summer, and this may have inhibited heat and moisture fluxes that cause rain. This is intriguing seeing that wind speed in the Gulf of Guinea (figure 6.8) is weak, while SST anomalies are negative. A possible explanation for this behaviour is that, the response of southeasterly winds to changes in temperature at the Gulf of Guinea region is rather a weak response, since the winds are driven largely by other factors in the South Atlantic. The cold tongue develops around 30°S but then affect the whole of the Gulf of Guinea region. The winds must have excited the ocean during early summer, and the cold tongue upwelling persists and maintained by the westerlies that appear anomalously high in 2005. The consequence is low moisture fluxes as well as the ability of the moisture to be driven onto land by the monsoon winds that become weak toward the end of summer.

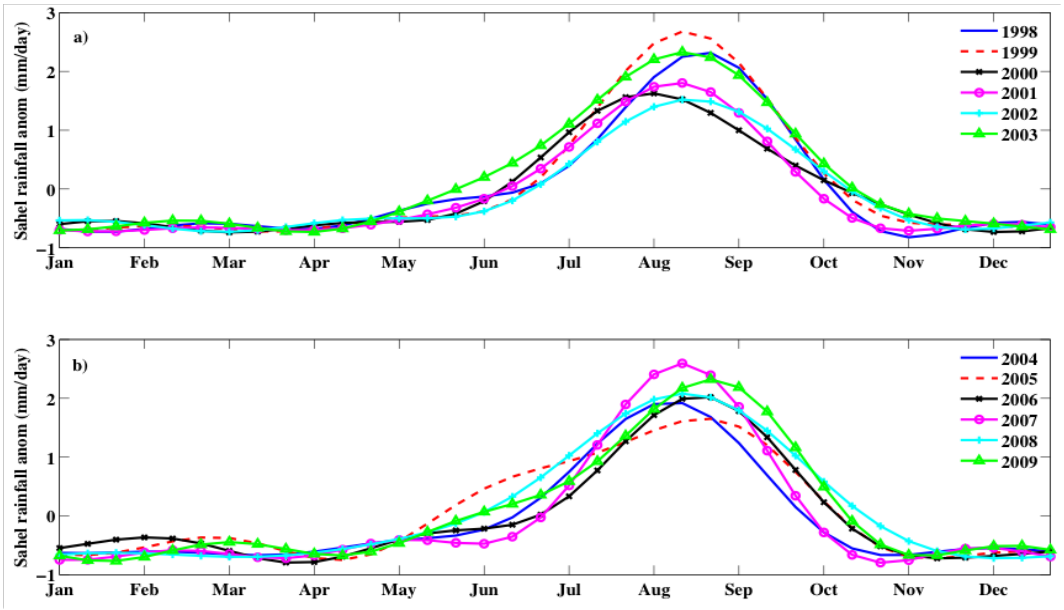

Figure 6.10. *The seasonal cycle of rainfall over Sahel averaged between (12°N-25°N, 10°W-16°E) for a) 1998-2003, b) 2004-2009.*

6.3.3.1 Interannual variability of anomalous SST and rainfall

The region of West Africa and the Sahel experiences fluctuations of rainfall, which vary from year to year. It is therefore pertinent to study the interannual variability of SST in the Gulf of Guinea. The SST anomalies are based on TMI daily data averaged to 3-day composites. The seasonal signals were removed based on the 12-year period (1998-2009), and the Hovmöller plots were extracted from a region in the Gulf of Guinea (2°N, 10°W-5°E) to highlight scales of variability.

In the tropical Atlantic Ocean, the cold tongue develops around mid-May in response to the intensification of the southeasterly winds. This strengthens upwelling of cold subsurface waters and consequentially impact on the air-sea processes. The seasonal cycle of the Gulf of Guinea is clearly manifest throughout the year as seen in the left panel of figure 6.11, with high positive SST anomalies in spring and very low signatures from mid-May to October. In the years 1998 and 1999, there were higher than normal SSTs during the boreal summer from May to August. This associated warming perhaps is connected to the monsoon system. A delay in the monsoon that drives the cold tongue would allow a

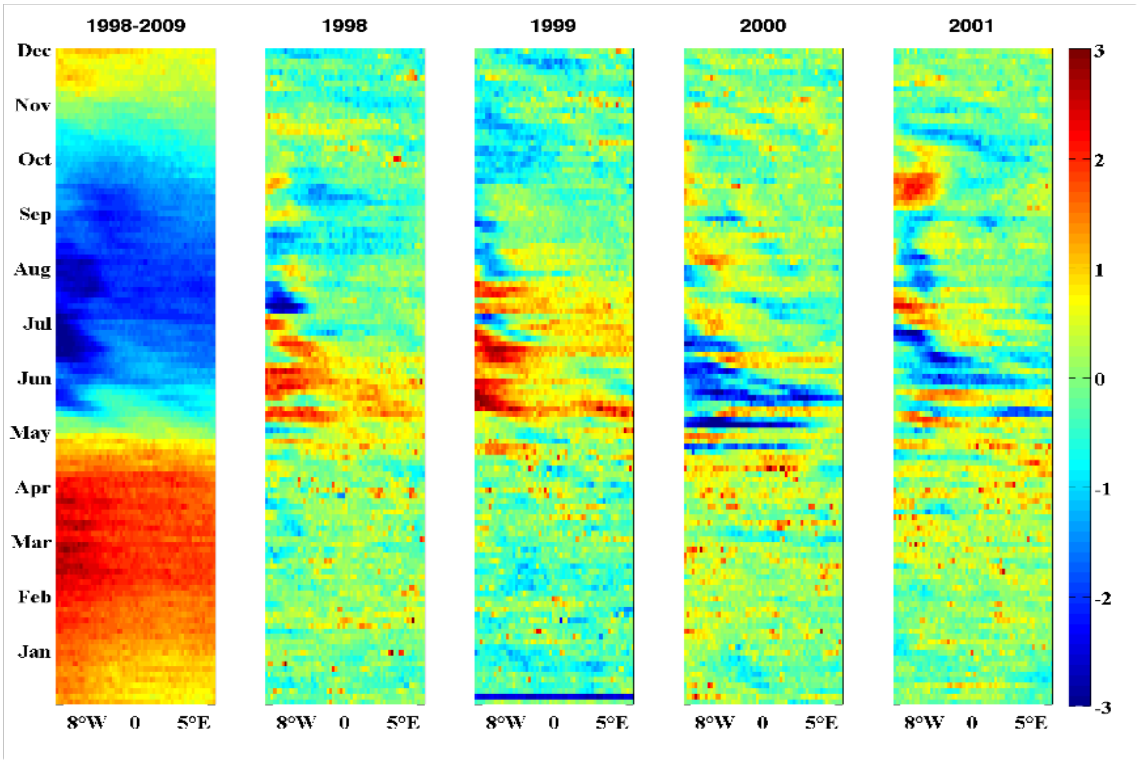

Figure 6.11. *Hovmöller plots of 3-daily averaged TMI SST anomalies (units in °C) averaged over 10° W5° E along 2° N. Left panel: averaged over the period 1998-2009, and right panels for various years. Seasonal cycles with respect to the long-term mean1(998-2009) were removed from each yearly plots on the right panel.*

significant warming to persist between these 2-3 months. Another possible explanation is that the monsoons winds were weak during those years due to associated large-scale atmospheric circulation.

The years 2000 and 2001 show a marked difference of temperatures during June-July months with ∼2-3°C low. This is contrary to the preceding years, and the presumption on further strengthening of the monsoons is probable.

Significant interannual variability is observed mostly in 1998, 1999 and 2000 from the SST anomaly plots (figure 6.11). The year 2000 recorded considerably negative SST anomalies during the summer (May-August) while the preceding years showed positive anomalies. This means that 1998 and 1999 had warmer summers than the average of all the 12 years in total. Hence, I study these anomalies in terms of rainfall to see if there are any connections with West Africa.

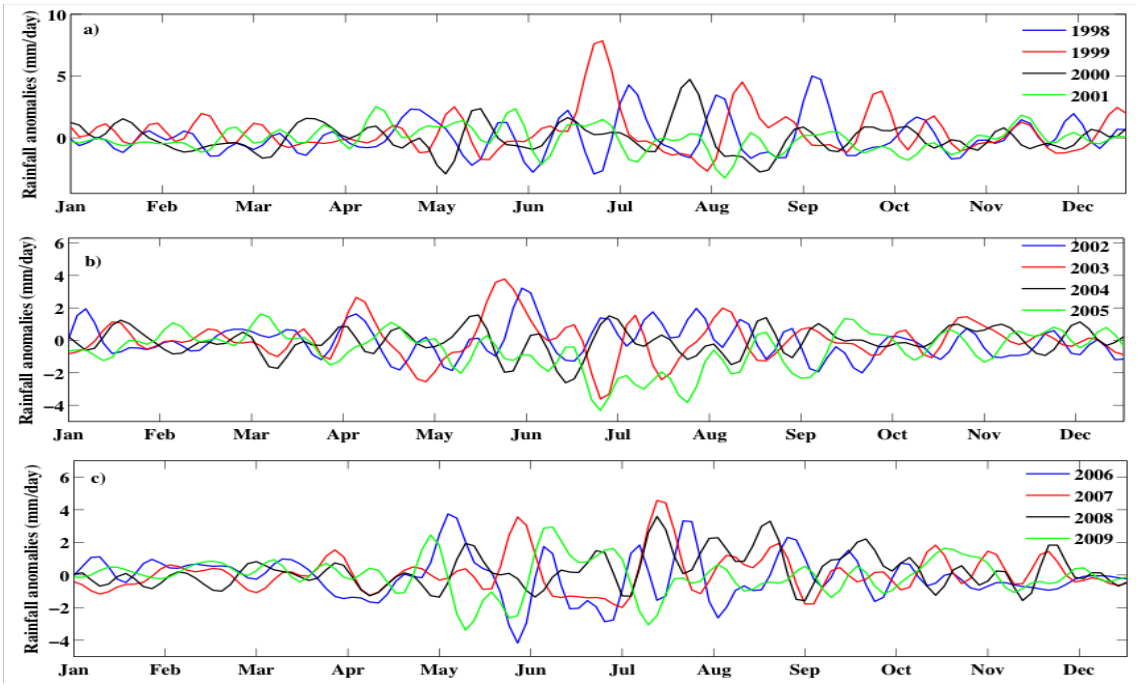

Figure 6.12. *The interannual variability of rainfall over West Africa averaged between [3° N-12° N, 10° W-16° E) for a) 1998-2001, b) 2002-2005 and c) 2006-2009. The long-term seasonal cycle based on the 12 years data were removed.*

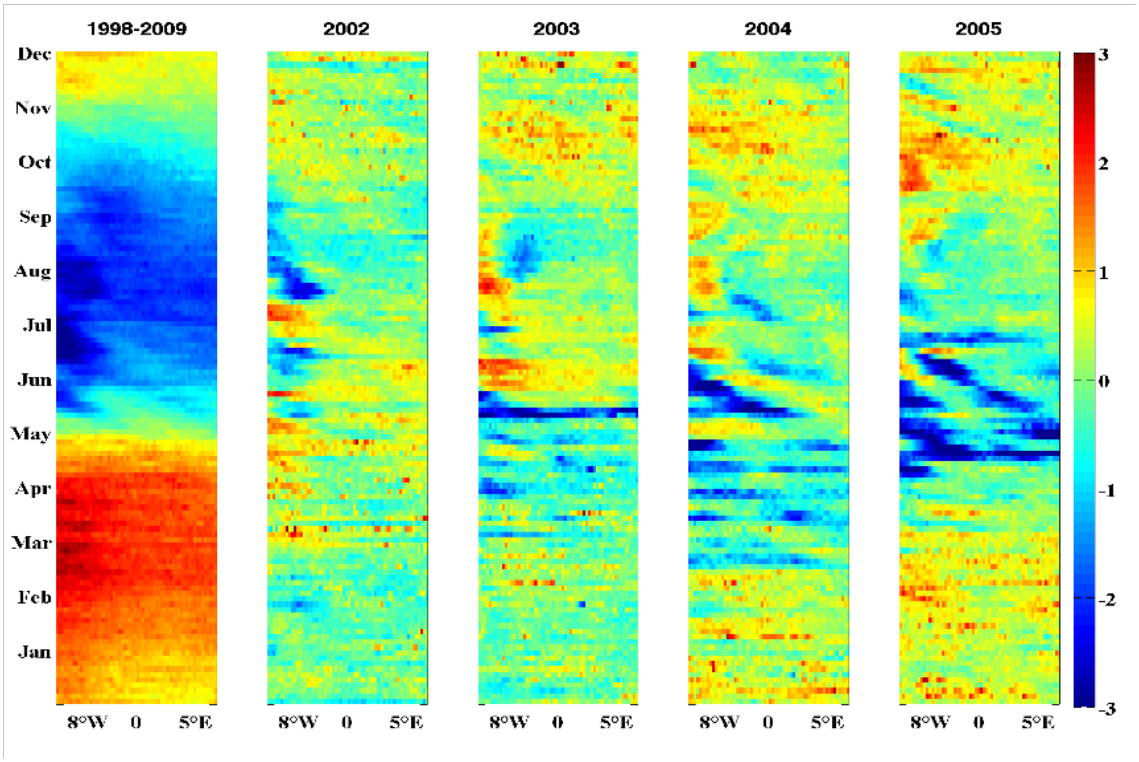

Figure 6.13. *The same as in figure 6.11, except for the difference in years.*

While the years 1998, 2000 and 2001 exhibits rainfall anomalies in the order of ±4mm/day, the year 1999 recorded a peak of positive anomaly of ∼7mm/day in June-July period. This is reflected in the SST anomaly of the same year (figure 6.11) when warming was exceedingly high ∼2°C. A persistent cooling follows from the SST plot that lasted over a month, signifying the maturity of the cold tongue. By implication, SST anomalies of the order of ∼2°C could have a great impact on rainfall over West Africa (figures 6.5b and 6.9a), and may even cause flooding. Interestingly, the June 1999 rainfall is approximately out of phase with rainfall of 1998. In the summer of 2005 (figure 6.13), strong negative SST anomalies are observed which did not occur in other years.

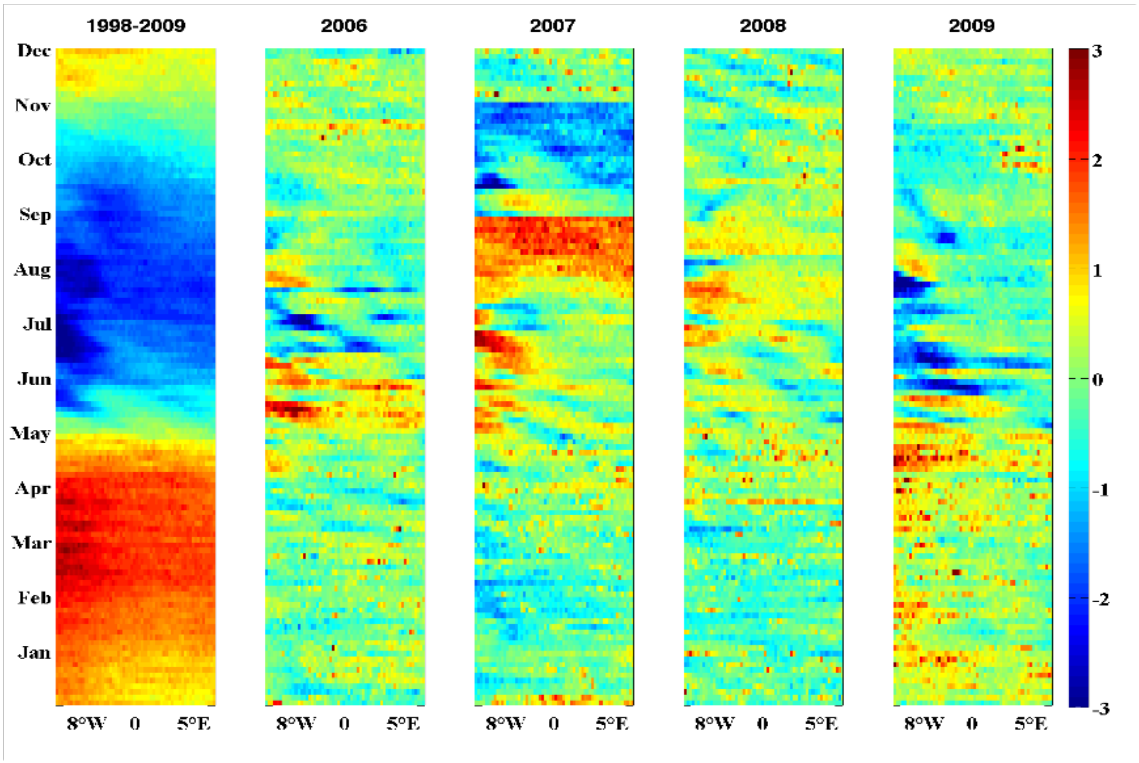

Figure 6.14. *The same as in figure 6.11, except for the difference in years.*

The years 2006, 2007 and 2008 showed significant warming during the summer contrary to what was observed in 2005 (figure 6.13). A significant cooling is observed during the summer of 2009. There is also a conspicuous warming from June-September 2007 from the SST anomalies. This has a consequence on the rainfall over West Africa that peaks in July with values above 4mm/day (figure

6.12c). This obvious SST anomaly is further investigated later to assess possible implication to local climate scenarios.

6.3.3.2 Gulf of Guinea Index vs West Africa and Sahel Rainfall indices

SST anomalies observed in 1999 (figure 6.11) that were found to have positive response from rainfall over West Africa (figure 6.12) also seem to have an impact on the Sahel rainfall (figure 6.15). Although, I characterised strong rainfall areas south of 12°N, and categorised the Sahel north of this boundary, the influence of Guinea Gulf SST still persists further north. This influence is rather prominent in August-September months when the ITCZ is farthest north carrying the rain band, compared to when it was at the south in previous months. However, while rainfall in 1999 showed an approximate positive peak only in August (figure 6.15a), the previous year (1998) recorded a negative peak in the same month, but with positive peak of an equal magnitude in September. The rainfall observed here seems to lag SST anomalies (figure 6.11) with about a month before peaking. Similarly, the cooling observed in June-July 2000 (figure 6.11) reflected on the Sahelian rainfall with a negative peak in August due to the one-month lag.

6.3.3.3 Potential causes of 2007 flooding over West Africa and the Sahel

Two important peaks of rainfall are observed in July-August and August-September 2007 (figure 6.15c) with a very short break in between these periods. The peak rain rates observed in July 2007 of both West Africa (figure 6.12c) and the Sahel region (figure 6.15c) may explain the flood patterns. It was suggested that heavy rainfall fell over dry soils, which led to heavy runoff and flooding of rivers such as the Niger and the Volta (Itiveh and Bigg, 2008). However from these results (e.g. figure 6.12c) the double peaks may explain that, after the dry land is saturated with rainfall in late-May to early-June due to heavy rains, it was only

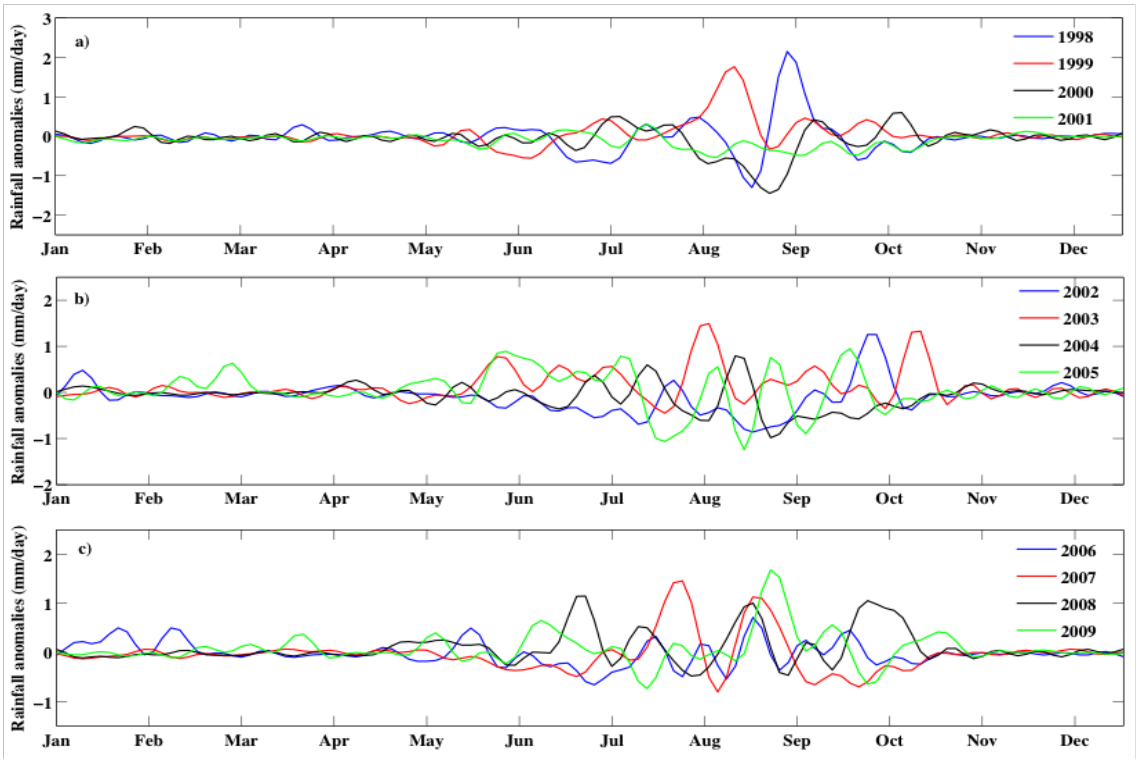

Figure 6.15. *The interannual variability of rainfall over the Sahel averaged between [12° N-25° N, 10° W-16° E) for a) 1998-2001, b) 2002-2005 and c) 2006-2009. The long-term seasonal cycle based on the 12 years data were removed.*

a matter of 3 weeks that heavier rainfall returned with the strongest downpour causing flood. For the Sahel region (figure 6.15c), the heavy downpour began first in late-July/early-August because the ITCZ has to maintain a northern-most position before atmospheric processes (e.g. Westerly Wind Jets) comfortably act to distribute rainfall. Within an approximate period of 10 days, another heavy rainfall began in late August and last until mid of September.

Tropical rains are generally heavier than in other global regions, hence any continuous rainfall that lasts more than one week tends to cause floods. For example, intense African Easterly Wave activity on convection, which is purely a tropical even suggests the ability of wave activity in modulating flood-producing rains.

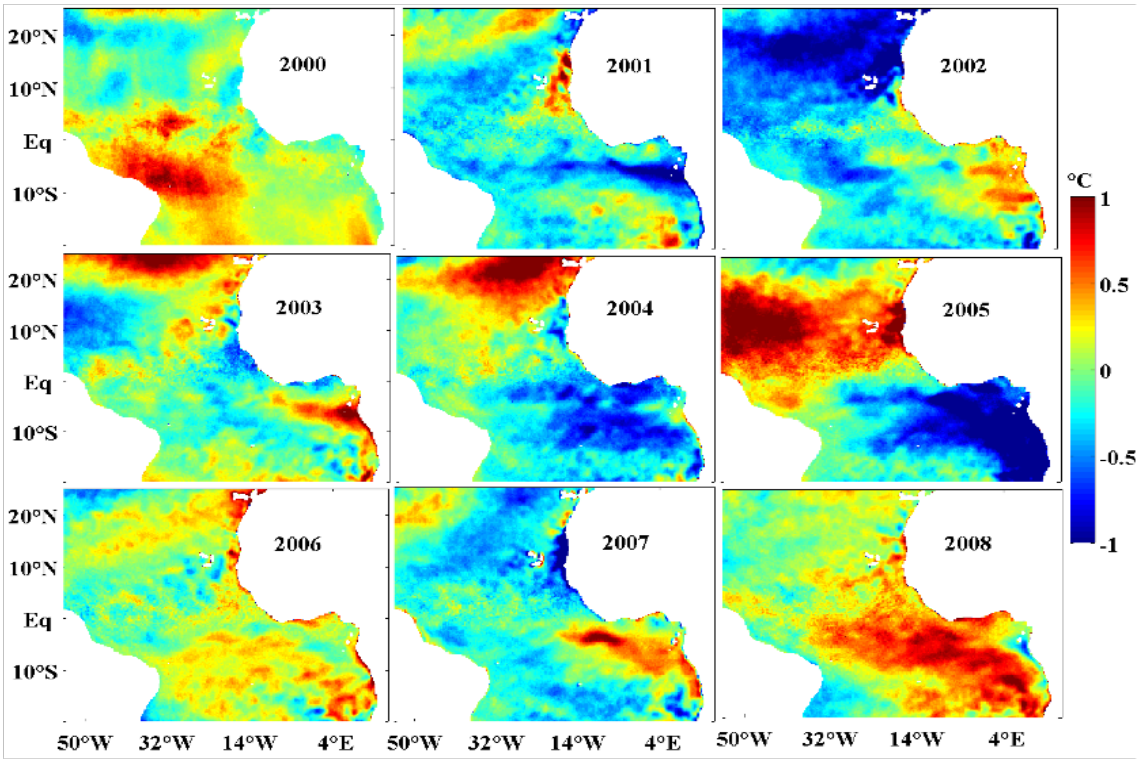

Figure 6.16. *Sea Surface Temperature anomaly for June-July-August (JJA) months in the Gulf of Guinea averaged. Seasonal cycle has been removed based on 1998-2009 climatological mean.*

6.3.3.4 Spectral analysis of SST and rainfall

To assess the impact of Gulf of Guinea SST to rainfall variability, I extend my analysis using Fourier techniques to help identify coherent signals that connect SST and rainfall. Coherence analysis considers discrete signals and identifies patterns of correlation, while cross power spectral density identifies the energy of correlation at each frequency interval. The phase spectrum identifies the direction of relationship between the two signals. Details of these methods are found in appendix A. I decomposition rainfall and SST signals with hope of finding coherent estimates in the absence of the obvious seasonality. The West African rainfall and Gulf of Guinea SST (figure 6.17) show strong coherence ($\sim$0.7) of the SST equivalent to a semi-annual cycle of the Gulf of Guinea, having the same phase and a significant energy (CPSD). This implies that variability of SST in the Gulf of Guinea is directly associated with rainfall variability

over West Africa. The 12-day peak with significant coherence, although having weaker power, is associated with high SST-rain covariability at the Guinea coast, where rainfall response quickly to a change in SST through heat fluxes.

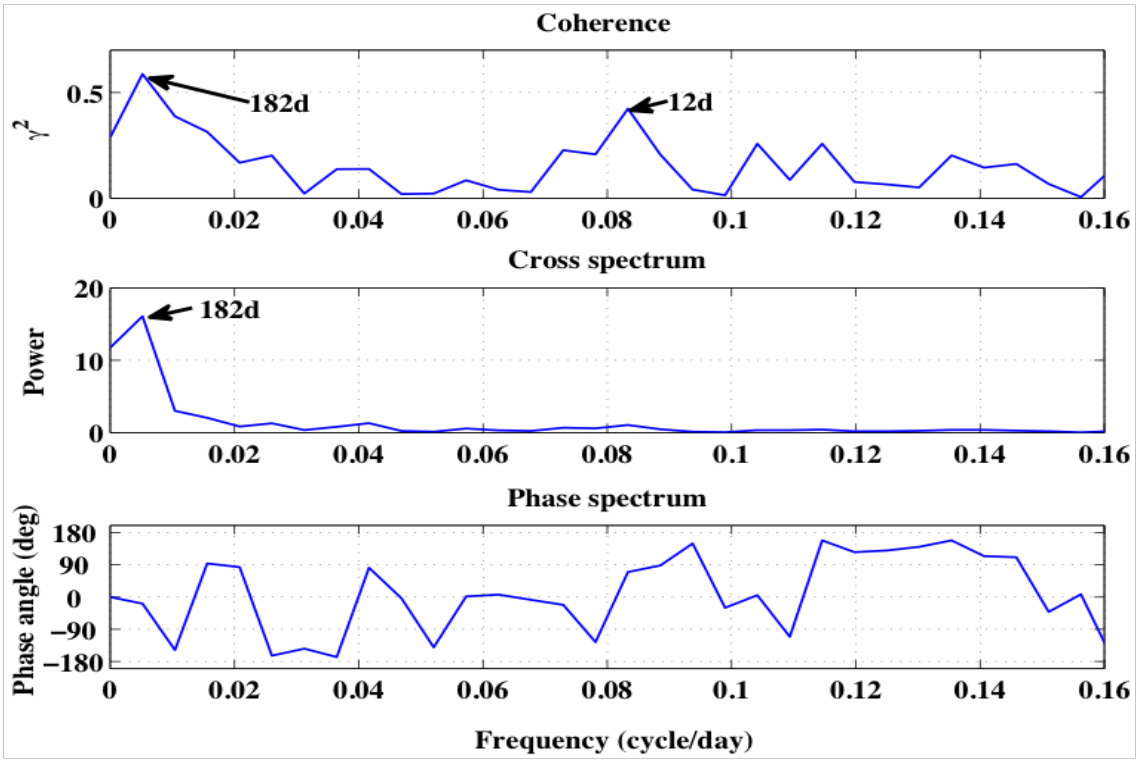

Figure 6.17. *Coherence squared amplitude, cross power spectral density (CPSD) and Phase Spectrum of non-seasonal signal between anomalies of Gulf of Guinea SST (7° S-7° N, 10° W-14° E) and the West African rainfall (3° N-12° N,18° W-16° E). Data is for the period (1998-2009). Both coherence and CPSD are estimated via Welch periodogram.*

The Sahel (figure 6.18) shows a weak coherence of ∼0.3 at 182-days, having stronger power that is associated with the semiannual cycle of the Gulf of Guinea. However, the phase is ∼180 degrees, indicating that rainfall changes in the Sahel is of opposite sign to that of SST in the Gulf of Guinea. This, by implication explains that low SSTs in the Gulf of Guinea correspond to high rainfall in the Sahel. The reason is that coherence estimates here is able to pick periods of strong variability in both Gulf of Guinea and the Sahel, which is summer (JJA months). At the Gulf, SSTs are already low due to intense cold tongue, while the Sahel at this period experiences strong rainfall due to the northward positioning of the rain-bearing ITCZ. The second and third peaks have high

coherence but weaker power at 12-day and 10-day that is associated with high frequency covariability of SST-rainfall. At the periods when the cold tongue doesn't exist, high SSTs in the Gulf of Guinea could correspond to high rainfall over the Sahel.

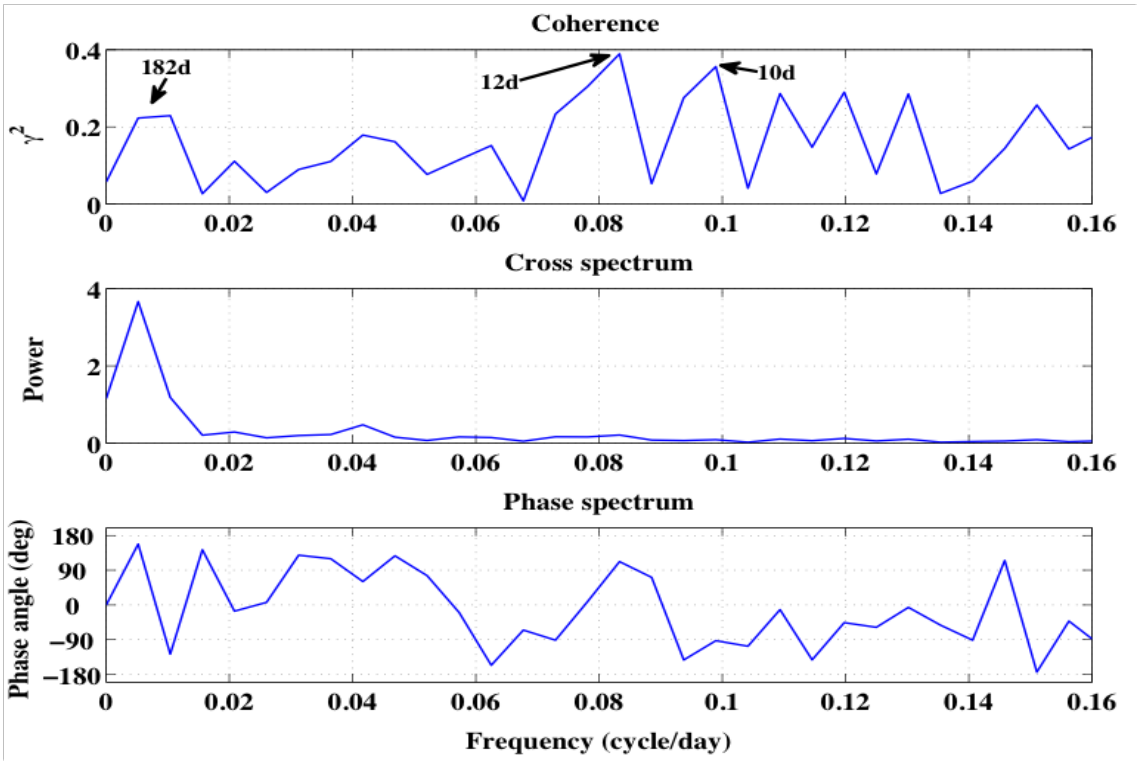

Figure 6.18. *Coherence squared amplitude, cross power spectral density (CPSD) and Phase Spectrum of non-seasonal signal between anomalies of Gulf of Guinea SST (7° S-7° N,10° W-14° E) and the Sahel rainfall region (12° N-25° N,18° W-16° E). Data is for the period (1998-2009). Both coherence and CPSD are estimated via Welch periodogram.*

6.3.4 The Gulf of Guinea Index and rainfall

The Gulf of Guinea SST is a major indicator of local climate anomaly in West Africa, and to some extent the Sahel. The Gulf of Guinea index (figure 6.19a) shows the seasonal cycle of SST and significant interannual variability with SST anomalies peaking in some years, notably 1998, 2001 and 2005, while others record less e.g. spring of 2008. The plots show stronger correlation with West Africa rainfall than with the Sahel, having a small difference. The correlation

curves also partially out of phase. This further highlights the relationship between rainfall and SST in the region through large-scale circulation and atmospheric moisture anomalies as suggested by Vizy and Cook (2001).

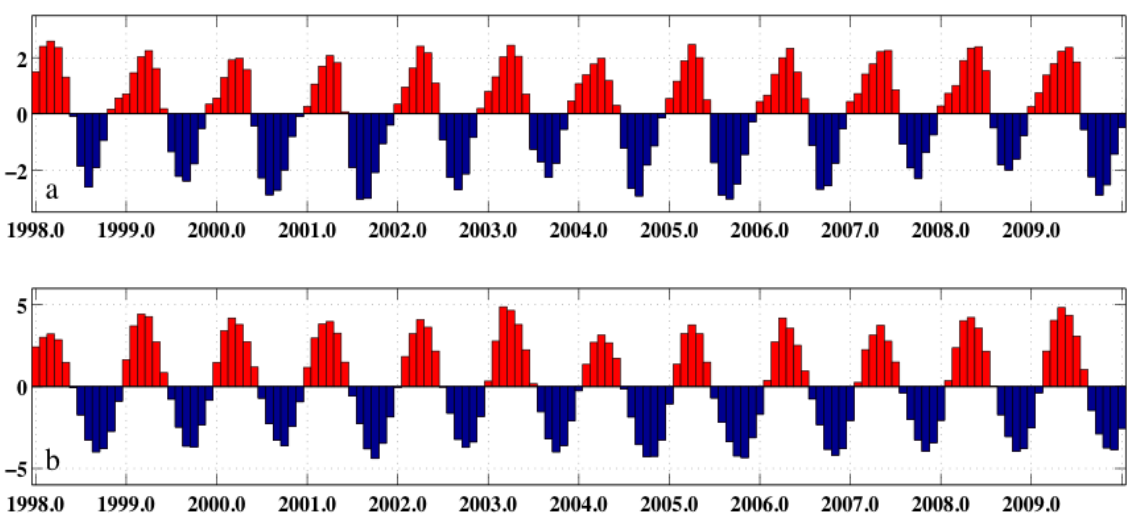

Figure 6.19. *The Atlantic SST indices calculated based on area averages a) Gulf of Guinea Index (GOGI) and b) Atlantic Meridional Mode Index (AMMI). GOGI is SST anomalies averaged over [7° S-7° N, 10° W-14° E] and AMMI [5° N-25° N,50° W-20° W]-[5° S-25° S,20° W-10° E]. Positive AMMI = warm tropical north Atlantic.*

The annual cycle is apparent in the correlation map (figure 6.20a). It is essential, therefore to compare the Gulf of Guinea SST with the rain data after removing the the seasonal cycle (long-term climatology) to determine the actual connection between them. The Gulf of Guinea SST anomalies lagged West Africa rainfall by 1-month (figure 6.21a) which is opposite to the analysis with seasonal cycle (figure 6.20a). This is because this correlation (figure 6.21a) is based on non-seasonal anomalies, hence covariability between rainfall and SST can occur due to seasonal difference of the GOGI or interannual variability. For example, SST in the Gulf of Guinea are affected by tropical instability waves that warm the region, and also large-scale atmospheric connections can modulate the Atlantic Niño which is also in the Gulf of Guinea region. On the contrary, the SST lags the Sahel by three months compared to a zero lag with the seasonal cycle present. This is not a surprise because the Sahel can be modified by a number

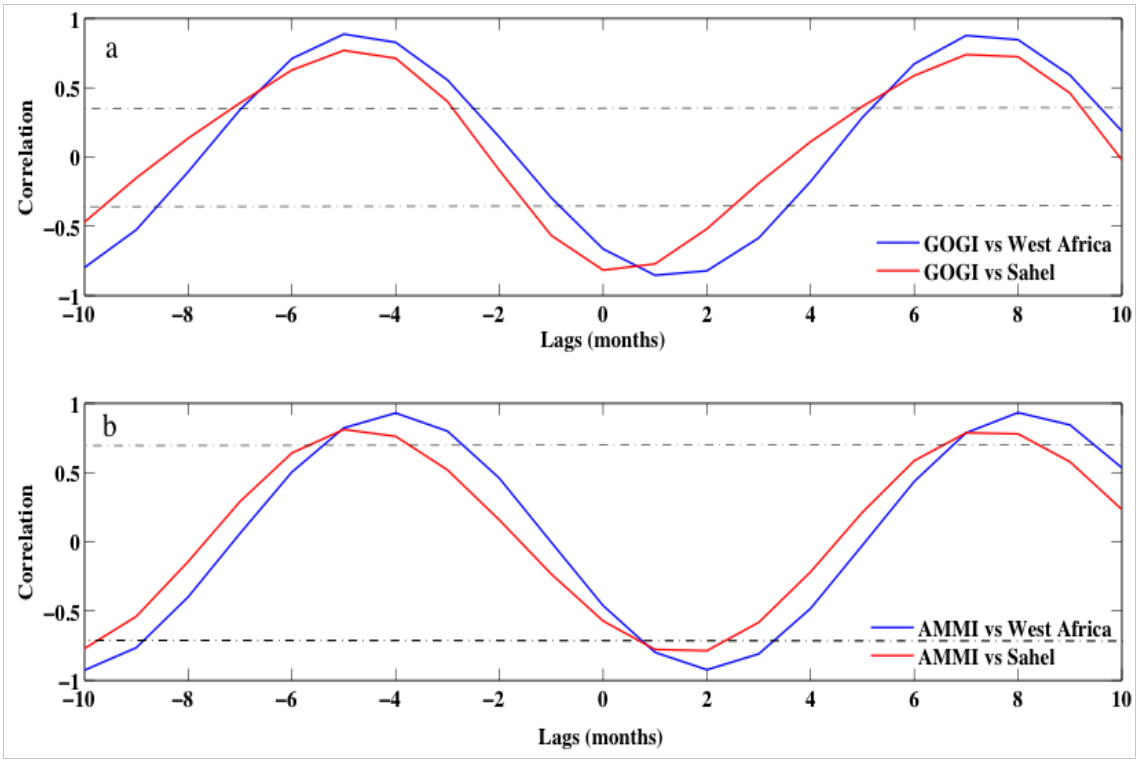

Figure 6.20. *Cross correlation between anomalies of a) Gulf of Guinea SST versus West Africa and Sahel rainfall. GOGI lags West Africa Rain and correlates well at zero lag with Sahel rainfall, b) Atlantic Meridional Mode Index (AMMI) and rainfall over West Africa and the Sahel. AMMI leads both West Africa and Sahel Rain. Lags are in months. Dash-dot lines indicate the 95% confidence limit. For a, positive x-axis means GOGI leads, and for b, positive means AMMI leads.*

of atmospheric factors such as the AEJ, AEWS, dry northeasterly winds etc as studied by Grist and Nicholson (2001); Gu and Adler (2004).

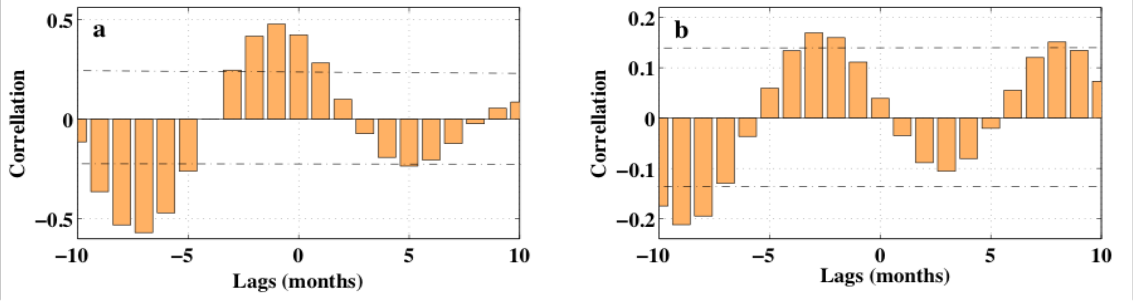

Figure 6.21. *Cross correlation between anomalies of Gulf of Guinea SST and a) West African rainfall anomalies, b) Sahel rainfall anomalies. Lags are in months, and seasonal cycle was removed. Data are based on 12 years (1998-2009). Dash-dot lines indicate the 95% confidence level. Positive x-axis means GOGI leads.*

6.3.5 The Atlantic Meridional Mode and Rainfall

The major modes of interannual variability in the tropical Atlantic are the equatorial mode analogous to Pacific Niño (also called Atlantic Niño), and the meridional mode characterised by an equatorial SST gradient, with significantly higher SST in the north than the south. The meridional inter-hemispheric SST gradient is referred to as the meridional mode because it is part of a coupled variability that exhibits north-south patterns, and has no Pacific counterpart (Servain et al., 1999).

The Atlantic Meridional Mode (henceforth AMM) is calculated from area averaged SST anomalies shown earlier in section 2.7.1. It is the main focus in this section, and has being found to have a major impact on rainfall over the Nordeste region of Brazil from observed data (Moura and Shukla, 1981). The area records high rainfall when the ITCZ is in its southernmost position (Xie and Carton, 2004). Drought in the region was found to be influenced by an anomalous northward shift of the ITCZ band that occurred in conjunction with an anomalous AMM, also referred to as Atlantic dipole.

Previous studies showed a very weak connection between AMM and rainfall anomaly over West Africa and the Sahel (Folland et al., 1986; Hastenrath, 1990; Lamb and Peppler, 1992; Lough, 1986). However, most of the studies were based on very short time data records or numerical simulations. Having the advantage of 12 years data record, I aim to improve the analysis of AMM′s influence over West African and Sahelian rainfall anomalies.

The link between AMM and the Atlantic equatorial mode has been studied (Servain et al., 1999). The Gulf of Guinea is in a sense, a part of the Atlantic equatorial mode, which is broadly studied in this chapter. In furtherance to my earlier analysis, I characterize the SST dipole mode to a standardized index (Atlantic Meridional Mode Index - AMMI), which is the difference of the area averaged SST anomalies of [5°N-25°N,50°W-20°W] and over [5°S-25°S,20°W-10°E].

The AMMI index (figure 6.19b) shows clearly the seasonal cycle of SST anomalies based on the difference between the two regions north and south of the equator. The seasonal cycle changes sign every 6 months, in response to basin-wide SST changes and the monsoon behaviour. An apparent interannual variability is observed, notably for the positive anomalies in some years such as 2003 and 2009. The years 1998 and 2004 accounted for weaker positive anomalies, with SSTs less than the average years.

Positive lags imply that AMMI leads West African rainfall (figure 6.20b). The GOGI correlates well with West Africa (WA) rainfall (r=0.95) and the Sahel rainfall (r=0.90) both at the 95% confidence level. Correlation of GOGI with WA is at one month lag, with GOGI leading, indicating that high rainfall in the region occurs after high SST occurs in the Gulf of Guinea. Correlation here has picked periods of strong variability, which is the summer period. During this time, the rain band is already over land due to the positioning of the ITCZ while at the same time, SST becomes cooler due to intense cold tongue upwelling. Therefore, the summer periods has dominated the SST-rainfall variability in the region. GOGI and the Sahel rainfall anomalies correlate at zero lag. It is possible that SST anomalies in the Gulf of Guinea initiate convection, and hence rainfall, then the rainfall is transmitted over to the Sahel by the monsoon at a period less than a month. This is because the monsoon convergence over the Sahel occur around 10°N, while Sahel is between 12°N-25°N.

In a Fourier analysis (not shown), coherence techniques using AMMI and West Africa rainfall time series with seasonal signals removed, two major coherent frequencies were determined. One at 333 days having the strongest power (calculated cross power spectral density) followed by a period of 53 days with a power half that of the annual cycle and both are in the same phase (negative). This confirms the cross correlation analysis shown in figure 6.20b, and the explanation is that the negative phase is a determining factor in this relationships. This implies that as the cold tongue develops, which by analogy is the main signal of the negative AMMI phase, the rain belt over West Africa is shifted northward, and hence a negative correlation results. This means that AMMI could strongly

influence the meridional shift of the ITCZ, by pushing the rain belt straddling the ITCZ northward and distributing moisture. Similar condition applies for the Sahel. A good knowledge of coupling between southerly winds and their interaction with SST in the tropical Atlantic is vital in this study, and it is a part of Chapter 8.

6.3.5.1 Similarity between Gulf of Guinea SST and the Atlantic Meridional Mode

Is there any similarity/dissimilarity between Gulf of Guinea SST and the Atlantic meridional mode? The Gulf of Guinea SST anomalies and the Atlantic meridional mode (AMM) can best be compared in terms of indices (figure 6.19). Although, they both exhibit the same seasonal cycle, the impact of each to a particular process may differ because they tend to differ in terms of their cold/warm phases. The cold and warm phases (figure 6.19) for example differ in the number of months. This provides a vivid explanation on why the AMMI lags an extra one-month more than GOGI over rainfall on West Africa and Sahel (figure 6.20). By inference, the tropical north and south Atlantic regions from which AMMI is extracted should lag more than the Gulf of Guinea SST by virtue of distance. I can speculate here that, by virtue of the composition of AMMI the lags are in order and have provided an expected result.

6.3.5.2 Connection with tropical instability waves (TIWs)

Severe flooding over West Africa and the Sahel in 2007 has been related to the changes in Gulf of Guinea SST (e.g. Itiveh and Bigg, 2008; Paeth et al., 2010). Because of this reason, and because the tropical instability waves (TIWs) have been thought to warm the Gulf of Guinea, this opens an avenue to search for why the September 2007 SST in the Gulf of Guinea was warmer than other years.

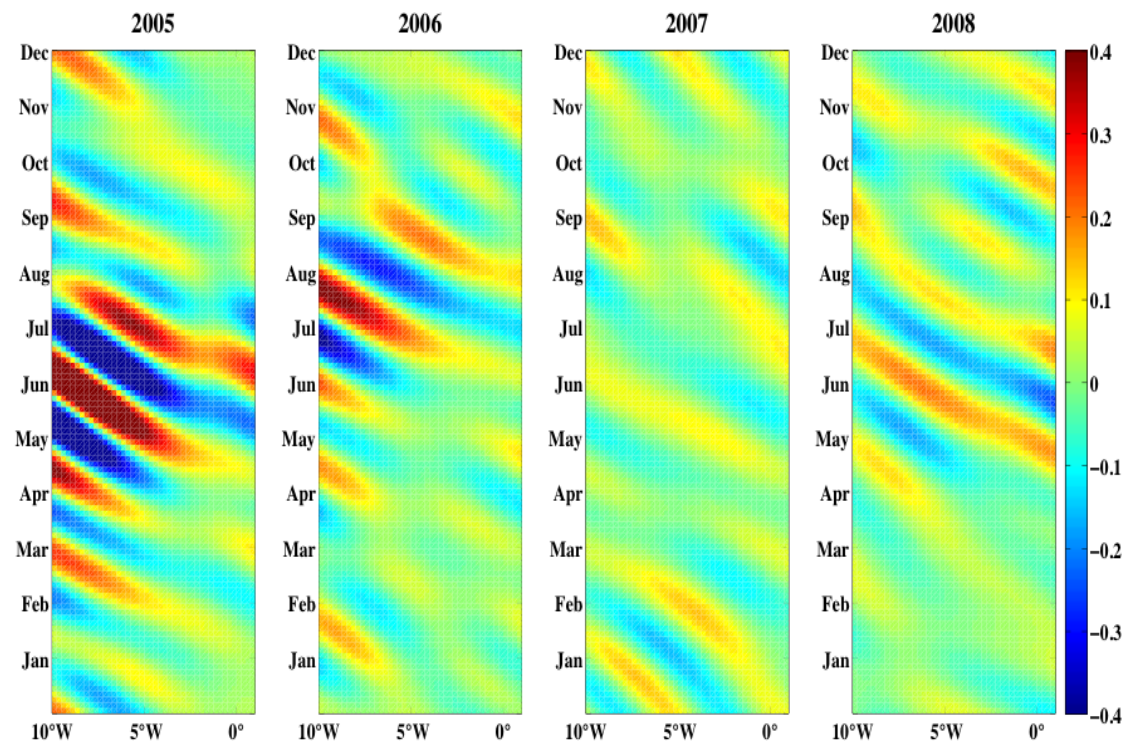

Figure 6.22. *Hovmöller plots of 3-day averaged TMI SST (units in °C) at [2°N, 10°W-1°E]: The long-term seasonal cycle based on 12 years of data (1998-2009) removed. Cold tongue weakens and warming persists.*

The evolution and maintenance of the cold tongue in the tropical oceans of both Atlantic and the Pacific is dependent on processes linked to TIWs such as vertical mixing, horizontal and vertical advection as well as heat flux divergence (Peter et al., 2006). Because of the role these waves play in the time evolution of heat fluxes and their importance to the near-surface heat budget (Grodsky et al., 2005; Peter et al., 2006; Weisberg and Weingartner, 1988), which are necessary for convection, I investigate further their link to warming of the region in September 2007.

I examine the interannual variability of TIWs in the Gulf of Guinea centred at [2°N, 10°W-1°E] during 2005-2008 (figure 6.22). The bandpass filtered SST reveals TIWs that have a period of 15-40 days and a wavelength of 500-1500km. The waves are quite prominent in 2005 and 2006, but very weak in 2007. These waves are believed to be generated by the shear of zonal currents (von Schuckmann et al., 2008) but are predominantly excited by the southeast trade winds

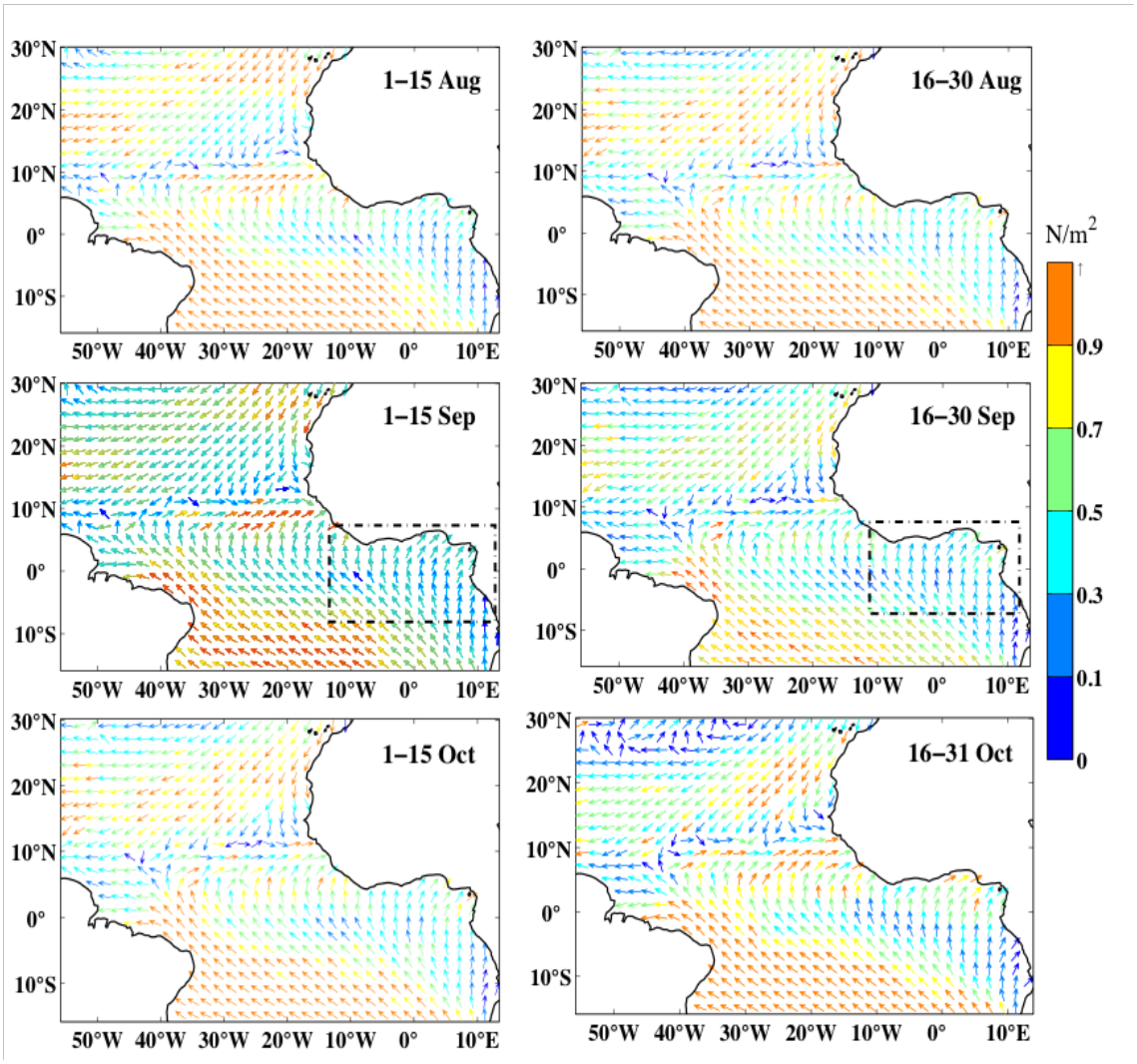

Figure 6.23. *Biweekly wind stress fields between August-October 2007. Weaker southeasterly winds observed in September in the Gulf of Guinea (boxes), with values less than 0.5 Nm^{-2}.*

that intensify in spring. Because the near-surface properties of the region are highly sensitive to high-frequency winds of e.g. 2-20 days (Athie et al., 2009), they can decrease remarkably the imprint of TIWs and their zonal signature on SST.

This analysis shows that the waves are almost non-existent in the summer of 2007 compared with other years. The question now is whether the high-frequency winds have damped the waves, allowing stability in the near-surface water properties and hence the increase in SST? Wind stress fields at sub-monthly time

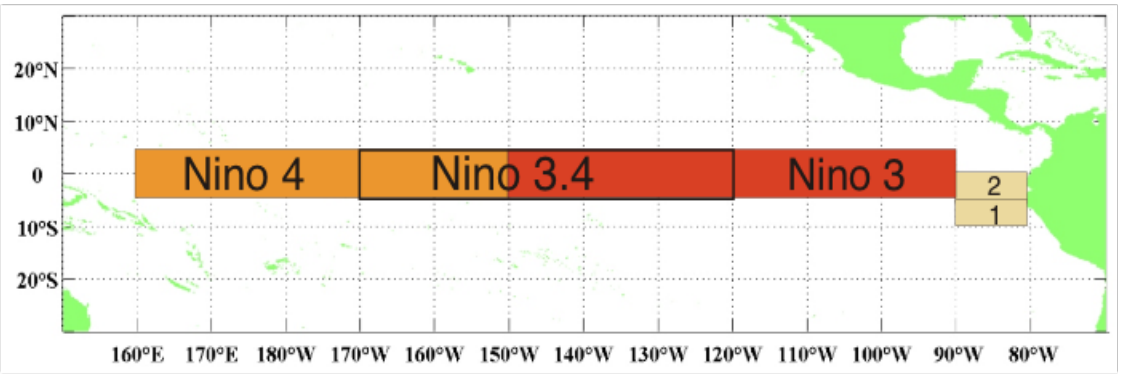

Figure 6.24. *The tropical Pacific Ocean showing the regions from which major climate indices are calculated. These include Niño 1+2, 3, 3.4 and 4.*

scales are presented (figure 6.23) between August and October 2007. In September, the winds are weak, leading to damping of the waves (figure 6.22), and hence allowing warming of SST to persist in September 2007. Therefore, I suggest that the weakening of the southeasterly winds leads to persistence in SST warming. Consequentially, the warming might have a profound effect on convection and hence the abnormal rainfall events observed in September 2007.

6.3.6 Teleconnection: Pacific ENSO

The El Niño /Southern Oscillation (ENSO) is recognised as one of the major climate indices that has a major impact on large-scale atmosphere-ocean processes. It was noted that while Atlantic SST anomalies are developing, the Pacific anomalies has already developed in the eastern tropical region and reach their maximum in March-April-May (Colberg et al., 2004; Hu and Huang, 2007; Münnich and Neelin, 2005). This suggests a connection between the two oceans possibly through thermodynamic processes. The ENSO-induced wind anomalies are responsible in driving the upper ocean temperatures by altering the Ekman pumping, meridional heat transport and net surface heat fluxes (Colberg et al., 2004). Similarly, ENSO was found to influence the western equatorial Atlantic wind stress, which in turn affects the general dynamics of the equatorial region (Münnich and Neelin, 2005). The description of the Pacific and Atlantic Niño

indices considered in this chapter are summarised in table 6.1. It is deemed necessary to repeat an earlier figure from chapter 2 that describes the regions from which the indices are calculated and this is shown in figure 24.

Table 6.1. *Description of Pacific El Niño Indices*

Index	Description
Niño 1+2	80°W-90°W and 0°-10°S
Niño 3	90°W-150°W and 5°S-5°N
Niño 3.4	120°W-170°W and 5°S-5°N
Niño 4	150°W-160°E and 5°S-5°N

Other studies reveal that there are connections between the Atlantic Niño and the Pacific ENSO events (Latif and Grötzner, 2000; Wang, 2006). Many authors studied the influence of the Pacific SST anomalies on the Sahelian rainfall (Janicot et al., 2001; Joly and Voldoire, 2010; Rowell, 2001). Results from these studies highlighted the important of atmospheric circulation in causing the Sahel drought. It is therefore importance to relate this phenomenon to rainfall variability in the study region. The aim of this subsection is to identify and describe the possible correlations between the Pacific Niño and rainfall over West Africa and the Sahel. This also provides the means to highlight the lead-lag relationships between the correlated indices. The locations of Pacific Niño indices are shown in figure 6.24.

Correlation analysis between West African and Sahel rainfall and the Niño indices (figure 6.25, and table 6.2) shows various indications of relationships between rainfall and the Pacific SST anomalies. In figure 6.25a, it is shown that rainfall and Niño 1+2 are correlates (r=-0.18) at zero lag, while Niño- 3 and 3.4 are correlated at r=0.17 and r=0.15 with rainfall leading for 3 and 2 months respectively. Niño 4 correlated with rainfall at r=0.17 and Niño leads with 1 month. For the Sahel (figure 6.25b), Niño 1+2 are correlated at r=-0.12 also at zero lag, while Niño 3 and 3.4 are correlated at r=0.15 and r=0.14 with rainfall leading with 4 and 3 months respectively. Niño 4 correlated with rainfall at r=0.18 and Niño leads with 1 month. All correlations are significant at 95% confidence interval, but they explain very little of the signal at these intervals.

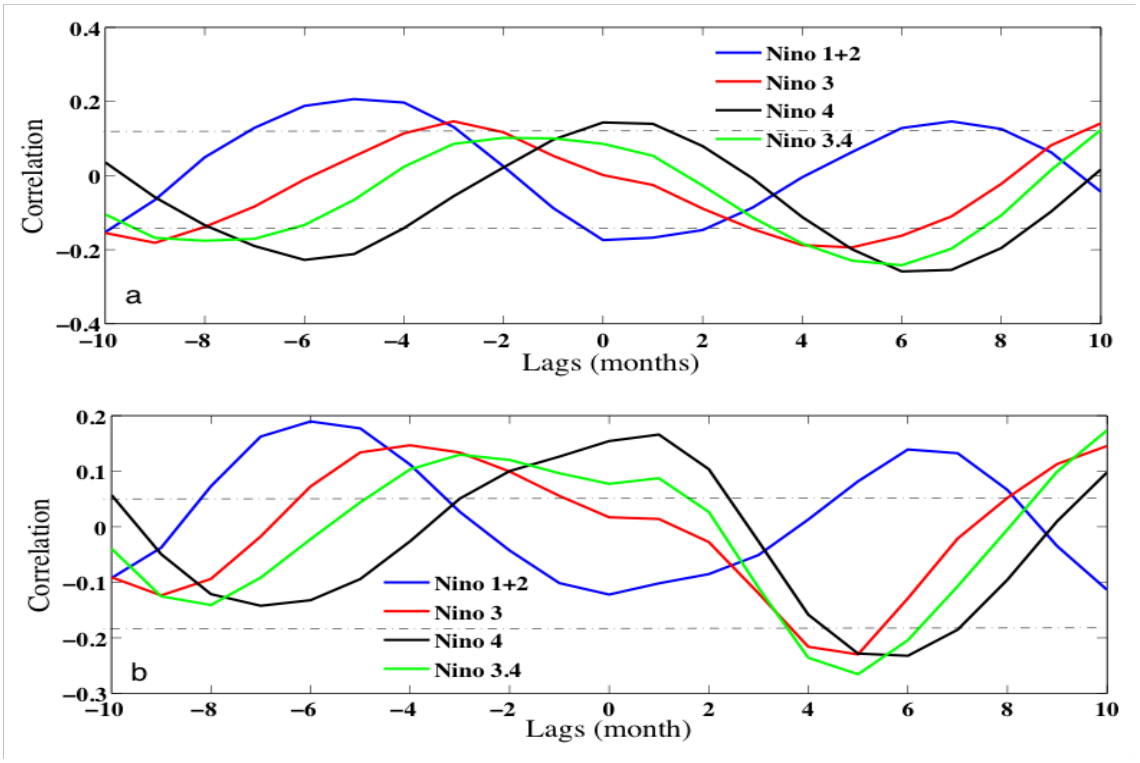

Figure 6.25. *Correlation analysis (lagged) between anomalies of Niño indices and anomalies of a) West Africa rainfall, b) Sahel rainfall. Dash-dot lines show the 95% confidence limits. Lags are in months. Integral time scale is based on 12 years of data (1998-2009). This correlation is prescribed in full seasonal cycle but with annual signals removed to correspond with the Niño data. Positive x-axis means Niño leads.*

Table 6.2. *Summary of correlations (r) between Niño Indices and West Africa and Sahel rainfall shown in figure 6.25.*

Correlations	Niño 1+2	Niño 3	Niño 3.4	Niño 4
West Africa rainfall	-0.18	+0.17	+0.15	+0.17
Sahel rainfall	-0.12	+0.15	+0.14	+0.18

When these are correlated at 99% confidence interval, the correlations showed better relationships.

6.3.7 Teleconnection: Benguela Niño

The Benguela Niño is the warm and cold episodes that are confined only to the Angola and Namibia regions in the south Atlantic (Florenchie et al., 2003; Shannon et al., 1986). Analogous to the Pacific, the warm phase is called Benguela

Niño and the cold phase Benguela Niña.

Carton and Huang (1994) suggested that the Benguela Niño might be remotely forced since it exhibits characteristics similar to the warming of the Atlantic Niño, which corresponds with weakening trade winds near Brazil. Most importantly, the Benguela Niño does not occur during its counterpart in the Pacific. It however, modulates local rainfall anomalies through heat and moisture fluxes in Angola/Namibia regions. This could result in flooding during warm years at the coasts and affect fisheries as well as feeding the dry inland regions with rainfall (Rouault et al., 2003a).

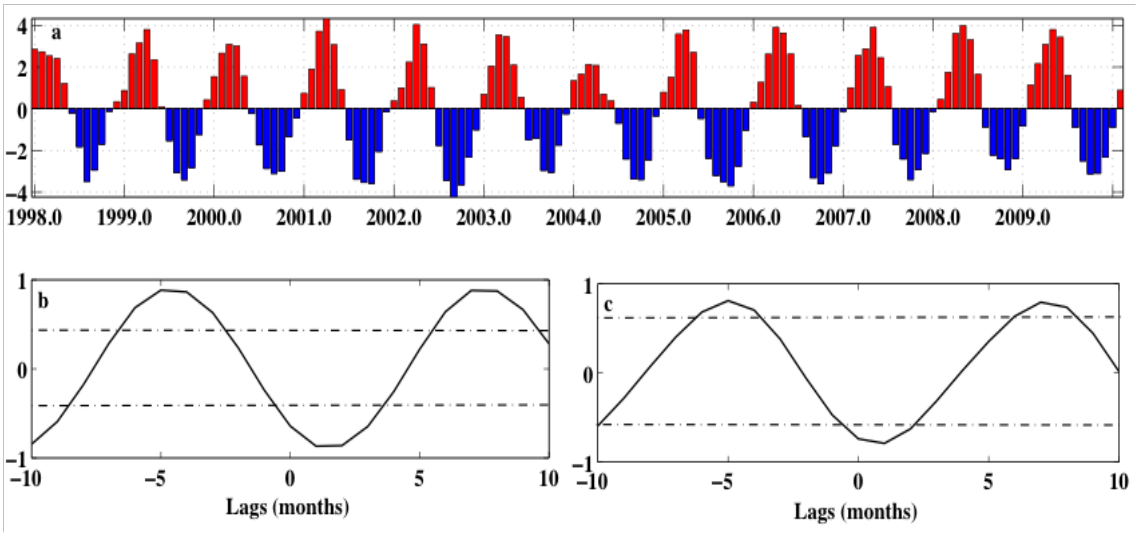

Figure 6.26. *a) Benguela Niño Index is the SST anomalies averaged over [10-20° S, 8-14° E], b) lagged correlation between Benguela Niño Index and West Africa rainfall anomaly and c) lagged correlation between Benguela Niño Index and Sahel rainfall anomaly. Lags are in months. Positive (negative) lags means that rainfall lags (leads) Benguela Niño Index. Dash-dot lines show the 95% confidence limits. Integral time scale is based on 12 years of data (1998-2009). Positive x-axis means Niño leads.*

Because Benguela Niño is a part of the global atmospheric circulation, warming events could impact atmospheric instability by enhancing or reducing the speed of the trade winds as well as moisture transport. Besides, the Benguela region is along the path of the southeast trade winds that convey moisture to West Africa (monsoon). Generally, south Atlantic SST is the source of moisture for both southern and West African regions throughout the year (Reason et al., 2006). It is therefore essential to find possible correlations between rainfall anomalies

in West Africa and the Sahel in response to changes in the Benguela Niño. This might imply possible reasons on why monsoon delays in some years.

I focus on this analysis by studying the correlations between the Benguela Niño and rainfall indices over West Africa and the Sahel. The Benguela Niño (figure 6.26a) is an averaged SST anomaly over the region (10-20°S, 8-14°E). The time series shows strong seasonality each year with warm events during the austral summer to austral autumn (December-May), and cold events during winter and spring. A remarkable interannual variability is observed especially in 2004, when warming is exceptionally low with SST anomalies 2°C less than other years. The years 1998 and 2000 also showed a reduced warming, while years 2003 and 2008 show weak negative anomalies. These kinds of anomalous warming/cooling may have an impact on the heat and moisture fluxes at the air-sea interface with resulting consequence on convection.

To describe the strength of relationships between rainfall in West Africa and the Benguela Niño index, lagged correlation is performed between the Niño indices and rainfall anomalies over West Africa and the Sahel (figure 6.26b and c) respectively. Rainfall over West Africa correlates well with Benguela Niño (-0.9) with the Niño leading by 1 month. The Sahel also correlates well (r=0.85) with the Niño leading by 1 month.

As mentioned earlier in this chapter, before the southeast trade winds strengthen and have any impact on the West Africa and Sahel, the rainfall belt has already shifted north along the ITCZ band. Therefore, in mid-summer (June) when the cold tongue is already matured the rain belt is already north and any correlation between the two would be negative with an appropriate time lag. The time lags obtained in these two analyses suggests an SST forcing from the Benguela region would have an impact on rainfall anomalies over West Africa and the Sahel at virtually the same time. As a result, interannual variability in the Benguela Niño will impact on changes in rainfall over the regions.

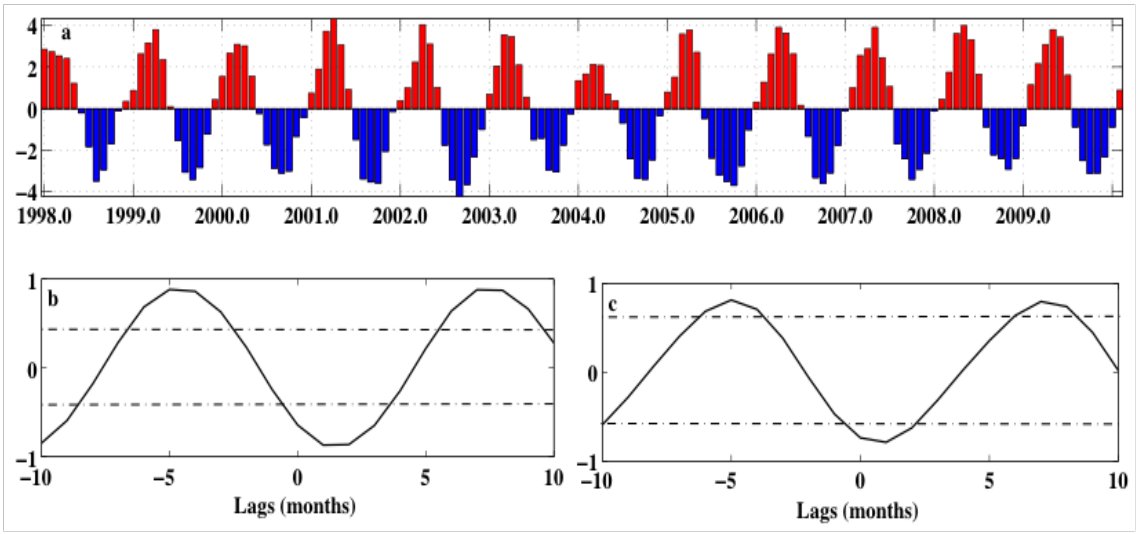

Figure 6.27. *a) Time series of Mediterranean SST anomalies index averaged over the whole region [31-40° N, 1° W-36° E], b) lagged correlation between Mediterranean Index and West Africa rainfall anomaly and c) lagged correlation between Mediterranean Index and Sahel rainfall anomaly. Lags are in months. Positive (negative) lag means that rainfall lags (leads) Mediterranean Index. Dash-dot lines show the 95% confidence limits. Integral time scale is based on 12 years of data (1998-2009). Positive x-axis means Niño leads.*

6.3.8 Teleconnection: Mediterranean SST

From the analysis using atmospheric general circulation models, Global Precipitation Climatology Project (GPCP) and gauge data, Rowell (2003) observed that warm Mediterranean SST primarily enhances moisture from its local origin and advect it through the mean flow into the Sahel region. He found that anomalies of SST in the Mediterranean Sea were correlate well with Sahel rainfall during boreal summer. During warmer SSTs, there were increased evaporation leading to higher moisture convergence that enhances rainfall over the Sahel. A similar study by Jung et al (2006) also confirms this with northerly winds helping to advect the moisture-laden air into the Sahel. I attempt to develop on these studies using more recently observed data that has higher spatial and temporal resolution than the previous studies. For example, both Rowell (2003) and Jung et al. (2006) used data of 2.5° by 2.5° grids or even coarser, as well longer time averages in their analysis. Here, I use SST and rainfall records that span 12

years with spatial and temporal resolutions of 0.25° by 0.25° and 3-day averages to analyse the impact of the Mediterranean SST on the Sahel and West African rainfall anomalies.

A Mediterranean index is formed, by averaging all point SST anomalies over twelve years (1998-2009) into monthly time series. This is then correlated in terms of lags with Sahel and West African rainfall anomaly indices. This is with the intent of gaining insight into the links between each of the rainfall regions and the SST. Results here should provide a view from observation data at inter-annual time scale, and may confirm previous model studies e.g. Rowell (2003), and is considered here.

The Mediterranean index (figure 6.27a) shows colder SST anomalies during the boreal winter and spring, and warmer SSTs during summer and autumn. The interannual variably is not strong here compared to with Benguela Niño or Gulf of Guinea SST anomalies observed earlier. However, SST anomalies in 2003 is about 1°C warmer compared to other years, and colder with -1°C in 2004 and 2005 years. The interannual signal is clearly visible (figure 6.27a) which shows a significantly higher positive SST anomalies in the order of 1-2 °C during the summer of 2003 compared to other years. A similar signature of ∼1-2°C of negative SST anomalies occurred in April of 2007 and 2008, when the region experiences significant cooling. A few studies (e.g. Rowell, 2003; Ward, 1994) were dedicated to the interaction of African rainfall and the Mediterranean Sea, and most of which focused only on the Sahel. Here, I focus my analysis on the connections between the Mediterranean Sea and rainfall over West Africa and the Sahel. I separated the analysis with West Africa to that of the Sahel. The 10-day peak observed from the coherence has weak power, and and considered here as less significant.

A correlation between West Africa rainfall and the SST index is high (∼-0.94) and SST index leads with 1 month. Similarly, Sahel rainfall also correlates high with the SST index (∼-0.9), and SST leads with 1 month. This concurs well with precious studies that suggested Mediterranean forcing of the Sahel. The

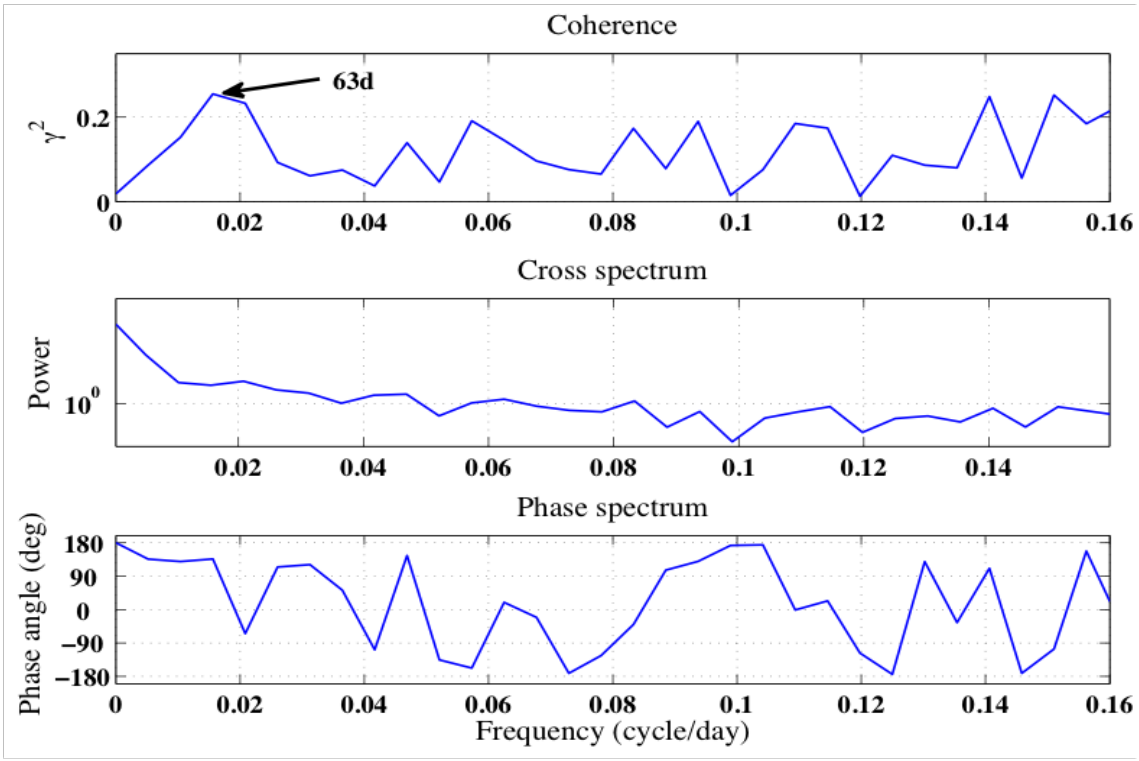

Figure 6.28. *Coherence squared amplitude, Cross Power Spectral Density (CPSD) and Phase Spectrum of the seasonal signal between anomalies of the Mediterranean SST and the West African rainfall (3° N-12° N,18° W-16° E). Data are for the period (1998-2009), and seasonal cycle from the long-term mean is removed. Both coherence and CPSD are estimated via Welch periodogram.*

strength of correlation and the lag indicates that the Mediterranean Sea is also capable of forcing West African rainfall with the same moisture advection as it does on to the Sahel. A possible explanation is that the northeasterly dry winds that originate in the Sahel called Harmattan are weak during the summer when the Mediterranean SSTs are warmer. Therefore, the moisture-laden winds from the Mediterranean Sea can flow across the Sahel and West Africa prior to the wintertime when the northeasterly winds become stronger.

To further my investigation on the time-varying connections between the Mediterranean Sea and rainfall, I decomposed the indices using Fourier analysis (figure 6.28). Rainfall over West Africa is coherent with the Mediterranean SST mainly at 63-day period, although with very small energy as shown from the

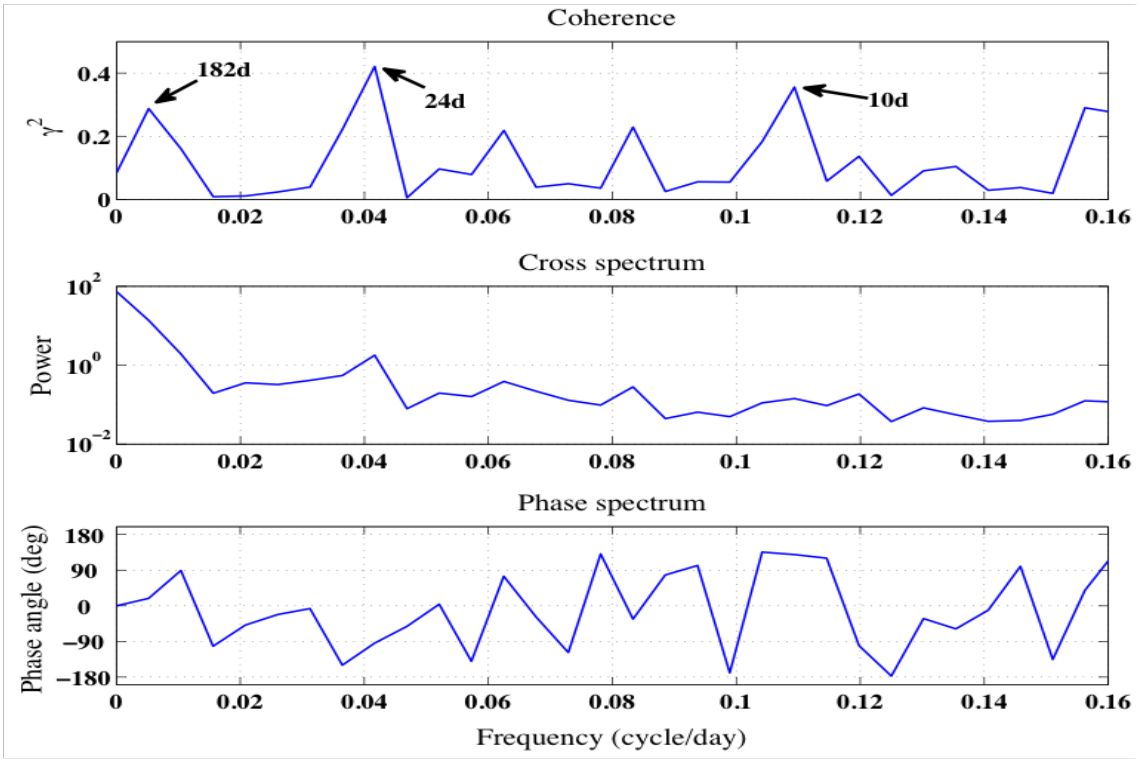

Figure 6.29. *Same as in figure 6.28, but for the Sahel rainfall region (12° N-25° N,18° W-16° E).*

power spectral density being that the data is devoid of seasonal cycle. Considering that the 63-day coherence exist at about 180° out of phase shows that they are negative correlated at this frequency. Therefore, warmer Mediterranean SST is equivalent to dry West Africa. Looking at the Mediterranean SST index, it can be deduced that convective anomalies over West African due to the former could only exist during the spring. However, because the Sahel is already dry during those periods, it may not have a strong effect compared to the influence of SSTs in the Gulf of Guinea or south Atlantic.

For the Sahel region, strong coherence exists at 24-day signal, showing a phase angle at ∼180° out of phase. This strong coherence (0.43) show a negative correlation rainfall over the Sahel. However, coherence at 182 days indicates a second harmonic signal that is associated with the Mediterranean SST (see figure 6.27a), but at the same phase (zero), indicating a mutual relationship. For the fact that both SST and rainfall have high coherency and are at the same

phase angle signifies that warmer Mediterranean SST coincides with wetter Sahel. This means that Mediterranean SST anomalies can cause positive rainfall anomalies over the Sahel.

6.4 Discussion

6.4.1 Rainfall variability

Drought conditions over West Africa have been attributed to both remote forcing and negative SST anomalies in the Gulf of Guinea (Fontaine and Janicot, 1996). This scenario however seems to occur either due to difference in time lag between SST forcing and rainfall, or connected to other forcing mechanisms rather than the Gulf of Guinea SST. For example, small magnitudes of rain rates are evident in the years 2004 and 2005 (figure 6.5). A likely possibility is that temperatures in the central tropical Atlantic could enhance convection and rainfall when the northeasterlies are strong.

A break in rainfall is observed off the Gulf of Guinea (south of 3°N) in February and early April of 2006, and later a high magnitude rain band become largely visible from late April to early May. This heavy rainfall pattern corresponds to the weakening of the equatorial winds and an increase in temperatures. In spring, the sun is directly overhead and the incident solar radiation raises SSTs to above 27°C from 8°S-5°N (Xie and Carton, 2004). This supports convection, especially at the Guinea coast and further north. As time goes on, southerly winds begin to strengthen, and the thermocline uplifting leads to cooling of SSTs. Since SSTs must reach a certain threshold (at least 26°C, e.g. Gu and Adler (2004)) for convection to initiate, the cooling effect due to the cold tongue would suspend the impact of SSTs on convection. This might explain the break in rains and dry spells observed during the years.

The West African monsoon system is in fact directly related to SSTs in the Gulf of Guinea, therefore an SST anomaly in that region is likely to influence rainfall

(Joly and Voldoire, 2010). Because SST is modulated by the monsoon winds, year-to-year variations of these winds could affect rainfall due to the modification of heat fluxes. Relaxation of trade winds due to other dynamical factors south of the Guinea Gulf therefore has potential impact on the SST anomalies. What appeared in 2001 and 2003 (figure 6.7) is, in a sense partly explained by the strengthening (weakening) of the winds in 2001 (2003) during the boreal summer. Contrasting these years in figure 6.8 shows that wind speed anomalies in 2001 are twice larger than that of 2003, thereby inducing stronger surface cooling in 2001 than in 2003.

Many studies for example (Grist and Nicholson, 2001; Gu and Adler, 2004) highlighted that the Sahel rainfall is primarily modulated by atmospheric phenomena related to African Easterly Jets (AEJ), African Easterly Waves (AEW), Tropical Easterly Jets (TEJ) and low-level southwesterly flow. Results here shows that SST anomalies of e.g. 1998, 1999 and 2003 (figure 6.7a) are concurrent with rainfall anomalies (figure 6.9a) of the same years. This means that SST anomalies could impact changes in precipitation, although this might not be independent done. The atmospheric winds, for example AEJ and AEJ could also influence rainfall either negatively or positively by interrupting the ITCZ, or independently modulating rainfall over the land.

Although, the influence of surface winds in the western basin modifies the eastern basin through Bjerknes feedback, changes in SSTs in the east (Gulf of Guinea) is largely due to amplified southerly winds that generate the cold tongue by intense upwelling. This occurs during the onset of the summer monsoon (Mitchell and Wallace, 1992). Busalacchi and Picaut (1983) demonstrated that the semi-annual signal in the Gulf of Guinea is driven by zonal and meridional wind stresses west of the Gulf.

While the annual cycle in the tropical Atlantic is due to the presence of the warmest SST north of the equator and the meridional march of the ITCZ that carries strongest rainfall, the semi-annual cycle is controlled by upwelling and downwelling which is only partially attributable to semiannual changes in the

wind (Philander and Pacanowski, 1986). Equatorial upwelling in the Gulf of Guinea is predominantly associated with the divergence of the meridional Ekman surface flow (Philander and Pacanowski, 1986). This flow is also associated with the variability of the cold tongue that helps to modulate the SSTs during the boreal summer.

6.4.2 SST vs drought

The cooling effect in 2005 is attributable to the basin-wide strengthening winds (figure 6.8), which induced a shallow thermocline consistent with the tropical Atlantic mode of variability (Houghton, 1989; Marin et al., 2009). The strengthening of winds north of the equator significantly weakens rain-bearing southeasterly monsoon winds, thereby inhibiting moisture convergence over West Africa and the Sahel regions. Hastenrath et al. (2007) attributed the cause of the 2005 drought in east Africa to pressure changes associated with strong westerlies while using NCEP/NCAR reanalysis data. My investigation here using satellite observations show that the strengthening of the westerlies (figure 6.8) north of the equator is largely a factor. However, the strengthening of southeasterlies in the Gulf of Guinea can dominate the influence of ocean forcing over West Africa since the monsoon winds are driven by the southeasterlies due to ocean-land-atmosphere temperature gradient.

Although, development of the cold tongue is based on the impact of trade winds that increases currents, which then shoals the thermocline (Houghton, 1989), seasonal evolution and maintenance of the cold tongue depends on dynamical processes. These processes include heat flux divergence, vertical and horizontal advection and vertical mixing due to tropical instability waves (Peter et al., 2006), which are common to both Atlantic and the Pacific oceans.

The summer of 2005 (figure 6.13) shows substantially strong negative SST anomalies than the preceding years. It has been indicated from Reynolds SST anomalies that such a strong negative anomaly was only recorded in 1983 and 1997

during the last decade (figure 6.13 Marin et al., 2009). Polo et al. (2008) pointed out that the Atlantic Niño leads the Pacific La Niña and the later is only connected to West African rainfall anomalies rather than the Sahel. The connection of the Pacific Niño to West Africa and Sahel rainfall anomalies are treated later in this chapter. Near surface processes that affect the development and maintenance of the cold tongue are essentially important factors in determining this kind of variability in SST. These processes and local wind effect are thought to be the major causes of this strong cooling in 2005 (Marin et al., 2009), while surface heat fluxes only act as negative feedback to the SST (Foltz et al., 2003; Foltz and McPhaden, 2006). The implication of this is that rainfall magnitudes are drastically reduced at times when SST can have an influence such as in late-May to mid-August (figure 6.12).

6.4.3 SST vs flood

The warmer SSTs in the later period of 2003 (figure 6.13) summer also show a simultaneous rainfall peak in August (figure 6.15b). Comparing SST anomalies for the whole decade (figures 6.11,6.13,6.14), the summer of 2007 exhibits an obvious positive SST anomalies that is greater than 2°C. This concurs well with the delayed summer season in West Africa (Levinson and Lawrimore, 2008; NIMET, 2008; Thomson, 2007).

The year 2007 shows two important peaks of rainfall in July-August and August-September (figure 6.15c) with a break in rainfall in-between the two periods. These coincide with the period of above average rainfall record in August-September 2007 that drew the attention of media and scientists in that year (Niles, 2007; Team, 2007). Although, the flood affected almost the whole of West Africa and the Sahel, it wasn′t widespread but affected some selected regions (Paeth et al., 2010).

While various studies, for example (Itiveh and Bigg, 2008; Paeth et al., 2010) were dedicated with interest to finding the causes of the flood in West Africa

and the Sahel, station data for the same period and places have not yet being documented. If SST might serve as explanation for the flood in West Africa, then Sahel may have been modulated by SST anomalies of the Mediterranean Sea or eastern tropical Pacific (Paeth et al., 2010). However, the intense SST anomaly of September 2007 in the Gulf of Guinea (figure 6.14) that has a magnitude of over three times that of other years should never be underestimated. Besides, the anomalous signature is not just a few patches but covers the whole Gulf of Guinea region, and may potentially explain the cause of the floods. Furthering this analysis with station data for all the affected areas by correlating with SST over the Guinea Gulf and other atmospheric variables is essential to provide further insight.

6.4.4 Teleconnection patterns

The Atlantic Meridional Mode Index (AMMI) correlates well with West Africa than with the Sahel (r=0.96 and 0.92 respectively) and leads West Africa by two months and Sahel by one month (figure 6.20b). The reason behind stronger correlation with West Africa is because AMMI influences the meridional migration of the ITCZ and the ITCZ path crosses over all of West Africa but not all of Sahel region. The repeat cycle in the lagged correlations show an annual cycle, which is the major mode of variability in the tropical Atlantic. In both cases, lagging of rainfall could explain that the negative AMMI phases have greater impact on rainfall than the positive phases. Since AMMI is a part of the WES-feedback mechanisms and the inter-hemispheric migration of ITCZ, it would play a significant role in determining the rainfall pattern through the SST. The interannual variability of AMM has also being studied previously (Mehta and Delworth, 1995; Moura and Shukla, 1981; Servain, 1991), and the out-of-phase relationship with opposite signs between the south and the north regions were apparently seen. The AMM involves a positive feedback between surface winds

of Wind-Evaporation-SST (WES). WES feedback involves response of southeasterly winds to strong northern equatorial SST gradients resulting in the weakening of northeasterly winds thereby warming the SSTs that once initiated the response. However, even though WES destabilises the AMM, it is not likely that AMM itself is by nature unstable (Vimont and Kossin, 2007).

From observational data and model output, the AMM index (AMMI) was studied to identify its connection with the Guinea Dome. Both positive and negative phases of AMMI are related to interannual variability of the Guinea dome that is connected to the meridional migration of the ITCZ (Doi et al., 2009). Guinea Dome is a region of strong wind-induced Ekman upwelling that develops off Dakar from late spring to summer. This study, as well as the studies of AMMI impact on South American rainfall raises a question as to whether AMMI has a potential impact on rainfall over West Africa and Sahel. This analysis is based on cross correlation analysis (figure 6.20b), which characterise the relationships in terms of period of occurrences.

Weak correlations are observed between West Africa and Sahel rainfall anomalies and the Pacific El Niño indices. A vivid analysis shows that Niño 1+2 is more correlated to West African rainfall than with Sahel rainfall. Niño 3 and Niño 3.4 are also better correlated with West African rainfall than the Sahel and both lags Sahel with 1 month more than West Africa. Notwithstanding, Niño 4 and rainfall correlated almost the same and leads both regions with 1 month. This may not be unconnected with the distance between Niño 4 region and the study regions. Rainfall correlations with Niño 3 and Niño 4 show interestingly the same results. These results show clearly that rainfall anomalies in West Africa and the Sahel region can be associated with Pacific El Niño. Drought over these regions is associated with positive SST anomalies of Pacific Niño 1+2, while positive rainfall anomalies are associated with positive anomalies of Pacific El Niño 3, 3.4 and 4.

Niño 4 leads rainfall in both regions with one-month lag, which is attributable to the Niño forcing rainfall variability through the eastward MJO. Unlike the

ENSO, which is standing pattern, the MJO manifest itself as a travelling pattern propagating itself at a phase speed of 4-8m/s through the atmosphere. My calculations show that if the MJO speed is at 8m/s, then it is capable of delivering precipitation anomalies over both West Africa and the Sahel within the one-month time lag. This is for the positive MJO phase. The MJO still explains the connection between Niño 3 and Niño 3.4 and the rainfall anomalies based on its positive (negative) phases that are associated with positive (negative) rainfall anomalies. Positive/negative anomalies of rainfall are associated with positive/negative anomalies of Niño 3 and Niño 3.4 through the MJO. These correlations are weak and this attests to the fact that MJO itself is weak in the Atlantic but strong Indian and Pacific Oceans.

Latif and Grötzner (2000) attempted to explain the mechanism of connection between Pacific ENSO and the Atlantic Ocean processes. During warm ENSO events, the easterly wind stress anomalies prevail over the equatorial Atlantic. This depresses the thermocline in the west and raises it in the east. Further, the equatorial Atlantic takes time to adjust to these variations in low frequency wind stress. The depressed thermocline in the west propagates eastward and air-sea interaction amplifies the signal. This signal connects with the equatorial westerlies that modulate Sahel rainfall (e.g. Grist and Nicholson, 2001) and affect rainfall over West Africa. The process could lead/lag rainfall anomalies based on the strength of coupling processes connecting the Pacific and the Atlantic oceans. The positive (negative) relationships are a consequence of warm (cold) phases of the ENSO signal respectively. However, a robust analysis of this is required to ascertain the mechanism put forward by Latif and Grötzner (2000) using both observational data and high-resolution general circulation models forced by ENSO.

6.5 Summary

The objectives of this chapter are to study and assess the impact of Gulf of Guinea SST on the West African and Sahel rainfall anomalies as well as teleconnections with Pacific Niño, Benguela Niño, Mediterranean SST and the Atlantic meridional mode from observational point of view. These SSTs and rainfall over land were characterised by various statistical means to highlight possible relationships.

The Gulf of Guinea SST was found to influence both West Africa and Sahel rainfall anomalies but at different time lags corresponding to the meridional shifting of the ITCZ. Coherence analysis illustrates that the links between both West Africa and the Sahel are directly related to the ITCZ positioning as well as the non-seasonal cycle of the Gulf of Guinea SST. High coherencies and stronger correlations were observed from the analysis, indicating lead/lag relationships.

A significantly enhanced rainfall over both West Africa and the Sahel was observed and this concurs well with warmer SSTs in the Gulf of Guinea. This is suggestive of the importance of Gulf of Guinea SST in Sahelian rainfall, which was previously thought to be modulated predominantly by moisture-laden westerlies (Grist and Nicholson, 2001; Gu and Adler, 2004). In fact, the northward low-level monsoon flow that aids in moisture advection was found to penetrate far north from the Guinea coast (5°N) to ∼20°N (Cook and Vizy, 2006). Therefore, the monsoons can still modulate rainfall anomalies over the Sahel (12-25°N). The influence of the SST on Sahel rainfall was more apparent in 2007, suggesting a non-dipole year from these studies due to positive correlations.

The interannual variability of SST at the Gulf of Guinea was clearly apparent and was evidently found to influence rainfall anomalies over West Africa and the Sahel. This is through the weakening (strengthening) of southeasterly winds that allow SSTs in the Gulf of Guinea to warm (cool) resulting in large (small) surface heat fluxes that enhance (reduce) rainfall. The consequences of these are flooding (e.g. in 2007) and drought (e.g. 2005). Both drought and flooding

of those years affected both regions. Results show that the period of flood corresponds with positive (warm) SST anomalies in the Gulf of Guinea, while the period of drought correspond to negative (colder) SST. Further research using station data from the affected regions to substantiate these findings is suggested.

Although, the tropical instability waves are known to warm the Gulf of Guinea SST, they are as well affected by high-frequency winds. This analysis shows that the undulating troughs and crest of the waves barely appear in summer/autumn of 2007 compared to other years. This is because high frequency winds (1-15 days) dampen the waves and allow stability in the near-surface water properties and hence the SST. This aids in convection that results in rainfall.

The Benguela Niño highly correlates with rainfall over West Africa (r=-0.9) and Sahel (r=-0.85) at the 95% confidence level, and lags by 1 month to both regions. This high correlation is indicative of its apparent non-seasonal cycle that varies according to the southeasterly winds. Because the Benguela region is along the path of the southerlies that convey monsoon convection over West Africa and the Sahel, variability in this region is important and any effect on it will undoubtedly affect rainfall.

The Mediterranean SST correlates well (r=$\sim$0.9) with both West Africa and the Sahel rainfall. The strength of the correlation indicates that the Mediterranean SST could influence even West Africa rainfall not only the Sahel by advecting moisture during its warm season. The seasonal cycle of the Mediterranean SST is linked to both West Africa and the Sahel rainfalls. The strongest coherence between this SST and rainfall over West Africa shows an annual cycle of the ITCZ convective band.

Analysis on teleconnection with Pacific ENSO shows that Niño- 1+2, 3, and 3.4 all correlates well with West Africa rainfall than with the Sahel. Also, Niño 4 correlates much better with the Sahel than West Africa rainfall. This may be connected with the distance between Niño 4 region and the study regions. However, Niño 4 can influence rainfall over Africa the two regions through the zonal

MJO pattern having a phase speed of 8m/s. Correlations for both rainfall regions and Niño 3 and Niño 4 show interestingly the same results.

The Atlantic Meridional Mode shows a similar seasonal cycle compared to Gulf of Guinea SST with differences in magnitude and the phases of warm/cold events. This difference in phases is apparent in the lagged correlation analysis, where West Africa leads AMM with 1 month and Sahel with 2 months. The strong correlation with West Africa rainfall (r=0.95) than the Sahel (r=0.9) indicates that AMM could influence the former much more than the later.

As a final note, both seasonal and annual signals related to the ITCZ and the Gulf of Guinea SST shows that, any forcing on West Africa and Sahel rainfalls cannot be entirely independent of the meridional shifting of the ITCZ or the influence of the local SSTs. Again, the region is better understood if we could know spatial and temporal variability of both the prevailing winds and the SST. Most importantly, specific regions and time of variability, direction of propagation, connections with other large-scale processes outside the tropical Atlantic domain could give a better insight to anomalous rainfall, and these are considered in chapter seven.

CHAPTER 7

Non-seasonal variability of SST and winds

7.1 Introduction

Climate fluctuations in the tropical Atlantic are dominated by two distinct patterns of coupled ocean-Atmosphere variability, collectively termed tropical Atlantic variability (TAV). These are the Atlantic Meridional Mode and the Zonal mode (also called the Atlantic Niño). These modes of variability are tightly phase-locked with the seasonal cycle and composed of the meridional sea surface temperature (SST) gradient and the zonal mode, also called the Atlantic Niño, which is a phenomenon analogous to Pacific El Niño. These variabilities play a vital role in the coupling processes with both local and large-scale winds, resulting in the modulation of upper ocean circulation and an impact on the atmospheric boundary layer. The modulation of the atmospheric boundary layer in turn is responsible for changes in the local climate and significantly contributes to the global atmosphere dynamics.

The tropical Atlantic variability modes are determined by the seasonal cycle due to solar radiation. The interannual variability of these modes are composed of

the mean, the anomaly, the seasonal cycle and the non-stationary part of the annual cycle, which is the interannual variability in the timing of the seasonal transitions. The non-seasonal variability is an important climate derivative, hence the knowledge of its underlying physical mechanisms are essential. Seager et al. (2001) hypothesised that cross-equatorial-SST gradient (CESG) is a determinant of the north-south migration of the ITCZ. I will test this hypothesis using non-seasonal variability in the region bounded by two trade winds, the northeasterly and the southeasterly winds.

This chapter focuses on investigation of spatial and temporal patterns of SST and wind fields based on non-seasonal variability. The stationary harmonic seasonal cycles are removed from the time series at each grid point to create non-seasonal anomalies for all variables (e.g. Venegas et al., 2008). The dominant space/time patterns of these fields are then studied using EOFs to highlight possible connections between the two. The main purpose of EOF analysis is to reduce the large number of variables of the original data that have been collected over time, while at the same time maintaining much of the explained variance. It is also important in discovering new meaningful underlying variables in data. I applied the Singular Value Decomposition (SVD) described by (von Storch and Navarra, 1999). These investigations also provide the means of identifying propagating signals in the SST data through the use of complex Hilbert empirical orthogonal functions CHEOF). These methods find the spatial patterns of variability inherent in each data, their time variations and give a measure of importance of each pattern. The wind data are also decomposed into the complex EOF to investigate further patterns of variability and their directions.

Datasets employed in this study are Tropical Rainfall Measuring Mission Microwave Imager (TMI) SST and QuickScat winds, both with spatial resolution of 0.25 x 0.25 and averaged over 3-days. Prior to processing, all gaps in the data have been optimally interpolated and for any missing data, an average of the previous 3-day and the next 3-day are used to replace the gap. Details of quality control of data are documented in chapter 3. Long term mean and seasonal

signal have been removed before calculation except for figure 7.1 and the atmospheric wind data.

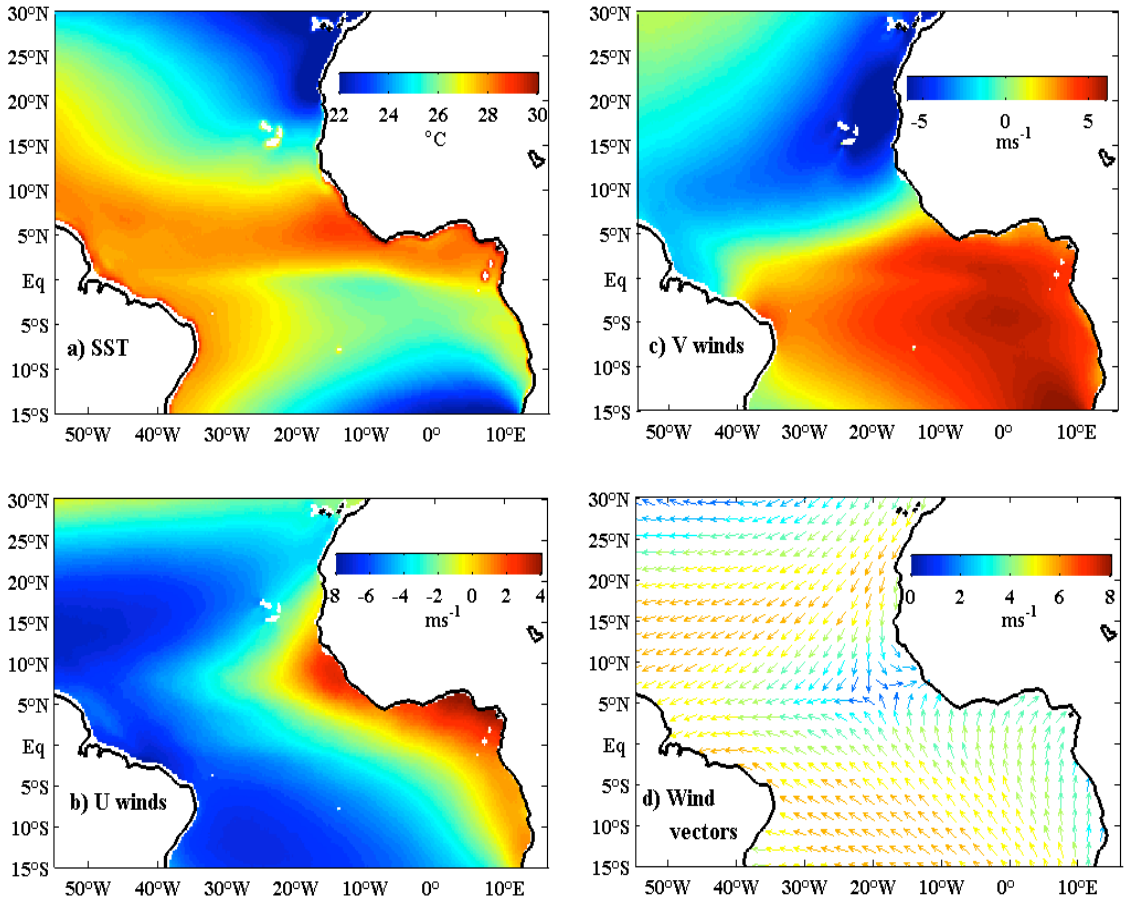

Figure 7.1. *Maps showing the mean composites of: a) SST, b) zonal wind speed, and c) meridional wind speed, d) vector of winds. Data is based on 3-day averaged composites for Jan 2000- Nov 2009 period.*

This chapter is organised as follows: 7.2) Methods 7.3) Results, 7.4) Discussion, 7.5 Summary.

7.2 Method

7.2.1 Empirical Orthogonal Function analysis

Empirical Orthogonal Function (EOF) analysis is a statistical tool used to decompose multivariate data into a set of linear, but uncorrelated functions of

the original data set. The functions are called modes and are usually ranked by their energy (variance) where the first few orders represent the principal behaviour of the decomposed signal. The main application of EOFs is that each component may be separately able to relate to different influences on the ocean signal (Robinson, 2004) Typically a few modes can provide the dominant information of the whole data in question.

7.2.2 Complex EOF analysis

The complexities associated with oceanic and atmospheric circulation in this region and their coupling warrants the need to identify both standing and propagating signals. However, EOF allows the analysis of only standing oscillations and does not take into account the propagation of the signal. That means it cannot be considered adequate for fully representing atmospheric and oceanic data since it does not provide information on propagating features (Alvera-Azcárate et al., 2005). Therefore, I thought of achieving the goal of understanding variances associated with the climate of equatorial Atlantic through the use of complex EOF and complex Hilbert EOF analyses. It is necessary to make a clear distinction between the CEOF and CHEOF here.

7.2.2.1 CEOF Analysis

This is complex EOF that employs the use of two vector fields, and its resulting outputs capable of showing amplitude and direction of a pattern. It is applicable to vector fields such as zonal and meridional winds. The zonal field is attributed to the real part of the complex vector, and the meridional to the imaginary part. The CEOF applied here is similar to Brink and Muench (1986), as discussed in (von Storch and Zwiers, 1999). Details are shown in appendix B.

7.2.2.2 CHEOF Analysis

This is Complex Hilbert EOF that is performed on a scalar field, whereby the scalar field is attributed to the real part of the complexified process and the imaginary as Hilbert transform of the scalar field. The standing oscillations of a mode are represented by the real part of both the spatial pattern and the temporal coefficients, which are similar to the conventional EOF. The additional information obtained comes from the imaginary part, which represents the signals that are identified to be related with the real part but at 90° out of phase (Cai and Baines, 2001). This allows both temporal and spatial phase relationships between the standing oscillation and its subsequent features to be determined.

Unlike the EOF that provide only standing oscillations as its variances, CHEOF has the advantage of providing an idea about propagation of the signal, and hence it can represent the data and allow estimation of both amplitude and phase fluctuations of the spatial and temporal modes of a signal. Investigating the evolution and displacement of a signal is essential in climate studies. Details of my application of CHEOF are shown in appendix B, and further details are obtainable in Jolliffe (1986) and von Storch and Zwiers (1999).

7.3 Results

7.3.1 The spatial and temporal distribution of SST and wind

The long-term spatial distribution of SST and zonal and meridional components of wind are shown in figure 7.1. SST, for example, varies between the two hemispheres, with north recording the highest temperatures. The equatorial north (∼0-12°N) stretching from the Gulf of Guinea to the west shows areas with higher SST values (figure 7.1a). The northeast region centred at 24°N/15°W is marked with lowest SST, signifying the southward flow of the North Equatorial Current (NEC). The fluctuations of the SST gradient, which is closely related to

the air-sea interaction (Czaja et al., 2002) plays a fundamental role in the current theories of tropical Atlantic variability.

For the zonal winds (figure 7.1b), stronger eastward winds are concentrated in the eastern tropical Atlantic north of the Gulf of Guinea, while stronger westward winds are at the western tropical Atlantic with maximum values centred at approximately 10°S/28°W and 15°N/45°W. The westward winds appear to be stronger than the eastward component. The meridional component (figure 7.1c), shows southeasterly trade winds to the south of the equator with maximum values of 6 m/s in the south-eastern part of the basin, and in the north, stronger northeast trade winds have a core at 18°N/16°W. The band separating the strong southward and northward winds is the average position of the ITCZ for all seasons. Interestingly, stronger zonal winds for both hemispheres are further east, if compared with the Atlantic meridional mode discussed in chapter 6 (e.g. Servain, 1991). The two wind regimes (northeast and southeast) and the SST are important elements that modulate the climate of the tropical Atlantic region.

The relationship between SST, wind and convection dominates the first harmonic of the annual cycle in response to the patterns of the ITCZ seasonal variability. Mitchell and Wallace (1992) proposed that, the reason for this behaviour lies in the response of the tropical ocean-atmosphere system to the variations of solar insolation in the presence of the north-south asymmetry of the distribution of landmasses around the equator. This is particularly apparent in figure 7.1a, where SST signatures are observed to be stronger north of the equator. This meridional dipole configuration is a part of the cross-equatorial SST gradient (CESG) discussed in chapter 4, whose interannual variability influences the coupled ocean-atmosphere system through mutual interaction with the ITCZ.

The SST anomaly time series (figure 7.2a) show the non-seasonal fluctuations of the tropical Atlantic SST. An interannual variability is clearly seen with variations of peaks and troughs during the 10-year period of the data. In these data, seasonal signal and long-term means have been removed. Therefore, the peaks

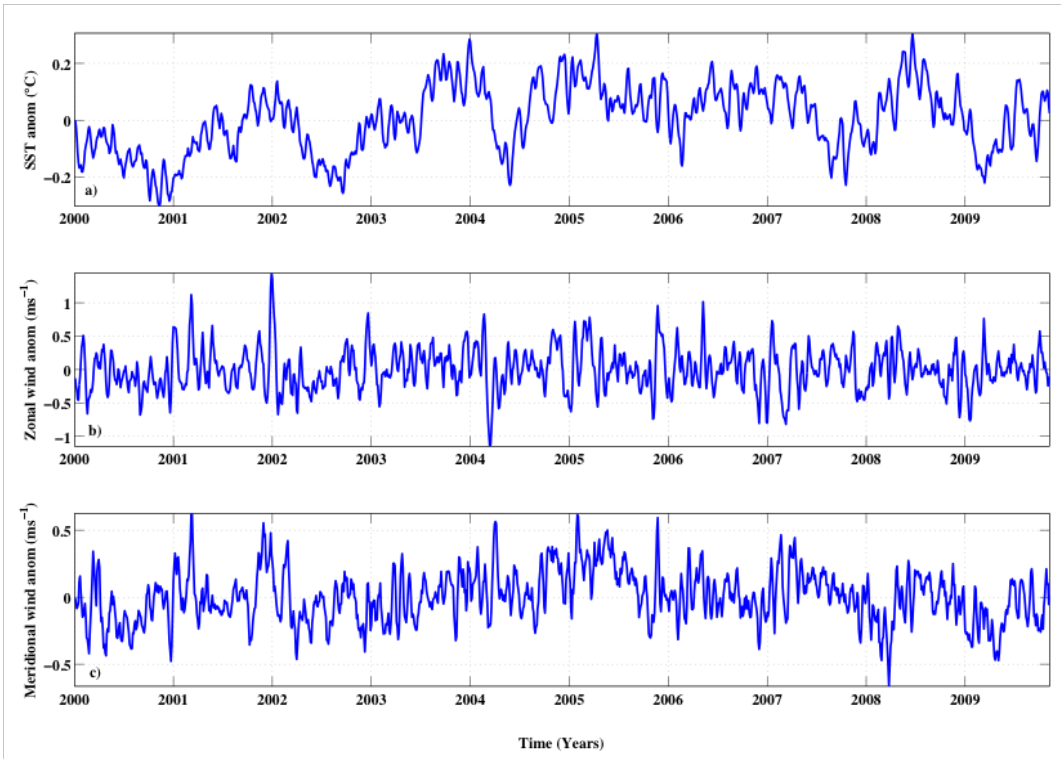

Figure 7.2. *The time series of spatially averaged a) SST, b) Zonal and c) Meridional wind components based on the 3-day means for the Jan 2000-Nov 2009 period. The time series covers the region shown in Figure 7.1, but with long-term mean and seasonal signal removed. The time series are further smoothed with a 21-day moving average.*

that appear show time variability of the signals, which highlights interestingly interannual variability. Even though the signals for each data set are smoothed with a 21-day moving average, high frequency variability is still observed in the wind data. The wind system changes faster than the SST. These time series show that zonal wind anomalies are twice as large as the meridional component.

Non-seasonal SST and wind fluctuations are best described by calculating the standard deviation. Standard deviation exceeding 1.4°C is observed from the long-term SST data (figure 7.3a) on the western flank of West Africa around Guinea Dome and north of it. The Guinea Dome is a permanent quasi-stationary feature on the eastern side of the tropical Atlantic centred at 10°N/22°W. The dome is part of a large-scale flow fields associated with the North Equatorial Countercurrent (NECC), the North Equatorial Current (NEC) and the North Equatorial Undercurrent (Siedler et al., 1992). Variability north of the Guinea

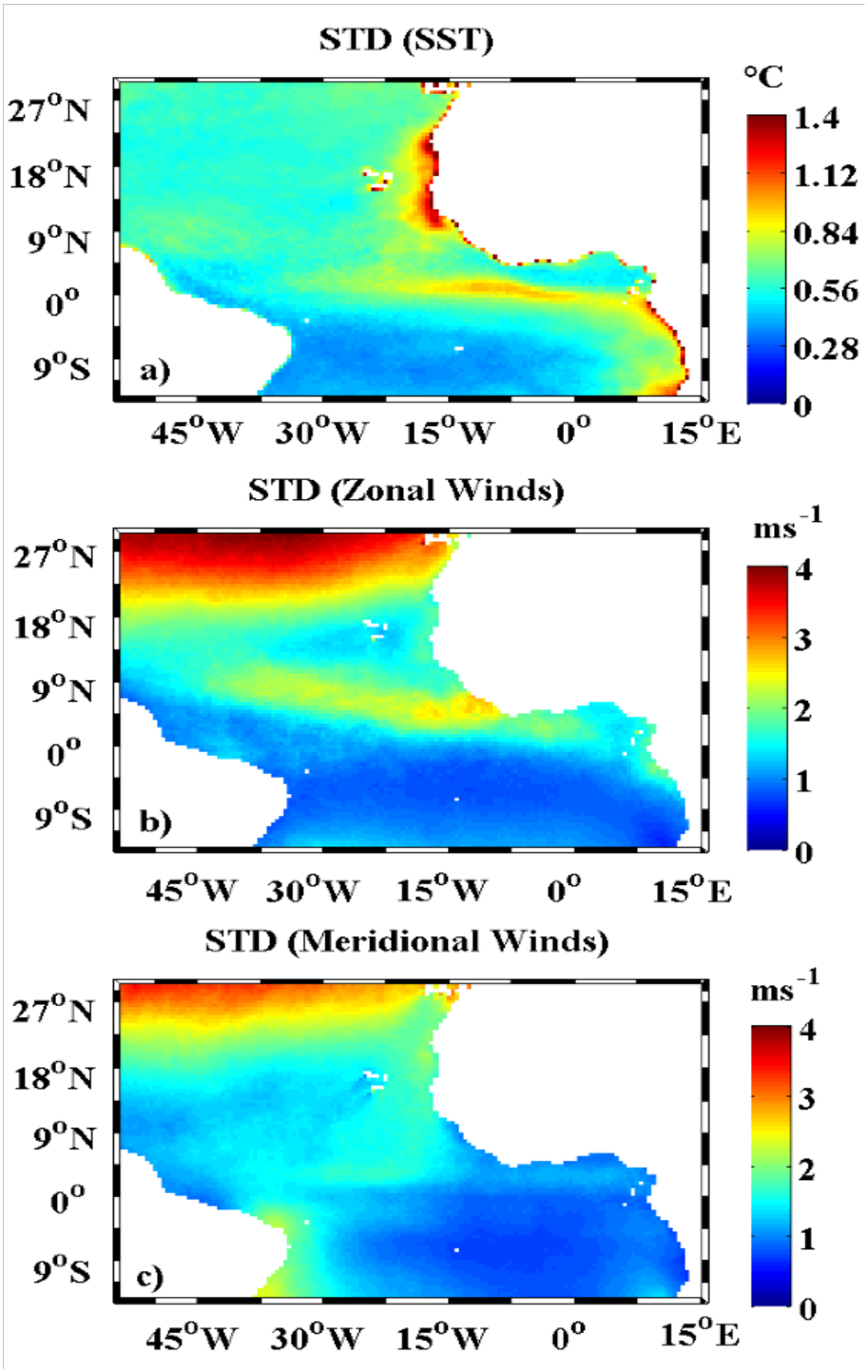

Figure 7.3. *The standard deviation of a) SST, b) zonal wind speed and c) meridional wind speed for the period 2000-2009.*

Dome is a quasi-temporary phenomenon that is associated with northward migration of the ITCZ. Westerly winds originating from the converging southeasterlies and northeasterlies cause anomalous circulation in the region resulting

wind-induced Ekman upwelling.

Another region of strong std is observed around the equator in the eastern part of the basin. This is the region of strong ocean-atmosphere coupling as a result of tropical instability waves that show strong signatures at the northern flank of the cold tongue during the boreal summer. Both zonal (figure 7.3b) and meridional (figure 7.3c) wind anomalies exhibit strong std north of 20°N that reached an std of 4m/s. Weaker std are observed south of the equator, especially around the region of the cold tongue. However, it is important to assess the long-term spatial patterns and temporal variability of both SST and wind to highlight areas and times of strongest variances. This is achievable using empirical orthogonal function (EOF) techniques.

7.3.2 EOF analysis of SST

The spatial patterns of EOF SST (figure 7.4) show areas with highest variance. The first three modes explained about 36% total variance. EOF 1 explains 17.5% of the total variance. It exhibits the tropical Atlantic dipole with an asymmetrically large variance north and south of the equator. Variations in SST between the north and south regions are the determinants of the Atlantic Meridional Mode (AMM), which is a large-scale climatic mode of the tropical Atlantic.

The second EOF shows strong variance (11.8%) accounting for about 33% of the total variance, covering the cold tongue region. The cold tongue occurs as a result of the strengthening of the southeasterly trade winds at the beginning of boreal summer that last for 5 months. Strong upwelling of near-surface cold waters from the southeastern tropical Atlantic spreads across the region and crosses the equator. The development of the cold tongue leads to a rise in sea level pressure over the equator, which further enhances the northward flow (Schott et al., 2003). The second EOF here represents changes in strength and duration of the cold tongue.

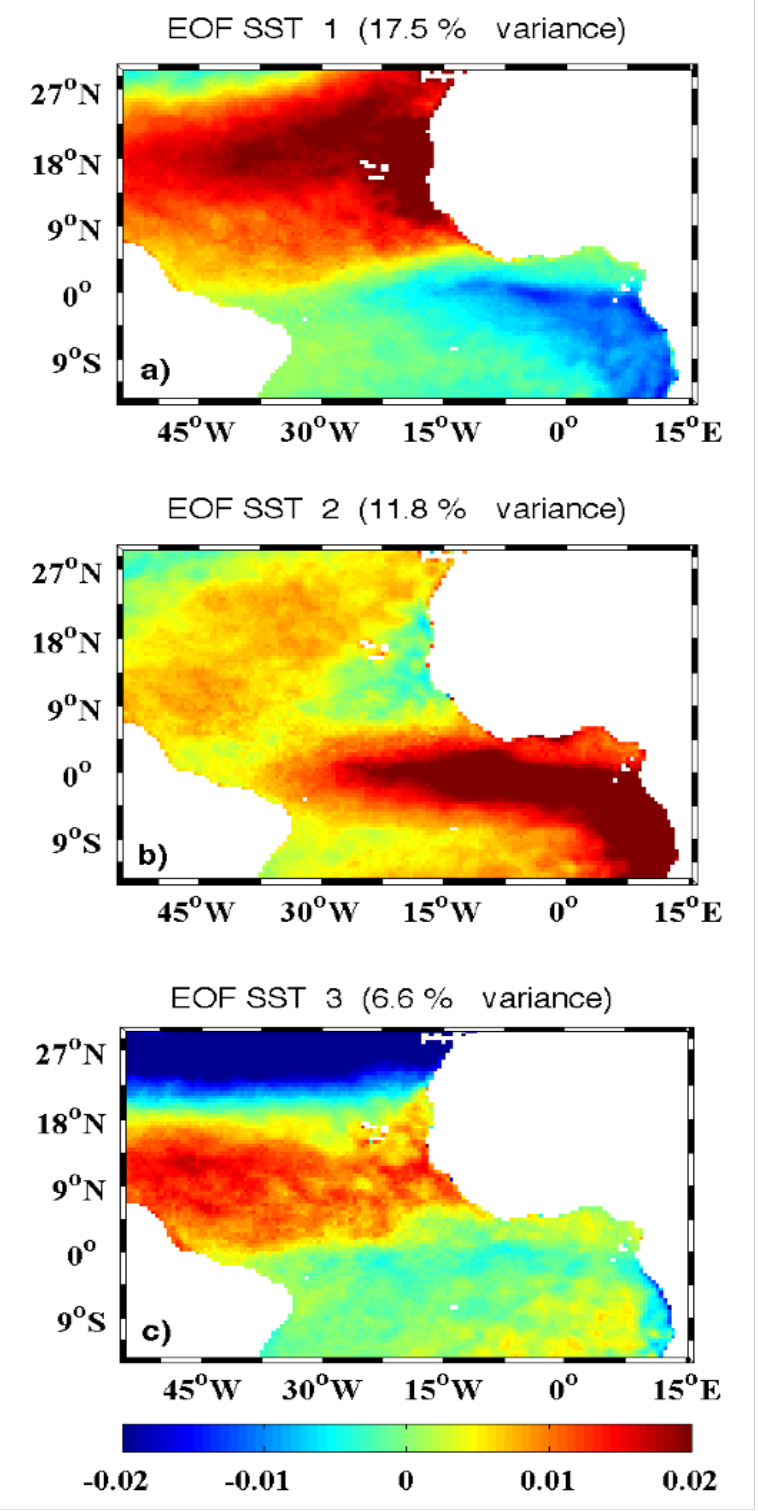

Figure 7.4. *Spatial patterns of EOF SST anomalies for the period 2000-2009. Calculations were done after removing the long-term mean based on the 2000-2009. Seasonal signal has been removed prior to EOF.*

The third EOF explains only 6.6% of the total variance and highlights two principal regions of strong variance. One between 0-18°N, owing to the northward positioning of the Intertropical Convergence Zone. These signatures represent a region where strong surface heat fluxes occur the most, leading to strong convection and rainfall during the boreal summer. The second, north of 25°N is due to other dynamical factors outside the tropical domain.

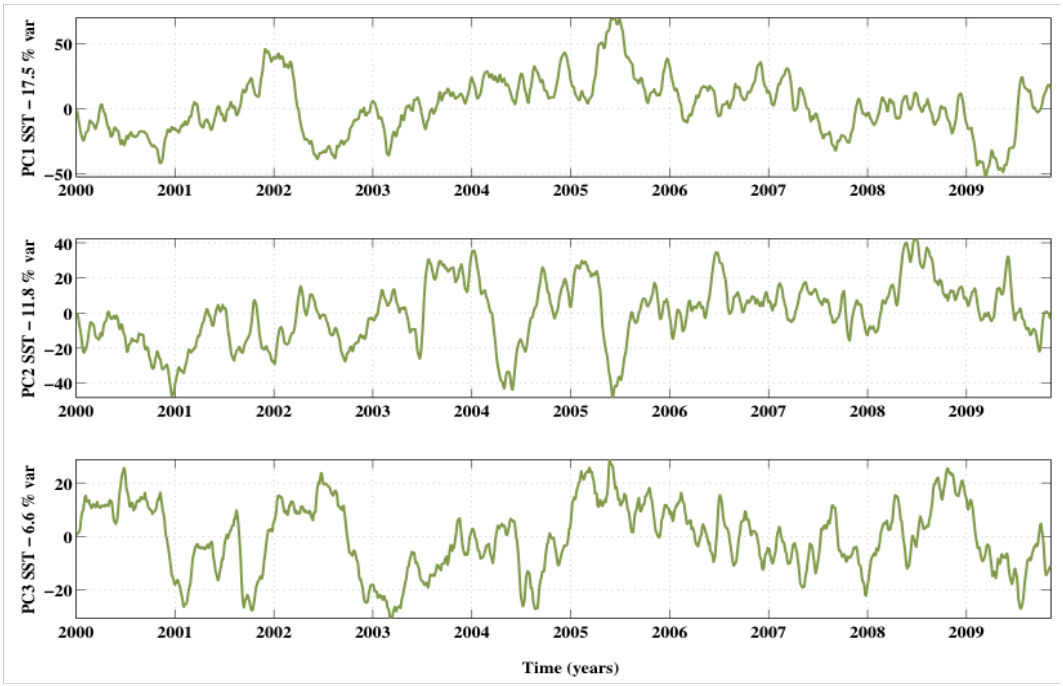

Figure 7.5. *The principal component (PC) time series of SST anomalies for the period of 2000-2009. Time series are smoothed with a 21-day moving average filter.*

The principal components (PCs) of SST are shown in figure 7.5. There are signatures of interannual variability for PC1 SST, and these occur in 2001, 2005 and 2009. Most notably in 2005, extremely cold temperatures were observed in the Gulf of Guinea as shown in chapter 6. This occurred as a result of stronger than usual intraseasonal intensification of the southeast trade winds that resulted in the rapid and intense cooling of SST in mid-May 2005. These signatures are also observed in PC2 and PC3 SST.

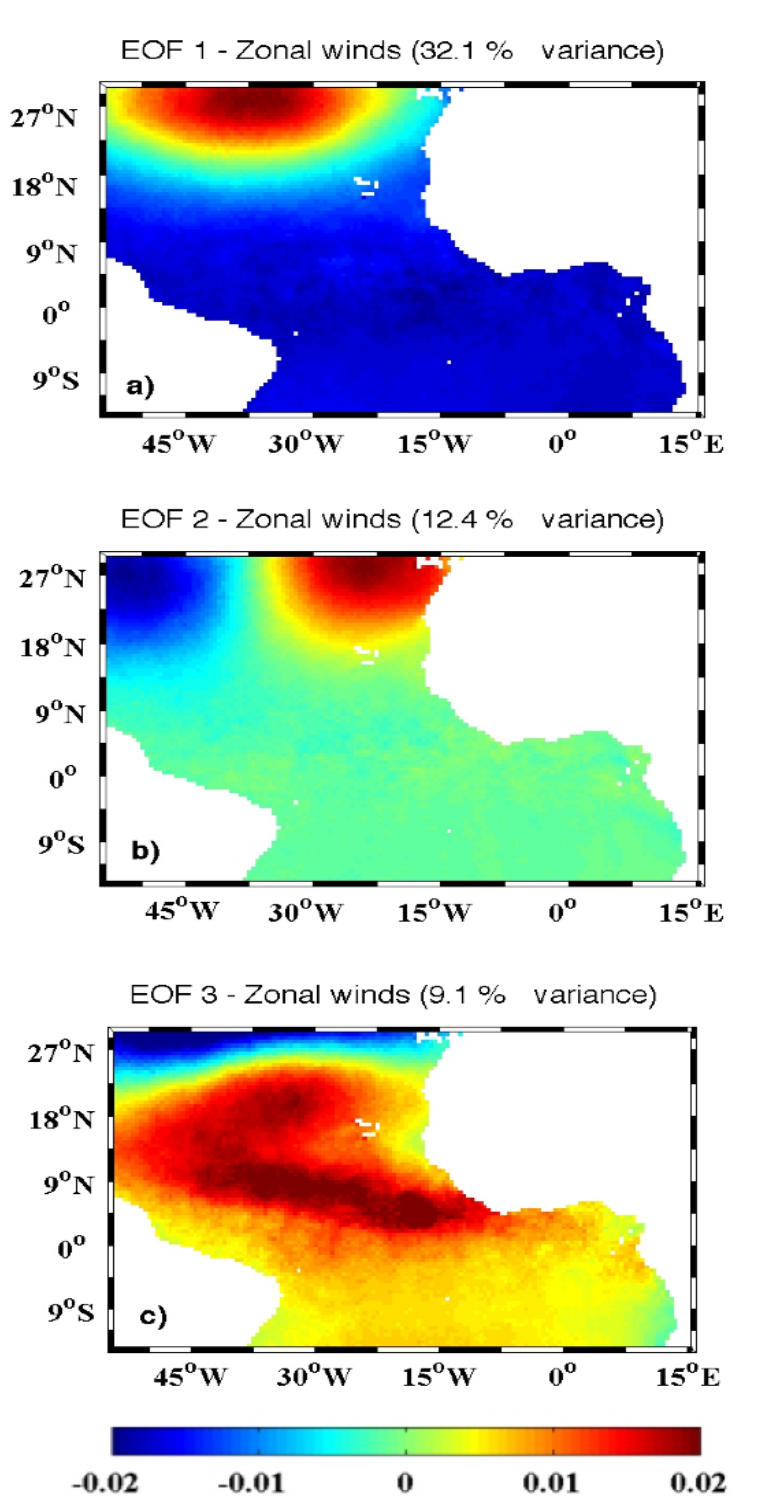

Figure 7.6. *Spatial patterns of EOF zonal wind anomalies for the period 2000-2009. Calculations were done after removing the long-term mean based on the 2000-2009. Seasonal signal has been removed prior to EOF.*

7.3.3 EOF analysis of zonal winds

The three EOF modes of zonal wind (figure 7.6) reveal total variances explained as 53.6%. The first mode (EOF 1) has a variance of 32.1% (60% of total variance explained of the first three modes). This strong variance is located north of 18°N. Similarly, EOF 2 with explained variance of 12.4% show double signatures in the same region while the rest of the region has close to zero variance. Although, they might be of the same location, their dynamic properties might differ. The third, EOF 3 has a variance of 9.1%, accounting for 17.0% of the total variance explained. Strong areas of variance are observed north of the equator between 2-25°N. A similar signature is observed in the variance plot of zonal winds (figure 7.3b), but these two do not align with the asymmetric positioning of the ITCZ (southwest-northeast) but instead crosses it (southeast-northwest). The positioning of this variance reveals high frequency variability in the region due to relative influence of southeast and northeast trade winds. The southeasterly winds that drive the cold tongue is much stronger the northeast and is more sensitive to cross equatorial SST gradient (CESG) north of the equator. When anomalous SST gradient north of the equator occur, the southeast trade winds response and eventually weakens the northeasterly winds through wind-evaporation-SST (WES). This high frequency variability associated with the non-seasonal anomalous winds lead to the occurrence and positioning of this variance.

The associated time series of zonal winds (figure 7.7) consists of a combination of local extrema and high frequency oscillations. Fluctuations of wind exhibiting local extrema in 2001, 2004, 2005 and 2007 are observed in PC1. For PC2, the peaks are observed in 2000, 2002, 2005 and 2006. High frequency variability is also observed in PC3 with very insignificant signs of interannual variability.

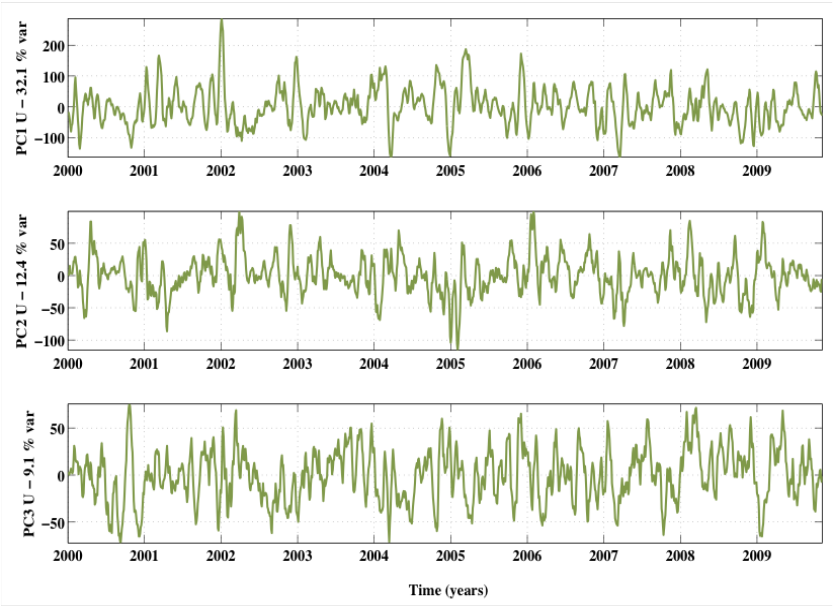

Figure 7.7. *The principal component (PC) time series of zonal wind anomalies for the period of 2000-2009. Time series are smoothed with a 21-day moving average filter.*

7.3.4 EOF analysis of meridional winds

The three leading modes of meridional wind EOFs together account for a total 45.8% variance (figure 7.8). The EOF1 exhibits a monopole pattern at two regions north of 10°N. This mode explains 21% of the total variance and is associated with the zonally propagating Madden-Julian Oscillation (MJO). To confirm whether these features are due to the MJO, investigated from zonally high-pass filtered 850hPa winds (figure 7.9) to highlight the phase of the signal. This shows that north of 10°N, atmospheric winds akin to the MJO do alter surface winds.

A similar strong variance is observed in EOF2 occurring also north of the equator that seems to be connected to that of EOF1. This EOF2 accounts for 16.9% of the total variance explained. Both EOF1 and EOF 2 show completely homogenous maps south of the equator. However, EOF3 that explains 7.9% of the total variance shows heterogeneous characteristics with larger variance west of the basin and another north of 20°N. This area of high variance west of the

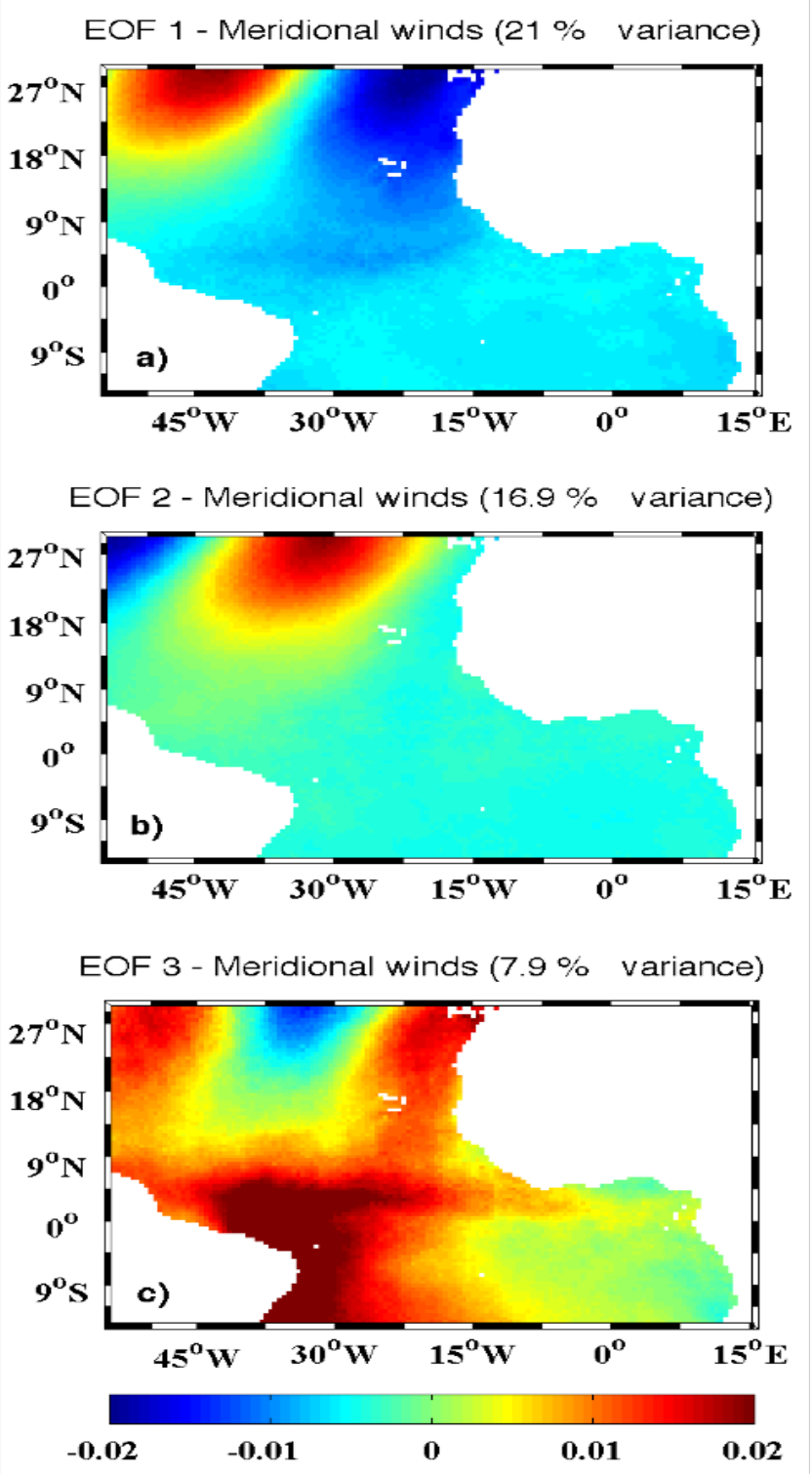

Figure 7.8. *Spatial patterns of EOF meridional wind anomalies for the period 2000-2009. Calculations were done after removing the long-term mean based on the 2000-2009. Seasonal signal has been removed prior to EOF.*

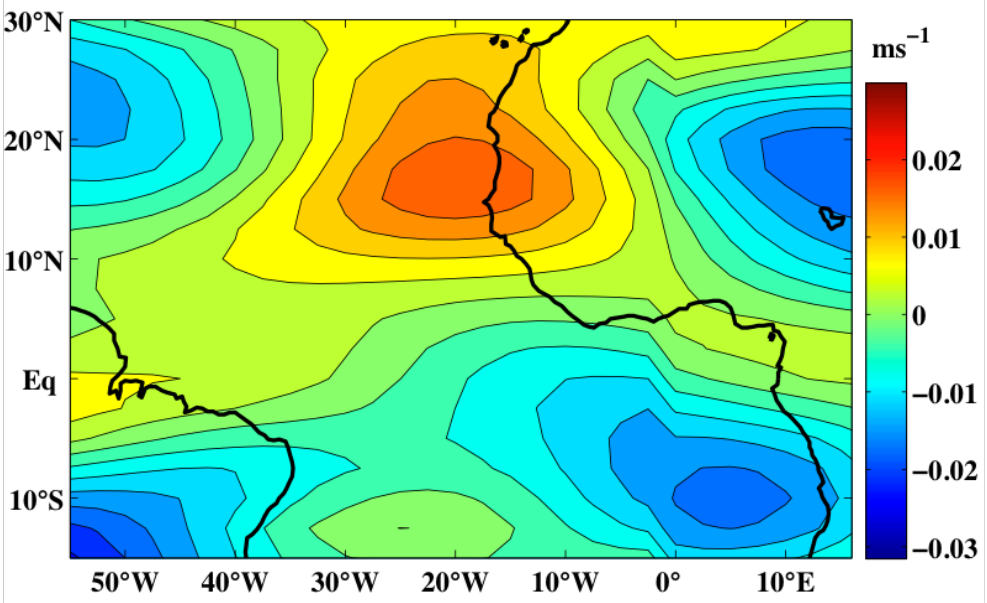

Figure 7.9. *EOF1 of the zonal 850hPa winds band-pass filtered at 30-90 day MJO pattern. Data is based on NCEP/NCAR reanalysis covering a period of 10-years (2000 to 2009).*

basin is co-located with the variability of the North Brazil Current (NBC). The fraction of the local variance explained decreases from west to east. These may effect the seesawing of the thermocline and the modulation of the Equatorial Undercurrent (EUC) and surface currents such as the seasonal North Equatorial Countercurrent (NECC). The principal components (PCs) associated with these modes are shown in figure 7.10. These consist of a combination of high frequency and interannual oscillations.

The EOF calculations described above are able to highlight regions having variances with strongest amplitudes of both known and unknown features. The known features include the dipole mode of the tropical Atlantic, the cold tongue region and the position of the ITCZ north of the equator in relation to Atlantic thermal equator. These appear very clearly in SST data despite using data devoid of mean and seasonal cycle. The three EOF patterns of zonal winds and EOF-1 and -2 of meridional winds are not clearly identified with known phenomena in the tropical Atlantic. However, EOF3 of meridional winds is identified with the changes in oceanic circulation akin to the flow of North Brazil Current (NBC). The associated expansion coefficients (PCs) also show amplitudes

of high frequency and interannual oscillations. However, some limitations exist in the use of EOFs without the ability to identify certain characteristic from the variance maps or their principal components. For example, the strong variance in EOF1 meridional winds east of the basin may be associated either with the MJO or variability of the northeasterly winds. The standard EOF analysis however, is not sufficient to ascribe this mode to any of them without knowing its directional characteristic. I therefore, advance this investigation by studying these variances and their expansion coefficients (PCs) based on information derived from both their standing oscillations and propagation characteristics using complex and complex Hilbert EOFs.

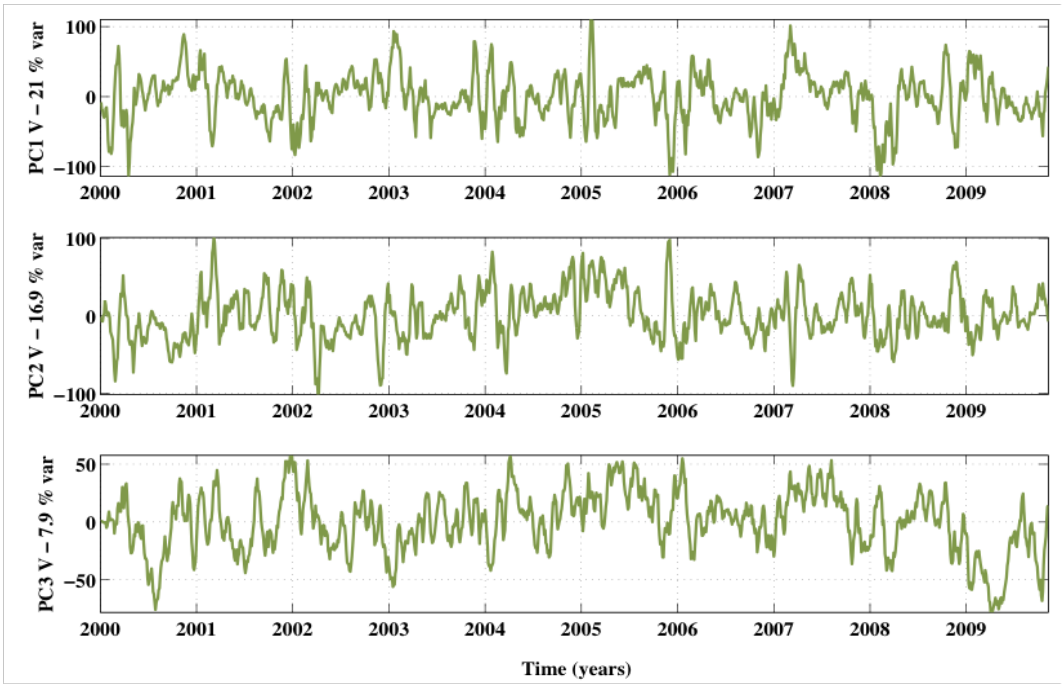

Figure 7.10. *The principal component (PC) time series of meridional wind anomalies for the period of 2000-2009. Time series are smoothed with a 21-day moving average filter.*

7.3.5 Simulation of EOF and CHEOF

For the benefit of extracting additionally important information from scalar fields, notably SST, which the standard EOF does not provide, I have done a number of experiments on these data. First, I experimented by calculating

CHEOF and then transforming it in the Hilbert space (HCHEOF), but the resulting output could not provide any useful information. The reason is that I expected to observed propagating signals as well as the ability of the HCHEOF to show most of the percentage variance from very few modes. I then applied CHEOF on the scalar field (SST) after running a simulation to verify its ability to provide additional information from data, which standard EOF does not.

The simulated Complex Hilbert EOF and the standard EOF results for the first 10 modes are plotted in figure 7.11. The EOFSST1 show patterns of variability with the first harmonic. The second, third and fourth showed second harmonic that are tilted differently but basically the same feature is repeated. The amplitude of CHEOF however showed consistent features all the time. The CHEOF phase shows the relative position of each amplitude assigned to its phase in degrees. The first three CHEOF Phases show first, second and third harmonics allowing the ability to infer more information of a signal than the standard EOF. In contrast, the EOF has to take more number of modes to give information of a particular scalar quantity, for example looking at the three harmonics which it produces in modes 6 and 7, the CHEOF produced that with the third mode. Therefore, complex Hilbert EOFs compress the temporal and spatial variability into the lowest possible number of spatial patterns (Tokmakian and Challenor, 1993). It can provide information on the scalar pattern, as well as amplitude and phase information.

7.3.6 The Complex Hilbert EOF of SST

The time and space evolution of the SST anomalies associated with seasonal and sub-seasonal events in the tropical Atlantic can be precisely described using the complex Hilbert EOFs. The percentage variances explained as well as their cumulative values for the first 3 CHEOFs are summarized in table 7.1 and contrasted with the standard EOF SST discussed in sub-section 7.3.1.1. The first 3 are able to account for about 37.4% of the total explained variance. It is

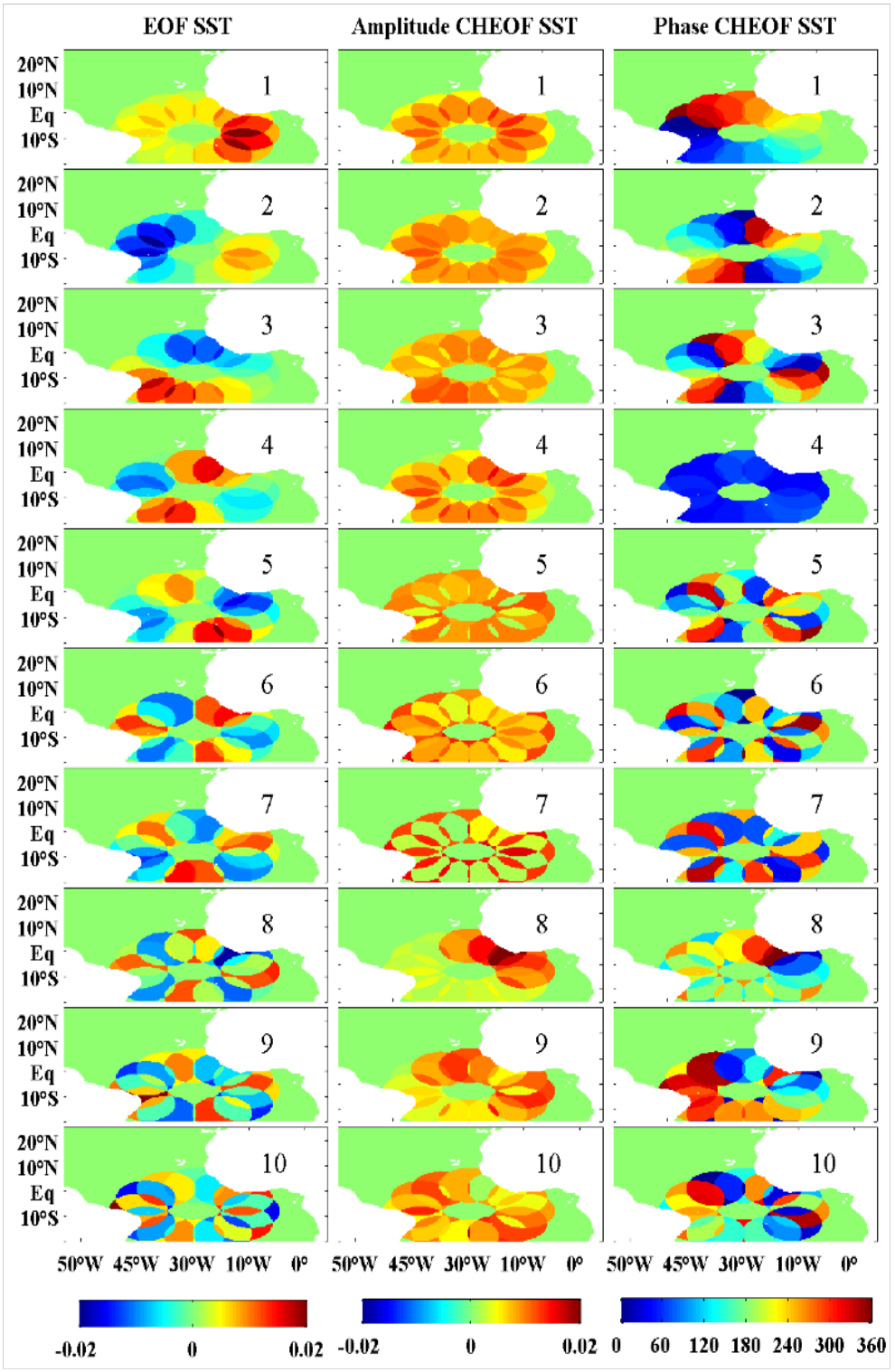

Figure 7.11. *Simulation of propagating signals in Complex Hilbert EOF (CHEOF) compared to standard EOF using SST data. Numbers represent modes of, a) EOF SST, b) amplitude of CHEOF SST and c) Phase of CHEOF SST.*

therefore, sufficient enough to focus only on the first 3 modes as they can explain both seasonal and high frequency variability in the region. Interestingly, the CHEOF is able to explain more of the percentage variances as well as the cumulative values when contrasted with the standard EOF.

Table 7.1. *Comparison of percentage variances explained by the first three leading EOFs and Complex Hilbert EOFs of SST anomalies during the period 2000-2009.*

Mode	Variance explained (%)		Cumulative variance (%)	
	EOF	CHEOF	EOF	CHEOF
1	17.5	19.1	17.5	19.1
2	11.8	12.7	29.3	31.9
3	6.6	5.6	35.9	37.4

The spatial amplitude of the leading SST anomalies (CHEOF-1 figure 7.12a) shows variance of 19.1% accounting for over 51% of the total variance of the first three modes. The strongest variances are located around the Guinea Dome and north of it. The location of the strong variances north of the equator and almost zero amplitude in the southwest explains strong variability associated with the tropical Atlantic dipole mode. This is separated by the mean position of the ITCZ as an anti-symmetric band of equatorial convection clearly delineated by a zero phase (figure 7.13a).

The CHEOF1 phase shows an anticlockwise direction of a propagation characteristic centered at ∼14°W/5°N. This shows that the strong variance of CHEOF1 is a feature that propagates in an anti-clockwise direction. This is attributable to SST variability that is associated with the southward flowing Canary and Guinea Currents. The North Equatorial Current (NEC) is also seen to propagate toward the southwest direction. This is interesting because the CHEOF can show propagating characteristics associated with these modes, which the standard EOF was unable to do. This CHEOF1 shows that coastal upwelling along the African coast around the Guinea Dome and North of it is associated with the southward flowing Canary Current. It is the most important non-seasonal variability associated with the tropical Atlantic circulation. The Canary Current

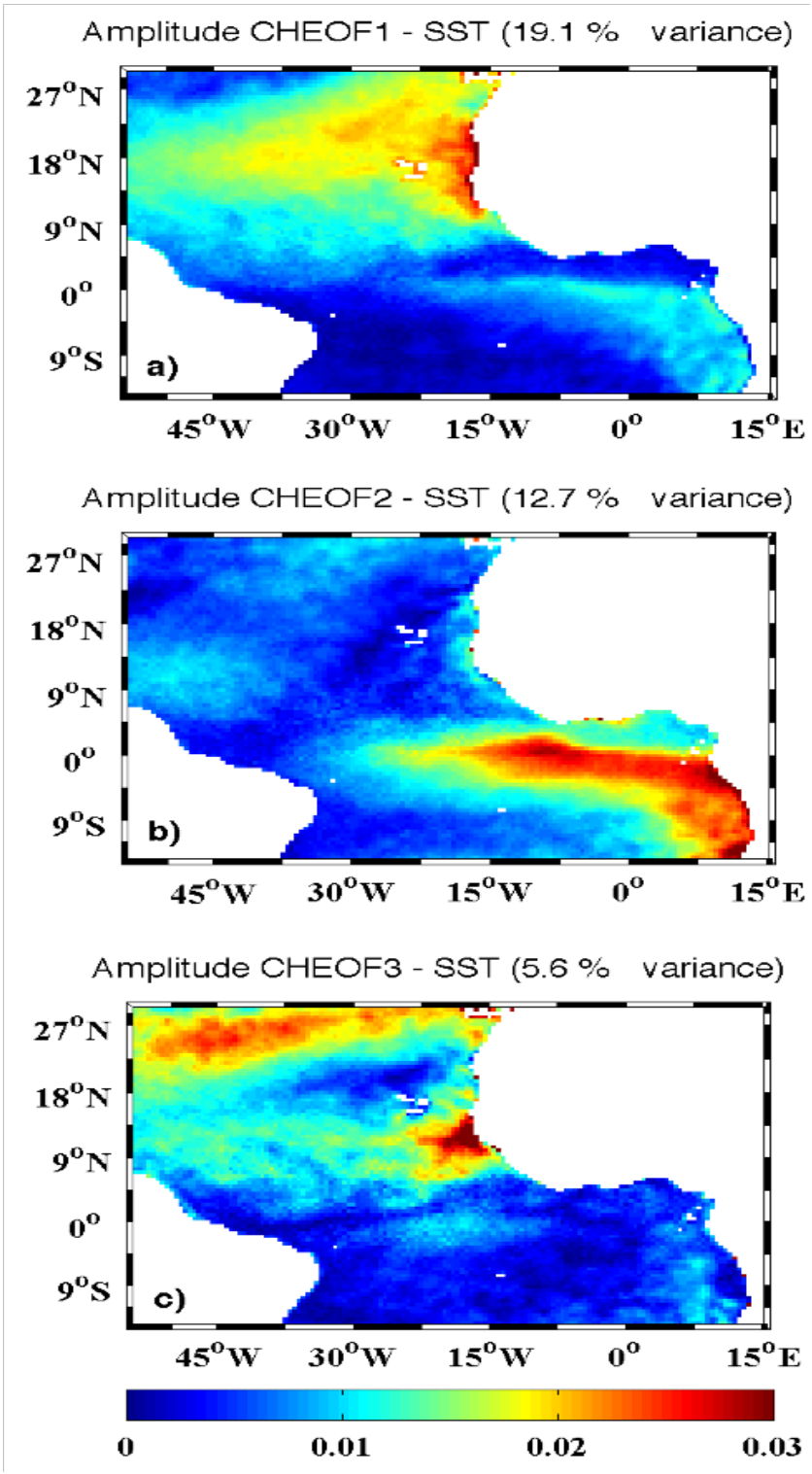

Figure 7.12. *The complex Hilbert EOF of SST anomalies for the period 2000-2009. a) CHEOF1, b) CHEOF2, c) CHEOF3. Calculations were done after removing the long-term mean based on the 2000-2009 data, as well as the linear trend.*

region (18°W, 12-18°N) is one of the large marine ecosystems in Africa that are associated with strong wind-driven coastal upwelling and primary productivity.

The second spatial amplitude of SST (CHEOF2) contributes to 12.7% of the total percentage variance. Stronger amplitudes are concentrated along at the path of the cold tongue and the Atlantic Niño region (3°S-3°N, 20°W-0°E), extending from the southeast and along the African coastline to form a strip of variance that crosses the equator. The CHEOF2 phase shows a northward and southward propagation, which is associated with the expansion of the cold tongue variability. This also explains the ability of upwelled waters of the cold tongue and equatorial upwelling to both propagate north and south, constituting the second largest variance associated with non-seasonal variability. This variability provides additional information necessary for the understanding of the Atlantic Niño and variability associated with the tropical instability waves.

The CHEOF3 shows strong amplitude at the Guinea Dome. The CHEOF3 phase of this mode shows that the amplitude is associated with southward propagation. This propagation is due to Canary Current that flows south to feed the Guinea Current. Fairly large amplitudes are also observed in the north, centred by zero amplitude at the western flank of the Cape Verde Islands (22°W, 20°N). Variances around this zero amplitude propagate in a clockwise direction. These are associated with the cold and saline Canary Current properties that originate from Mediterranean Sea and Azores Current as well as the NEC as discussed by Zhou et al. (2000). The usual southwest flow is deflected due to Coriolis force and this rotation allows water properties associated with these currents be transported northward again and into the subtropics.

The connection between the CHEOF patterns and their time varying signatures can be further supported by their principal components. The amplitude of complex Hilbert principal component (CHPC - figure 7.14) of the three CHEOFs show non-seasonal variability of the equatorial Atlantic based on time and cycle of events. Strong amplitudes appear in 2000, 2001, 2002, 2005 and 2009 signifying interannual variability of the CHEOF1 amplitude shown in figure 7.12a.

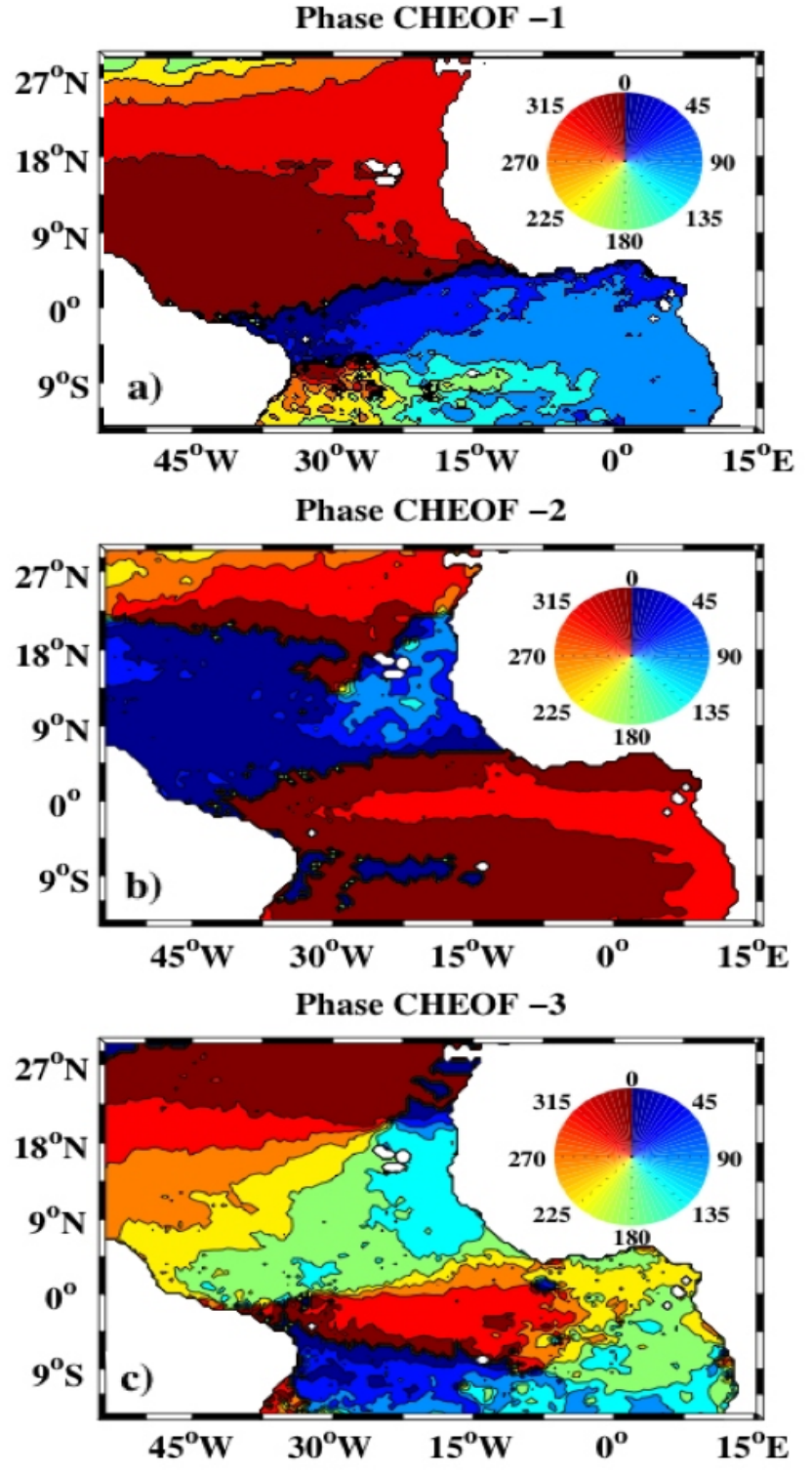

Figure 7.13. *The spatial phase of complex Hilbert EOF of SST anomalies for the period 2000-2009. Units are in degrees. Increased spatial phase indicates the direction of propagation for an increasing temporal phase.*

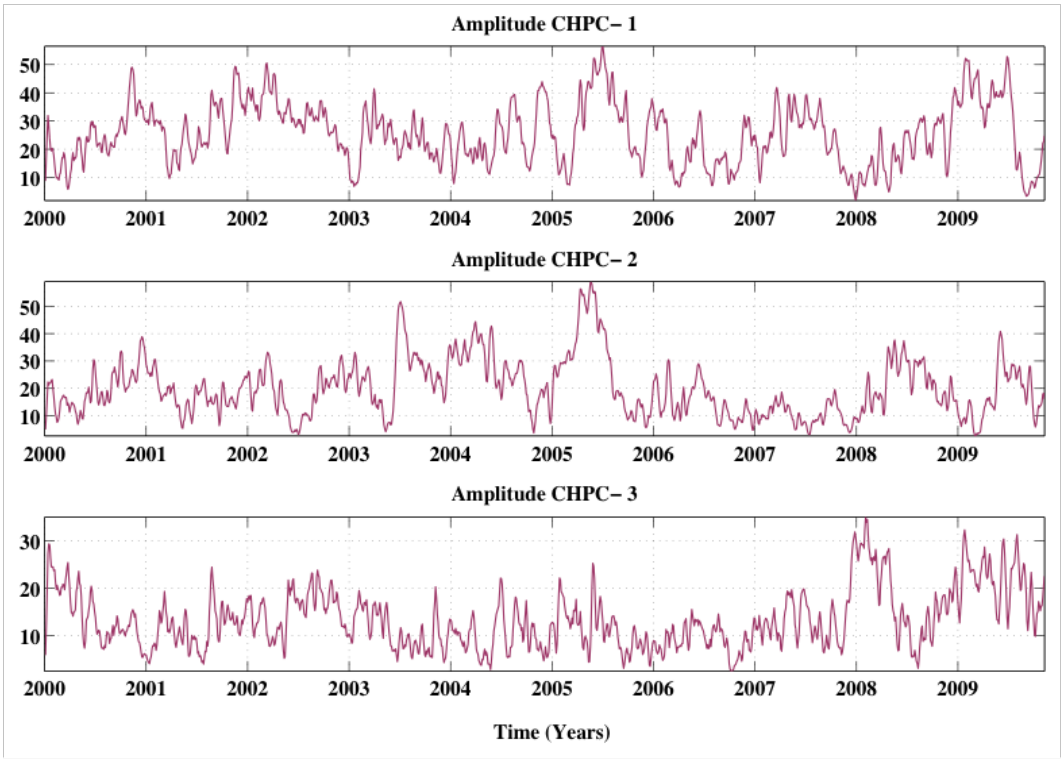

Figure 7.14. *The temporal amplitude of CHEOF principal components of SST anomalies for the period 2000-2009. The amplitudes are smoothed by a 21-day moving average.*

Analysis of temporal amplitude and phase requires the background information of the features observed in the spatial CHEOFs. The first and third CHPCs are associated with variability of upwelling in the Guinea Dome. The Guinea Dome develops seasonally from late spring to late fall owing to the wind-induced Ekman upwelling associated with the meridional migration of the ITCZ. The second, CHPC2 is associated with variability of the cold tongue, Atlantic Niño and the tropical instability waves. The analysis of complex time series and their respective phases provide time variability results of the features observed from the spatial plots.

Let us look at the phase and amplitude plots closely. In year 2000, CHPC1 amplitude peak is observed in winter and become weaker by early spring the following year. The corresponding CHPC1 phase shows a change in phase from 90 to -50 degrees during this period. This shows anti-clockwise propagation of the amplitude. This is similar to the rotation observed in and CHEOF1 phase.

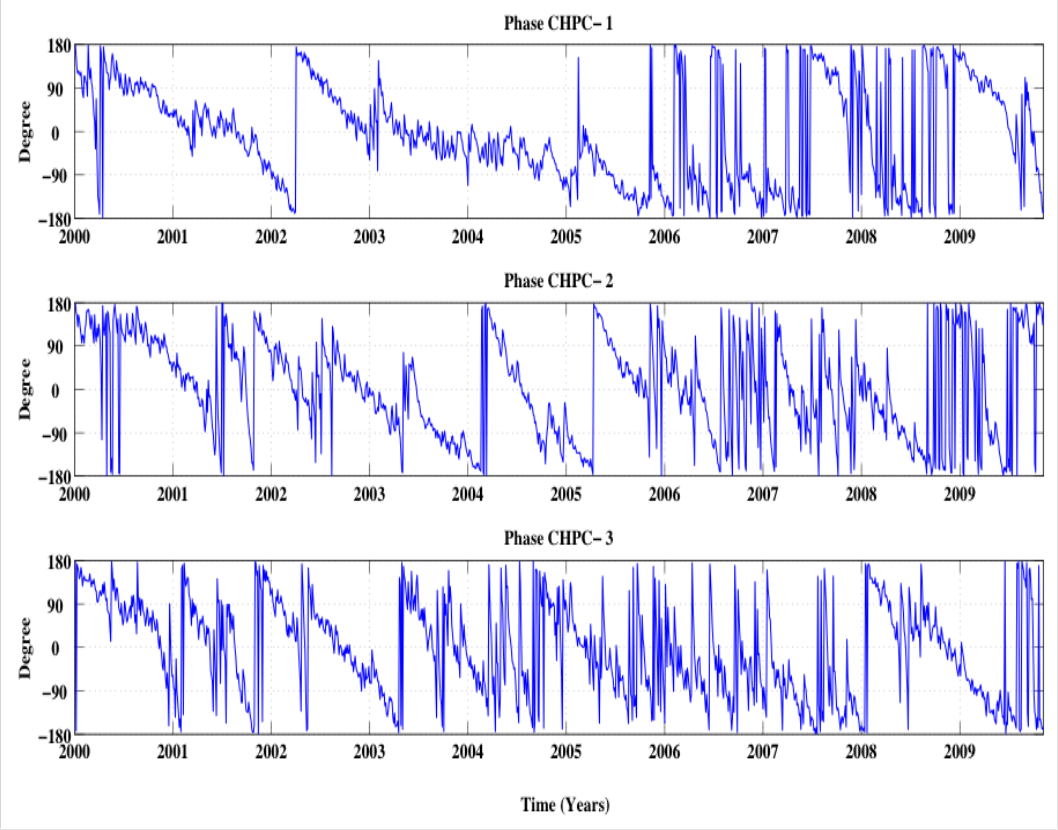

Figure 7.15. *The temporal phase of CHEOF principal components of SST anomalies for the period 2000-2009. Increased spatial phase indicates the direction of propagation for an increasing temporal phase.*

The peak in 2005 (figure 7.14) however shows a clockwise rotation (figure 7.15) by a change in phase from -90 to -180 degrees toward end of the year. These two phenomena can be explained by the variability of the ITCZ associated with the strengthening northeasterly and southeasterly winds. The anticlockwise change in phase in 2000 is attributable to the strengthening of the northeasterly winds that results in the enhancement of southerly flow, which obeys Ekman theory. These winds become strong during the boreal autumn and modulate the Guinea Dome variability (see Doi et al., 2009). The clockwise rotation in 2005 began in mid of the year, when the southeasterly winds become strong, and with the emergence of North Equatorial Countercurrent (NECC) that flows northeastward aid in forcing variability at the Guinea Dome region. This enhances upwelling and affect water properties in the region.

Let me consider the peak in CHPC2 in 2005 further, and its change in amplitude from around May to September. It has a corresponding phase show a change from 90 to 0 degrees, showing an anti-clockwise rotation. This is attributable to propagation of tropical instability waves at the southern edge of the cold tongue. The intensification of the cold tongue is associated with the strengthening of the waves both north and south of the equator. The cold tongue was found to be exceptionally strong in 2005 owing to strong anomalous southeasterly winds (see chapter 6).

The third, CHPC3 amplitude shows a peak in January of 2008. The corresponding phase (CHPC3 phase) shows a change in phase form 180 to 0 degrees. This is reflected in the spatial phase (figure 7.13) that showed a clockwise rotation. This is attributable to change in the southwest flowing North Equatorial Current that is deflected by the Coriolis in addition to strengthening of southeasterly winds.

The interannual variability associated with these CHPCs can have a significant contribution to the local climate, which can be weighted by the magnitude of their respective variances.

7.3.7 The Complex EOF of winds

Associated with the SST warming/cooling is the overlying atmosphere. The complex EOF of winds is calculated based on the formulations outlined in appendix B. The percentage variance explained for the first 3 modes (table 7.2) indicate that the first three modes are sufficient in explaining the major modes of variability in the tropical Atlantic. The three CEOFs accounts for a total variance of 51.3%, with the first, second and third are having 32.1%, 21.8% and 8.5% respectively.

The leading spatial amplitude and direction of the winds (CEOF1) is shown figure 7.16 showing large amplitude north of the region. The direction of this amplitude is averagely eastward, and that dominates the region north of 15°N. It

Table 7.2. *Fraction of percentage variance explained by the first three leading Complex EOFs of wind anomalies during the period 2000-2009.*

CEOF	Variance explained (%)	Cumulative variance (%)
1	30.8	30.8
2	12.2	43.0
3	8.3	51.3

appears that the amplitudes associated with the southeasterly winds are also strong north of the equator. The second, CEOF2 show two maxima centered at 48°W/22°N associated with southwesterly winds and 17°W/20°N associated with westerly winds. These patterns are associated with strong atmospheric dynamics such as the intraseasonal 30-90-day Madden-Julian Oscillation (MJO), as indicated by the west to east direction shown in figure 7.9. The MJO is the largest element of tropical intraseasonal atmospheric variability and significantly modulates the tropical convective system (Maloney and Shaman, 2008). However, the MJO is weaker in the Atlantic compared to the Pacific and the Indian Oceans. For CEOF2, the western pattern is associated with southwesterly flow, and the eastern being a feature of MJO.

These winds originate from the tropical Pacific region and modulate the atmospheric boundary layer at a non-seasonal scale that influences the 10-m scatterometer wind fields. African Easterly Jets (AEJ) that is driven by temperature contrast between land and ocean that spans 10-15 °N may tend to weaken the influence of the eastward MJO on the near-surface ocean.

The third spatial amplitude (figure 7.16c) accounts for 8.3% variance and dominating the equatorial band of 1°S-5°N. This pattern exhibits a location that is completely opposite to the positioning of the ITCZ, and far away from the horizontally aligned TIWs frontal zones (2-6°N). This mode clearly shows variability associated with southeasterly winds. These winds response to SST gradient north of the equator through the WES feedback, and by Coriolis, deflects over to the African continent carrying moisture, hence called the monsoon winds. Although, this pattern, to my knowledge has not appeared in the literature, it

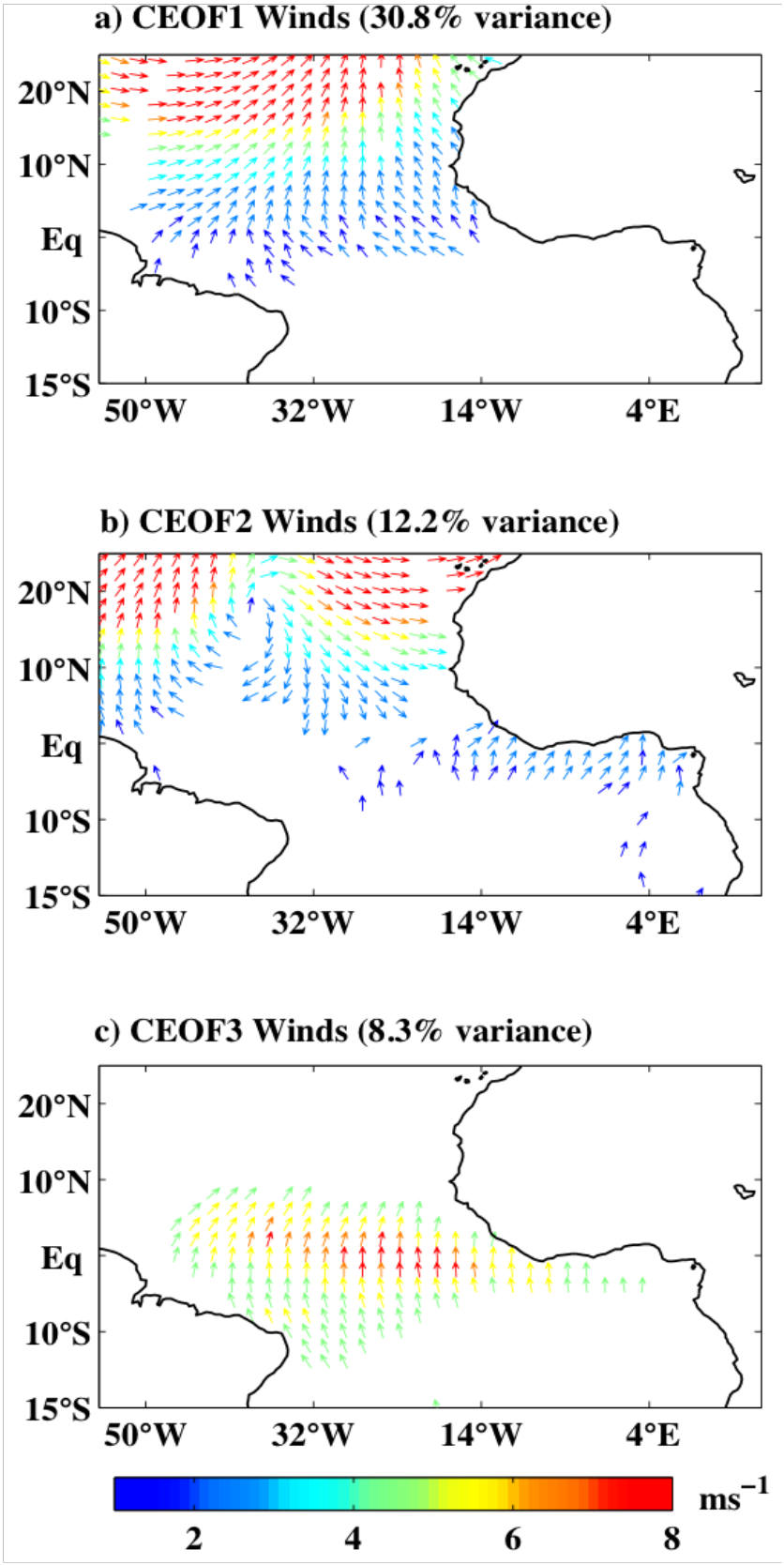

Figure 7.16. *Spatial structure of complex EOF of wind anomalies for the period 2000-2009. The amplitude is shown in colors (ms^{-1}) and direction by arrows. The long-term mean based on the 2000-2009 data and linear trend were removed prior to calculation. Winds are anticyclonic in the northern hemisphere and cyclonic in the southern hemisphere.*

should be given a special consideration in spite of its relatively low variance in the future.

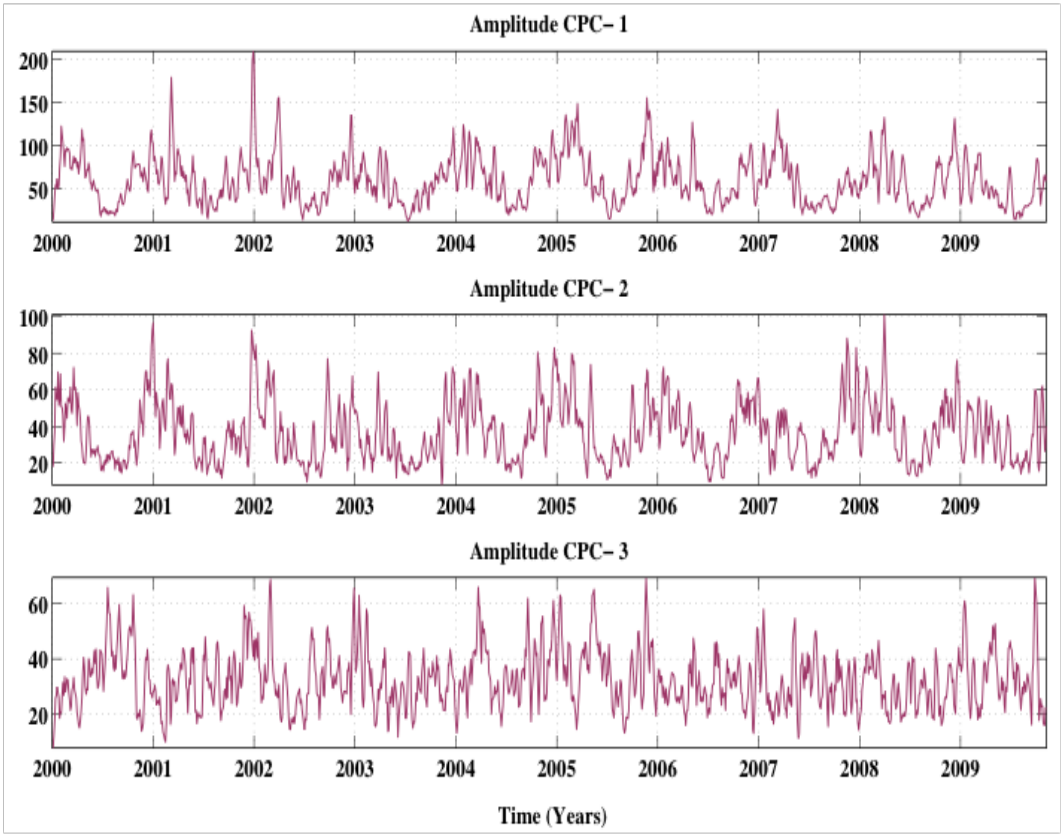

Figure 7.17. *The temporal amplitude of CEOF principal components of wind anomalies for the period 2000-2009. The amplitudes are smoothed by a 21-day moving average.*

The time variability of the complex EOFs of wind are shown as amplitude time series (figure 7.17) and directions of amplitude time series (figure 7.18). The amplitude CPC1 shows periodic signals each year with no apparent interannual variability. The highest peaks are observed in the boreal winter of each year, with winter of 2001 having the highest peak, while lowest peaks in the boreal summer. The corresponding temporal phase of this principal component (figure 7.18) shows the direction of this amplitude to 180 degrees, indicating southward. It appears that the mechanism driving this signal is responsible for other peaks in boreal winter such as 2002, 2003, 2005 and 2008.

The second amplitude (CPC2) also shows high frequency variability. This is due to fast changing wind patterns comparable to SST, which takes longer time.

The peak amplitudes during boreal winter of 2000 correspond to zero degrees of phase (figure 7.18b) and differ with that of 2001, which is at 180 degrees. That means the driving mechanism of winter variability of 2000 is completely opposite to that of 2001. The amplitudes of CPC3 show peaks that are not restricted to the boreal winter, but spread to other seasons depending on the year. For example, the phase corresponding to the amplitude of highest peak in 2000 show 180 degrees, which occurred in summer time. This has the same phase with amplitudes of boreal winter observed in 2001, 2002 and 2005.

By implication, both CPC1 and CPC2 that show large amplitudes north of 18°N are associated with an MJO phase during the winter. Maloney and Shaman (2008) observed that intraseasonal variability of the MJO do vary during winter in connection to North Atlantic Oscillation (NAO).

The third, CPC3 amplitude time series shows high frequency variability associated with the changes in wind pattern north of the equator. It should be noted that, the spatial amplitude of this mode (figure 7.16) showed variability in the region north of the equator that is also attributable to variability of the tropical instability waves. Fluctuations of winds at the SST frontal zones of TIWs are highly variable due to the coupling of the winds with warm and cold phases of the waves. The peaks show significant interannual variability with weaker events in 2006, 2007 and 2008.

7.3.8 Connection with mid and high level winds

The large-scale variability observed north of the tropical Atlantic are essential to the understanding of the ocean-atmosphere-land. I advance this study by looking at the variability of atmospheric wind data at 850hPa (roughly 1.5 km - or 1mile) based on NCEP/NCAR reanalysis products. The 850hPa is roughly the top of the convective boundary layer. This choice of height is in consideration of wind influence over both the ocean and land at this height, and in the region

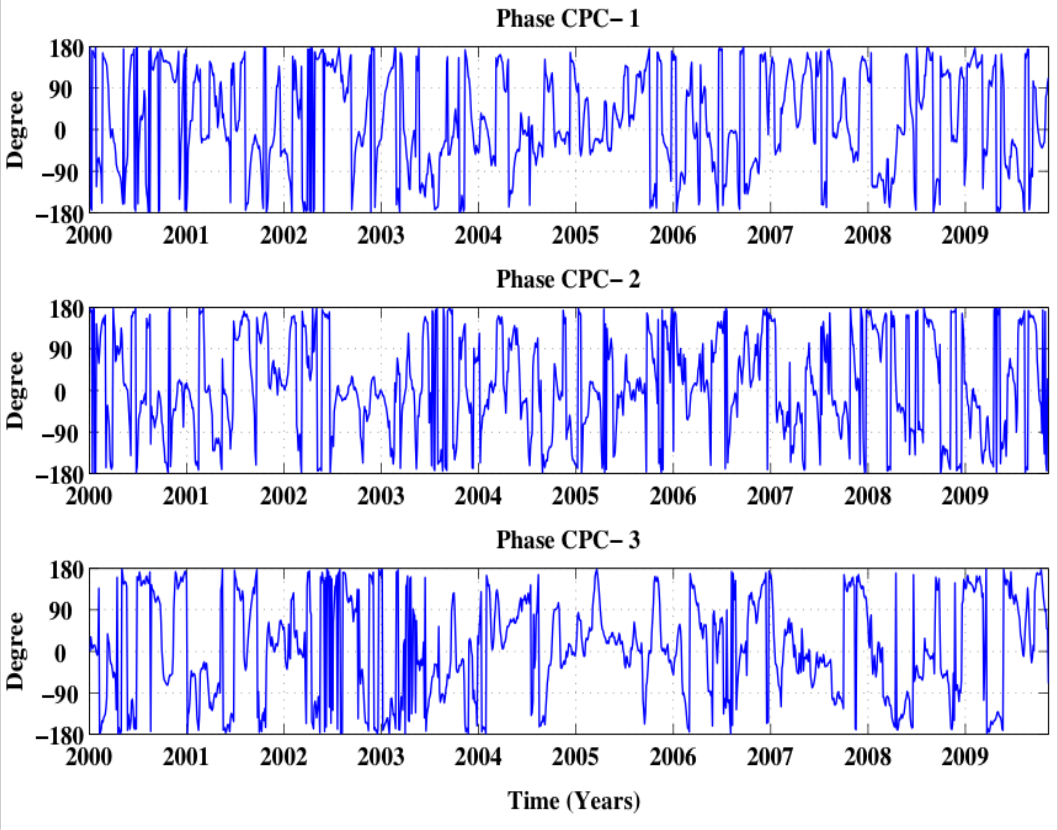

Figure 7.18. *The temporal phase of CEOF principal components of wind anomalies for the period 2000-2009. Units (in degrees) show direction of amplitude for each mode. X-axis labels are end of year.*

having significant mountain ranges. The major aim here is to find the relationship between atmospheric winds and the scatterometer 10-m wind field results of the CEOF (section 7.2.6).

The standard deviation of the zonal winds (figure 7.19a) shows strong variance north of 30°N, outside the tropical domain. This has reproduced the amplitude observed from the scatterometer winds (figure 7.16). This is due to large-scale wind region akin to the MJO, which are also modulated by the continental geography over Africa,

The first 3 EOFs are shown (figure 7.20), having a total variance of 35.8%. EOF1 (16.6% variance) shows two peaks north of the equator and centred at 25°W/20°N and 20°W/43°N. These variances are caused by different mechanisms and both may have significant impact on the 10-m scatterometer winds. This is through buoyancy and mixing in the lower boundary layer caused by large-scale heat

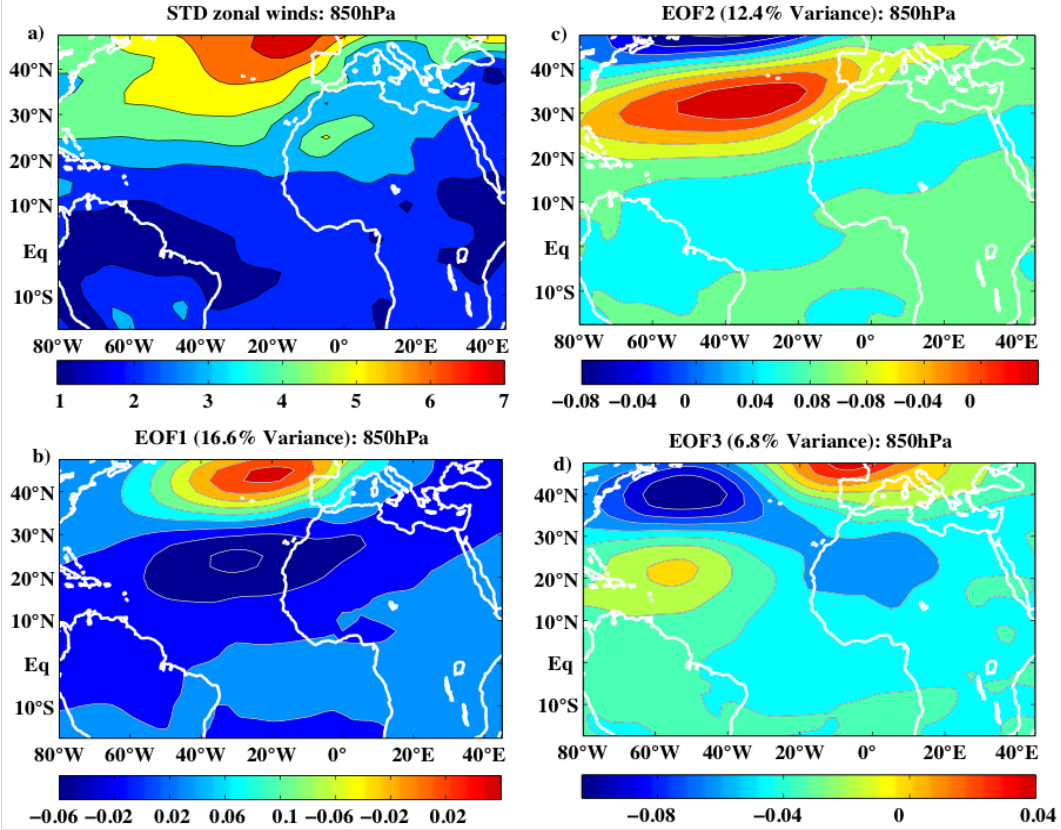

Figure 7.19. *Spatial variability of 850hPa NCEP zonal winds, a) Standard deviation, b) EOF1, c) EOF2 and d) EOF3. Daily data is averaged to 3-day to correspond with the period of SST and 10-scatterometer winds used in this chapter. The long-term mean and seasonal signal has been removed based on the length of data (2000 to 2009) prior to EOF calculation.*

fluxes. In between these variances are frontal zones that determine the boundary between eastward winds and westward African Easterly Jets (AEJ). EOF2 reproduced the pattern observed in the scatterometer winds (figure 7.16a) centred at 37°W/30°N, confirming that the largest variances observed from the CEOF winds north of 18°N are due to the influence of atmospheric winds. These interesting features further highlight the impact of tropospheric winds to ocean surface thereby enhancing coupling of ocean-atmosphere resulting in the distribution of moisture and heat, especially in the Sahel region. EOF3 also show strong variances north of the equator, one centred at 58°W/21°N and another 55°W/40°N.

In order to determine the direction of these features observed from the EOF

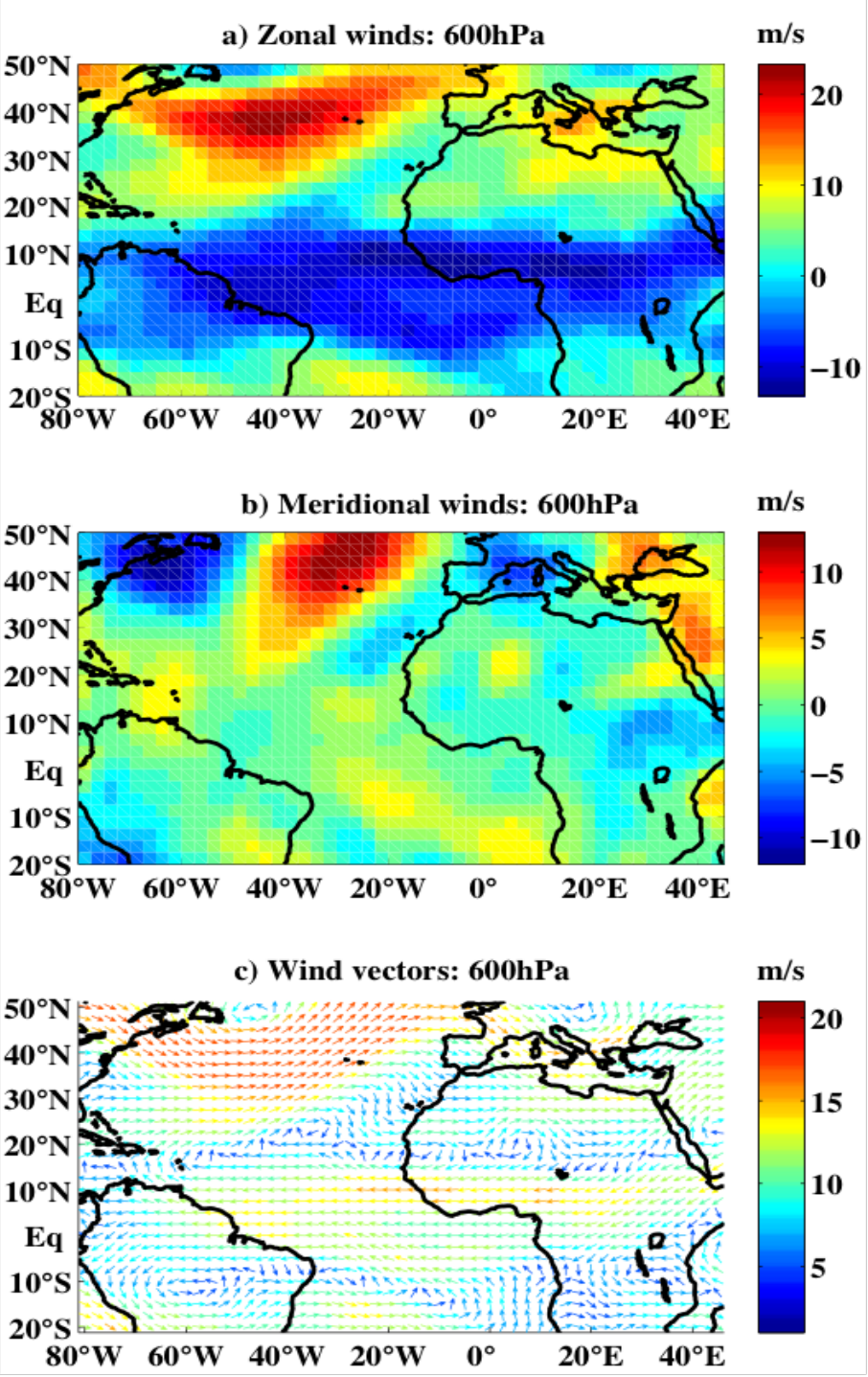

Figure 7.20. *Spatial variability of 600hPa NCEP winds for the period 15 May - 14 June 2010, a) Zonal winds, b) Meridional winds, c) Wind vectors.*

plots, I show wind distribution in the region at 600hPa (roughly 4km) (figure 7.20). The most active period of atmospheric circulation in West Africa, the Sahel and the tropical Atlantic is during the summer and mostly at 600hPa.

These are periods when African Easterly Waves (AEWs), which are disturbances unique to the region, develop and propagate westward, resulting in cyclogenesis (figure 7.21). Strong westward winds (figure 7.20a) dominate the equatorial region, while eastward winds are weak except north of 30°N. The meridional winds (figure 7.20b) show very weak signature in the tropics but show strong northward and southward signature. The wind vectors (figure 7.20c) show strong activity at the equatorial region between 8-30°N. This can be explained as follows: During the boreal summer, the northward monsoon southeasterlies that cross the equator are forced to turn eastward due to Coriolis force, hence called monsoon southwesterlies. This is accelerated due to steep pressure gradients and converges into thermal trough and the ITCZ. These rise upward and expelled outwards of the Saharan high pressure zone to become African Easterly Jet (AEJ). The AEJ clearly manifest in 11°N (figure 20c).

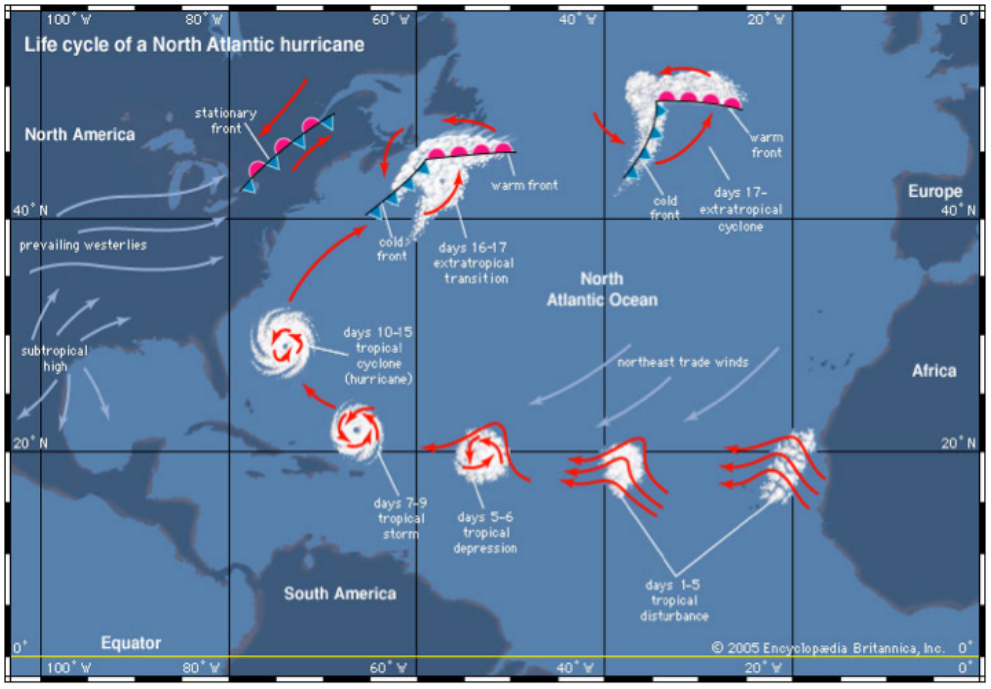

Figure 7.21. *The synoptic-scale development and strengthening of cyclonic circulation in the tropical Atlantic. Image source: Encyclopaedia Britannica 2005.*

Instabilities associated with the AEJ leads to the formation of African Easterly Waves (AEW). This is either barotropic instability, which is associated with horizontal shear produced by deep convection near the AEJ, or baroclinic, which is

associated with vertical wind shear with monsoon southwesterlies flowing over easterly jet and the temperature, moisture and pressure gradients. All these are found near the AEJ. The turning of the low-level 10-m winds (figure 7.1d) is due to barotropic instability, while the difference between the southwesterlies (monsoon winds) and jet easterlies (AEJ - figure 7.21c) is baroclinic instability. Instability theories of atmospheric circulation are beyond the scope of this chapter.

7.4 Discussion

7.4.1 The EOFs

The spatial and temporal patterns of non-seasonal SST and wind vectors are investigated. The first and second EOF SST modes depict the Atlantic meridional and the zonal modes respectively. The third EOF SST showed spatial pattern associated with the meridional mode but positioned north of the equator depicting the boreal summer positioning of the ITCZ centred at 10°N. This shows a different result compared to an earlier study by Houghton and Tourre (1992) based on analyses of EOF SST anomalies, where the inter-hemispheric dipole mode appeared in the first two modes. This shows that removing linear trend would explain more of variability associated with the tropical Atlantic region.

While EOF1 SST pattern (17.5% variance) is associated with the seasonal northeasterly and southeasterly winds, EOF1 of zonal winds (32.1% Variance) show patterns associated with tropospheric winds. Meridional EOF1 (21% variance), however showed a large pattern in the east that is associated with EOF1 SST, with another pattern in the west linked to tropospheric dynamics. This simply explains that the meridional mode of variability is explained by the first EOFs of both SST and meridional winds. The meridional mode, also called the dipole mode of the tropical Atlantic is thought to be driven by heat-fluxes and therefore, thermodynamic in nature (Foltz and McPhaden, 2010). Looking at the

EOF-1, and -3 of SST, this analysis confirms Seager et al. (2001) hypothesis, that CESG determines the meridional positing of the ITCZ.

The second, EOF2 SST is characterized by the zonal mode of the tropical Atlantic. This however, did not appear either in any of the first three zonal or meridional EOF modes of wind speed, despite the cold tonguebeing a strong feature of tropical Atlantic variability. I conclude that the cold tongue event is purely seasonal and driven by seasonal southeasterlies, therefore is not expected to appear in this analysis. Therefore, variability of the zonal mode here illustrates changes in the intraseasonal signals associated with any or all of the following: the cold tongue, the Atlantic Niño and the tropical instability waves.

The first and second modes of both zonal and meridional modes are north of 18°N. The positioning of these modes demonstrates influence of subtropical atmospheric circulation of the MJO. At latitude 30°N, I expect northeasterly trade winds and westerly winds (which are southwesterlies) to modulate the atmospheric boundary layer and influence the transport of heat and moisture in connection with the MJO.

The MJO is the largest element of intraseasonal variability in the tropical atmosphere, which couples with the ocean at zonal scales of 30-90 days and wavelengths of about 1000km (Maloney and Shaman, 2008). Yu et al. (2011) investigated the MJO from outgoing longwave radiation and QuikScat scatterometer winds and found that the north equatorial Atlantic is strongly influenced by the MJO. They observed that 30-70 day surface winds of the MJO progresses from the Pacific into the Atlantic through Panama and this occur during boreal spring and winter. In a similar investigation, (Han et al., 2008) found out that the MJO event contributes to 40-60 day zonal wind variability in the equatorial Atlantic Ocean.

Contrasting EOF3 of zonal winds and EOF3 of SST, a similar structure is observed, attributable to the meridional mode, which explains the point of convergence of northeasterly and southeaster winds as a non-seasonal variability. Even

though, EOF3 SST and EOF3 zonal winds accounts for only 6.6% and 9.1% respectively, they suggest an important signature that could advance the knowledge of cross-equatorial SST gradient influence on southeasterly winds. The southeasterly winds have stronger influence on the Atlantic Meridional Mode (AMM) variability. Therefore, prescribing the EOFs based on non-seasonal variability will indeed highlight changes associated with the AMM. The AMM is essentially the major mode of tropical Atlantic variability that affects local climate with significant contribution to large-scale variability. It is modulated chiefly by cross-equatorial SST gradient (CESG) (Schott et al., 2003). and is also connected with the zonal mode through Bjerknes feedback mechanism (Foltz and McPhaden, 2010).

Strong variance of meridional winds (EOF3-7.9% variance) is associated with the North Brazil Current, and that did not appear in the SST EOF3 or the EOF3 of the zonal winds. I attribute the lack of associated variability from the SST EOF to ocean damping effect on emerging SST anomalies by horizontal advection at the intraseasonal scale, which Seager et al. (2001) suggested to be either mean or Ekman.

7.4.2 The Complex Hilbert EOFs

The complex Hilbert EOF is able to highlight details on the spatial and temporal patterns associated with the variability of the tropical Atlantic. The major features observed are the variability associated with the Guinea Dome and that of the cold tongue/Atlantic Niño/TIWs regions.

The dome develops seasonally off Dakar from late spring to late fall due to wind-induced Ekman upwelling, and its evolution and physical characteristics is associated with the Atlantic Meridional Mode (AMM) (Doi et al., 2009). It serves as a point of convergence of southeasterly and northeasterly winds during the boreal summer, where moisture is driven toward West Africa and southern Sahel. The interannual variability of the Guinea Dome is an essential constituent

of tropical Atlantic climate variability. These results present non-seasonal interannual variability of the dome and the region north of it. Because the dome is associated with the northward migration of the ITCZ, it is a part of the basin-wide wind-evaporation-SST (WES) feedback mechanism that controls heat and moisture in the north.

The second mesoscale variability studied by the complex Hilbert EOF is variability at the cold tongue/Atlantic Niño/TIWs regions. These features are interwoven in terms of the largest amplitude of CHEOF2 location. The cold tongue occurs due to intense upwelling due to strengthening of the southeasterly winds during the boreal summer. North and south of the cold tongue are tropical instability waves that arise from barotropic instability of currents. The Atlantic Niño is the second major mode of variability in the tropical Atlantic. The nature of rotation of the CHEOF2 and CHPC2 phases explains variability associated with the tropical instability waves having a second dominant feature in the region.

Generally, large SST variability in the Gulf of Guinea occurs as a result of the shallowness of the thermocline and upwelling along the equator and the coasts during the boreal summer (Merle, 1980). Upwelling in this region however, cannot be solely explained by the local wind regimes (Houghton, 1976; Volturiez, 1981), but is influenced by winds over the whole basin via the equatorial Kelvin waves (Houghton, 1983; Katz, 1997; McCreary et al., 1984). Vertical and horizontal advection, vertical mixing and fluxes associated with instability waves also contribute to changes in upwelling (Foltz et al., 2003; Gouriou and Reverdin, 1992).

7.4.3 The Complex EOFs

The CEOF results show that the largest two variances of non-seasonal variability in the tropical Atlantic are associated with the intraseasonal MJO. The third CEOF showed the ability of the southeasterly winds to response strongly on

the cross-equatorial SST gradient (CESG). This showed interannual variability with strong amplitudes in 2000, 2002, 2003, 2005 and 2009. This response of the winds to CESG induces variability of the ITCZ, which is an indicative of Wind-Evaporation-SST feedback. The WES feedback is believed to play an important role in the tropical Atlantic variability (Mahajan et al., 2009).

7.4.4 The upper level winds

The connection between scatterometer 10-m winds and atmospheric winds are investigated to confirm the influence of intraseasonal tropospheric MJO on the 10-m winds. The standard deviation of 850hPa reproduced the variances observed in the complex EOF plots, demonstrating that these variances in the EOFs are caused by atmospheric winds. Further investigation to ascertain the direction of these atmospheric winds confirmed them to be zonal that are a part of intraseasonal variability of the global tropics, the MJO. The African Easterly Jets appear between 18-20°N, flowing westward. This confirms the positioning of the AEJ discussed by Grist and Nicholson (2001). These jets could significant affect the phasing of the MJO winds and its southward expansion.

7.5 Summary

In this chapter, I investigated non-seasonal variability of the tropical Atlantic Ocean based on SST, zonal and meridional wind components. I employed EOF, complex EOF and complex Hilbert EOF techniques in order to identify leading modes of variability in the region and also to find the relationship of the coupled SST and wind fields. I have examined the observed non-seasonal characteristics of SST and wind through both spatial patterns and temporal time series. The observations show significant interannual variability that contributes to the non-seasonal variability. These variabilities may modulate the crossequatorial SST gradient, thereby influencing a change in the wind-evaporation-SST (WES)

feedback mechanism. The WES feedback mechanism is a low-frequency natural variability of the tropical Atlantic that determines the Atlantic meridional mode and the migration of the meridional ITCZ.

My investigations showed that non-seasonal variability of SST (EOF-1 and -3) in the region are associated with the meridional mode, while EOF-2 SST is associated with the zonal mode. Interesting results were obtained based on the application of complex Hilbert EOF of SST. Variability at the Guinea Dome region is found to be connected with the southward flowing Canary Current. This variability is the most important non-seasonal variability associated with the tropical Atlantic circulation. The second most important variability is associated with the tropical instability waves.

I observed a strong meridional variance associated with North Brazil Current from EOF analysis, which is independent of seasonal fluctuations. This explains that the cooling of SSTs west of the tropical basin is not only associated with seasonal variability but also with non-seasonal changes. This observed feature could significantly affect the meridional migration of the ITCZ due to meridional wind forcing.

My study shows that the interannual variability exhibited by the complex Hilbert EOFs and their principal components agrees well with the hypothesis put forward by Seager et al. (2001) that the cross-equatorial-SST gradient (CESG) is responsible for the meridional migration of the ITCZ. However, it is necessary to explain other possible scenarios that may affect CESG. The southeasterly winds respond to SST frontal zone of the tropical instability waves could alter the SST and that may either delay or speed up the ITCZ migration. This depends on the strength of the cold tongue that determines the strength of the waves.

When these regions of high EOF amplitudes observed in scatterometer winds are compared with NCEP reanalysis winds, an almost exact match of spatial amplitudes is observed north of 20°N. My analysis suggests that tropospheric winds have a significant connection with the ocean than in the equatorial part due to the large-open North Atlantic Ocean. This is through turbulent heat

fluxes that create instability in the marine atmospheric boundary layer, which may result in barotropic instability of the upper layers in response to the fluxes. The interaction of atmospheric zonal winds such as MJO winds and African Easterly Jets together could affect surface winds, and hence the meridional migration of the ITCZ.

This chapter has shown that variability of the tropical Atlantic SSTs can be explained simply as the response of surface heat fluxes forced by variations in the strength of trade winds. The response of each hemisphere to the changes in wind pattern however differs. The northern hemisphere appears to respond strongly to variations of southeasterly winds due to the northward positioning of the Atlantic thermal equator ($\sim 5°$N) and the SST gradient. Consequently, variations on the SST gradient at non-seasonal scale lead to interannual variability of the wind system and that have subsequent effect to local climate. However, the wind systems are also modulated by large-scale cross equatorial SST-gradient as reported earlier by Seager et al. (2001). Overall, variability of the tropical Atlantic is better understood as a coupled system that can be modulated by anomalous SST signatures, especially at the TIW frontal zones as well as high frequency oscillations. These are independently considered in chapter eight.

CHAPTER 8

Ocean-atmosphere coupling and high frequency variability

8.1 Introduction

At the equatorial Atlantic region, tropical instability waves (TIW) propagate from east to west, having strong signatures of mesoscale variability of 20-40 days, with wavelengths of 1000-2000km and phase speed of 0.3-0.6cm/s (Qiao and Weisberg, 1995). These values may however, differ significantly as a function of longitude, latitude and time of year (Strutton et al., 2001). At the mesoscale level, the major SST signals that couple with winds are the TIWs. These waves are important in the time evolution of heat fluxes and the near-surface heat budget (Grodsky et al., 2005; Weisberg and Weingartner, 1988). Because the waves are stronger north of the equator than south, their impact on atmospheric processes are asymmetric with respect to the equator. Since the tropical atmosphere is influenced by the mesoscale activities of these waves (Chelton et al., 2001; Hayes et al., 1989), their interannual variability could influence the local climate as well as large-scale atmosphere circulation (Wu and Bowman, 2007b).

I aim to find the interannual variability of these waves, and the resulting consequences of their coupling with the winds in the equatorial Atlantic. I characterise them both at the south and north of the equator due to their relevance to local air-sea interaction and convection. Because of the strong signatures of negative/positive undulations in the waves from satellite sea surface temperature, I hypothesize that winds will respond accordingly to these undulations based on the strength of the waves.

Recent studies of TIWs variability in the Atlantic showed that the waves are only active in some years but not in others. Caltabiano et al. (2005) demonstrated from a suite of satellite data, that these waves vary from year to year and that they couple with the atmosphere to impact on the ITCZ. Interannual variability was observed from their analysis using 4 years of SST and 2.5 years of wind data while focusing north of the equator. A similar analysis by Wu and Bowman (2007a) based on the period of June-July-August months showed a slight year-to-year variability. Focusing on interannual variability of these waves north and south of the equator is essential in understanding their variability by region and their capacity to influence the climate. Using 12 years satellite products of SST and 9 years wind data, I characterise the interannual variability of the waves. The advantage of using a longer time series allows interannual variability to be determined based on both spatial and temporal scales.

Tropical instability waves occur in both the Pacific and Atlantic oceans. While no consensus has been reached about the exact nature of tropical instability waves in the Atlantic (Athie and Marin, 2008) they certainly exhibit stronger signatures north of the equator than to the south. Bunge et al. (2007) found no relationship between the north and south signatures, suggesting that they are of different dynamical origin. Also, because these waves couple with the atmosphere through SST and wind as a result of buoyancy instability and mixing (Liu et al., 2000), wind shear in the atmospheric boundary layer over the waves is reduced. This results in higher evaporative cooling over the warm phase of the waves resulting in a negative thermal feedback.

The state of the cold tongue in the Atlantic might be tied to the interannual variability of the Atlantic TIWs. The cold tongue itself is directly connected to the Atlantic Niño. However, due to limited observations in the Atlantic Niño, it is difficult to assess its relationship with the TIWs.

Bunge et al. (2007) observed biweekly oscillations in the ocean velocity measurements in the equatorial Atlantic as reminiscent of Yanai waves (mixed Rossby-gravity waves), having similar signatures to those observed earlier that Houghton and Colin (1986) attributed to meridional wind stress. Although, quasi-biweekly oscillations in winds have also been observed by various authors (Grodsky and Carton, 2001; Janicot and Sultan, 2001), their relationship with SST in terms of coupling is not yet understood. However, sub-monthly variability is important in the equatorial dynamics due to the short time variability of seasonal winds and their coupling with SST. I develop this analysis by characterising the dominant quasi-biweekly oscillations (5-20 days) in the tropical region to study their areas of influence and possible relationships with TIWs. I attempt to answer a question: What are the roles of 5-20 day oscillations in wind-driven ocean variability in the tropical Atlantic?

Many recent studies of air-sea interaction focus on oceanic fronts and eddies, and have shown positive correlation between sea surface temperature, wind speed and heat fluxes out of the ocean (Chelton et al., 2001; Hashizume et al., 2001). This indicates that the ocean is forcing the atmosphere, and that is contrary to large-scale climate modes, where negative correlations indicate that atmosphere is driving an ocean response (Small et al., 2008). There are various reasons why the atmosphere is affected by ocean fronts and eddies and these are explained in (Small et al., 2008). As the wind blows over an SST gradient, an air-sea temperature difference and air-sea humidity difference are generated. This leads to changes in near-surface stability and surface stress as well as latent and sensible heat fluxes (Hayes et al., 1989). During the boreal summer monsoon, the south-east trade winds are stronger, influencing the formation of the cold tongue and coupling with mesoscale SST north of the equator. The surface currents of ocean

fronts and/or eddies produce a relative motion between the ocean and the atmosphere, acting to change the surface stress, thus affecting the atmosphere as well as feeding back to the ocean (Cornillon and Park, 2001; Kelly et al., 2001). In this analysis, an attempt is made to find out whether correlations at the major TIW frontal zones differ from those in other regions of the equatorial Atlantic. I hypothesis that the positive correlation between SST and wind stress fields at the TIW frontal zones dominate the tropical Atlantic region.

Datasets employed in this study are 12 years of TMI SST (1998-2009) and 9 years of QuickScat wind, both with spatial resolution of 0.25° x 0.25° and averaged over 3-days. Prior to processing, all gaps in data have been optimally interpolated and for any missing data, an average of the previous 3-day and the next 3-day are used to replace the gap. For the time series at each location, the seasonal signal is estimated and removed to leave non-seasonal and interannual anomalies. All correlations are calculated as r and not r^2.

This chapter is organised as follows: 8.2) Methods 8.3) Results, 8.4) Discussion, 8.5 Summary.

8.2 Method

8.2.1 Tropical Instability Waves

I applied a Fourier filter designed using prior knowledge of TIWs approximate range of wavelengths and periods, having 5-14° in longitude and a 15-40 days window (Qiao and Weisberg, 1995). This is applied to both SST and the wind data sets and are analysed in sub-section 8.3.1.

8.2.2 Correlation

The Spearman's correlation (r) is applied to non-seasonal SST and wind stress fields covering the period of 2000 to 2008. These correlations are spatial, where

every pixel of SST is correlated with a corresponding pixel of wind stress component covering the 9 years period of the 3-daily data sets. This method is also applied in the correlations of SST and wind stress curl, wind stress divergence and wind speed in section 8.3.6.

8.2.3 Wind stress

To estimate surface wind stress, τ, for each scatterometer 10-m wind vector, the bulk formula based on Smith (1988) as detailed in Piolle and Bentamy (2002) is used.

8.2.4 Wavelet analysis of SST and wind stress

Due to ambiguity in the coupled relationship between atmospheric and oceanic processes, various methods are applied to infer these relationships. In section 8.3.2 of this chapter, spatial cross-correlation between wind stress fields and SST has been determined. I advance this analysis by implementing a different approach, a more rigorous statistical technique using wavelet analysis to assess the inter-relationships between wind stress fields and SST.

The wavelet is a function, which represents a waveform that is contained within a finite domain (Graps, 1995). This is in contrast to the sine and cosine functions used in Fourier analysis that extend out to negative/positive infinity (being globally uniform in time and have finite span) (Lau and Weng, 1995). The wavelet's ability to consider finite domain allows it to do better work by approximating sharp spikes in data, than does Fourier analysis. A common ground between Fourier and wavelets is that they both treat data series as signals and decompose them into coefficients that represent variance (Lindsay et al., 1996). However, the wavelets rapidly decrease to zero about a finite point, interval, space or time (Si and Farrell, 2004). This allows it to produce a coefficient associated with a specific location and, unlike Fourier, retain the localised context of

data. Even though, Fourier analysis is well suited to quantifying constant periodic components in a time series, it is not able to characterise the signals whose frequency content changes with time (Cazelles et al., 2007). In essence, wavelet analysis allows localised investigations of co-variability between the two signals as well as their phase relationships.

There are two classes of wavelet transform: the Continuous Wavelet Transform (CWT) and its discrete counterpart (DWT). The CWT is good for feature extraction while the DWT represents data in compact form and is important for noise reduction (Grinsted et al., 2004). In this analysis, the CWT is chosen to enable me to extract relationships between SST and wind stress fields. The CWT has an advantage of high resolution and gives a smooth spectral structure in time-frequency domain (Setoh et al., 1999).

In order to understand the coupling characteristics of SST and wind stress fields and their relative effect on climate, I advanced my analysis using the 3-daily averaged datasets that are devoid of long-term mean based on the data length and seasonal signal. By removing the seasonal cycle before calculation using cross-wavelet and wavelet coherence, important signals that vary from year to year can be studied at different periods and magnitudes, as well as sub-seasonal variability. Because changes in the winds are much faster than that of SST, I maintained the data to 3-daily averages before analysis covering 2000 to 2009 to allow high frequency variability to be determined.

8.2.4.1 Continuous wavelet transform (CWT)

Continuous wavelets are not orthogonal, and therefore, there is overlap and redundant information between wavelet coefficients of all locations and scales. This makes continuous wavelet transform very important for scale analysis (Si and Farrell, 2004) and hence good at extracting features. The CWT is very resistant to noise. Therefore, its application for climate studies is ideal, for example extracting relationships between a coupled SST and wind fields. The continuous wavelet transform (CWT) of a dataset $h(t)$ is given by

$$CWT(u,s) = \int_{-\infty}^{+\infty} h(t) \frac{1}{\mid s \mid^{0.5}} \psi^* \left(\frac{t-u}{s} \right)$$

where, s is scale, u is displacement, ψ is the mother wavelet used, and $*$ means complex conjugate. The CWT is therefore, the convolution of the data with a scaled version of the mother wavelet. The adjustable parameter, Morlet is set 8, as this yields the best resolution level for both frequency and time. The Morlet wavelet is defined as:

$$\Psi(x) = \frac{1}{\pi f_b} e^{2\pi i f_{c^x e}^{\frac{-x^2}{f_b}}}$$

where f_b controls the wavelet bandwidth, and f_c is the wavelet centre frequency. A value of 1.0 is chosen for f_c, so that scale becomes equivalent to wavelength.

8.2.4.2 Cross wavelet transform (XWT)

In order to compare the two time series, cross wavelet transform (Torrence and Compo, 1998) is used. Cross-wavelet transform shows the time frequencies where time series have common power. The wavelet coherence shows time frequencies where time series co-vary. Since the coherence does not show the power at those frequencies, it can be inferred directly from the cross-wavelet plots. The lead-lag relationships can also be determined from the phase represented by arrows. The structure of the equation is like calculating a product-moment correlation coefficient, which is defined by Torrence and Compo (1998) as the ratio of joint variation to total variation of two variables. This is given by

$$CWT_{1,2} = CWT_1 . CWT_2^*$$

is a complex quantity having an amplitude (the cross-wavelet power) given by

$$A = \mid CWT_{1,2} \mid$$

and local phase ϕ :

$$\phi = arctan\left[\frac{\Im(CWT_{1,2})}{\Re(CWT_{1,2})}\right]$$

The phase ϕ can range between $-\pi$ to π as a measure of phase correlation between the two data sets.

8.2.4.3 Wavelet Transform Coherence (WTC)

Wavelet coherence is another important quantity used to find frequencies in space where the two time series covary, but may not have the same power. By studying the cross-wavelet and coherence wavelet, both the power of co-variability and frequencies of strongest coherence can be studied. Wavelet coherence does not rely on stationarity, but does provide location specific information (Yates et al., 2007). The wavelet coherence (WTC) is given by:

$$CWT^2(s,t) = \frac{\left|\langle s^{-1}W_{xy}(s,t)\rangle\right|^2}{\langle s^{-1}\left|W_x(s,t)\right|^2\rangle\langle s^{-1}\left|W_y(s,t)\right|^2\rangle'}$$

where $\langle ...\rangle$ is the smoothing in time and scale, and other factor s^{-1} converts wavelet power to energy density. Wavelet coherence can be considered as localised cross-correlation coefficient between two time series in frequency-space. The phase relationships between wavelet coherence time series can be determined as in cross-wavelet transform, except that their results would differ due to smoothing applied to data in coherence calculations. The confidence intervals are determined using Monte Carlo method (Grinsted et al., 2004).

8.2.5 High frequency variability

I use 10 years of data and filtered SST and zonal and meridional wind stress to particularly assess the spatial and temporal patterns of variability. The data

comprising SST and wind stress fields have had their long-term mean and seasonal cycle removed. The data are then subjected to 5-20 days time and 5-10° spatial grid windowing using a bandpass filter based on Fourier analysis. The filtered data are then subjected to EOF analysis described in chapter 7. This is analysed in section 8.3.7.

8.3 Results

8.3.1 Interannual variability of TIWs in the Gulf of Guinea

In this section, I study the interannual variability of the waves at latitudes 3°S and 3°N, and along longitudes 20°W to 5°E. The interannual anomalies of SST and wind stress magnitudes are passed through a bandpass filter (keeping only 15-40 day signals) in order to highlight the waves. The latitude belts of 3°S and 3°N are chosen as they represent the southern and northern edges of the Atlantic Niño (3S-3°N, 20°W-0°E), while still on the edges of the TIWs. This may provide an insight into how interannual variability of the waves could aid in the warming/cooling of the Atlantic Niño. Characterising these waves and attempting to contrast them based on north-south locations from a decade of satellite observed data therefore, might provide a better hint on their temporal and spatial extent.

8.3.1.1 Tropical instability waves at 3°S

The tropical instability waves at 3°S (figure 8.1) show significant spatial and temporal variability at interannual scale. The waves become apparent from May and persist toward end of year. However, a substantial longitudinal variability is evident in all the years. For example, in 1999 the waves exist only within 17-20°W and did not appear in the eastern basin, compared to 2002 and 2003 when they appeared along the whole longitude band.

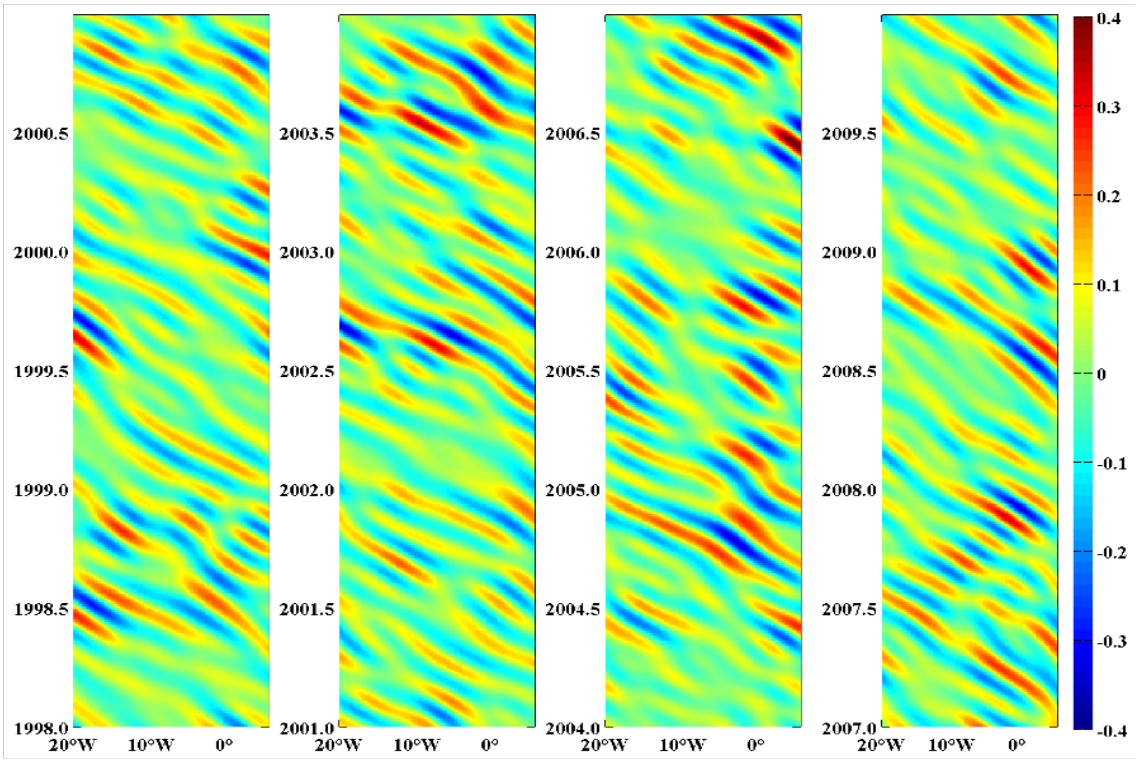

Figure 8.1. *Longitude-time bandpass-filtered SST anomalies along 20° W to 5° E on latitude 3° S. The plots cover a period of 12 years (1998 to 2009). Units are in °C.*

The wind stress magnitude of the TIWs is shown in figure 8.2. There are considerably weaker TIW events in most of the years with the exception of 2005 and 2006. The signals in 2005 appear during the early half of the year having strong amplitudes east of 5°W. This is interesting because in the far eastern Gulf of Guinea, the waves would have been expected to be weaker due to proximity to land to the north and east. This is reflected in the SST for the same period (figure 8.1). During the mid-2006, the waves are stronger east of 0°E from the wind data that is also reflect in the SST data. This suggests that the waves in the region are affected not by remote forcing but by direct winds that act to modify the SST. Although, the signatures of these waves are weaker from these plots (figure 8.1 and 8.2), this does not mean that they are generally weaker. The signals of TIW are tied to the seasonal signal of the tropical Atlantic, which has been pre-filtered. Hence, the representation here highlights non-seasonal variability and interannual signatures of the waves. The waves were also weaker in 2007 and 2008 and these are associated with reduced cold tongue due to the

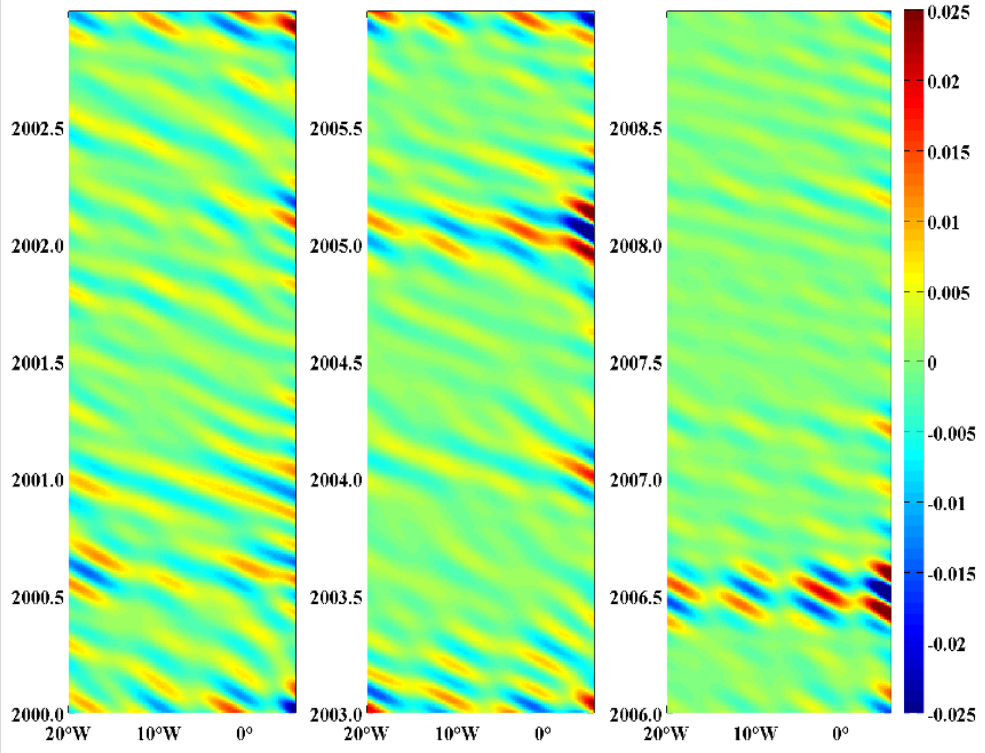

Figure 8.2. *Longitude-time bandpass-filtered wind stress magnitude anomalies along 20° W to 5° E on latitude 3° S. The plots cover a period of 9 years (2000 to 2008). Units are in* Nm^{-2}.

weakening of the southeasterlies.

8.3.1.2 Tropical instability waves at 3°N

The TIWs at 3°N (figure 8.3) show significant interannual variability with obvious signatures that begins in May, and ends in September/October. The waves are stronger in 2000, 2002, 2003, 2005 and 2009 due to negative non-seasonal SST anomalies observed in the ATL3 region (figure 8.5) that helped to enhance them. This is in contrast to the years 1998, 1999 and 2008 where they showed weak signatures due to warmer waters in the ATLT3 region that facilitates in suppressing the waves. In 2001, the waves were only strong east of 10°W and lasted only for about 3 months. In a similar study using data from 1998-2002, Caltabiano et al. (2005) compared the strength of the waves along latitudes 1-4°N and found a covariability of the waves with zonal and meridional winds. Wind stress magnitude of these waves (figure 8.4) reproduced the strong wave

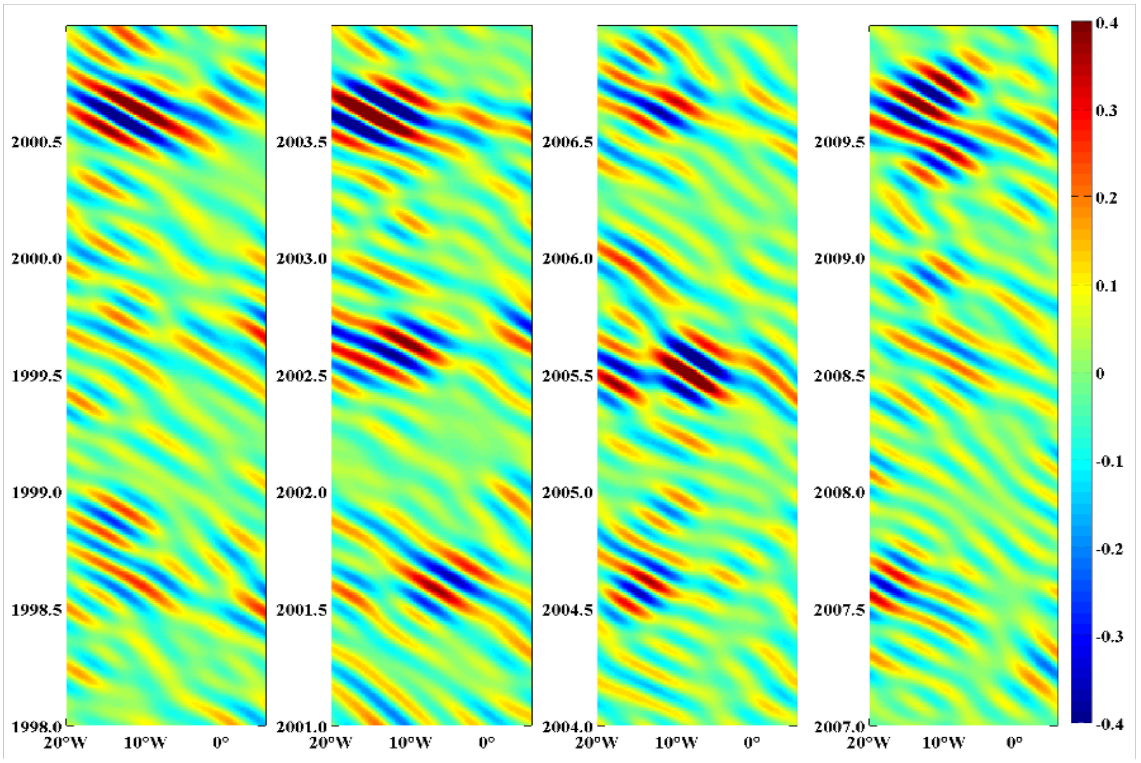

Figure 8.3. *Longitude-time bandpass-filtered SST anomalies along 20° W to 5° E on latitude 3° N. The plots cover a period of 12 years (1998 to 2009). Units are in °C.*

signatures observed in the SST for some years, e.g. 2001, 2002, 2005. However, the strong signatures observed from the winds in 2008 did not appear in the SST plots. This is due to warming of SSTs that suppresses the waves (figure 8.5). In 2006, the waves pick-up from around April and lasted until August, appearing west of 0°E. During the years 2001, 2002, 2005 and 2006, coupling between the overlying atmosphere and the SSTs at mesoscale level is expected to be strong.

8.3.2 Spatial correlation of SST and wind stress fields

Ocean-atmosphere interaction in the tropics is quite unusual due to the interplay of coupled effects. At large-scales, each medium is strongly controlled by the boundary conditions imposed by the other (Neelin and Dijkstra, 1995). The upper ocean circulation is largely controlled by the previous wind stress with little

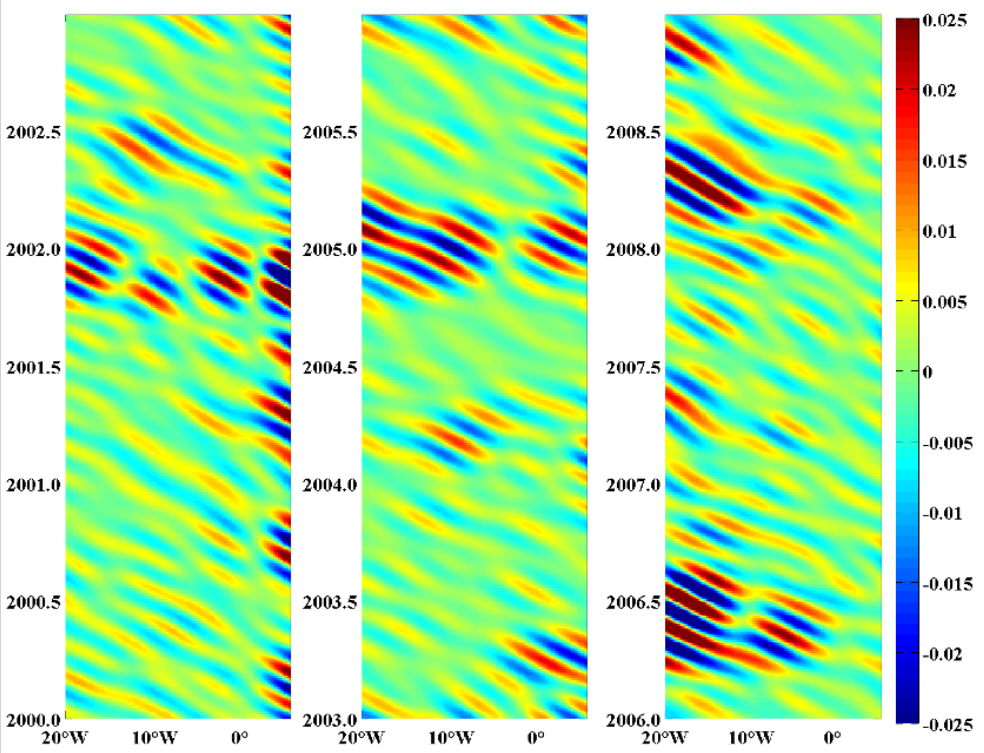

Figure 8.4. *Longitude-time bandpass-filtered wind stress magnitude anomalies along 20° W to 5° E on latitude 3° N. The plots cover a period of 9 years (2000-2008). Units are in* Nm^2.

internal variability. The major features in the tropical atmospheric circulation are determined by the SST, with internal variability confined to time scales between 1-2 months. These occur due to conditional instability and SST signatures at frontal zones. This contrasts with the mid-latitude variations where internal variability between both the ocean and the atmosphere are large.

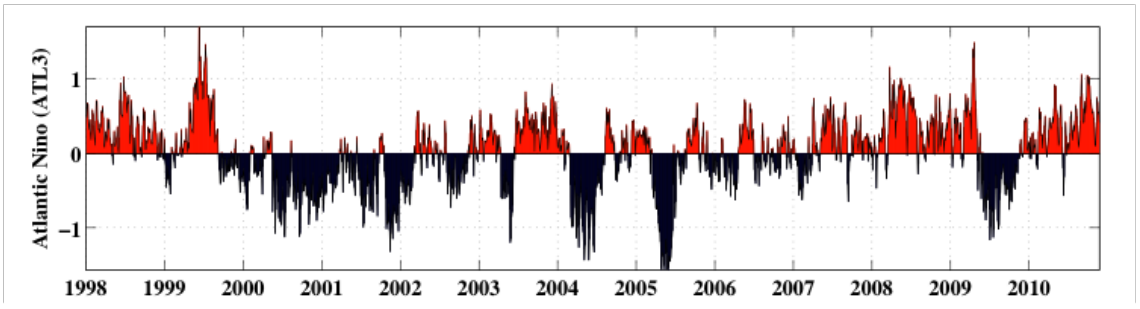

Figure 8.5. *time series of high frequency year-to-year variability of the Atlantic Niño (ATL3). Plot is produced from TMI SST anomalies bounded by the region [20° W-0°, 3° S-3° N]. Data are based on 3-day averages with long-term mean and seasonal signal removed.*

The year-to-year variability in the Atlantic Niño region (figure 8.5) exhibits about a 4.5 year cycle. This indicates the frequency of Atlantic Niño, and shows significant interannual variability. While interannual variability of the TIWs affect the SST, the latter also affects the atmosphere through a lead-lag relationship. The most important variability in the tropical Atlantic due either to the meridional mode or the zonal mode (Atlantic Niño), occurs during the boreal summer. The response of SST forcing to the overlying atmosphere and vice-versa are important in driving variability such as the cross-equatorial SST gradient and may modulate the climate through wind-evaporation-SST feedback. This section highlights spatial correlation between the non-seasonal fields of SST and zonal and meridional wind stresses during the boreal summer (June-July-August) with data spanning 2000-2009. The time series of every pixel of SST is correlated with corresponding pixels of wind stress field for the period of the data (1202 points).

The surface wind stress drives the dynamics of ocean-atmosphere boundary layer, and is therefore expected on physical grounds to be related most directly to the generation of surface waves and the roughness detected by radars, as well as having a wide importance in the production of wind-driven surface currents and the mixing processes of the upper ocean (Robinson, 2004).

Strong correlation (r=∼0.5) of zonal wind stress and SST is observed north of the equator between 8-18°N (figure 8.6a) just outside the region of the seasonal TIWs. Another considerable correlation (r=∼-0.3) is observed along River Amazon output centred at 40°W/2°N and at the south centred at 0°E/7°S. The rest of the basin is characterised by weak correlations, implying that relationships between zonal wind stress and SST are not significant in the absence of seasonal cycle.

The meridional wind stress and SST correlations also showed strong positive correlations (r=0.55) at the same location north of the equator. However, the plot shows a secondary correlation (r=∼0.4) around the equator in the Gulf of

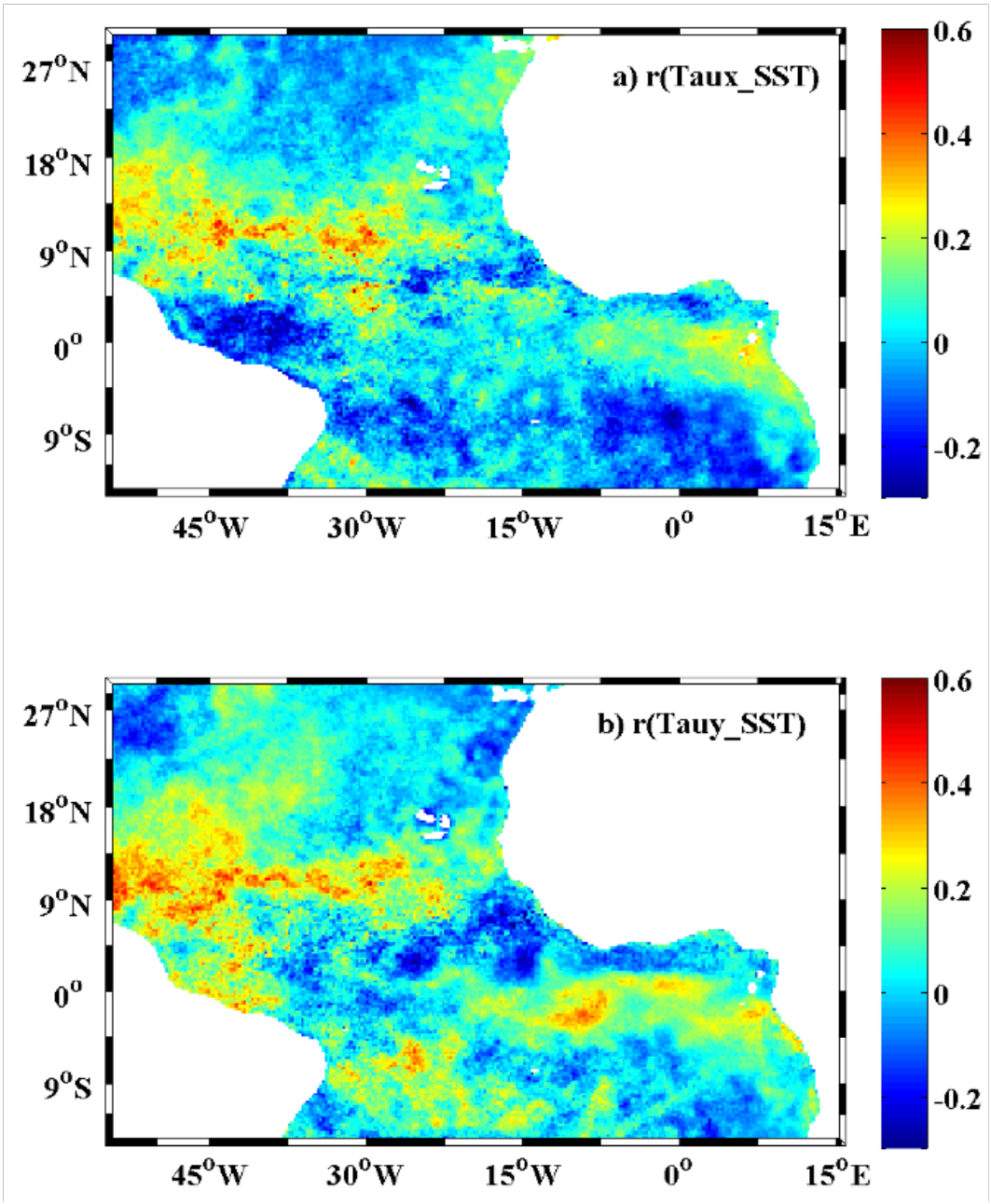

Figure 8.6. *Spatial correlation of anomalies between SST and a) zonal wind stress, b) meridional wind stress during JJA period. Data are based on 3-day averages spanning 2000 to 2008.*

Guinea. SST gradients influence the wind stresses through instability of atmospheric boundary layer, hence increased SST result in equivalent strong wind stresses. It is important however to note that momentum transfer varies with atmospheric stability. Highly unstable lower atmosphere entails stronger momentum. Anomalous wind stresses have an additional effect on ocean circulation as a secondary circulation is ensued. This results in stronger surface currents which

themselves act to alter the relative motion between the ocean surface and the stress fields (Small et al., 2009).

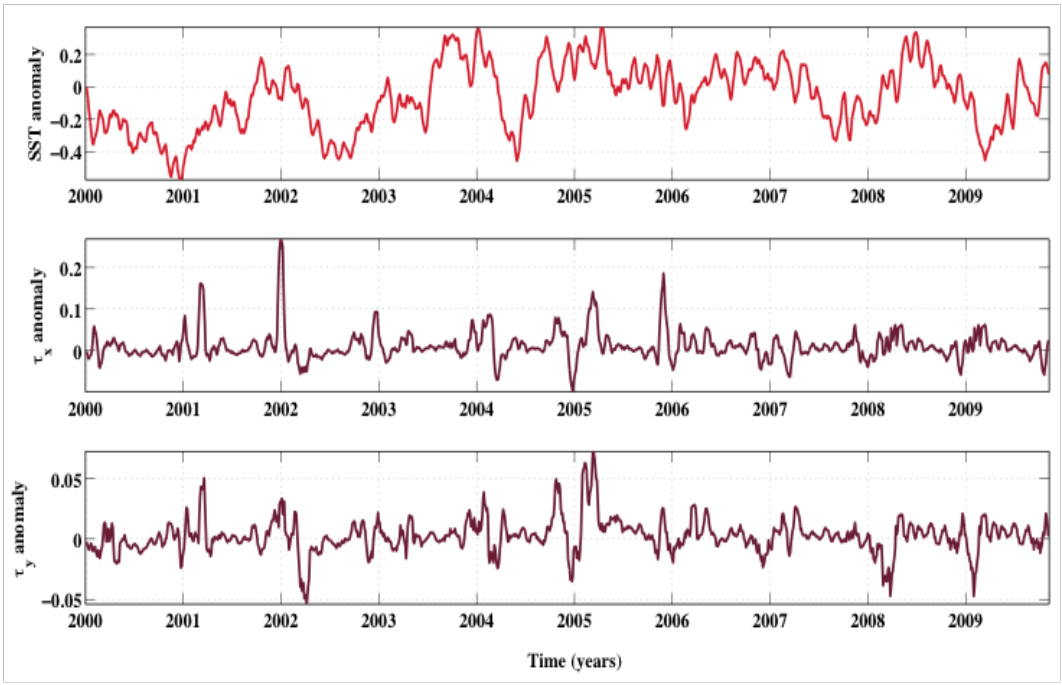

Figure 8.7. *time series of spatially averaged SST and wind stress fields covering the whole domain. time series are smoothed with a 21-day moving average.*

8.3.3 SST and Wind Stress (CWT)

The time series plot (figure 8.7) show non-seasonal characteristics of both SST and wind stress fields. High amplitudes are recorded that signify either warming or cooling from the SST, with peaks showing interannual variability. The zonal wind stress shows substantial peaks in 2001, 2004 and 2005. The meridional counterpart also shows peaks with substantial interannual variability. Both interannual and short-term periodicities of these data suggest a superposition of different frequencies in time. I advance investigate their type and occurrences using Morlet 'mother' wavelet.

Continuous wavelet transform (CWT) for the SST and wind stress fields (figure 8.8) are computed using Morlet wavelet following (Torrence and Compo, 1998).

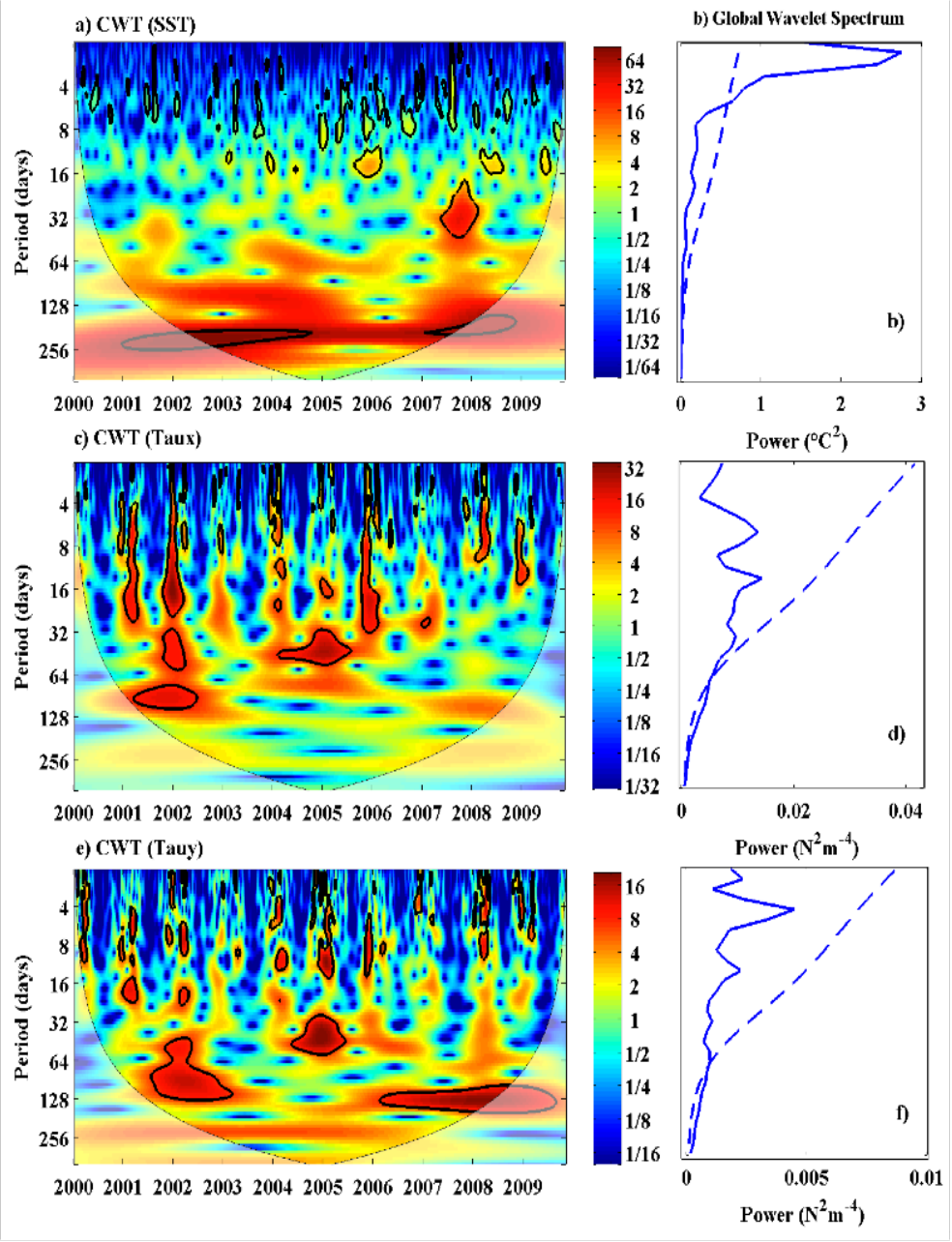

Figure 8.8. *The Continuous wavelet transform (CWT) of SST and wind stress fields (left panel) calculated using Morlet function. The thick black line designate the 95% confidence levels against red noise and the cone of influence (COI) where edge effects might distort the picture is shown in lighter shade. The global wavelet power spectral density (PSD) for each variable (right panel) shows amplitudes and the 95% confidence level as dashed lines.*

The CWT has artefacts because it is not completely localised in time. Therefore, it is necessary to introduce the cone of influence (COI) in which the edge

effects cannot be ignored (Grinsted et al., 2004). The COI here is taken as the area in which the wavelet power caused by the discontinuity of edge dropped to e^{-2} of the edge value.

Apparent intraseasonal variations with a period of 17-40 days were observed in the SST data (figure 8.8a) in 2007 having stronger amplitude PSD (figure 8.8b). This is the most significant intra-seasonal variability in the SST at 95% confidence level, and is associated with the variability of TIWs. This suggests an important characteristic associated with the SST in that year. An anomalously high SST anomaly greater than 2°C was observed in the Gulf of Guinea during the summer of 2007 (see chapter 6) that was associated with flooding in West Africa and the southern Sahel (Paeth et al., 2010).

The SST also exhibits a feature at a period of 200 days between 2002 and 2004 but that did not appear in the wind stress plots. These are not connected to the intra-seasonal variability but are related to interannual variability of the cold tongue that is characterised by a semi-annual cycle. Interannual variability of the cold tongue is caused by the weakening of the southeast trade winds that force the ocean at the cold tongue region. These affect temperatures in the Gulf of Guinea leading to cooler/warmer SSTs as observed by Marin et al. (2009).

There are evidently common features between the two wind stress components in the wavelet power such as the significant peaks in 35-50 day around 2004/2005. Another similar feature with ∼90 days around 2001/2002 exists but the zonal one appeared earlier and short-lived. This strongest magnitude shows the inherent intraseasonal variability in the time series. The PSD of the respective wind stress time series differ, with the zonal magnitude more than 3 times the meridional magnitude (figure 8.8d,e). Other peaks apparent within the 95% confidence level are in the wind stress fields, such as the ∼4-24 day bands that occur in 2001, 2002 and 2005 which last longer in the zonal wind stress than the meridional counterpart. Each of these peaks has shown significant PSD amplitudes.

8.3.4 SST and zonal wind stress (XWT and WTC)

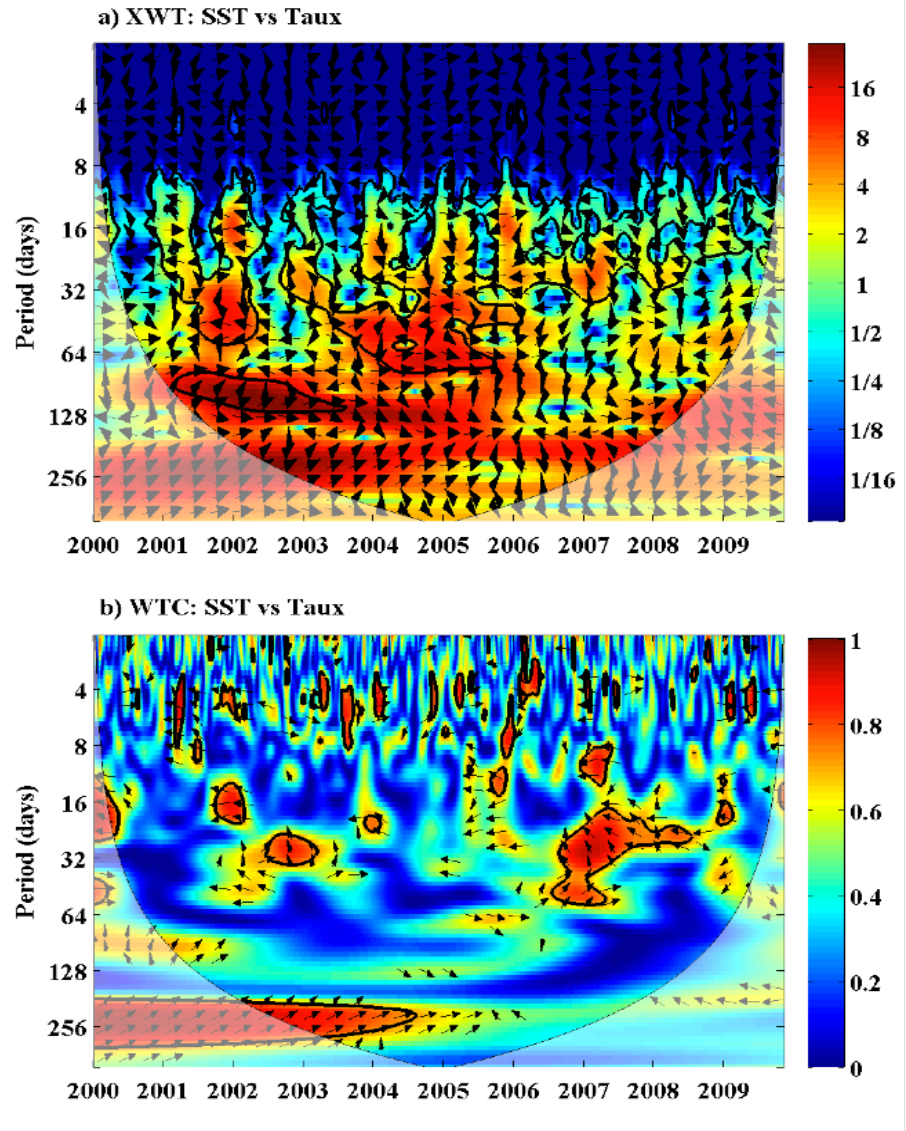

Figure 8.9. *Cross Wavelet Transform (XWT- top panel) showing period and time where SST and zonal wind stress have high common power. Wavelet Transform squared Coherence (WTC-lower panel), indicating period and time where SST and zonal wind stress covary. The 95% confidence levels determined through Monte Carlo are bounded by black contours. The directions of arrows indicate phase relationship. In phase relationship (0°) is right, anti-phase (±180°) is left, SST leading zonal wind stress by 90° (down), and zonal wind stress leading SST -90° (up).*

The cross wavelet transform (XWT) between SST and zonal wind stress are

shown in figure 8.9a. The abscissa is the timescale and the ordinate is the frequency while the colour is magnitude of the observed frequencies. Highest magnitudes occur during the years 2001 to 2004 where a pronounced signal occurs with period of 70-128 days. The arrows at these periods face right, showing relative phase difference between the time series, indicating an in-phase relationship with zero lag. This simply explains coupling between the zonal winds and SST, where one responds to the changes of another. These amplitudes are due to the peaks observed in the time series in figure 8.7 occurring in the same period. However, the wavelet coherence (WTC-figure 8.9b) shows strong coherence (0.6) only in 2001 but not in 2002. I associate this with current anomalies that act to dampen the stress fields as well as SST, particularly at the tropical instability waves (TIW) frontal zones. Earlier studies by Small et al. (2009) showed that surface currents at the TIW region alter the stress fields and results in damping the waves. It may also explain the impact of the Amazon output on wind stress and SST fields west of the equatorial Atlantic.

Strong amplitudes are apparent between 2003 and 2005 and a period of 32-70 days whose phase relationship is rather complex. Although, this falls within the 95% confidence limit, the corresponding wavelet coherence (figure 8.9b) is rather weak. A significant coherence ($\sim$0.85) is observed during the period of 18-50 days that appears in late 2006 to 2008 showing an out of phase relationship. Part of this shows considerable amplitude in the cross wavelet plot. These also appear in the SST-zonal wind stress spatial correlations north of 10°N shown in figure 8.6a. These amplitudes and coherence might be attributable to intraseasonal fluctuations of the tropical oceans, the Madden-Julian Oscillations.

During 2004 and mid-2005, strong amplitude is observed at a period of $\sim$20-40 days having an anti-phase relationship (figure 8.9). These are periods of the TIW that couple with the atmosphere. The anti-phase relationship explains an increase in wind speed and hence wind stress over the waves, thereby cooling the SST. This explains that SST at the TIW frontal zones of a threshold (26-29°C) affect the heat and moisture fluxes resulting in instability in the atmospheric

boundary layer (ABL). A moderate coherence (∼0.6) is apparent but that is restricted to a period of 32-40 days that lasts from mid-2004 to early 2005.

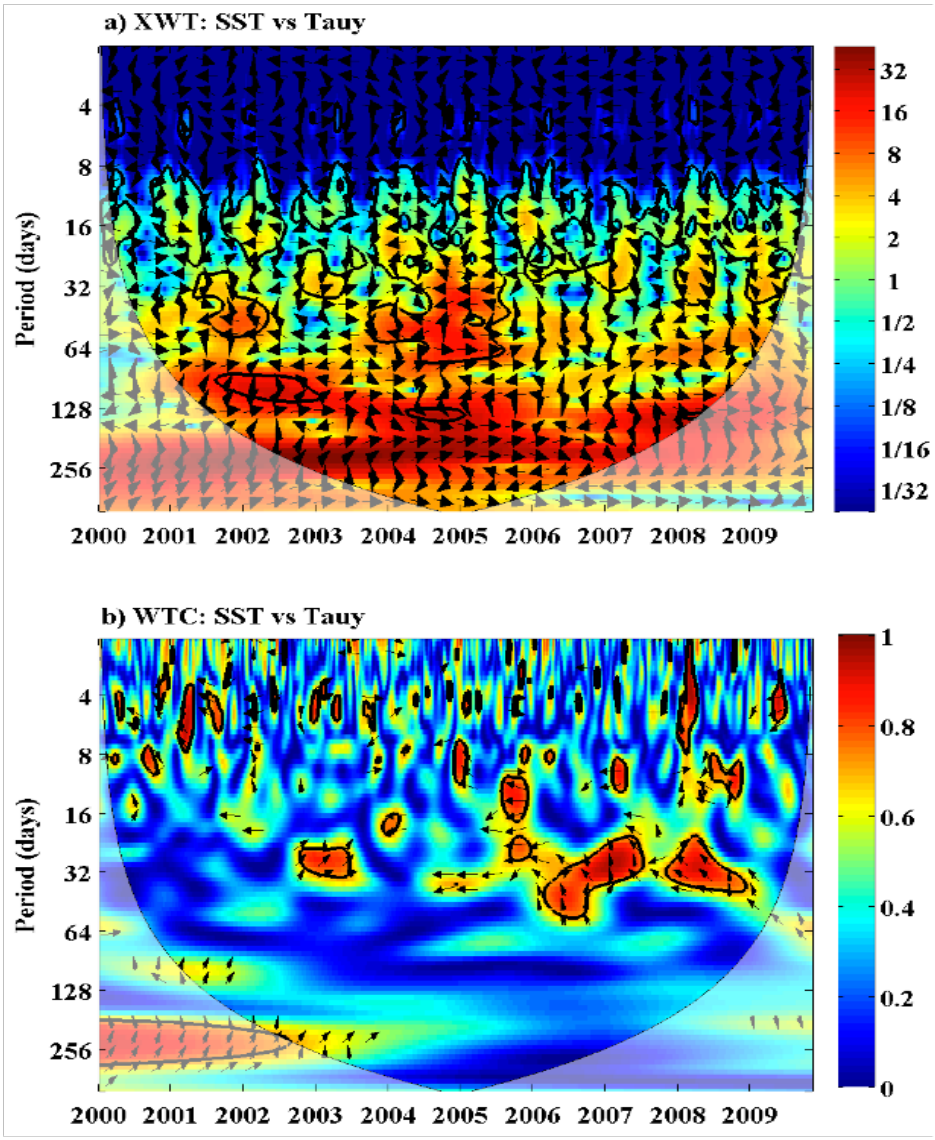

Figure 8.10. *Cross Wavelet Transform (XWT - top panel) showing period and time where SST and meridional wind stress show high common power. Lower panel shows Wavelet Squared Coherence (WTC), indicating in period and time where SST and zonal wind stress covary. The 95% confidence levels determined through Monte Carlo are bounded by black contours. The directions of arrows indicate phase relationship. In phase relationship (0°) is right, anti-phase (±180°) is left, SST leading meridional wind stress by 90° (down), and meridional wind stress leading SST -90° (up).*

8.3.5 SST and meridional wind stress (XWT and WTC)

The cross wavelet transform (XWT) between SST and meridional wind stress are shown in figure 8.10a. Strong coherence (WTC 0.9) exists between 2006 and early 2007 (figure 8.10b) at a period that varies between 20-55 days. Although, these are represented with weaker amplitudes in the cross wavelet transform, they are important having exhibited that meridional wind stress leads SST (upward arrows). This is related to large-scale cross equatorial SST gradient that causes wind anomalies north of the equator resulting in a wind-evaporation-SST feedback process. In the WES-feedback mechanism, the anomalous SST gradient is impacted with anomalous southwesterly winds that weaken northeasterly winds resulting in the warming of the SST (Mahajan et al., 2009). This anomalous SST gradient may partly play a role in determining the local climate of West Africa and the Sahel region through convective processes and rainfall. A separate band of strong coherence (0.85) is observed in 2008 for the period of ∼20-40 days showing an anti-phase relationship which is represented by arrows facing left corresponding to ±180°. This could be the response of wind stress over cold SST as it crosses over the cusp-shaped features of tropical instability waves.

8.3.6 Air-sea coupling

The region of tropical instability waves is a prime candidate for mesoscale SST and wind coupling, particularly at the SST fronts. The off-equatorial SST front anomalies in the tropical instability waves (TIW) region are associated with the changes in the strength of wind on either side of the equator. The influence of these winds on SST as well as subsequent impacts on the near-surface circulation extends beyond the region of the cold tongue. The coupled characteristics

of SST and wind are assessed here based on wind stress fields and the corresponding divergence/convergence, stress curl and speed. The wind stress divergence and stress curl are calculated using the finite difference method described by (Piolle and Bentamy, 2002).

The wind stress field becomes stronger as the winds descend over warmer SST (figure 8.11a). Wind stress increases from 0.2 to 0.6 Nm^{-2} and this coincides with the sharp SST front with a threshold of 26-28°C between 1° and 4°N. The impact of these stresses creates divergence and hence Ekman upwelling along the SST threshold as is clearly delineated in figure 8.11b. Associated with the SST fronts of the TIWs and their coupling with the overlying atmosphere is wind stress curl (figure 8.11c). As the wind blows over the SST isotherms of the northern TIW fronts, positive wind stress curl is generated. This leads to an observed linear relationship between the ocean and the crosswind (meridional gradient) component of the overlying atmosphere.

During the period of TIWs (May to October), an increase in wind speed (figure 8.11) results in an equivalent increase in wind stress. This induces positive wind stress curl whose strength depends on how strong the SST is, as threshold of 26-29°C corresponds to stronger curl. At the centre of the cold tongue, where SST remains low, wind stress curl becomes negative.

The centre of the basin (14-18°W, 3-4.5°N - figure 8.11) shows interesting peaks for both wind stress and wind stress curl but not with wind divergence. These peaks do not correspond to the SST threshold (26-29°C) of the divergence, but with SST between 28.5-29°C. This explains that the wind stress divergence can occur at smaller SST signatures compared to the other two components. This is because strong SST fronts are related to the crosswind (perpendicular gradient) in terms of meridional stresses and stress curl, but it is associated with divergence by alongwind direction (parallel gradient). That means, wind stress fields and stress curl can have larger magnitudes depending on the strength of the SST, regardless of any threshold compared to divergence.

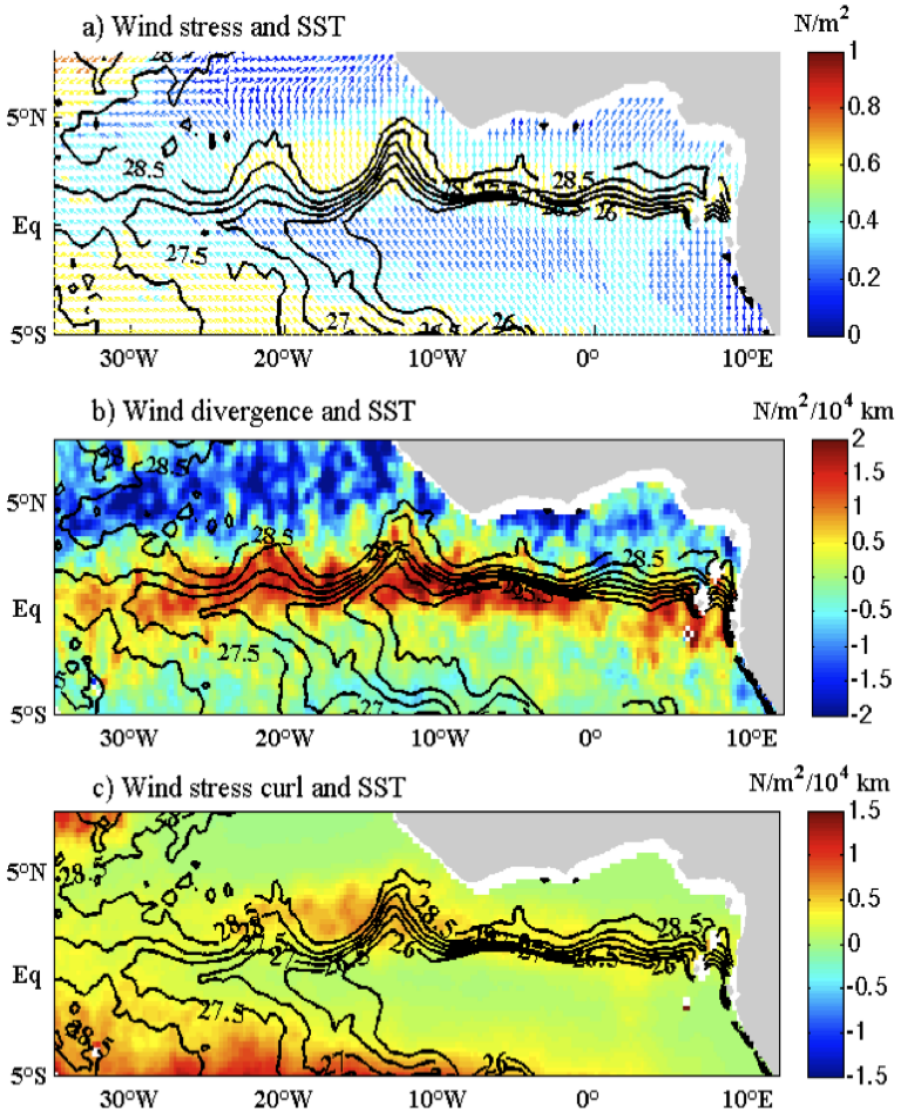

Figure 8.11. *Ten-day average maps for 11-20 June 2005 showing TIW signatures. The components of wind are in colour, and each is overlaid with SST contours, a) Wind stress vectors, b) wind stress divergence, and c) Wind stress curl. Isotherm intervals are 0.5° C.*

8.3.6.1 Correlations of SST and wind stress curl

Wind stress curl at the edges of the tropical instability vortices is associated with upwelling and downwelling as well as advection of temperature at the near surface. These are very important features that significantly affect ocean circulation (Chelton et al., 2004). Understanding the coupling of wind and SST at

the SST fronts is important so as to give further background basis to numerical model estimates of sensible and latent heat fluxes, which are also likely to be underestimated especially when the model/s resolution is 1° or more (Rouault et al., 2003b).

The spatial correlation of SST and wind stress curl was conducted based on 3-day data spanning ∼10 years (2000-2009 -figure 8.12) covering the boreal summer months (JJA). Strong positive correlations (r=0.6) are observed in the Gulf of Guinea extending from about 16°W to 3°E that falls within the Atlantic Niño region. Other high positive correlations appear north of the equator centred at 40°W/28°N, 22°W/25°N and north of the Guinea Dome between the continental boundary of Africa and Cape Verde Islands. Strong negative correlation (r=∼0.5) is observed between 10°-15°N.

The strong negative correlations (r=∼ -0.5) in the western basin both north and south of the equator show signatures of the positioning of the ITCZ, where the thermal equator is sandwiched by these phenomena. The negative correlation around the equator shows that cold SSTs in that region are associated with northward positioning of the ITCZ at the beginning of summer, when the south-east trade winds are stronger. The negative anomalies at about 10°-15°N are linked to the southward positioning of the ITCZ when the northeast trade winds are stronger towards the end of summer. These are dynamics corresponding to the Atlantic meridional mode. The two positive correlations north of 20°N explain the connections between the northeasterlies and the ocean circulation. These correlations occur in late summer when the winds become stronger as the ITCZ retreats to the south. However, the winds are accelerated westward by the African easterly jets (AEJs) that lie between 5-15°N, instead of south-westward. The accelerated winds then act as stress on the warm ocean surface and with the beta effect, leads to an anticyclonic circulation (curl). These two features are important in the ocean circulation due to their connection to the tropical high system and the generation of African easterly waves (AEW). The AEWs are the energy sources for the extratropical cyclogenesis.

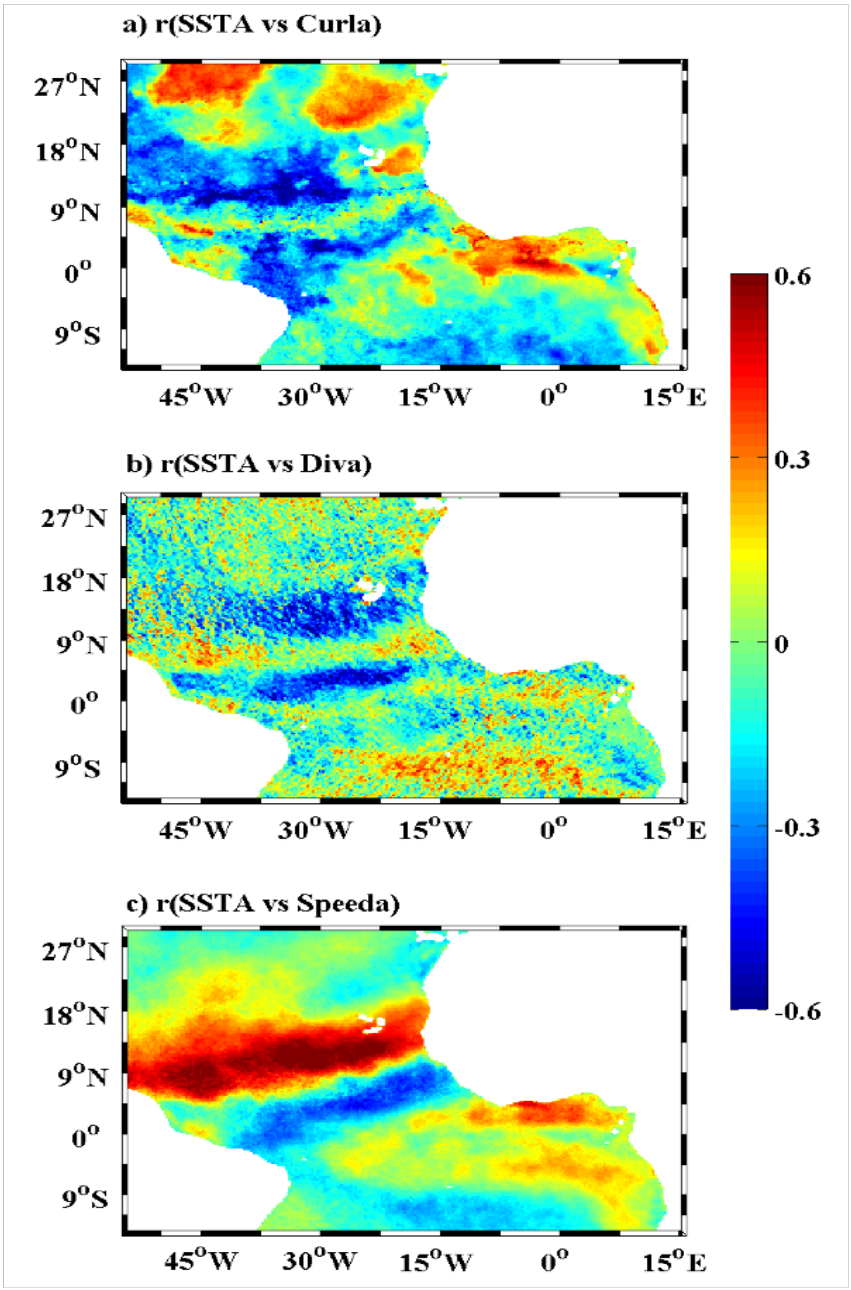

Figure 8.12. *Spatial correlation (r) between SST anomalies and a) wind stress curl anomalies b) wind stress divergence anomalies, and c) wind speed anomalies. Data is based on 3-day averages spanning 2000 to 2009, and for the June-July-August (JJA) period only.*

8.3.6.2 Correlations of SST and wind stress divergence

To further assess the region most influenced by wind stress divergence in the equatorial Atlantic, a temporal correlation between SST and wind stress was

calculated based on their anomalies (figure 8.12b). This shows negative correlation dominating two regions along the ITCZ pathway, one along 4°N and another centred at 28°W/14°N. Weak positive correlations exist south of 7°S and along the Atlantic thermal equator at 8°N. While wind stress divergence computed from a 10-day data (Figure 8.11b) corresponds to an SSTTIW of a threshold of 26-29°C exhibiting a zonal relationship, correlation coefficients of the JJA seasonal data here shows an asymmetric positioning with the equator that highlights a negative feedback. The reason is that SSTs of this threshold are required for maximum divergence to occur. With these calculations using anomalies of data, the correlations exhibit a scenario that is driven by the meridional mode, rather than the zonal signature associated with the SST threshold.

The negative correlation around the equator having an asymmetric nature may elucidate the findings of Chelton et al. (2004) on ocean eddies, that linear response exists between divergence and alongwind SST gradient. In essence, meridional SST gradients are associated with meridional wind gradients. Wallace et al. (1989) formulated a hypothesis to explain SST-wind divergence relationship. They explained that, the near-surface wind becomes unstable when passing across SST front towards warmer waters, leading to enhanced mixing in the marine atmospheric boundary layer. Momentum from upper easterly jets is then brought down to accelerate the surface winds. While divergence enhances the fluxes into the boundary layer, convergence aids in sinking warmer surface waters into the mixed layer.

A similar correlation was conducted using data with full seasonal signal and mean (not shown), during the period of TIWs, and the results showed a high negative correlation (r=-0.8) along the SST frontal zone. This is not surprising considering the fact that the wind stress divergence field only appears as strong signatures when the SST fronts of TIWs reach the threshold of 26-29°C that last for 6 weeks in the Atlantic. This is an indication that the SST frontal zones are regions of strong convergence that leads to entrainment of warmer surface waters

into the mixed layer as a result of wind shear associated with the waves. Surface patches of TIW cyclones are created due to divergence (Jochum and Murtugudde, 2006), thereby thinning the mixed layer. The latter is responsible for zonal temperature advection, which is as large as meridional temperature advection. The atmosphere heats the water and then this heat is transferred into the mixed layer through the patches due to convergence.

It should be noted that with temperatures below and above the threshold, the tropical Atlantic SST-divergence relationship would be mere random perturbations.

This SST-wind stress divergence correlation suggests that the meridional mode of the tropical Atlantic and the air-sea interaction at the TIW frontal zones dominate the mesoscale ocean-atmosphere interaction that determines heat fluxes in and out of the ocean. In addition, coupled ocean-atmosphere models that simulate surface heat and moisture fluxes must give special consideration to the tropical instability waves frontal zones, especially the 26-29°C SST threshold to be able to simulate them correctly.

8.3.6.3 Correlations of SST and wind speed

Correlation analysis of SST and wind speed (figure 8.12c) showed two parallel maxima that are of opposite sign. These are associated with the meridional mode of the tropical Atlantic. A strong positive correlation (r=0.6) is apparent between 7-12°N, while a secondary but negative correlation (r=-0.4) appeared between 0-8°N. The SSTs around the equator become cold after the warm, rain-bearing ITCZ band moves northward, and also due to the presence of cold tongue waters. This leads to a negative correlation around the equator when the southeast trade winds flow to the north. The positive correlation north of 8°N falls within the northernmost position of the ITCZ during the late boreal summer. The northeasterly winds correlate well with the warm SSTs and this correlation is facilitated by the upper layer atmospheric winds resulting from instability in the atmospheric boundary layer due to heat fluxes. These winds aid

in the southward migration of the ITCZ. Along the West African coast, however, positive correlation (r=∼0.5) is observed which is associated with the warming of the Gulf of Guinea during the TIWs period.

This analysis suggests that the ocean drives atmospheric variability and pushes the rain band southward. This occurs as a result of strengthening of the north-east trade winds accompanied by a weakening of southeasterly winds during late summer.

8.3.7 High frequency (5-20 days) oscillations

A 2-20 day oscillation additionally forces intra-seasonal variability in the upper layer of the Atlantic Ocean (Athie et al., 2009). Houghton and Colin (1987) suggested that 15-day oscillations cool the mixed layer significantly in the Gulf of Guinea in contrast with the net warming due to tropical instability waves (TIWs) in the central and western parts of the equatorial Atlantic. Biweekly oscillations were found to dominate the eastern equatorial Atlantic (Athie and Marin, 2008), using SST and sea level data from 1999-2005, with results showing significant interannual variability. High-pass filtered wind stress anomalies covering the period of May-June 2003 overlie the anomalies of SST for the same period at the western boundary currents (Gulf Stream, Kuroshio, South Atlantic and Agulhas) (see Nonaka and Xie, 2003; Small et al., 2008). However, these studies did not focus on 5-20 day oscillations and their analysis depended mostly on short data records. The goal of this sub-section is to assess the spatial and temporal variability of oceanic and atmospheric processes at sub-monthly periods (5-20 days). The motivation is to attempt to answer the question: *What are the roles of 5-20 day oscillations in wind-driven ocean variability in the tropical Atlantic?*

This analysis is based on pre-filtered data sets. I consider only the first EOF spatial variability and standard deviation of the filtered data, which together would show regions with strongest variability. Longitude-time plots (not shown)

covering the period of the data set in this section showed that the features just north of the equator are westward moving and are characteristics of TIWs.

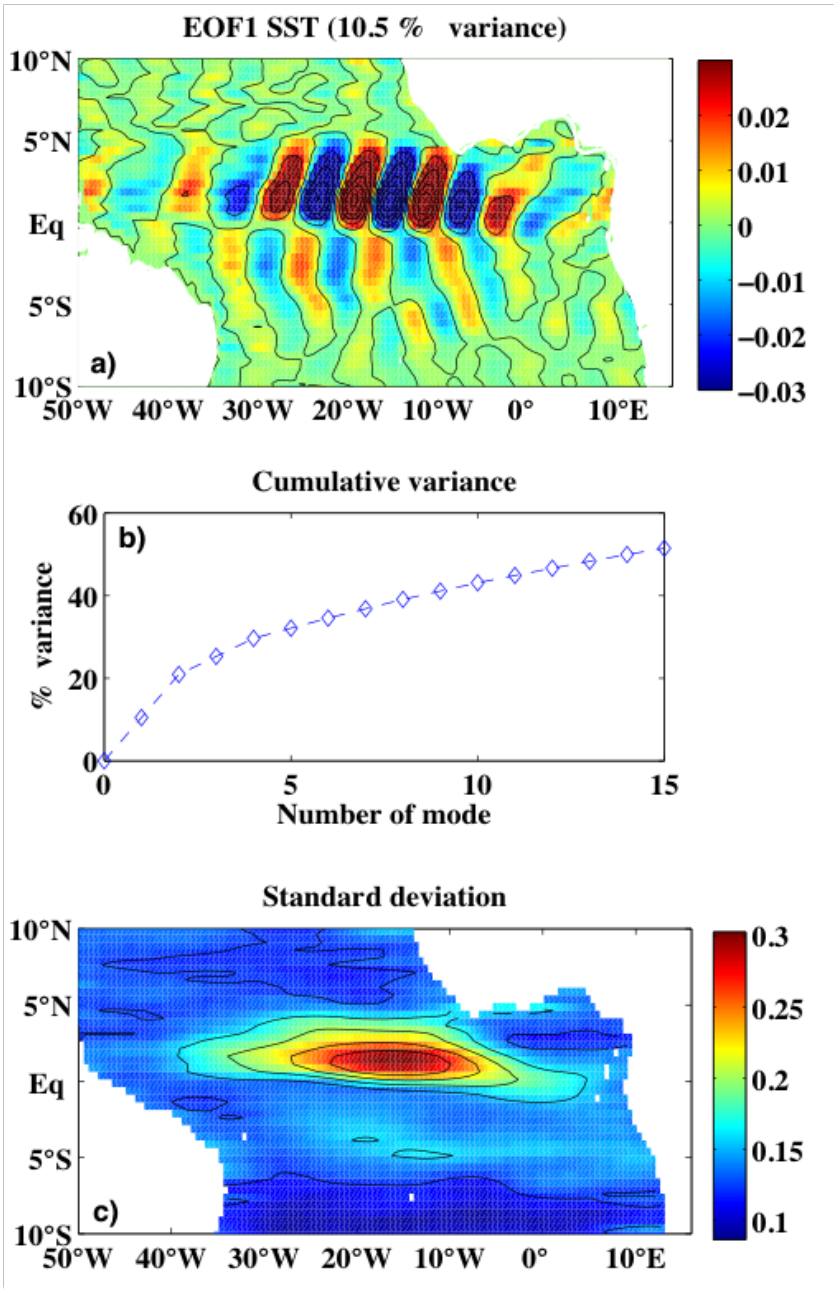

Figure 8.13. *Analysis of high frequency variability of 5-20 days and longitude span of 1-5° based on band-pass filtered SST data. These are, a) EOF1 SST, b) cumulative percentage variance of EOF, c) standard deviation of filtered data (°C). Data are based on TMI SST of 3-daily averages spanning the period of 2000-2009.*

8.3.7.1 Dominant patterns of SST

The 5-20 day filtered EOF1 of SST and EOF cumulative variance are shown in figure 8.13. The strongest variance associated with EOF1 SST at the submonthly period are concentrated north of the equator between 0-4°N and longitude span of 34°-1°W.

The analysis demonstrates that the first few EOFs explain most of the variability, with the first EOF explaining over 10% of the total variance despite using a non-seasonal anomaly data. The first 5, 10 and 15 EOF modes explain about 38%, 47% and 54% of the variance of SST respectively (figure 8.13b). To quantify the degree to which the dominant EOF1 represent the total variability in the data, I present the standard deviation (std) of the filtered data for the period of investigation. A very high std is observed north of the equator mirroring the position of the high variance observed in EOF1. This is because SST gradients are by far larger north of the equator than the south, and that the waves are created by a current shear between the North Equatorial Countercurrent (NECC) and the northern branch of South Equatorial Current (nSEC).

8.3.7.2 Dominant patterns of zonal wind stress

The analysis presented in figure 8.14 show EOF1 of zonal wind stress, EOF cumulative percentage variance and standard deviation of the filtered data based on the submonthly periods (5-20 days). The spatial pattern of EOF1, having over 16% variance (figure 8.14) shows a fairly homogenous distribution across the whole equatorial basin with no distinction between north and south of the equator. Strong variances are observed off Brazil in the west and Congo in the east. Westward moving features have been observed from a movie created from a series of filtered images of this data prior to EOF (not shown) and that dominate but do not compare with large variances north of the equator observed from the SST data seen earlier in figure 8.13. The cumulative variance show that the first 5, 10 and 15 EOF modes explain about 53%, 60% and 62% of the

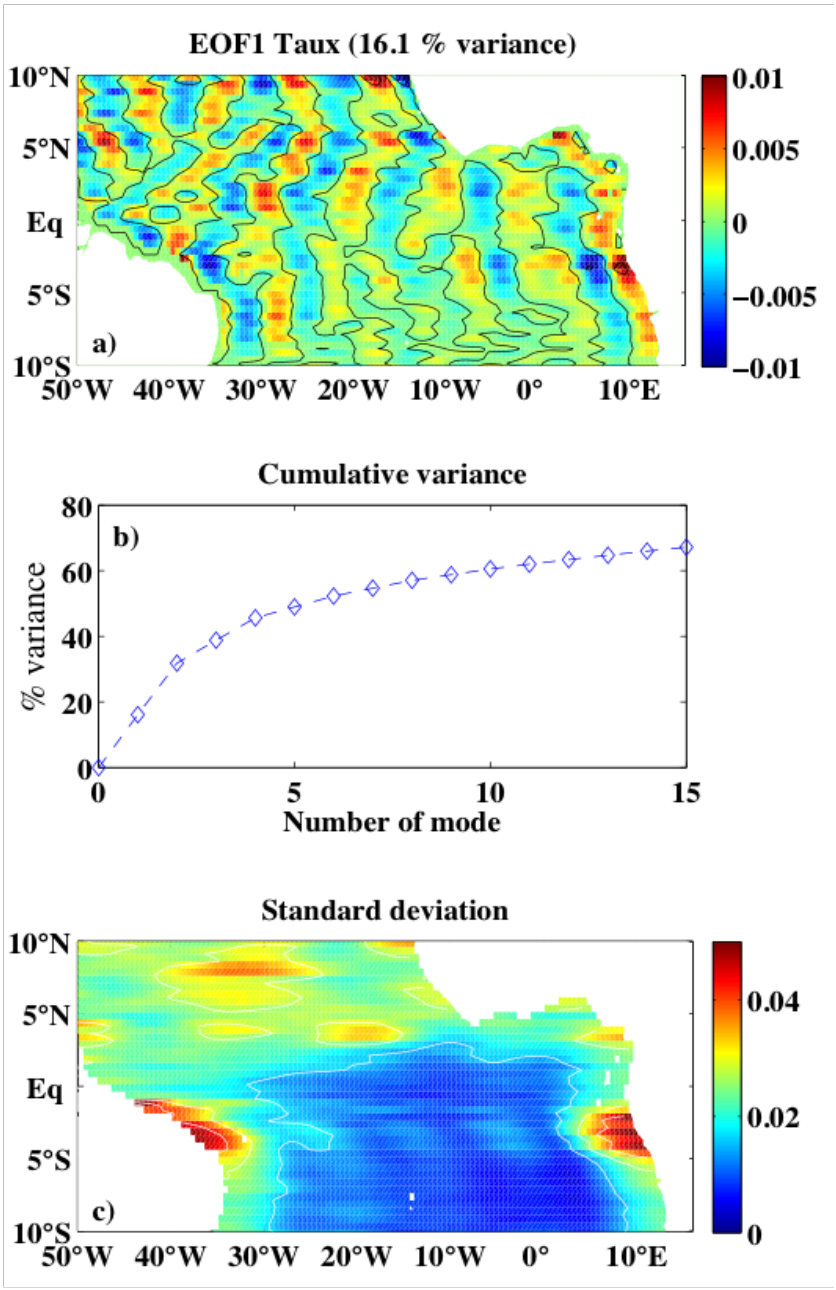

Figure 8.14. *Analysis of high frequency variability of 5-20 days based on bandpass filtered zonal wind stress data. These are, a) EOF1 zonal wind stress, b) cumulative percentage variance of EOF, c) standard deviation of filtered data (m/s). Data are based on QuikScat scatterometer winds of 3-daily averages spanning the period of 2000-2009.*

variance of zonal wind stress respectively (figure 8.14b). The degree to which the dominant EOF1 represent the total variability in the data is presented by the standard deviation of the filtered data. A fairly high std is observed east of

the basin centred at 10°E/4°S and at 37°W/3°S, which is slightly reflected in the EOF1 plot.

8.3.7.3 Dominant patterns of meridional wind stress

The spatial pattern of EOF1 of meridional wind stress is shown in figure 8.15a, exhibiting over 18% of the total variance. A basin scale homogenous characteristic is observed showing westward moving features with significant variance centred at 10°E/4°S and at 37°W/3°S. These variances are apparent from the std plot (figure 8.15c), and also appeared in the zonal wind stress plots in figure 8.14. The cumulative percentage variances of the EOF decomposition are shown in figure 8.15b, which demonstrates that the first 5, 10 and 15 modes explains about 63%, 76% and 80% of the variance of meridional wind stress respectively.

8.3.7.4 Time variability of 5-20 days oscillations at 3°N

The spatial patterns of variability associated with SST and wind stress components (subsection 8.3.7) showed significant variances, with SST demonstrating stronger signatures north of the equator, while wind stress at the western and eastern extreme ends. Here, I show time variability and longitude dependency of these signatures and attempt to explain what makes those variances differ in the spatial distribution shown above. I focus on 3°N, to allow comparison with SST signatures observed in the SST EOF variance shown in figure 8.13a.

The 5-20 day bandpass filtered SST data (figure 8.16a) show oscillations at submonthly periods that are associated with TIWs. These signatures stretch from around 30°W to 5°W, and appear from early July to mid-September. The zonal wind stress (figure 8.16b) reveals strong signatures that span 22°-12°W. These waves however, are short-lived and appeared only in July. Their time and space features however overlap with that of SST, typifying a connection between ocean and atmosphere at these periods and space. The signature of the waves in the meridional wind stress however is weak, but interestingly showed a different

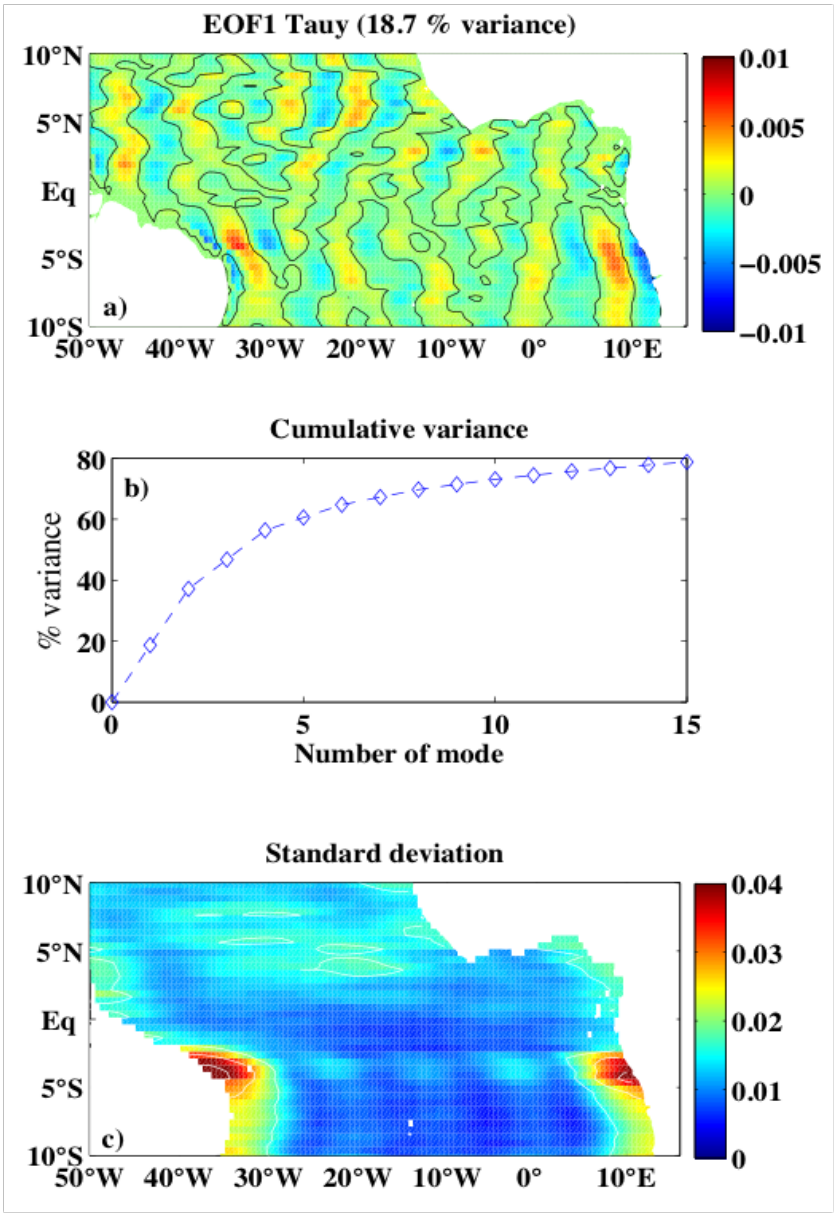

Figure 8.15. *Analysis of high frequency variability of 5-20 days based on bandpass filtered meridional wind stress data. These are, a) EOF1 meridional wind stress, b) cumulative percentage variance of EOF, c) standard deviation of filtered data (m/s).*

timing. Their features exhibit monthly variability, appearing in June, July and September/October periods but not in July. This attests to the fact that the zonal and meridional wind stresses are independent, although an overlap is evident in July months. In July, the meridional wind stress occurs mostly in the east, and the subsequent appearance in September/October occurs to the west.

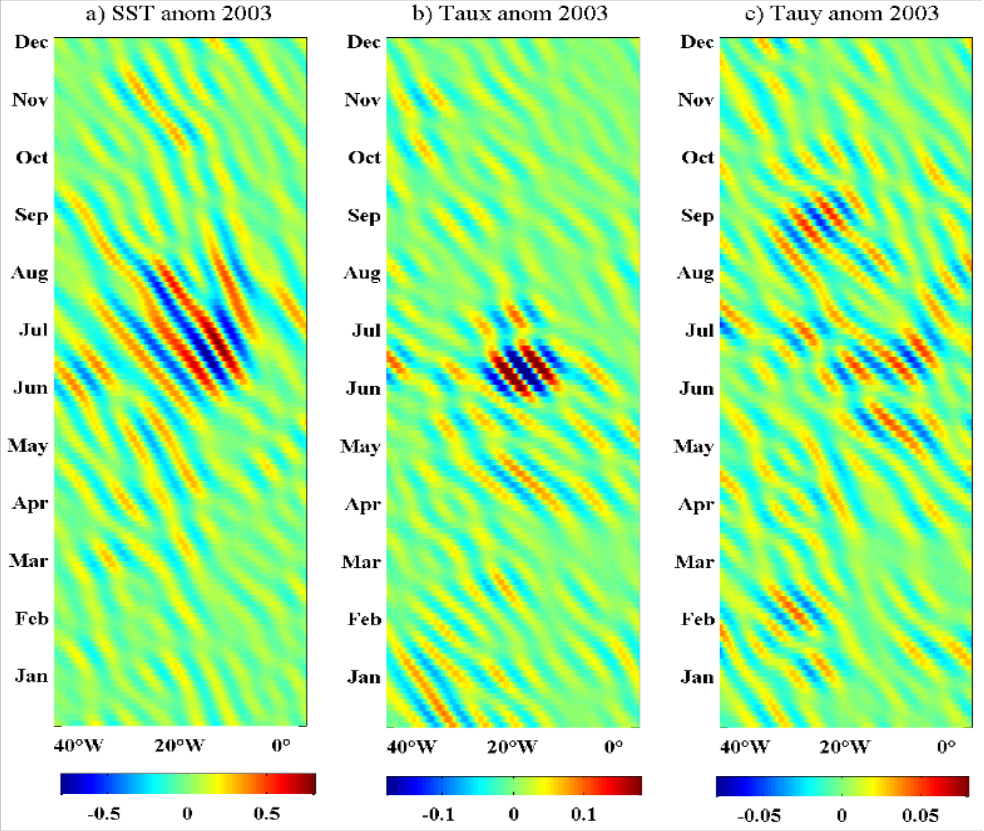

Figure 8.16. *High frequency variability of 5-20 days based on band-pass filtered SST and wind stress anomaly data at 3° N. These are longitude-time plots of, a) SST, b) zonal wind stress and, c) meridional wind stress. Data are based on TMI SST and QuikScat scatterometer winds of 3-daily averages for the year 2003.*

I have characterized 5-20 days oscillations in the equatorial Atlantic based on anomalous SST and wind stress data. Strong variances associated with tropical instability waves are apparent from the spatial SST variance and standard deviation but restricted to north of the equator. These observed characteristics point to the fact that the 5-20 day oscillations are features of TIWs, and hence are important to ocean circulation especially in the modification of the upper layer heat content as well as important coupling with the atmosphere. Other parts of tropical Atlantic however show a clear homogeneous behavior, suggesting that the 5-20-day periods are associated with the tropical instability rather than other physical phenomena.

The wind stress patterns for both zonal and meridional components exhibit

characteristics having large variances to the east and west of the basin. Their appearance in the eastern and western parts of the basin corresponds to areas of strong river outflow. High variances in the eastward region occur at the River Congo output and variances in the west at River Amazon output. River Congo output is situated along the Angola Current and River Amazon at the North Brazil Current. This implies that wind stress fields appear to be modulated by 5-20 days oscillations associated with these currents that are significantly maintained by river output.

The main findings of this sub-section is that SST and zonal wind stress reveal robust covariability of 5-20 days oscillations in July, but atmospheric forcing in September/October is altered by an ocean response that damps the stress fields. River output of Amazon and Congo do alter wind stresses and these could influence the local climate through modification of heat fluxes and hence convection.

8.4 Discussion

8.4.1 Tropical Instability Waves

A marked longitudinal variability is observed at 3°S (figure 8.1) from SST data. The reason is that SSTs were warm in 1999, leading to a weak wave activity due to a reduced cold tongue (Wu and Bowman, 2007a). This year-to-year variability is due to different dynamical factors that cause or modulate the waves. For example, the strength of the cold tongue, as well as the background winds west of the tropical Atlantic facilitates the shallowing of the thermocline in the eastern basin. These winds at the western basin influence the eastern basin via equatorial Kelvin waves (Houghton, 1983; McCreary et al., 1984).

The interannual variability exhibited by the TIWs north and south of the equator may not be explained by a single mechanism. This is due to the highly varying nature of the Atlantic Niño region, which is also linked to the Atlantic meridional mode (Foltz and McPhaden, 2010) and the equatorial Kelvin waves. Positive feedback between SST, thermocline depth and winds (Bjerknes feedback) also tends to sustain the Atlantic Niño region where these waves are sampled, especially during the boreal spring and summer (Chang et al., 2001; Keenlyside and Latif, 2007). Because the zonal temperature gradient is associated with the Walker circulation, the weakening or strengthening of the latter through large-scale ENSO modes such as the Pacific El Niño will undoubtedly cause an effect on Atlantic Niño.

This explains the interannual variability observed in the TIWs at the southern (3°S) and northern (3°N) boundaries of the Atlantic Niño. The inability of both SST and wind fields to fully show covariability in their signatures on year-to-year basis and along longitudes partially disqualify my earlier hypothesis that this would occur. This essentially points to the fact that the 10-m wind fields are forced by different dynamics that oppose the SST forcing, but that depends on the year and longitude space. This could be large-scale ENSO forcing that weakens the southeasterly winds. TIWs are caused by instabilities of current anomalies, hence their signatures will persist despite weak southeasterlies.

The equatorial Kelvin waves also play an important role in the evolution of SSTs in the eastern equatorial Atlantic. Strong easterly (westerly) winds in the western basin generate anomalous upwelling (downwelling) that propagates eastward along the equator waveguide as Kelvin waves reaching the boundary 1-2 months later (Servain et al., 1982). In the absence of Coriolis force, the northward branch of the South Equatorial Current (nSEC) flows westward along the equatorial band, opposite to the direction of the Kelvin waves. This anomalous east-west circulation, in addition to variability of the strength of the cold tongue explains the reason why the waves differ north and south of the equator.

8.4.2 Spatial correlations

Spatial correlations between SST and wind stress vectors (figure 8.6) provide a clear picture of how the ocean and atmosphere couples during the boreal summer, which is a period of dynamical importance. For example, SST gradients north of the equator are thought to create coupling anomalies through the wind-evaporation-SST feedback (Mahajan et al., 2009). The resulting anomalous winds at the marine atmospheric boundary layer (ABL) cause convergence of water vapour leading to deep convection. The low-level moisture convergence at the ABL north of the equator is directed eastward based on the WES hypothesis arising from deflection due to Coriolis effect. The magnitude of this anomaly will affect the local climate of the surrounding continent. Orographic influence may aid in such influence either positively or negative. While these correlations concentrate on the boreal summer months, other seasons may also play a part in determining the tropical Atlantic climate variability. The earlier hypothesis that positive correlation between SST and wind stress fields at the TIW frontal zones will dominate the tropical Atlantic region is disproved. Correlations from SST-zonal wind stress were rather weak, and those of SST-meridional wind stress are negative. I observed that high positive correlations occur between these variables but within a certain threshold of SST (26-29°C).

8.4.3 Sub-seasonal variability

The apparent sub-seasonal variability observed from SST and wind stress vectors from wavelets analysis suggest an important coupled relationship between them. The 4-24 days periodicity (figure 8.8) are related to high frequency atmospheric variability in the region. These are thought to be important parts of the intra-seasonal variability of the tropical Atlantic (Bunge et al., 2006). However, correlated variability between ocean and atmosphere can occur at any frequency between the 4-24 days. For example, Garzoli (1987) observed significant coherence between the ocean and atmosphere with two predominant peaks at 5 and

7 days. Grodsky and Carton (2001) observed 15-day oscillations between the ocean and atmosphere from velocity measuring.

Interannual variability is observed in the SST associated with intraseasonal variability of the tropical Atlantic caused by tropical instability waves having 17-40 day cycle. This variability is prominent in 2007, when the boreal summer SST anomaly in the Gulf of Guinea was observed to be more than 2°C. This anomalous TIWs SST may explain significantly the cause of 2007 flooding in the adjoining continent of Africa particularly West Africa and the southern Sahel. A wind forced intraseasonal variability of 4-24 days cycle is observed from the wind stress data for both zonal and meridional components. This occurred in 2001, 2002 and 2005 signifying an interannual variability.

However, the similarities shown by these periods may not fully explain in detail the connection between SST and the stress fields. Therefore, I investigate further the spectral co-variability between the time series using the cross wavelet transform and wavelet transform coherence.

This analysis highlights the covariability of SST and wind stress fields based on non-seasonal anomaly data. High frequency intraseasonal variability of 4-24 days are apparent in the wind stress data, which signifies the scale of influence of atmosphere to the ocean. Although, the zonal and meridional wind stresses are not of comparable strength, with the zonal almost 3 times the meridional, they certainly covary, especially at the 4-24 day periods. The interannual variability observed from the intraseasonal signals could modulate the Atlantic meridional mode (AMM) and the Atlantic Niño. The anomalous meridional mode will force variability according to the wind-evaporation-SST feedback and that results in anomalous convective processes due to enhanced heat and moisture fluxes. Anomalous AMM could also affect the zonal intraseasonal tropospheric variability of the Madden-Julian Oscillation (MJO).

8.4.4 SST frontal zone and winds

The strong concurrence between SST and wind stress (figure 8.11) highlights a coupled phenomenon typical of TIW frontal zones. The result of this is an increase in perturbation of surface heat fluxes. Previous observational studies revealed a negative feedback of these fluxes due to the evolving TIWs SST. A correlation was found (Deser and Blackmon, 1993) between SST and stratocumulus cloudiness, where increased cloudiness over a warm ocean reduces incoming solar radiation fluxes thereby cooling the ocean. In the same vein, increased latent and sensible heat fluxes are found (Thum et al., 2002) over the warm phase of the TIWs that is attributable to strong coupling between SST and winds. Weaker winds and warmer SSTs do not allow the growth of wave activity. Therefore, the TIWs are suppressed as discussed in subsection 8.3.1.

Associated with the SST fronts is the wind stress curl. A similar scenario was observed in the Pacific (Chelton et al., 2001), where the TIWs exhibit longer life span than the Atlantic. Perturbations in wind stress curl are produced as a result of TIW-induced SST gradient (Chelton et al., 2001), which generates perturbation Ekman pumping over the TIWs. In a similar study, Spall (2007) explained that Ekman pumping dampen the baroclinic instability in the ocean in the presence of strong background southerly winds. From a model study, Seo et al. (2007) showed that Atlantic TIW Ekman pumping variability is negligible compared with dynamically induced variability by upwelling, arguing that TIW-induced wind stress curl would not modify baroclinic instability processes in the Atlantic. This indicates a further interest in studying the wind stress curl, as it generates a secondary circulation that can have a resulting influence on the mesoscale atmospheric processes. Small-scale variability caused by the positive/negative wind stress curl may also generate upwelling and downwelling in the open ocean, and these are vital to the dynamics, thermodynamics, as well as the biology of the upper ocean Gill (1982).

Atmospheric response to variations of SST results in wind stress curl anomalies.

Xie (2004) emphasised how the winds respond to changes in SST of about 27°C, which is remarkably different to those temperatures below it. Two important scenarios may explain this positive correlation observed in the Gulf of Guinea.

One is the warming of the surface waters by TIWs during the JJA months between 0°-4°N that coincides with the northern edge of the TIWs. The TIWs were found to warm the Gulf of Guinea region during the boreal summer through advection (see chapter 4). The second is, the relaxation of the southeasterly summer monsoon winds that allow warming of the waters to the threshold of 26-29°C as shown in figure 8.11. Each of these will enhance heat and moisture fluxes in the atmospheric boundary layer. The winds will respond to these changes in the temperature and hence the enhanced wind stress curl. The wind stress curl is calculated as in Stewart (2004). While Ekman pumping velocity is related to the wind stress curl, $W_e = -curl\frac{\tau}{\rho f}$, positive wind stress curl is related to divergence and indicates upward flow. Therefore, negative wind stress curl indicates convergence of Ekman transport that pumps water downward into the ocean interior. This results in the warming of the mixed layer, and cooling of the surface layer during the JJA months. That is, warmer surface waters are entrained into the mixed layer. However, a similar analysis for the other seasons (not shown) indicates a different circumstance, where wind stress curl showed negative correlation with SST. I present here that, even though the Bjerknes feedback associated with zonal mode tends to sustain and prolong the Atlantic Niño mode during boreal spring and summer (Hormann and Brandt, 2007; Keenlyside and Latif, 2007), the dynamics associated with the summer period of the Atlantic Niño north of the equator is largely due to ocean front-atmosphere interaction. The Bjerknes feedback may contribute but to a lesser degree in the summer months, but larger in spring when the northeast trade winds are weak.

8.4.5 High frequency variability

Interesting results were seen in the high frequency 5-20 days and 2-5 longitude filtered data. Homogeneity in the long-term intra monthly variability as indicated from the wind data justifies that at large-scale, the fast changing wind patterns do not always correlate with SST. However, relationships exist at a time lag that typically depends on both the relaxation and strengthening of the winds and the warming/cooling of the SST. These westward moving waves have been found to interact with the atmosphere through thermodynamic processes (Chelton et al., 2001), and hypothesized by Wallace et al. (1989) to modify the atmospheric boundary layer stability.

It should be noted that the appearance of the waves in September/October in the meridional plots (Figure 8:16c) did not reflect in the SST data (Figure 8:16a). This does not mean that the ocean did not respond to the atmospheric forcing to mirror features of these perturbations. The ocean may be experiencing strong surface currents that dampens the strength of the stress fields thereby inhibiting their imprint on the SST. An analysis by Small et al. (2009) showed that ocean surface currents act to weaken wind stress fields thereby altering their effect on the ocean surface. I deduce here that the emergence of North Equatorial Countercurrent (NECC) in July and its strengthening in August/September may have helped adjust the usual response of the ocean from the inherent atmospheric perturbations. The September/October signature observed in the meridional plot points to an atmosphere forcing the ocean. Whether this phenomenon is related to the Atlantic Niño II observed by Okumura and Xie (2006) that appear in November/December period, or the secondary bloom observed during late spring by Grodsky et al. (2008) are a matter of future investigations outside this thesis.

8.5 Summary

I have examined the observed characteristics of non-seasonal variability in the tropical Atlantic region using satellite data. My findings are summarized as follows:

Variability in the interannual signatures of tropical instability waves investigated at the Atlantic Niño region show that both Bjerknes and ENSO feedback mechanisms are responsible for driving such year-to-year variability. The equatorial Kelvin waves that propagate from the west to the eastern basin significantly modulate the near-surface and thermocline depth in the Atlantic Niño region through Bjerknes feedback. The inability of the oceanic imprints of TIWs to cause a relative response to overlying winds in some years points to the fact the 10-m wind fields are sometimes modulated by different dynamics that opposes coupling with SST. I propose that large-scale ENSO modes are responsible for weakening the southeasterly winds. SST signatures of TIWs however, persist at these periods despite weaker winds since they are driven by instabilities of current anomalies and not by the winds.

Coherent 18-50 days intraseasonal signals of Madden-Julian Oscillation (MJO) feedback onto the tropical Atlantic Ocean is observed, with SST forcing the atmosphere, which also shows interannual variability. I suggest that this clear connection between the ocean and intraseasonal tropospheric variability are due to anomalous cross equatorial SST gradient (CESG) that occurs north of the equator. While the CESG-induced variability influences the north-south migration of the ITCZ, it also couples with the MJO through wind-evaporation-SST (WES) feedback and may influence variability of the MJO through eastward transfer of heat and moisture.

My results show that 5-20 day oscillations in the tropical Atlantic SST fields are associated with the signals of tropical instability waves based on both spatial and temporal signatures. These also represent regions of largest variances captured by EOF and standard deviation. However, the zonal and meridional

wind stresses showed variances along River Amazon and River Congo outputs, where North Brazil Current (NBC) and Angola Currents (AC) are located respectively. This implies that 5-20 day wind stress fields are significantly modulated and maintained by these currents due to mainly river outputs.

Spatial correlations between SST and wind stress fields during boreal summer show strong positive correlations north of the equator, and negative correlation around the equator. The positive correlations illustrate a region that influences the Atlantic meridional mode through WES feedback mechanism. High positive correlations signify higher heat and moisture fluxes in the marine atmospheric boundary layer and higher rainfall over land in the east. Correlations between SST and wind stress divergence suggests that the meridional mode of variability and the TIWs SST frontal zones dominate mesoscale air-sea coupling that determines heat fluxes out of the ocean. I suggest here that coupled ocean-atmosphere models that simulate heat and moisture fluxes must consider the TIW frontal zones, especially the 26-29°C SST threshold in order to be able to simulate them correctly. I observed that high positive correlations occur between SST and wind stress divergence but within SST threshold of 26-29°C.

A 17-40 day variability in the SST observed in 2007 from cross wavelet transform of SST and zonal wind stress is associated with the intraseasonal variability of the TIWs. This also corresponds to an abnormally high SST in the Gulf of Guinea that caused anomalous convection leading to flooding over West Africa and the Sahel in 2007 as previously examined in chapter 6.

The relative effects of SST and wind stress fields at 5-20 day signals are investigated. At the tropical instability region, the response of meridional wind stress to SST forcing is hampered by current anomalies that act to dampen the strength of the winds. These current anomalies associated with the North Equatorial Countercurrent (NECC) weaken the signatures of TIWs imprint in September/October months.

CHAPTER 9

Conclusions, Future Directions and Final Remarks

9.1 Conclusions

In this section, the main conclusions of this thesis are drawn and some thought about future investigations in the Gulf of Guinea, West Africa and Sahel regions are given. The conclusions are linked with the questions raised in the motivation and that covers the five main results chapters.

9.1.1 Temperature advection

What are the scales of contributions of TIWs to horizontal temperature advection?

Meridional temperature advection is found to be larger than the zonal advection component from both satellite and drifter data when calculated at the centre of the basin (3-8°N/18-34°W). However, in the Gulf of Guinea, zonal temperature advection is larger and about three times larger than the meridional

component, but this occur only in July months when TIWs are strong. The explanation behind these is that current anomalies associated with TIWs such as North Equatorial Countercurrent that develops during the boreal summer enhances advection of temperatures north of the equator. To further confirm whether these advections are caused by the waves, we decomposed the advection term into the mean an anomaly components. Results showed that the strong anomalous meridional temperature advections are due to current anomalies associated with tropical instability waves. My results here have contradicted coupled ocean-atmosphere model results of Jochum and Murtugudde (2006), which showed that zonal temperature advection is as large as the meridional component. The authors however, have suggested the use of observational data to verify their results.

South of the equator at 10-12°S, where zonal currents are weak, zonal temperature advection is even weaker. This area is largely controlled by mean advection rather than anomalous advection due to the absence of current shear that can flow against the westward South Equatorial Current.

Do the TIWs warm the Gulf of Guinea region?

At the Gulf of Guinea, zonal temperature advection is larger than meridional advection. During boreal summer when the cold tongue is fully developed, zonal advection associated with anomalous currents and temperatures warms the region. This anomalous warming could sufficient alter the Atlantic Niño and subsequently the local climate through an increase in heat and moisture fluxes.

9.1.2 Water properties

Variability of the Equatorial Undercurrent (EUC) and its northern and southern branches have been examined. The variability of the EUC is heavily influenced by the seasonal southeasterly winds that lift the thermocline during the boreal summer.

I observed that perturbations of flow associated with the tropical instability waves (TIWs) exhibited by a strong northward flow destabilises the vertical positioning of the EUC during the boreal summer. A local maximum of salinity representing the North Equatorial Undercurrent (NEUC) is observed at 5°N from a float that sampled between 3 and 8°N. This confirms previous investigations by Stramma and Schott (1999).

Is the EUC shallowing in the Gulf of Guinea linked to the strengthening of the seasonal winds?

I show that vertical fluctuations of the EUC in the Gulf of Guinea as indicated by Brunt-Väisälä frequency is accompanied by warmer and less dense water due to current shear associated with bathymetry. Stratification observed in winter/spring of 2007 and 2008 are associated with weakening of the monsoon winds and the zonal pressure gradient initiated from the western basin. Two phases of warm temperatures exist at this location: One during the summer, when solar radiation is at maximum at the equator, and another during winter, when the SSTs and upper temperatures remain high due to absence of strong winds. This results in four phases, each per season of thermocline adjustment to atmospheric forcing. Although, bathymetry and current shear also contribute to these vertical fluctuations of the thermocline, atmospheric influence is the primary contributor. The consequence of this is the modulation of SSTs at the Atlantic Niño region, which is an important climate determinant. The EUC shallowing in the Gulf of Guinea is therefore, linked to the strengthening of the seasonal winds, and its anomalous flow due to density variations associated with hydrological cycle could impact the coastlines.

Does the EUC vary seasonally at any of its branches?

Seasonal variability of the EUC is prominent due to its alignment with the equator where it interacts with other currents such as the northern and southern branches of South Equatorial Current. This also applies to the northern branch, the NEUC which also interacts with North Equatorial Countercurrent. However,

this is not the same with its southward branch, the South Equatorial Undercurrent (SEUC) which do not show seasonal variability by virtue of its position.

The mean annual position of EUC varies at each of the four chosen locations and that depends on various factors that determine their variability. The EUC position centred at 5°E/2°N is influenced by basin-wide wind system, bathymetry as well as river runoff and strong rainfall. This makes it vary in every season, with stronger signatures in summer and weaker in winter. Heavy runoff from Rivers Niger and Volta in late summer/autumn could alter the structure of the EUC and that ultimately weakens it by winter due to freshening.

9.1.3 Rainfall and Sea Surface Temperature

I investigate the influence of Gulf of Guinea SST to changes in rainfall over West Africa and the Sahel region using 12-years of TRMM rainfall and TMI SST satellite data. Teleconnections with Pacific El Niño, Benguela Niño, Mediterranean SST and Atlantic Meridional Mode were examined.

Is there any influence of the Gulf of Guinea SST on West Africa and Sahel rainfall from observational means, and at what scales?

Sea Surface temperature anomalies in the Gulf of Guinea is found to influence rainfall over West Africa and the Sahel with a time lag of one month. Interannual variability of rainfall patterns over these regions concur well with the variability of Gulf of Guinea SST (GG SST). The influence of this SST however varies, depending on whether rainfall exhibits a dipole pattern between the Guinea coast and the Sahel region or not. The ′dipole′ years are periods when anomalous rainfall of opposite sign prevail in the Guinea Coast and the Sahel, while non-dipole are years with ubiquitous positive or negative anomalies throughout as reported earlier by Nicholson (2009). Dipole years occur due to anomalous positioning of the Intertropical convergence zone (ITCZ) far north at about 12°N. The influence of GG SST is apparent in 2007, with an anomalously high rainfall over both West Africa and the Sahel region, suggesting a non-dipole

year. This positive rainfall anomalies as a result of positive SST anomalies lead to flooding that affected both regions in that year.

Strengthening of southeasterly winds in 2005 leads to increased wind stress resulting in cooler GG SST as shown by Marin et al. (2009). This cold temperature reduces the amount of heat fluxes out of the ocean, and that caused negative convective anomalies. The consequences of this are negative anomalies of rainfall over both West Africa and the Sahel region leading to the well-documented drought of 2005.

Is there any remote forcing that controls the moisture convergence over West Africa and the Sahel other than the Gulf of Guinea SST?

The Pacific El Niño (Niño 4) correlates with both West Africa and the Sahel rainfall anomalies, with Niño 4 leading by one month. Other Pacific Niño indices (Niño 3 and 3.4) show weaker correlations and both lead rainfall with one month. The exact mechanism driving the relationship between Pacific El Niño and these rainfall anomalies are not well understood. However, it is known that ENSO builds up positive SST anomalies and that increases surface heat fluxes in the Atmospheric Boundary Layer (ABL). It is therefore, likely that Pacific El Niño influences the African rainfall anomalies through a connection with the intraseasonal Madden-Julian Oscillation (MJO). The anomalous SSTs in the Pacific create east-west sea level pressure (SLP) gradients, and that drives wind anomalies of MJO.

9.1.4 Non-seasonal variability of SST and winds

What are the scales and propagation characteristics of non-seasonal variability?

Are non-seasonal variability in the tropical Atlantic a part of the TIWs?

I identified two regions in the tropical Atlantic where non-seasonal variability of SST vary the most, and these are the regions of Guinea Dome and of Tropical Instability Waves. A key issue in this investigation is the ability to find the direction of propagation of these large variances of SST and that was achieved using complex Hilbert EOF. The largest variance observed at the Guinea Dome is associated with the southward flowing Canary Current. This is suggestive of the influence of northeasterly winds that perturb SSTs of the southward flowing currents. The second strongest variance is connected with the seasonal TIWs that have strong influence on oceanic mesoscale activity at the equatorial region. The southern branch of variance associated with the waves is found to propagate southward.

When I compared the variances of wind patterns with those of SST, the two largest variances appear to be independent of the SST. Investigations of the winds were then advanced, and that showed large-scale mid and high level winds do modulate the surface winds between 18-30°N. I observed that these tropospheric winds do alter the surface winds resulting in the modulation of surface fluxes that are connected to the MJO.

9.1.5 Ocean-atmosphere coupling and high frequency variability

Interannual variability of tropical instability waves was observed from both SST and wind data. A connection between SST and wind at the TIW regions do not always co-vary, as year-to-year variability between each variable differs.

Are 5-20day oscillations in the tropical Atlantic related to the TIWs?

SST and wind stress fields of 5-20 day intraseasonal variability are found to be features of TIWs. These waves observed in 2003 appear to last longer in SST from July to early September but they only exist in July in the zonal wind

stress fields. The waves however appeared for the second time in September/October in the meridional wind stress but the SST did not present any imprint during that time.

Anomalously high SST signature in the Gulf of Guinea showed strong covariability with zonal wind stress anomalies at 17-40day in 2007. This is associated with intraseasonal variability of TIWs. It was expressed earlier that the waves warm the Gulf of Guinea during the boreal summer, resulting in the increase in surface heat and moisture fluxes that cause rainfall. These anomalous warming of the region due to the waves has caused an increase in rainfall pattern over West Africa and the Sahel in that year. Sea surface temperature in the Gulf of Guinea positively correlates with West Africa and Sahel regions, and in both cases rainfall lagging SST with one month. Therefore, it takes approximately a month for the ITCZ convective rain band to transport moisture over these regions.

9.2 Future Directions

Investigating the contribution of temperature advection in the equatorial heat budget can be improved by focusing on observed data that includes currents and temperatures. For the time being, investigations of temperature advection from observations in tropical Atlantic can only be determined from satellite SST/-geostrophic currents and drifter surface fields. Availability of moorings fitted with current meters and most importantly ADCP as well as temperature sensors will increase our knowledge of heat transport in the tropical Atlantic region especially at depth. Coupled ocean-atmosphere models can improve their simulations on the tropical Atlantic region if TIW SST is fully considered based on its variability north and south of the equator.

Rain gauge data products spread over West Africa and the Sahel regions can be contrasted with satellite radar precipitation and together with SST in order to assess impact of SST anomalies on drought and floods affect the regions.

For a proper understanding of the fate of EUC in the eastern tropical Atlantic, river discharge from Volta and Niger are required as these determine water density due to influx of freshwater. This will provide the opportunity to calculate heat balance to carter for influx of heat in and out of the mixed layer due to solar radiation and evaporation.

The connection between Pacific El Niño and the MJO if investigated could highlight properly the forcing of West Africa and Sahel rainfall variability by Pacific El Niño.

Further investigation of the origin of high variances that appear to propagate between 18 and 30°N from the meridional winds is required. Large EOF variances along the NBC can be further studied to highlight the influence of winds to ocean circulation and its connection to precipitation anomalies at the Nordeste region of Brazil (2°-12°S, 36°-43°W).

At the TIW frontal zones, evolving anomalous SST signatures could couple with the atmosphere to produce changes in the atmospheric boundary layer, and hence heat and moisture fluxes. This could result in momentum transfer due to instability created by temperature difference where upper level winds can exert significant stress over the ocean surface. Future investigations on the coupled variability of the TIW frontal zones and the upper winds and temperatures may give greater insight into how these could translate into large-scale climate variability.

9.3 Final Remarks

Looking at the bigger picture, ocean-atmosphere interaction in the tropical Atlantic falls within the realm of the wind-evaporation-SST feedback (WES) mechanism, the inclusively ocean-atmosphere activities due to tropical instability waves demonstrates a uniquely interesting process. The response of the southeasterly winds to crossequatorial SST gradient affect heat fluxes. However, SST

frontal zones of TIWs couples with the atmosphere in a unique way, by exhibiting a threshold of SST between 26 and 29°C to alter an atmospheric response. While ocean-atmosphere processes are important to the tropical Atlantic climate, the influence of the ocean itself to the coupling is equally important. For example, the shoaling of the thermocline in the Gulf of Guinea is associated with large heat fluxes in the atmospheric boundary layer. The response of winds to these fluxes is enormous, and in the presence of the ITCZ, moisture is transported over long distance as rainfall.

This thesis has contributed in advancing the present knowledge of the tropical Atlantic variability based on observational data.

APPENDIX A

Coherence and Cross Power Spectral Density

A.1 Coherence

The magnitude squared coherence (C_{xy}) of input signals X and Y are calculated based on Welchs averaged, modified periodogram method. The application here is based on Emery and Thomson (2001) and the mathworks implementation. The magnitude squared coherence is a function of the power spectral densities between the two signals $P_{xx}(f)$ and $P_{yy}(f)$ of X and Y and the cross power spectral density $P_{xy}(f)$ of X and Y. Coherence squared C_{xy} is given as

$$C_{x,y}f = \frac{|P_{xy}f|^2}{P_{xx}fP_{yy}f} \tag{A.1}$$

X and Y must be the same length. Coherence estimates uses Fourier analysis to determine frequencies at which the coherence is estimated. This can be determined by the sampling frequency, using periodic windowing (Hamming) to obtain eight equal sections of X and Y. The number of overlap between these sections can also be determined.

A.2 Cross Power Spectral Density

The cross power spectral density (cpsd) calculates the distribution of power per unit frequency based on Fourier analysis. It is calculated based on Welchs averaged, modified periodogram as is defined as:

$$P_{x,y}\omega = \sum_{m=-\infty}^{\infty} R_{xy}(m)e^{j\omega m} \tag{A.2}$$

The cross correlation sequence is defined as:

$$R_{xy}(m) = E\left[x_{n+m}y_n^*\right] = E\left[x_n y_{n-m}^*\right]$$

where

x_n and y_n are jointly stationary random processes, $-\infty < n\infty$, $*$, and E are the expected value operator.

The CPSD uses periodic windowing (Hamming) and considers number of overlapping sections in its estimates.

APPENDIX B

Complex EOF and Complex Hilbert EOF Analysis

Statistical techniques of complex EOF (CEOF) and complex Hilbert (CHEOF) analyses and their terminologies are briefly described, following closely Tokmakian and Challenor (1993), Ueki et al. (2000) and Terradas et al. (2004).

Let $U_{(x_j,t)}$ be an anomaly scalar field derived by subtracting the time-mean, x... corresponds to spatial position and$t$, the time. The core of the CEOF and CHEOF analysis consists in finding the eigenvalues and eigen vectors of a covariance matrix C.

$$C_{ij} = \langle U^*(x_i,t)U(x_j,t)\rangle_t \tag{B.1}$$

B.1 Complex EOF as applied to wind data

The asterisk denotes complex conjugate, the brackets $\langle ...\rangle$ indicate time-averaging.

Here, C represents the cross-spectral matrix and is Hermitian by construction and posses m real non-negative eigenvalues n and complex eigenvectors, *En(x)*,

n=1,2,.m. Once the spatial eigenvectors are calculated, their corresponding time evolution is obtainable by the timeseries An(t) which is obtained by projecting the data series *U(x,t)* onto the appropriate eigenvectors *En(x)*, and summing all over the locations.

$$A_n(t) = \sum_j U(x_j, t) E_n(x_j). \tag{B.2}$$

The *nth* CEOF or CHEOF mode consists of a spatial part, i.e the pattern *En(x)*, and a temporal part *An(t)*, such that the product of the two $E_n^*(x)A_n(t)$ corresponds to a representative oscillatory component present in the field. Consequently, the spatial and temporal behaviour of the nth mode can be derived by taking the real part of $E_n^*(x)A_n(t)$. The original complex data field *U(x,t)* can be easily and completely reconstructed by adding the empirically found statistical modes,

$$U_{(x,t)} = \sum_{n=1}^{m} E_n^*(x) A_n(t), \tag{B.3}$$

B.2 Complex EOF as applied to wind data

The complex field $U_{(x_j,t)}$ shown in B.1 is

$$U_{(x,t)} = U_{(x_j,t)} + iV_{(x_j,t)}, \tag{B.4}$$

Where $U_{(x_j,t)}$ is the complex field, u and v are the zonal and meridional components of wind respectively, $i = \sqrt{-1}$, and t is time.

B.3 Complex Hilbert EOF as applied to SST data

The complex field $U_(x_j, t)$ shown in B.1 is defined as having real and imaginary parts equal to the scalar data field of the data and the Hilbert transform respectively.

$$U_{(x,t)} = X_{(x_j,t)} + i\breve{X}_{(x_j,t)}, \tag{B.5}$$

By definition, the Hilbert transform of a data series has Fourier components with the same amplitude as the original scalar field, while the phase is advanced by $\pi/2$. At a given position *xj*, the spectral decomposition of $X_{(x_j,t)}$is given by

$$X_{(j,t)} = \sum_w \cos(wt) + b_i(w)\sin(wt) \tag{B.6}$$

and its Hilbert transform $\breve{X}_{(x_j,t)}$ is given by

$$\breve{X}_{(x_j,t)} = \sum_w b_i \cos(wt) - a_j(w)\sin(wt) \tag{B.7}$$

In a situation where the data series described by a single frequency oscillation, the Hilbert transform would be proportional to its time derivative. In a general case, the Hilbert transform provides information at each grid point locally in frequency domain about the time change of the scalar data. The ability to retain information about the phase of the scalar field is the reason CHEOF is able to detect propagating signals.

B.4 Decomposition of the complex signal

More conveniently, we could rewrite the decomposition of the data field $U_{(x_j,t)}$ onto a complex basic functions $En_{(xj)}$ with complex coefficients$An_{(t)}$given by

equation B3 using real valued functions.

$$U_{(x_j,t)} = \sum_{n=1}^{m} S_n(x_j) e^{i\theta_n(x_j)} R_n(t) e^{i\phi_n(t)}, \tag{B.8}$$

or, for the original data $X(xj,t)$ which is simply the real part of $U(xj,t)$,

$$X_{(x_j,t)} = \sum_{n=1}^{m} R_n(t) \cos[\phi_n - \theta_n(x_j)]. \tag{B.9}$$

Four real-valued signals $S_n(x_j), \theta_n(x_j), R_n(t), \phi_n(t)$ obtained from the complex field describes different oscillatory behaviour.

B.5 Spatial amplitude function

$$S_n(x_j) = [E_n(x_j) E_n^*(x_j)]^{1/2} \tag{B.10}$$

This shows the spatial distribution of variability associated with each mode and may be interpreted as EOF analysis. The spatial distribution gives a measure of spatial homogeneity in the magnitude of X field associated with each mode.

B.6 Spatial phase function

$$\theta_n(x_j) = arctan\left[\frac{Im(E_n(x_j))}{Re(E_n(x_j))}\right]. \tag{B.11}$$

The spatial phase represents a measure of the relative phase difference for a given mode among the various locations where X is defined. The phase varies continuously between $-\pi$ and π, and its derivative is equal to the phase speed of the propagating signal. The use of atan2 is to get the range from $-\pi$ to π, and that allows direction to be determined.

B.7 Temporal amplitude function

This is a measure of temporal variability in the magnitude associated with a given mode. It may be interpreted in the same way as the principal component time series of a standard EOF.

$$R_n(t) = [A_n(t)A_n^*(t)]^{1/2}\,. \tag{B.12}$$

B.8 Temporal phase function

$$\phi_n(t) = arctan\left[\frac{Im(A_n(t))}{Re(A_n(t)}\right]. \tag{B.13}$$

The temporal phase describes the temporal variation of the phase of the nth eigen mode associated with the periodicities in the X field. Locally, its derivative is equal to the frequency of the propagating signal. It varies between $-\pi$ and π. The use of atan2 is to get the range from $-\pi$ to π, and that allows direction to be determined.

References

Allersma, E. and Tilmans, W. M. K. (**1993**). "Coastal conditions in West Africa–A review." *Ocean and Coastal Management*, 19(3): 199–240. URL http://www.sciencedirect.com/science/article/B6VG5-4876KHK-37/2/dca056c11bcd3f5fa2a0d15b6942a4a8.

Alvera-Azcárate, A., Barth, A., Rixen, M., and Beckers, J. (**2005**). "Reconstruction of incomplete oceanographic data sets using empirical orthogonal functions: application to the Adriatic Sea surface temperature." *Ocean Modelling*, 9(4): 325–346. URL http://adsabs.harvard.edu/abs/2005OcMod...9..325A.

An, S.-I. (**2008**). "Interannual variations of the Tropical ocean instability waves and ENSO." *Journal of Climate*, 21(15): 3680–3686. URL http://journals.ametsoc.org/doi/full/10.1175/2008JCLI1701.1.

Arhan, M., Treguier, A., Bourlès, B., and Michel, S. (**2006**). "Diagnosing the annual cycle of the Equatorial Undercurrent in the Atlantic Ocean from a general circulation model." *Journal of Physical Oceanography*, 36(8): 1502–1522. URL http://journals.ametsoc.org/doi/abs/10.1175/JPO2929.1.

Athie, G. and Marin, F. (**2008**). "Cross-equatorial structure and temporal modulation of intraseasonal variability at the surface of the Tropical Atlantic Ocean." *Journal of Geophysical Research*, 113(C8): C08 020. URL http://europa.agu.org/?view=article&uri=/journals/jc/jc0808/2007JC004332/2007JC004332.xml&t=jc,2008,athie.

Athie, G., Marin, F., Treguier, A.-M., Bourlès, B., and Guiavarc'h, C. (**2009**). "Sensitivity of near-surface Tropical Instability Waves to sub-monthly wind forcing in the tropical Atlantic." *Ocean Modelling*, 30(4): 241–255. URL http://www.sciencedirect.com/science/article/pii/S1463500309001395.

Bah, A. (**1987**). "Towards the prediction of Sahelian rainfall from sea surface temperatures in the Gulf of Guinea." *Tellus A*, 39(1): 39–48. URL http://onlinelibrary.wiley.com/doi/10.1111/j.1600-0870.1987.tb00287.x/abstract.

Bakun, A. (**1996**). "Patterns in the ocean: ocean processes and marine population dynamics." *Ocean processes and marine population dynamics. University of California Sea Grant, California, USA*. URL http://www.paperbackswap.com/Patterns-Ocean-Ocean-Andrew-Bakun/book/1888691018/.

Benson, C. and Clay, E. J. (**1998**). *The impact of drought on sub-Saharan African economies: a preliminary examination*. World Bank Publications. URL http://publications.worldbank.org/index.php?main_page=product_info&cPath=1&products_id=21311.

Biasutti, M., Battisti, D., and Sarachik, E. (**2003**). "The Annual Cycle over the Tropical Atlantic, South America and Africa." *Journal of Climate*, 16(15): 2491–2508. URL http://journals.ametsoc.org/doi/pdf/10.1175/1520-0442(2003)016%3C2491%3ATACOTT%3E2.0.CO%3B2.

Bischof, B., Mariano, A., and Ryan, E. A. (**2004**). "The North Equatorial Counter Current: Ocean Surface Currents." *Rosenstiel School of Marine and Atmospheric Science: Accessed 9 July 2011*. URL http://oceancurrents.rsmas.miami.edu/atlantic/north-equatorial-cc.html.

Bourlès, B., Busalacchi, A. J., Campos, E., Hernandez, F., Lumpkin, R., McPhaden, A., M.J.and Moura, Nobre, P., Planton, S., Servain, J., and Trotte, J. (**2006**). *PIRATA (Pilot Research Moored Array in the*

Tropical Atlantic): Accomplishments of PIRATA: 1997-2005, Status and perspectives. Document prepared for a PIRATA review by CLIVAR -AIP - and OOPC, 89pp. URL http://www.brest.ird.fr/pirata/pirata.php.

Bourlès, B., Molinari, R., Johns, E., Wilson, W., and Leaman, K. (**1999**). "Upper layer currents in the western tropical North Atlantic (1989–1991)." *Journal of Geophysical Research*, 104(C1): 1361–1375. URL http://europa.agu.org/?view=article&uri=/journals/jc/1998JC900025.xml&t=jc,1999,bourles.

Brink, K. and Muench, R. (**1986**). "Circulation in the Point Conception–Santa Barbara Channel Region." *Journal of Geophysical Research*, 91(C1): 877–895. URL http://europa.agu.org/?uri=/journals/jc/JC091iC01p00877.xml&view=article.

Bunge, L., Provost, C., and Kartavtseff, A. (**2007**). "Variability in horizontal current velocities in the central and eastern equatorial Atlantic in 2002." *Journal of Geophysical Research*, 112. URL http://www.agu.org/journals/ABS/2007/2006JC003704.shtml.

Bunge, L., Provost, C., Lilly, J., D, M., Orgeville, Annie, K., and Melice, J.-L. (**2006**). "Variability of the Horizontal Velocity Structure in the Upper 1600 m of the Water Column on the Equator at 10W." *Bulletin of the American Meteorological Society*, 36(7): 1287–1304. URL http://journals.ametsoc.org/doi/abs/10.1175/JPO2908.1.

Busalacchi, A. J. and Picaut, J. (**1983**). "Seasonal Variability from a Model of the Tropical Atlantic Ocean." *Journal of Physical Oceanography*, 13(9): 1564–1588. URL http://journals.ametsoc.org/doi/abs/10.1175/1520-0485%281983%29013%3C1564%3ASVFAMO%3E2.0.CO%3B2.

Cai, W. and Baines, P. (**2001**). "Forcing of the Antarctic circumpolar wave by El Niño-Southern Oscillation teleconnections." *Journal of Geophysical Research*, 106(C5): 9019–9038. URL http://europa.agu.org/?uri=/journals/jc/2000JC000590.xml&view=article.

Caltabiano, A., Robinson, I., and Pezzi, L. (**2005**). "Multi-year satellite observations of instability waves in the Tropical Atlantic Ocean." *Ocean Science Discussions*, 2(1): 1–35. URL http://www.ocean-sci-discuss.net/2/1/2005/osd-2-1-2005.html.

Carton, J. (**1991**). "Effect of Seasonal Surface Freshwater Flux on Sea Surface Temperature in the Tropical Atlantic Ocean." *Journal of Geophysical Research*, 96(C7): 12,593–12,598. URL http://dx.doi.org/10.1029/91JC01256.

Carton, J. A., Cao, X., Giese, B. S., and Da Silva, A. M. (**1996**). "Decadal and Interannual SST Variability in the Tropical Atlantic Ocean." *Journal of Physical Oceanography*, 26(7): 1165–1175. URL http://journals.ametsoc.org/doi/abs/10.1175/1520-0485%281996%29026%3C1165%3ADAISVI%3E2.0.CO%3B2.

Carton, J. A. and Huang, B. (**1994**). "Warm Events in the Tropical Atlantic." *Journal of Physical Oceanography*, 24(5): 888–903. URL http://journals.ametsoc.org/doi/abs/10.1175/1520-0485%281994%29024%3C0888%3AWEITTA%3E2.0.CO%3B2.

Cazelles, B., Chavez, M., Magny, G., Guégan, J., and Hales, S. (**2007**). "Time-dependent spectral analysis of epidemiological time-series with wavelets." *Journal of the Royal Society Interface*, 4(15): 625–636. URL http://www.ncbi.nlm.nih.gov/pubmed/17301013.

Challenor, P., Cipollini, P., Cromwell, D., Hill, K., Quartly, G., and Robinson, I. (**2004**). "Characteristics of mid-latitude Rossby wave propagation from multiple satellite datasets." *International Journal of Remote Sensing*, 25(7-8): 1297–1302. URL http://adsabs.harvard.edu/abs/2004IJRS...25.1297C.

Chang, P., Ji, L., and Li, H. (**1997**). "A decadal climate variation in the tropical Atlantic Ocean from thermodynamic air-sea interactions." *Nature*, 385(6616): 516–518. URL http://dx.doi.org/10.1038/385516a0.

Chang, P., Ji, L., and Saravanan, R. (**2001**). "A hybrid coupled model study of tropical Atlantic variability." *Journal of Climate*, 14(3): 361–390. URL http://adsabs.harvard.edu/abs/2001JCli...14..361C.

Chang, P., Yamagata, T., Schopf, P., Behera, S., Carton, J., Kessler, W., Meyers, G., Qu, T., Schott, F., Shetye, S., et al. (**2006**). "Climate fluctuations of tropical coupled systems-The role of ocean dynamics." *Journal of Climate*, 19(20): 5122–5174. URL http://journals.ametsoc.org/doi/full/10.1175/JCLI3903.1.

Chauvin, F., Roehrig, R., and Lafore, J.-P. (**2010**). "Intraseasonal Variability of the Saharan Heat Low and Its Link with Midlatitudes." *Journal of Climate*, 23(10): 2544–2561. URL http://journals.ametsoc.org/doi/abs/10.1175/2010JCLI3093.1.

Chelton, D., Schlax, M., Freilich, M., and Milliff, R. (**2004**). "Satellite measurements reveal persistent small-scale features in ocean winds." *Science*, 303(5660): 978. URL http://www.sciencemag.org/content/303/5660/978.

Chelton, D., Wentz, F., Genremann, C., de Szoeke, R., and Schlax, M. (**2000**). "Satellite microwave SST observations of transequatorial tropical instability waves." *Geophysical Research Letters*. URL http://www.agu.org/journals/ABS/2000/1999GL011047.shtml.

Chelton, D. B., Esbensen, S. K., Schlax, M. G., Thum, N., Freilich, M. H., Wentz, F. J., Gentemann, C. L., McPhaden, M. J., and Schopf, P. S. (**2001**). "Observations of Coupling between Surface Wind Stress and Sea Surface Temperature in the Eastern Tropical Pacific." *Journal of Climate*, 14(7): 1479–1498. URL http://journals.ametsoc.org/doi/abs/10.1175/1520-0442%282001%29014%3C1479%3AOOCBSW%3E2.0.CO%3B2.

Colberg, F., Reason, C., and Rodgers, K. (**2004**). "South Atlantic response to El Niño–Southern Oscillation induced climate variability in an ocean general circulation model." *Journal of Geophysical Research*, 109(C12):

C12 015. URL http://www.agu.org/journals/ABS/2004/2004JC002301.shtml.

Contreras, R. (**2002**). "Long-Term Observations of Tropical Instability Waves." *Journal of Physical Oceanography*, 32(9): 2715–2722. URL http://journals.ametsoc.org/doi/abs/10.1175/1520-0485-32.9.2715.

Cook, K. and Vizy, E. (**2006**). "Coupled model simulations of the West African monsoon system: Twentieth-and twenty-first-century simulations." *Journal of Climate*, 19(15): 3681–3703. URL http://journals.ametsoc.org/doi/full/10.1175/JCLI3814.1.

Cornillon, P. and Park, K. (**2001**). "Warm core ring velocities inferred from NSCAT." *Geophysical Research Letters*, 28(4): 575–578. URL http://www.agu.org/pubs/crossref/2001/2000GL011487.shtml.

Cuny, J., Rhines, P. B., Niiler, P. P., and Bacon, S. (**2002**). "Labrador Sea Boundary Currents and the Fate of the Irminger Sea Water." *Journal of Physical Oceanography*, 32(2): 627–647. URL http://journals.ametsoc.org/doi/abs/10.1175/1520-0485%282002%29032%3C0627%3ALSBCAT%3E2.0.CO%3B2.

Czaja, A., van der Vaart, P., and Marshall, J. (**2002**). "A Diagnostic Study of the Role of Remote Forcing in Tropical Atlantic Variability." *Journal of Climate*, 15(22): 3280–3290. URL http://journals.ametsoc.org/doi/abs/10.1175/1520-0442%282002%29015%3C3280%3AADSOTR%3E2.0.CO%3B2.

Deser, C., Alexander, M., Xie, S., and Phillips, A. (**2010**). "Sea surface temperature variability: patterns and mechanisms." *Annual Review of Marine Science*, 2: 115–143. URL http://www.ncbi.nlm.nih.gov/pubmed/21141660.

Deser, C. and Blackmon, M. (**1993**). "Surface climate variations over the North Atlantic Ocean during winter: 1900–1989." *Journal of Climate*, 6(9): 1743–1753. URL http://journals.ametsoc.org/doi/abs/10.1175/1520-0442%281993%29006%3C1743%3ASCVOTN%3E2.0.CO%3B2.

Deser, C., Capotondi, A., Saravanan, R., and Phillips, A. (2006). " Tropical Pacific and Atlantic climate variability in CCSM3." *Journal of Climate*, 19: 2451–2481. URL http://adsabs.harvard.edu/abs/2006JCli...19.2451D.

DeWitt, D. G. and Schneider, E. (1999). "The Processes Determining the Annual Cycle of Equatorial Sea Surface Temperature: A Coupled General Circulation Model Perspective." *Monthly Weather Review*, 127(3): 381–395. URL http://journals.ametsoc.org/doi/abs/10.1175/1520-0493%281999%29127%3C0381%3ATPDTAC%3E2.0.CO%3B2.

Doi, T., Tozuka, T., and Yamagata, T. (2009). "Interannual variability of the Guinea Dome and its possible link with the Atlantic Meridional Mode." *Climate Dynamics*, 33(7): 985–998. URL http://www.springerlink.com/content/g70q71x7050721mp/.

Dong, S., Sprintall, J., Gille, S., and Talley, L. (2008). "Southern Ocean mixed-layer depth from Argo float profiles." *Journal of Geophysical Research*, 113(C6): C06 013. URL http://www.agu.org/journals/ABS/2008/2006JC004051.shtml.

Eden, C. and Dengler, M. (2008). "Stacked jets in the deep equatorial Atlantic Ocean." *Journal of Geophysical Research*, 113. URL http://eprints.ifm-geomar.de/7210/.

Emery, W. J. and Thomson, R. E. (2001). *Data Analysis Methods in Physical Oceanography*. Elsevier. URL http://www.sciencedirect.com/science/book/9780444507563.

Falco, P. and Zambianchi, E. (2011). "Near-surface structure of the Antarctic Circumpolar Current derived from World Ocean Circulation Experiment drifter data." *Journal of Geophysical Research*, 116(C5): C05 003. URL http://www.agu.org/pubs/crossref/2011/2010JC006349.shtml.

Fischer, J. and Schott, F. (**1997**). "Seasonal transport variability of the Deep Western Boundary Current in the equatorial Atlantic." *Journal of Geophysical Research*, 102(C13): 27 751–27. URL http://europa.agu.org/?uri=/journals/jc/97JC02327.xml&view=article.

Florenchie, P., Lutjeharms, J., Reason, C., Masson, S., and Rouault, M. (**2003**). "The source of Benguela Niños in the South Atlantic Ocean." *Geophysical Research Letters*, 30(10): 1505. URL http://www.agu.org/journals/ABS/2003/2003GL017172.shtml.

Folland, C., Palmer, T., and Parker, D. (**1986**). "Sahel rainfall and worldwide sea temperatures, 1901–85." *Nature*, 320(6063): 602–607. URL http://www.nature.com/nature/journal/v320/n6063/abs/320602a0.html.

Foltz, G. and McPhaden, M. (**2010**). "Interaction between the Atlantic meridional and Niño modes." *Geophysical Research Letters*, 37(L18604). URL http://www.agu.org/pubs/crossref/2010/2010GL044001.shtml.

Foltz, G. R., Grodsky, S. A., Carton, J. A., and McPhaden, M. J. (**2003**). "Seasonal mixed layer heat budget of the tropical Atlantic Ocean." *Journal of Geophysical Research*, 108(C5): 3146. URL http://dx.doi.org/10.1029/2002jc001584.

Foltz, G. R. and McPhaden, M. J. (**2006**). "The Role of Oceanic Heat Advection in the Evolution of Tropical North and South Atlantic SST Anomalies." *Journal of Climate*, 19(23): 6122–6138. URL http://journals.ametsoc.org/doi/abs/10.1175/JCLI3961.1.

Fonseca, C., Goni, G., Johns, W., and Campos, E. (**2004**). "Investigation of the North Brazil Current retroflection and North Equatorial Countercurrent variability." *Geophysical Research Letters*, 31: L21 304. URL http://europa.agu.org/?view=article&uri=/journals/gl/gl0421/2004GL020054/2004GL020054.xml&t=gl,2004,fonseca.

Fontaine, B., Garcia-Serrano, J., Roucou, P., Rodriguez-Fonseca, B., Losada, T., Chauvin, F., Gervois, S., Sijikumar, S., Ruti, P., and

Janicot, S. (**2010**). "Impacts of warm and cold situations in the Mediterranean basins on the West African monsoon: observed connection patterns (1979–2006) and climate simulations." *Climate Dynamics*, 35(1): 95–114. URL http://www.springerlink.com/content/21x6h2753n8u5q76/.

Fontaine, B. and Janicot, S. (**1996**). "Sea Surface Temperature Fields Associated with West African Rainfall Anomaly Types." *Journal of Climate*, 9(11): 2935–2940. URL http://journals.ametsoc.org/doi/abs/10.1175/1520-0442%281996%29009%3C2935%3ASSTFAW%3E2.0.CO%3B2.

Fontaine, B., Roucou, P., and Trzaska, S. (**2003**). "Atmospheric water cycle and moisture fluxes in the West African monsoon: Mean annual cycles and relationship using NCEP/NCAR reanalysis." *Geophysical Research Letters*, 30(3): 1117. URL http://www.agu.org/journals/ABS/2003/2002GL015834.shtml.

Gammelsrød, T., Bartholomae, C., Boyer, D., Filipe, V., and Otoole, M. (**1998**). "Intrusion of warm surface water along the Angolan-Namibian coast in February–March 1995: the 1995 Benguela Niño." *South African Journal of Marine Science*, 19(1): 41–56. URL http://www.informaworld.com/smpp/content~db=all~content=a921027542.

Garfinkel, C. and Hartmann, D. (**2010**). "Influence of the quasi-biennial oscillation on the North Pacific and El Niño teleconnections." *Journal of Geophysical Research*, 115(D20116). URL http://www.agu.org/pubs/crossref/2010/2010JD014181.shtml.

Garzoli, S. (**1987**). "Forced oscillations on the equatorial Atlantic basin during the Seasonal Response of the Equatorial Atlantic Program (1983–1984)." *Journal of Geophysical Research*, 92(C5): 5089–5100. URL http://europa.agu.org/?uri=/journals/jc/JC092iC05p05089.xml&view=article.

Garzoli, S. and Richardson, P. (**1989**). "Low-frequency meandering of the Atlantic North Equatorial countercurrent." *Journal of Geophysical Research*, 94(C2): 2079–2090. URL http://www.agu.org/pubs/crossref/1989/JC094iC02p02079.shtml.

Giannini, A., Saravanan, R., and Chang, P. (**2003**). "Oceanic Forcing of Sahel Rainfall on Interannual to Interdecadal Time Scales." *Science*, 302(5647): 1027–1030. URL http://www.sciencemag.org/content/302/5647/1027.abstract.

Giarolla, E., Nobre, P., Malagutti, M., and Pezzi, L. (**2005**). "The Atlantic Equatorial Undercurrent: PIRATA observations and simulations with GFDL Modular Ocean model at CPTEC." *Geophysical Research Letters*, 32(10): L10 617. URL http://www.agu.org/journals/ABS/2005/2004GL022206.shtml.

Gill, A. (**1982**). *Atmosphere-Ocean Dynamics*. Academic Press, New York. URL http://catalogue.nla.gov.au/Record/69108.

Gouriou, Y. and Reverdin, G. (**1992**). "Isopycnal and Diapycnal Circulation of the Upper Equatorial Atlantic Ocean in 1983-1984." *Journal of Geophysical Research*, 97(C3): 3543–3572. URL http://www.agu.org/pubs/crossref/1992.../91JC02935.shtml.

Graps, A. (**1995**). "An introduction to wavelets." *Computational Science & Engineering, IEEE*, 2(2): 50–61. URL http://ieeexplore.ieee.org/xpls/abs_all.jsp?arnumber=388960&tag=1.

Grinsted, A., Moore, J. C., and Jevrejeva, S. (**2004**). "Application of the cross wavelet transform and wavelet coherence to geophysical time series." *Nonlinear Processes in Geophysics*, 11(5/6): 561–566. URL http://www.nonlin-processes-geophys.net/11/561/2004/.

Grist, J. P. and Nicholson, S. E. (**2001**). "A study of the dynamics factors influencing the rainfall variability in the West African Sahel." *Journal of Climate*, 14: 1337–1359. URL http://cat.inist.fr/?aModele=afficheN&cpsidt=1025282.

Grodsky, S. and Carton, J. (**2001**). "Coupled land/atmosphere interactions in the West African Monsoon." *Geophysical Research Letters*, 28(8): 1503–1506. URL http://www.agu.org/pubs/crossref/2001/2000GL012601.shtml.

Grodsky, S., Carton, J., and McClain, C. (**2008**). "Variability of upwelling and chlorophyll in the equatorial Atlantic." *Geophysical Research Letters*, 35(L03610). URL http://europa.agu.org/?uri=/journals/gl/gl0803/2007GL032466/2007GL032466.xml&view=article.

Grodsky, S., Carton, J., Provost, C., Servain, J., Lorenzzetti, J., and McPhaden, M. (**2005**). "Tropical instability waves at 0°N,23°W in the Atlantic: A case study using Pilot Research Moored Array in the Tropical Atlantic (PIRATA) mooring data." *Journal of Geophysical Research*, 110(C08010). URL http://dx.doi.org/10.1029/2005jc002941.

Gu, G. and Adler, R. (**2004**). "Seasonal Evolution and Variability Associated with the West African Monsoon System." *Journal of Climate*, 17(17): 3364–3377. URL http://journals.ametsoc.org/doi/abs/10.1175/1520-0442%282004%29017%3C3364%3ASEAVAW%3E2.0.CO%3B2.

Gutzler, D. and Harrison, D. (**1987**). "The structure and evolution of seasonal wind anomalies over the near-equatorial eastern Indian and western Pacific Oceans." *Monthly Weather Review*, 115: 169–192. URL http://journals.ametsoc.org/doi/abs/10.1175/1520-0493%281987%29115%3C0169%3ATSAEOS%3E2.0.CO%3B2.

Han, W., Webster, P. J., Lin, J.-L., Liu, W. T., Fu, R., Yuan, D., and Hu, A. (**2008**). "Dynamics of Intraseasonal Sea Level and Thermocline

Variability in the Equatorial Atlantic during 2002-03." *Journal of Physical Oceanography*, 38(5): 945–967. URL http://journals.ametsoc.org/action/showCitFormats?doi=10.1175%2F2008JPO3854.1.

Hashizume, H., Xie, S.-P., Liu, T., and Takeuchi, K. (**2001**). "Local and remote atmospheric response to tropical instability waves: A global view from space." *Journal of Geophysical Research*, 106(D10): 10,173–10,185. URL http://dx.doi.org/10.1029/2000JD900684.

Hastenrath, S. (**1990**). "Decadal-scale changes of the circulation in the tropical atlantic sector associated with Sahel drought." *International journal of climatology*, 10(5): 459–472. URL http://onlinelibrary.wiley.com/doi/10.1002/joc.3370100504/abstract.

Hastenrath, S., Polzin, D., and Mutai, C. (**2007**). "Diagnosing the 2005 drought in equatorial East Africa." *Journal of Climate*, 20(18): 4628–4637. URL http://journals.ametsoc.org/doi/pdf/10.1175/JCLI4238.1.

Hayes, S. P., McPhaden, M. J., and Wallace, J. M. (**1989**). "The Influence of Sea-Surface Temperature on Surface Wind in the Eastern Equatorial Pacific: Weekly to Monthly Variability." *Journal of Climate*, 2(12): 1500–1506. URL http://journals.ametsoc.org/doi/abs/10.1175/1520-0442%281989%29002%3C1500%3ATIOSST%3E2.0.CO%3B2.

Hazeleger, W., de Vries, P., and Friocourt, Y. (**2003**). "Sources of the Equatorial Undercurrent in the Atlantic in a high-resolution ocean model." *Journal of Physical Oceanography*, 33(4): 677–693. URL http://journals.ametsoc.org/doi/abs/10.1175/1520-0485%282003%2933%3C677%3ASOTEUI%3E2.0.CO%3B2.

Helber, R. W., Weisberg, R. H., Bonjean, F., Johnson, E. S., and Lagerloef, G. S. E. (**2007**). "Satellite-Derived Surface Current Divergence in Relation to Tropical Atlantic SST and Wind." *Journal of Physical Oceanography*, 37(5): 1357–1375. URL http://journals.ametsoc.org/doi/abs/10.1175/JPO3052.1.

Hisard, P. and Hénin, C. (**1987**). "Response of the Equatorial Atlantic Ocean to the 1983-1984 Wind From the Programme Français Océan et Climat Dans l'Atlantique Equatorial Cruise Data Set." *Journal of Geophysical Research*, 92: 3759–3768. URL http://dx.doi.org/10.1029/jc092ic04p03759.

Hormann, V. and Brandt, P. (**2007**). "Atlantic Equatorial Undercurrent and associated cold tongue variability." *Journal of Geophysical Research*, 112: C06 017. URL http://www.agu.org/journals/ABS/2007/2006JC003931.shtml.

Houghton, R. (**1983**). "Seasonal variations of the subsurface thermal structure in the Gulf of Guinea." *Journal of Physical Oceanography*, 13(11): 2070–2081. URL http://journals.ametsoc.org/doi/abs/10.1175/1520-0485%281983%29013%3C2070%3ASVOTST%3E2.0.CO%3B2.

Houghton, R. (**1991**). "The Relationship of Sea Surface Temperature to Thermocline Depth at Annual and Interannual Time Scales in the Tropical Atlantic Ocean." *Journal of Geophysical Research*, 96: 15,173–15,185. URL http://dx.doi.org/10.1029/91jc01442.

Houghton, R. and Colin, C. (**1986**). "Thermal Structure along 4°W in the Gulf of Guinea during 1983-1984." *Journal of Geophysical Research*, 91(C10): 11,727–11,739. URL http://www.agu.org/pubs/crossref/1986/JC091iC10p11727.shtml.

Houghton, R. and Colin, C. (**1987**). "Wind-driven meridional eddy heat flux in the Gulf of Guinea." *Journal of Geophysical Research*, 92(C10): 10 777–10. URL http://www.agu.org/journals/ABS/1987/JC092iC10p10777.shtml.

Houghton, R. W. (**1976**). "Circulation and Hydrographic Structure over the Ghana Continental Shelf during the 1974 Upwelling." *Journal of Physical Oceanography*, 6(6): 909–924. URL http://journals.ametsoc.org/doi/abs/10.1175/1520-0485%281976%29006%3C0909%3ACAHSOT%3E2.0.CO%3B2.

Houghton, R. W. (**1989**). "Influence of Local and Remote Wind Forcing in the Gulf of Guinea." *Journal of Geophysical Research*, 94: 4816–4828. URL http://dx.doi.org/10.1029/jc094ic04p04816.

Houghton, R. W. and Tourre, Y. M. (**1992**). "Characteristics of Low-Frequency Sea Surface Temperature Fluctuations in the Tropical Atlantic." *Journal of Climate*, 5(7): 765–772. URL http://journals.ametsoc.org/doi/abs/10.1175/1520-0442%281992%29005%3C0765%3ACOLFSS%3E2.0.CO%3B2.

Houseago-Stokes, R. and Challenor, P. (**2004**). "Using PPCA to estimate EOFs in the presence of missing values." *Journal of Atmospheric and Oceanic Technology*, 21(9): 1471–1480. URL http://journals.ametsoc.org/doi/abs/10.1175/1520-0426%282004%29021%3C1471%3AUPTEEI%3E2.0.CO%3B2.

Hu, Z. and Huang, B. (**2007**). "Physical processes associated with the tropical Atlantic SST gradient during the anomalous evolution in the southeastern ocean." *Journal of Climate*, 20(14): 3366–3378. URL http://journals.ametsoc.org/doi/abs/10.1175/JCLI4189.1.

Huang, B., Schopf, P., and Shukla, J. (**2004**). "Intrinsic ocean-atmosphere variability of the tropical Atlantic Ocean." *Journal of Climate*, 17(11): 2058–2077. URL http://journals.ametsoc.org/doi/full/10.1175/1520-0442%282004%29017%3C2058%3AIOVOTT%3E2.0.CO%3B2.

Itiveh, K. O. and Bigg, G. R. (**2008**). "The variation of discharge entering the Niger Delta system, 1951-2000, and estimates of change under global warming." *International Journal of Climatology*, 28(5): 659–666. URL http://onlinelibrary.wiley.com/doi/10.1002/joc.1568/abstract.

Jackett, D. and Mcdougall, T. (**1995**). "Minimal adjustment of hydrographic profiles to achieve static stability." *Journal of Atmospheric and Oceanic Technology*, 12(2): 381–389. URL http://adsabs.harvard.edu/abs/1995JAtOT..12..381J.

Janicot, S. (**1992**). "Spatiotemporal Variability of West African Rainfall. Part I: Regionalizations and Typings." *Journal of Climate*, 5: 489–497. URL http://journals.ametsoc.org/doi/abs/10.1175/1520-0442%281992%29005%3C0489%3ASVOWAR%3E2.0.CO%3B2.

Janicot, S. and Sultan, B. (**2001**). "Intra-seasonal modulation of convection in the West African monsoon." *Geophysical Research Letters*, 28(3): 523–526. URL http://europa.agu.org/?view=results.

Janicot, S., Trzaska, S., and Poccard, I. (**2001**). "Summer Sahel-ENSO teleconnection and decadal time scale SST variations." *Climate Dynamics*, 18(3): 303–320. URL http://www.springerlink.com/content/d3a95a1w9xench38/.

Janowiak, J. (**1988**). "An investigation of interannual rainfall variability in Africa." *Journal of Climate*, 1: 240–255. URL http://adsabs.harvard.edu/abs/1988JCli....1..240J.

Jenkins, G. (**1997**). "The 1988 and 1990 summer season simulations for West Africa using a regional climate model." *Journal of Climate*, 10(6): 1255–1272. URL http://journals.ametsoc.org/doi/abs/10.1175/1520-0442(1997)010%3C1255%3ATASSSF%3E2.0.CO%3B2.

Jochum, M., Deser, C., and Phillips, A. (**2007**). "Tropical Atmospheric Variability Forced by Oceanic Internal Variability." *Journal of Climate*, 20(4): 765–771. URL http://journals.ametsoc.org/doi/abs/10.1175/JCLI4044.1.

Jochum, M. and Murtugudde, R. (**2004**). "Internal variability of the tropical Pacific Ocean." *Geophysical Research Letters*, 31: L14 309. URL http://www.agu.org/journals/ABS/2004/2004GL020488.shtml.

Jochum, M. and Murtugudde, R. (**2006**). "Temperature Advection by Tropical Instability Waves." *Journal of Physical Oceanography*, 36(4): 592–605. URL http://journals.ametsoc.org/doi/abs/10.1175/JPO2870.1.

Jolliffe, I. T. (**1986**). *Principal Component Analysis*. Springer Series in Statistics., 2nd edition. URL http://www.springer.com/statistics/statistical+theory+and+methods/book/978-0-387-95442-4?detailsPage=reviews.

Joly, M. and Voldoire, A. (**2010**). "Role of the Gulf of Guinea in the inter-annual variability of the West African monsoon: what do we learn from CMIP3 coupled simulations?" *International Journal of Climatology*, 30(12): 1843–1856. URL http://onlinelibrary.wiley.com/doi/10.1002/joc.2026/full.

Jung, T., Ferranti, L., and Tompkins, A. (**2006**). "Response to the summer of 2003 Mediterranean SST anomalies over Europe and Africa." *Journal of Climate*, 19(20): 5439–5454. URL http://journals.ametsoc.org/doi/full/10.1175/JCLI3916.1.

Kalnay, E., Kanamitsu, M., Kistler, R., Collins, W., Deaven, D., Gandin, L., Iredell, M., Saha, S., White, G., Woollen, J., et al. (**1996**). "The NCEP/NCAR 40-year Reanalysis Project." *Bulletin of the American Meteorological Society*, 77: 437–470.

Katz, E. J. (**1997**). "Waves along the Equator in the Atlantic." *Journal of Physical Oceanography*, 27(12): 2536–2544. URL http://journals.ametsoc.org/doi/abs/10.1175/1520-0485%281997%29027%3C2536%3AWATEIT%3E2.0.CO%3B2.

Keenlyside, N. and Latif, M. (**2007**). "Understanding equatorial Atlantic interannual variability." *Journal of Climate*, 20(1): 131–142. URL http://journals.ametsoc.org/doi/abs/10.1175/JCLI3992.1.

Kelly, B., Meyers, S., and O'Brien, J. (**1995**). "On a generating mechanism for Yanai waves and the 25-day oscillation." *Journal of Geophysical Research*, 100: 10,589–10,612. URL http://dx.doi.org/10.1029/94jc02911.

Kelly, K., Dickinson, S., McPhaden, M., and Johnson, G. (**2001**). "Ocean currents evident in satellite wind data." *Geophysical Research Letters*, 28(12): 2469–2472. URL http://www.agu.org/journals/ABS/2001/2000GL012610.shtml.

Kushnir, Y., Robinson, W., Chang, P., and Robertson, A. (**2006**). "The Physical Basis for Predicting Atlantic Sector Seasonal-to-Interannual Climate Variability." *Journal of Climate*, 19(23): 5949–5970. URL http://journals.ametsoc.org/doi/abs/10.1175/JCLI3943.1.

Lamb, P. and Peppler, R. (**1992**). "Further case studies of tropical Atlantic surface atmospheric and oceanic patterns associated with sub-Saharan drought." *Journal of Climate*, 5(5). URL http://journals.ametsoc.org/doi/abs/10.1175/1520-0442%281992%29005%3C0476%3AFCSOTA%3E2.0.CO%3B2.

Latif, M. and Grötzner, A. (**2000**). "The equatorial Atlantic oscillation and its response to ENSO." *Climate Dynamics*, 16(2): 213–218. URL http://www.springer.com/earth+sciences+and+geography/geophysics/journal/382.

Lau, K. and Weng, H. (**1995**). "Climate signal detection using wavelet transform: How to make a time series sing." *Bulletin of the American Meteorological Society*, 76(12). URL http://adsabs.harvard.edu/abs/1995BAMS...76.2391L.

Lawrence, S. and Angell, J. (**2000**). "Evidence for Rossby wave control of tropical instability waves in the Pacific Ocean." *Geophysical Research Letters*, 27(15): 2257–2260. URL http://www.agu.org/journals/ABS/2000/1999GL002363.shtml.

Le Barbé, L., Lebel, T., and Tapsoba, D. (**2002**). "Rainfall variability in West Africa during the years 1950-1990." *Journal of Climate*, 1151(15): 187–202. URL http://www.mendeley.com/research/rainfall-variability-in-west-africa-during-the-years-195090/.

Lee, T., Fukumori, I., and Tang, B. (**2004**). "Temperature Advection: Internal versus External Processes." *Journal of Physical Oceanography*, 34(8): 1936–1944. URL http://journals.ametsoc.org/doi/abs/10.1175/1520-0485%282004%29034%3C1936%3ATAIVEP%3E2.0.CO%3B2.

Legeckis, R. (**1977**). "Long waves in the eastern equatorial Pacific Ocean: A view from a geostationary satellite." *Science*, 197(4309): 1179. URL http://www.sciencemag.org/content/197/4309/1179.abstract.

Levinson, D. and Lawrimore, J. (**2008**). "State of the climate in 2007." *Bulletin of the American Meteorological Society*, 89(7): 1–179. URL http://cat.inist.fr/?aModele=afficheN&cpsidt=20578933.

Lin, J.-L., Kiladis, G. N., Mapes, B. E., Weickmann, K. M., Sperber, K. R., Lin, W., Wheeler, M. C., Schubert, S. D., Del Genio, A., Donner, L. J., Emori, S., Gueremy, J.-F., Hourdin, F., Rasch, P. J., Roeckner, E., and Scinocca, J. F. (**2006**). "Tropical Intraseasonal Variability in 14 IPCC AR4 Climate Models. Part I: Convective Signals." *Journal of Climate*, 19(12): 2665–2690. URL http://journals.ametsoc.org/doi/abs/10.1175/JCLI3735.1.

Lindsay, R., Percival, D., and Rothrock, D. (**1996**). "The discrete wavelet transform and the scale analysis of the surface properties of sea ice." *Geoscience and Remote Sensing, IEEE Transactions*, 34(3): 771–787. URL http://ieeexplore.ieee.org/xpls/abs_all.jsp?arnumber=499782.

Lindzen, R. S. and Nigam, S. (**1987**). "On the Role of Sea Surface Temperature Gradients in Forcing Low-Level Winds and Convergence in the Tropics." *Journal of the Atmospheric Sciences*, 44(17): 2418–2436. URL http://journals.ametsoc.org/doi/abs/10.1175/1520-0469%281987%29044%3C2418%3AOTROSS%3E2.0.CO%3B2.

Liu, W., Xie, X., Polito, P., Xie, S., and Hashizume, H. (**2000**). "Atmospheric manifestation of tropical instability wave observed by QuikSCAT and Tropical Rain Measuring Mission." *Geophysical Research Letters*, 27(16):

2545–2548. URL http://www.agu.org/pubs/crossref/2000/2000GL011545.shtml.

Liu, W. T., Katsaros, K. B., and Businger, J. A. (**1979**). "Bulk Parameterization of Air-Sea Exchanges of Heat and Water Vapor Including the Molecular Constraints at the Interface." *Journal of the Atmospheric Sciences*, 36(9): 1722–1735. URL http://journals.ametsoc.org/doi/abs/10.1175/1520-0469%281979%29036%3C1722%3ABPOASE%3E2.0.CO%3B2.

Liu, Z., Philander, S., and Pacanowski, R. (**1994**). "A GCM study of tropical-subtropical upper-ocean water exchange." *Journal of Physical Oceanography*, 24(12): 2606–2623. URL http://direct.bl.uk/bld/PlaceOrder.do?UIN=023472600&ETOC=EN&from=searchengine.

Lough, J. M. (**1986**). "Tropical Atlantic Sea Surface Temperatures and Rainfall Variations in Sub-saharan Africa." *Monthly Weather Review*, 114(3): 561–570. URL http://journals.ametsoc.org/doi/abs/10.1175/1520-0493%281986%29114%3C0561%3ATASSTA%3E2.0.CO%3B2.

Lumpkin, R. and Garraffo, Z. (**2005**). "Evaluating the Decomposition of Tropical Atlantic Drifter Observations." *Journal of Atmospheric and Oceanic Technology*, 22(9): 1403–1415. URL http://journals.ametsoc.org/doi/abs/10.1175/JTECH1793.1.

Lumpkin, R. and Garzoli, S. (**2005**). "Near-surface circulation in the tropical Atlantic Ocean." *Deep Sea Research Part I: Oceanographic Research Papers*, 52(3): 495–518. URL http://www.mendeley.com/research/nearsurface-circulation-in-the-tropical-atlantic-ocean/.

Madden, R. A. and Julian, P. R. (**1994**). "Observations of the 4050-Day Tropical OscillationA Review." *Monthly Weather Review*, 122(5): 814–837. URL http://journals.ametsoc.org/doi/abs/10.1175/1520-0493%281994%29122%3C0814%3AOOTDTO%3E2.0.CO%3B2.

Mahajan, S., Saravanan, R., and Chang, P. (**2009**). "The role of the wind-evaporation-sea surface temperature (WES) feedback in air-sea coupled tropical variability." *Atmospheric Research*, 94(1): 19–36. URL http://adsabs.harvard.edu/abs/2009AtmRe..94...19M.

Malanotte-Rizzoli, P., Hedstrom, K., Arango, H., and Haidvogel, D. (**2000**). "Water mass pathways between the subtropical and tropical ocean in a climatological simulation of the North Atlantic ocean circulation." *Dynamics of Atmospheres and Oceans*, 32(3-4): 331–371. URL http://adsabs.harvard.edu/abs/2000DyAtO..32..331M.

Maloney, E. and Shaman, J. (**2008**). "Intraseasonal variability of the West African monsoon and Atlantic ITCZ." *Journal of Climate*, 21(12): 2898–2918. URL http://journals.ametsoc.org/doi/full/10.1175/2007JCLI1999.1.

Maloney, E. D., Chelton, D. B., and Esbensen, S. K. (**2008**). "Subseasonal SST Variability in the Tropical Eastern North Pacific during Boreal Summer." *Journal of Climate*, 21(17): 4149–4167. URL http://journals.ametsoc.org/doi/abs/10.1175/2007JCLI1856.1.

Marengo, J. (**2006**). *Eastern Africa. In State of the climate in 2005. (edited by K. A. Shein)*. Bulletin of the American Meteorological Society, 87, S70.

Marin, F., Caniaux, G., Giordani, H., Bourlès, B., Gouriou, Y., and Key, E. (**2009**). "Why Were Sea Surface Temperatures so Different in the Eastern Equatorial Atlantic in June 2005 and 2006?" *Journal of Physical Oceanography*, 39(6): 1416–1431. URL http://journals.ametsoc.org/doi/abs/10.1175/2008JPO4030.1.

Matthews, A. J. (**2004**). "Intraseasonal Variability over Tropical Africa during Northern Summer." *Journal of Climate*, 17(12): 2427–2440. URL http://journals.ametsoc.org/doi/abs/10.1175/1520-0442%282004%29017%3C2427%3AIVOTAD%3E2.0.CO%3B2.

McCreary, J., Julian, P., Picaut, J., and Moore, D. (**1984**). "Effects of remote annual forcing in the eastern tropical Atlantic Ocean." *Journal of*

Marine Research, 42(1): 45–81. URL http://www.ingentaconnect.com/content/jmr/jmr/1984/00000042/00000001/art00004.

McCreary Jr, J. and Lu, P. (**1994**). "Interaction between the subtropical and equatorial ocean circulations: The subtropical cell." *Journal of Physical Oceanography*, 24(2): 466–497. URL http://journals.ametsoc.org/doi/abs/10.1175/1520-0485%281994%29024%3C0466%3AIBTSAE%3E2.0.CO%3B2.

McGlade, J., Koranteng, K., and Cury, P. (**2002**). *The Gulf of Guinea Large Marine Ecosystem - Environmental Forcing & Sustainable Development of Marine Resources*, volume 11. Elsevier. URL http://www.sciencedirect.com/science/article/pii/S1570046102800234.

Mehta, V. and Delworth, T. (**1995**). "Decadal Variability of the Tropical Atlantic Ocean Surface Temperature in Shipboard Measurements and in a Global Ocean-Atmosphere Model." *Journal of Climate*, 8: 172–190. URL http://journals.ametsoc.org/doi/abs/10.1175/1520-0442%281995%29008%3C0172%3ADVOTTA%3E2.0.CO%3B2.

Merle, J. (**1980**). "Seasonal heat budget in the equatorial Atlantic Ocean." *Journal of Physical Oceanography*, 10(3): 464–469. URL http://journals.ametsoc.org/doi/abs/10.1175/1520-0485%281980%29010%3C0464%3ASHBITE%3E2.0.CO%3B2.

Millard, R., Owens, W., and Fofonoff, N. (**1990**). "On the calculation of the Brunt-Väisälä frequency." *Deep Sea Research Part A. Oceanographic Research Papers*, 37(1): 167–181. URL http://www.sciencedirect.com/science/article/B757K-48B0X0M-5G/2/dabb8f4260815cbe80bddbe481f554ed.

Mitchell, T. P. and Wallace, J. M. (**1992**). "The Annual Cycle in Equatorial Convection and Sea Surface Temperature." *Journal of Climate*, 5(10): 1140–1156. URL http://journals.ametsoc.org/doi/abs/10.1175/1520-0442%281992%29005%3C1140%3ATACIEC%3E2.0.CO%3B2.

Mitchelson-Jacob, E. G. (**1996**). "Variations in the Odden, Greenland Sea - an interpretation of Special Sensor Microwave/ Imager ice concentration data." *International Journal of Remote Sensing*, 17(5): 1019–1029. URL http://www.tandfonline.com/doi/abs/10.1080/01431169608949061.

Moura, A. and Shukla, J. (**1981**). "On the dynamics of droughts in northeast Brazil: Observations, theory and numerical experiments with a General Circulation Model." *Journal of the Atmospheric Sciences*, 38: 2653–2675. URL http://adsabs.harvard.edu/abs/1981JAtS...38.2653M.

Münnich, M. and Neelin, J. (**2005**). "Seasonal influence of ENSO on the Atlantic ITCZ and equatorial South America." *Geophysical Research Letters*, 32: L21 709. URL http://www.agu.org/journals/ABS/2005/2005GL023900.shtml.

Neelin, J. D. and Dijkstra, H. A. (**1995**). "Ocean-Atmosphere Interaction and the Tropical Climatology. Part I: The Dangers of Flux Correction." *Journal of Climate*, 8(5): 1325–1342. URL http://journals.ametsoc.org/doi/abs/10.1175/1520-0442%281995%29008%3C1325%3AOAIATT%3E2.0.CO%3B2.

Nicholson, S. (**1993**). "An overview of African rainfall fluctuations of the last decade." *Journal of Climate*, 6(7): 1463–1466. URL http://journals.ametsoc.org/doi/abs/10.1175/1520-0442%281993%29006%3C1463%3AAOOARF%3E2.0.CO%3B2.

Nicholson, S. (**2009**). "On the factors modulating the intensity of the tropical rainbelt over West Africa." *International Journal of Climatology*, 29(5): 673–689. URL http://onlinelibrary.wiley.com/doi/10.1002/joc.1702/abstract.

Nicholson, S. and Palao, I. (**1993**). "A re-evaluation of rainfall variability in the sahel. Part I. Characteristics of rainfall fluctuations." *International Journal of Climatology*, 13(4): 371–389. URL http://onlinelibrary.wiley.com/doi/10.1002/joc.3370130403/abstract.

Nicholson, S. E., Some, B., McCollum, J., Nelkin, E., Klotter, D., Berte, Y., Diallo, B. M., Gaye, I., Kpabeba, G., Ndiaye, O., Noukpozounkou, J. N., Tanu, M. M., Thiam, A., Toure, A. A., and Traore, A. K. (**2003**). "Validation of TRMM and Other Rainfall Estimates with a High-Density Gauge Dataset for West Africa. Part II: Validation of TRMM Rainfall Products." *Journal of Applied Meteorology*, 42(10): 1355–1368. URL http://journals.ametsoc.org/doi/abs/10.1175/1520-0450%282003%29042%3C1355%3AVOTAOR%3E2.0.CO%3B2.

Niles, C. (**2007**). "In West Africa flood response, UNICEF focuses on the most vulnerable children." *UNICEF: Accessed 11 July 2011*. URL http://www.unicef.org/emerg/index_40993.html.

NIMET (**2008**). "Nigerian Climate Review Bulletin 2007." *Nigerian Meteorological Agency*. URL http://www.nimetng.org/.

Nobre, P. and Shukla, J. (**1996**). "Variations of Sea Surface Temperature, Wind Stress, and Rainfall over the Tropical Atlantic and South America." *Journal of Climate*, 9(10): 2464–2479. URL http://journals.ametsoc.org/doi/abs/10.1175/1520-0442%281996%29009%3C2464%3AVOSSTW%3E2.0.CO%3B2.

Nonaka, M. and Xie, S. (**2003**). "Covariations of sea surface temperature and wind over the Kuroshio and its extension: Evidence for ocean-to-atmosphere feedback." *Journal of Climate*, 16(9): 1404–1413. URL http://journals.ametsoc.org/doi/full/10.1175/1520-0442%282003%2916%3C1404%3ACOSSTA%3E2.0.CO%3B2.

Okamoto, S., Hirawake, T., and Saitoh, S.-I. (**2010**). "Interannual variability in the magnitude and timing of the spring bloom in the Oyashio region." *Deep Sea Research Part II: Topical Studies in Oceanography*, 57(17-18): 1608 – 1617. URL http://www.sciencedirect.com/science/article/B6VGC-4YN5PBN-1/2/a4bde3c9b9d70af4554fd4f37b23697d.

Okumura, Y. and Xie, S.-P. (**2004**). "Interaction of the Atlantic Equatorial Cold Tongue and the African Monsoon." *Journal of Climate*, 17(18): 3589–3602. URL http://journals.ametsoc.org/doi/abs/10.1175/1520-0442%282004%29017%3C3589%3AIOTAEC%3E2.0.CO%3B2.

Okumura, Y. and Xie, S.-P. (**2006**). "Some Overlooked Features of Tropical Atlantic Climate Leading to a New Niño-Like Phenomenon." *Journal of Climate*, 19(22): 5859–5874. URL http://journals.ametsoc.org/doi/abs/10.1175/JCLI3928.1.

Paeth, H., Fink, A. H., Pohle, S., Keis, F., Mächel, H., and Samimi, C. (**2010**). "Meteorological characteristics and potential causes of the 2007 flood in sub-Saharan Africa." *International Journal of Climatology*, page n/a. URL http://onlinelibrary.wiley.com/doi/10.1002/joc.2199/abstract.

Pazan, S. E. and Niiler, P. P. (**2001**). "Recovery of Near-Surface Velocity from Undrogued Drifters." *Journal of Atmospheric and Oceanic Technology*, 18(3): 476–489. URL http://journals.ametsoc.org/action/showCitFormats?doi=10.1175%2F1520-0426%282001%29018%3C0476%3ARONSVF%3E2.0.CO%3B2.

Peter, A.-C., le Henaff, M., du Penhoat, Y., Menkes, C. E., Marin, F., Vialard, J., Caniaux, G., and Lazar, A. (**2006**). "A model study of the seasonal mixed layer heat budget in the equatorial Atlantic." *Journal of Geophysical Research*, 111. URL http://dx.doi.org/10.1029/2005jc003157.

Philander, S. and Pacanowski, R. (**1986**). "The mass and heat budget in a model of the tropical Atlantic Ocean." *Journal of Geophysical Research*, 91(C12): 14 212–14. URL http://europa.agu.org/?view=article&uri=/journals/jc/JC091iC12p14212.xml.

Picaut, J., Hayes, S., and McPhaden, M. (**1989**). "Use of the geostrophic approximation to estimate time-varying zonal currents at the equator." *Journal of Geophysical Research*, 94: 3228–3236. URL http://europa.agu.org/?view=results.

Piolle, J. and Bentamy, A. (**2002**). *Mean Wind Fields (MWF product) - User Manual*. CERSAT, Plouzané. URL http://www.cersat.ifremer.fr/content/download/704/3684/file/mutwqscat.pdf.

Polo, I., Rodríguez-Fonseca, B., Losada, T., and García-Serrano, J. (**2008**). "Tropical Atlantic Variability Modes (1979-2002). Part I: Time-Evolving SST Modes Related to West African Rainfall." *Journal of Climate*, 21(24): 6457–6475. URL http://journals.ametsoc.org/doi/full/10.1175/2008JCLI2607.1.

Provost, C., Arnault, S., Chouaib, N., Kartavtseff, A., E., L. B., and Sultan (**2004**). "TOPEX/Poseidon and Jason Equatorial Sea Surface Slope Anomaly in the Atlantic in 2002: Comparison with Wind and Current Measurements at 23°W." *Marine Geodesy*, 27: 31– 45. URL http://www.tandfonline.com/doi/abs/10.1080/01490410490465274.

Qiao, L. and Weisberg, R. (**1995**). "Tropical instability wave kinematics: Observations from the tropical instability wave experiment." *Journal of Geophysical Research*, 100(C5): 8677–8693. URL http://europa.agu.org/?view=article&uri=/journals/jc/95JC00305.xml&t=jc,1995,qiao.

Quartly, G., Buck, J., Srokosz, M., and Coward, A. (**2006**). "Eddies around Madagascar–The retroflection re-considered." *Journal of Marine Systems*, 63(3-4): 115–129. URL http://adsabs.harvard.edu/abs/2006JMS...63..115Q.

Reason, C., Landman, W., and Tennant, W. (**2006**). "Seasonal to Decadal Prediction of Southern African Climate and Its Links with Variability of the Atlantic Ocean." *Bulletin of the American Meteorological Society*, 87: 941–955. URL http://adsabs.harvard.edu/abs/2006BAMS...87..941R.

Rhein, M., Stramma, L., and Send, U. (**1995**). "The Atlantic Deep Western Boundary Current: Water masses and transports near the equator." *Journal of Geophysical Research*, 100: 2441–2457. URL http://europa.agu.org/?view=article&uri=/journals/jc/94JC02355.xml.

Richardson, P. and McKee, T. (**1984**). "Average seasonal variation of the Atlantic equatorial currents from historical ship drifts." *Journal of Physical Oceanography*, 14(7): 1226–1238. URL http://journals.ametsoc.org/doi/abs/10.1175/1520-0485%281984%29014%3C1226%3AASVOTA%3E2.0.CO%3B2.

Richardson, P. and Reverdin, G. (**1987**). "Seasonal cycle of velocity in the Atlantic North Equatorial Countercurrent as measured by surface drifters, current meters, and ship drifts." *Journal of Geophysical Research*, 92(C4): 3691–3708. URL http://europa.agu.org/?uri=/journals/jc/JC092iC04p03691.xml&view=article.

Robinson, I. S. (**2004**). *Measuring the oceans from space: the principles and methods of satellite oceanography*. Springer Verlag. URL http://www.praxis-publishing.co.uk/9783540426479.htm.

Robinson, I. S. (**2010**). *Discovering the Ocean from Space*. Springer Berlin Heidelberg. URL http://www.springer.com/earth+sciences+and+geography/geophysics/book/978-3-540-24430-1.

Rouault, M., Florenchie, P., Fauchereau, N., and Reason, C. (**2003**a). "South East tropical Atlantic warm events and southern African rainfall." *Geophysical Research Letters*, 30(5): 8009. URL http://www.agu.org/journals/ABS/2003/2002GL014840.shtml.

Rouault, M., Reason, C. J. C., Lutjeharms, J. R. E., and Beljaars, A. C. M. (**2003**b). "Underestimation of Latent and Sensible Heat Fluxes above the Agulhas Current in NCEP and ECMWF Analyses." *Journal of Climate*, 16(4): 776–782. URL http://journals.ametsoc.org/doi/abs/10.1175/1520-0442%282003%29016%3C0776%3AUOLASH%3E2.0.CO%3B2.

Rowell, D. (**2001**). "Teleconnections between the tropical Pacific and the Sahel." *Quarterly Journal of the Royal Meteorological Society*, 127(575): 1683–1706. URL http://onlinelibrary.wiley.com/doi/10.1002/qj.49712757512/abstract.

Rowell, D. P. (**2003**). "The Impact of Mediterranean SSTs on the Sahelian Rainfall Season." *Journal of Climate*, 16(5): 849–862. URL http://journals.ametsoc.org/doi/abs/10.1175/1520-0442%282003%29016%3C0849%3ATIOMSO%3E2.0.CO%3B2.

Schott, F., Dengler, M., Brandt, P., Affler, K., Fischer, J., Bourlès, B., Gouriou, Y., Molinari, R., and Rhein, M. (**2003**). "The zonal currents and transports at 35°W in the tropical Atlantic." *Geophysical Research Letters*, 30(7): 1349. URL http://www.agu.org/pubs/crossref/2003/2002GL016849.shtml.

Schott, F., McCreary, J., and Johnson, G. (**2004**). "Shallow overturning circulations of the tropical-subtropical oceans." *Earth Climate: The Ocean–Atmosphere Interaction, Geophysical Monograph*, 147: 261–304. URL http://www.ocean-sci.net/7/389/2011/os-7-389-2011.xml.

Schouten, M., Matano, R., and Strub, T. (**2005**). "A description of the seasonal cycle of the equatorial Atlantic from altimeter data." *Deep Sea Research Part I: Oceanographic Research Papers*, 52(3): 477–493. URL http://adsabs.harvard.edu/abs/2005DSR....52..477S.

Seager, R., Kushnir, Y., Chang, P., Naik, N., Miller, J., and Hazeleger, W. (**2001**). "Looking for the Role of the Ocean in Tropical Atlantic Decadal Climate Variability." *Journal of Climate*, 14(5): 638–655. URL http://journals.ametsoc.org/doi/abs/10.1175/1520-0442%282001%29014%3C0638%3ALFTROT%3E2.0.CO%3B2.

Semazzi, F. and Sun, L. (**1997**). "The role of orography in determining the Sahelian climate." *International Journal of Climatology*, 17(6): 581–596. URL http://onlinelibrary.wiley.com/doi/10.1002/(SICI)1097-0088(199705)17:6%3C581::AID-JOC134%3E3.0.CO;2-E/abstract.

Seo, H., Jochum, M., Murtugudde, R., and Miller, A. (**2006**). "Effect of ocean mesoscale variability on the mean state of tropical Atlantic climate." *Geophysical Research Letters*, 33(9). URL http://www.agu.org/pubs/crossref/2006/2005GL025651.shtml.

Seo, H., Jochum, M., Murtugudde, R., Miller, A., and Roads, J. (**2007**). "Feedback of tropical instability wave-induced atmospheric variability onto the ocean." *Journal of Climate*, 20(23): 5842–5855. URL http://journals.ametsoc.org/doi/abs/10.1175/JCLI4330.1.

Servain, J. (**1991**). "Simple Climatic Indices for the Tropical Atlantic Ocean and Some Applications." *Journal of Geophysical Research*, 96(C8): 15 137–15 146. URL http://europa.agu.org/?view=article&uri=/journals/jc/91JC01046.xml.

Servain, J., Clauzet, G., and Wainer, I. (**2003**). "Modes of tropical Atlantic climate variability observed by PIRATA." *Geophysical Research Letters*, 30(8003): 1997–2000. URL http://europa.agu.org/?uri=/journals/gl/gl0305/2002GL015124/2002GL015124.xml&view=article.

Servain, J., Picaut, J., and Merle, J. (**1982**). "Equator waveguide as Kelvin waves reaching the boundary 1-2 months later." *Journal of Physical Oceanography*, 12(5): 457–463. URL http://dx.doi.org/10.1175/1520-0485(1982)012<0457:EORFIT>2.0.CO;2.

Servain, J., Wainer, I., McCreary Jr, J., and Dessier, A. (**1999**). "Relationship between the equatorial and meridional modes of climatic variability in the tropical Atlantic." *Geophysical Research Letters*, 26(4): 485–488. URL http://www.agu.org/journals/ABS/1999/1999GL900014.shtml.

Setoh, T., Imawaki, S., Ostrovskii, A., and Umatani, S. (**1999**). "Interdecadal variations of ENSO signals and annual cycles revealed by wavelet analysis." *Journal of Oceanography*, 55(3): 385–394. URL http://www.springerlink.com/content/k784vpx816075078/.

Shannon, L., Boyd, A., Brundrit, G., and Taunton-Clark, J. (**1986**). "On the existence of an El Niño-type phenomenon in the Benguela system." *Journal of Marine Research*, 44(3): 495–520. URL http://www.ingentaconnect.com/content/jmr/jmr/1986/00000044/00000003/art00005.

Si, B. and Farrell, R. (**2004**). "Scale-dependent relationship between wheat yield and topographic indices: A wavelet approach." *Soil Science Society of America*, 68(2): 577–587. URL http://www.mendeley.com/research/scaledependent-relationship-between-wheat-yield-topographic-indices-wavelet-a

Siedler, G., Church, J., and Gould, J. (**2001**). *Ocean Circulation and Climate: In International Geophysics Series*. Academic Press, London and San Diego. URL http://www.elsevier.com/wps/find/bookdescription.cws_home/679268/description#description.

Siedler, G., Zangenberg, N., Onken, R., and Morlière, A. (**1992**). "Seasonal changes in the tropical Atlantic circulation: observation and simulation of the Guinea Dome." *Journal of Geophysical Research*, 97(C1): 703–715. URL http://www.agu.org/pubs/crossref/1992/91JC02501.shtml.

Small, R. J., deSzoeke, S. P., Xie, S. P., O'Neill, L., Seo, H., Song, Q., Cornillon, P., Spall, M., and Minobe, S. (**2008**). "Air-sea interaction over ocean fronts and eddies." *Dynamics of Atmospheres and Oceans*, 45(3-4): 274–319. URL http://adsabs.harvard.edu/abs/2008DyAtO..45..274S.

Small, R. J., Richards, K. J., Xie, S.-P., Dutrieux, P., and Miyama, T. (**2009**). "Damping of Tropical Instability Waves caused by the action of surface currents on stress." *Journal of Geophysical Research*, 114. URL http://www.agu.org/journals/ABS/2009/2008JC005147.shtml.

Smith, S. D. (**1988**). "Coefficients for sea surface wind stress, heat flux, and wind profiles as a function of wind speed and temperature." *Journal of Geophysical Research*, 93(C12): 15 467–15. URL http://www.agu.org/journals/ABS/1988/JC093iC12p15467.shtml.

Spall, M. (**2007**). "Midlatitude wind stress-sea surface temperature coupling in the vicinity of oceanic fronts." *Journal of Climate*, 20(15): 3785–3801. URL https://darchive.mblwhoilibrary.org/handle/1912/4119.

Stewart, R. (**2004**). *Introduction to Physical Oceanography*. Texas A & M University. URL http://oceanworld.tamu.edu/home/course_book.htm.

Stramma, L., Fischer, J., and Reppin, J. (**1995**). "The North Brazil Undercurrent." *Deep Sea Research I*, 42: 773–795. URL http://www.sciencedirect.com/science/article/pii/096706379500014W.

Stramma, L. and Schott, F. (**1999**). "The mean flow field of the tropical Atlantic Ocean." *Deep Sea Research-Part II-Topical Studies in Oceanography*, 46(1): 279–304. URL http://cat.inist.fr/?aModele=afficheN&cpsidt=1756188.

Strutton, P., Ryan, J., and Chavez, F. (**2001**). "Enhanced chlorophyll associated with tropical instability waves in the equatorial Pacific." *Geophysical Research Letters*, 28(10): 2005–2008. URL http://www.agu.org/journals/ABS/2001/2000GL012166.shtml.

Sultan, B., Janicot, S., and Diedhiou, A. (**2003**). "The West African Monsoon Dynamics. Part I: Documentation of Intraseasonal Variability." *Journal of Climate*, 16(21): 3389–3406. URL http://journals.ametsoc.org/doi/abs/10.1175/1520-0442%282003%29016%3C3389%3ATWAMDP%3E2.0.CO%3B2.

Team, N. (**2007**). "Natural Hazards: Floods in West Africa." *Earth Observatory NASA*. URL http://earthobservatory.nasa.gov/NaturalHazards/view.php?id=19084.

Terradas, J., Oliver, R., and Ballester, J. (**2004**). "Application of statistical techniques to the analysis of solar coronal oscillations." *The Astrophysical Journal*, 614: 435–447. URL http://iopscience.iop.org/0004-637X/614/1/435.

Thomson, A. (**2007**). "Deadly floods and disease afflict Africas arid Sahel." *Reuters: Accessed 9 July 2011*. URL http://uk.reuters.com/article/2007/08/15/science-africa-floods-dc-idUKL1581162120070816.

Thum, N., Esbensen, S., Chelton, D., and McPhaden, M. (**2002**). "Air-sea heat exchange along the northern sea surface temperature front in the eastern tropical Pacific." *Journal of Climate*, 15(23): 3361–3378. URL http://journals.ametsoc.org/doi/full/10.1175/1520-0442%282002%29015%3C3361%3AASHEAT%3E2.0.CO%3B2.

Tokmakian, R. T. and Challenor, P. G. (**1993**). "Observations in the Canary Basin and the Azores Frontal Region Using Geosat Data." *Journal of Geophysical Research*, 98(C3): 47614773. URL http://www.agu.org/journals/jc/v098/iC03/92JC02624/.

Tomczak, M. and Godfrey, J. S. (**2003**). *Regional Oceanography: An introduction*. Daya Publishers, Delhi. URL http://www.es.flinders.edu.au/~mattom/regoc/pdfversion.html.

Torrence, C. and Compo, G. (**1998**). "A practical guide to wavelet analysis." *Bulletin of the American Meteorological Society*, 79(1): 61–78. URL http://paos.colorado.edu/research/wavelets/.

Ueki, I., Kutsuwada, K., Inaba, H., and Kaneko, A. (**2000**). "Quasi-2-day signals observed in the warm pool region during TOGA/COARE IOP." *Journal of Oceanography*, 56(5): 539–552. URL http://www.springerlink.com/content/r7548n542u780j51/.

Venegas, R., Strub, P., Beier, E., Letelier, R., Thomas, A., Cowles, T., James, C., Soto-Mardones, L., and Cabrera, C. (**2008**). "Satellite-derived variability in chlorophyll, wind stress, sea surface height, and temperature in the northern California Current System." *Earth Climate: The Ocean–Atmosphere Interaction, Geophysical Monograph*, 113(C3): C03 015. URL http://europa.agu.org/?uri=/journals/jc/jc0803/2007JC004481/2007JC004481.xml&view=article.

Vimont, D. J. and Kossin, J. P. (**2007**). "The Atlantic Meridional Mode and hurricane activity." *Geophysical Research Letters*, 34(7). URL http://www.agu.org/journals/ABS/2007/2007GL029683.shtml.

Vizy, E. and Cook, K. (**2001**). "Mechanisms by which Gulf of Guinea and eastern North Atlantic sea surface temperature anomalies can influence African rainfall." *Journal of Climate*, 14(5): 795–821. URL http://journals.ametsoc.org/doi/abs/10.1175/1520-0442%282001%29014%3C0795%3AMBWGOG%3E2.0.CO%3B2.

Volturiez, B. (**1981**). "The equatorial undercurrents north and south and the formation of tropical thermal domes (Les sous-courants equatoriaux nord et sud et la formation des dmes thermiques tropicaux)." *Oceanologica Acta*, 4(4): 497–506.

von Schuckmann, K., Brandt, P., and Eden, C. (**2008**). "Generation of tropical instability waves in the Atlantic Ocean." *Journal of Geophysical Research*, 113: C08 034. URL http://www.agu.org/journals/ABS/2008/2007JC004712.shtml.

von Storch, H. and Navarra, A. (**1999**). *Analysis of Climate Variability: Applications of Statistical Techniques*. Springer. URL http://www.springer.com/earth+sciences+and+geography/meteorology+%26+climatology/book/978-3-540-66315-7.

von Storch, H. and Zwiers, F. (**1999**). *Statistical Analysis in Climate Research*. Cambridge University Press. URL http://www.cambridge.org/gb/knowledge/isbn/item1144478/?site_locale=en_GB#.

Wainer, I., Clauzet, G., Servain, J., and Soares, J. (**2003**). "Time scales of upper ocean temperature variability inferred from the PIRATA data (1997–2000)." *Geophysical Research Letters*, 30(5): 8004. URL http://europa.agu.org/?uri=/journals/gl/gl0305/2002GL015147/2002GL015147.xml&view=article.

Wallace, J. M., Mitchell, T. P., and Deser, C. (**1989**). "The Influence of Sea-Surface Temperature on Surface Wind in the Eastern Equatorial Pacific: Seasonal and Interannual Variability." *Journal of Climate*, 2(12): 1492–1499. URL http://journals.ametsoc.org/doi/abs/10.1175/1520-0442%281989%29002%3C1492%3ATIOSST%3E2.0.CO%3B2.

Wang, C. (**2006**). "An overlooked feature of tropical climate: Inter-Pacific-Atlantic variability." *Geophysical Research Letters*, 33: L12 702. URL http://www.agu.org/journals/ABS/2006/2006GL026324.shtml.

Wang, C. and Weisberg, R. H. (**2001**). "Ocean circulation influences on sea surface temperature in the equatorial central Pacific." *Journal of Geophysical Research*, 106: 19,515–19,526. URL http://dx.doi.org/10.1029/2000jc000242.

Ward, M. (**1998**). "Diagnosis and short-lead time prediction of summer rainfall in tropical North Africa at interannual and multidecadal timescales." *Journal of Climate*, 11(12): 3167–3191. URL http://journals.ametsoc.org/doi/abs/10.1175/1520-0442%281998%29011%3C3167%3ADASLTP%3E2.0.CO%3B2.

Ward, M. N. (**1994**). *Tropical North African rainfall and worldwide monthly to multidecadal climate variations: Ph.D. thesis p313*. Available from the National Meteorological Library, Meteorological Office, London Road, Bracknell, Berkshire RG12 2SZ, United Kingdom.

Weisberg, R. H. and Weingartner, T. J. (**1988**). "Instability Waves in the Equatorial Atlantic Ocean." *Journal of Physical Oceanography*, 18(11): 1641–1657. URL http://journals.ametsoc.org/doi/abs/10.1175/1520-0485%281988%29018%3C1641%3AIWITEA%3E2.0.CO%3B2.

Willett, C. S., Leben, R. R., and Lavn, M. F. (**2006**). "Eddies and Tropical Instability Waves in the eastern tropical Pacific: A review." *Progress In Oceanography*, 69(2-4): 218 – 238. URL http://www.sciencedirect.com/science/article/B6V7B-4K427N0-2/2/

9e4ec052f65962244e04915d11aa4bfc. A Review of Eastern Tropical Pacific Oceanography.

Wu, Q. and Bowman, K. (**2007**a). "Interannual variations of tropical instability waves observed by the Tropical Rainfall Measuring Mission." *Geophysical Research Letters*, 34(9): 9701. URL http://www.agu.org/journals/ABS/2007/2007GL029719.shtml.

Wu, Q. and Bowman, K. P. (**2007**b). "Multiyear satellite observations of the atmospheric response to Atlantic tropical instability waves." *Journal of Geophysical Research*, 112(D19). URL http://www.agu.org/journals/ABS/2007/2007JD008627.shtml.

Xie, L., Yan, T., Pietrafesa, L., Morrison, J., and Karl, T. (**2005**). "Climatology and interannual variability of North Atlantic hurricane tracks." *Journal of Climate*, 18(24): 5370–5381. URL http://journals.ametsoc.org/doi/full/10.1175/JCLI3560.1.

Xie, S. (**2004**). "Satellite observations of cool ocean-atmosphere interaction." *Bulletin of the American Meteorological Society*, 85(2): 195–208. URL http://citeseerx.ist.psu.edu/viewdoc/summary?doi=10.1.1.145.490.

Xie, S.-P. (**1999**). "A Dynamic Ocean-Atmosphere Model of the Tropical Atlantic Decadal Variability." *Journal of Climate*, 12(1): 64–70. URL http://journals.ametsoc.org/doi/abs/10.1175/1520-0442%281999%29012%3C0064%3AADOAMO%3E2.0.CO%3B2.

Xie, S.-P. and Carton, J. A. (**2004**). "Tropical Atlantic Variability: Patterns, Mechanisms, and Impacts, in Earths Climate: The Ocean-Atmosphere Interaction and Climate Variability." *Geophysical Monograph , AGU,Washington, D. C*, 147: 121–142. URL http://iprc.soest.hawaii.edu/users/xie/.

Yates, T., Si, B., Farrell, R., and Pennock, D. (**2007**). "Time, location, and scale dependence of soil nitrous oxide emission, water, and temperature

using wavelet coherency analysis." *Journal of Geophysical Research*, 112: D09 104. URL http://www.agu.org/pubs/crossref/2007/2006JD007662.shtml.

Yu, J. and Liu, W. (**2003**). "A linear relationship between ENSO intensity and tropical instability wave activity in the eastern Pacific Ocean." *Geophysical Research Letters*, 30(14): 1735. URL http://www.agu.org/journals/ABS/2003/2003GL017176.shtml.

Yu, W., Han, W., Maloney, E., Gochis, D., and Xie, S. (**2011**). "Observations of eastward propagation of atmospheric intraseasonal oscillations from the Pacific to the Atlantic." *Journal of Geophysical Research*, 116(D2): D02 101. URL http://www.agu.org/pubs/crossref/2011/2010JD014336.shtml.

Zhou, M., Paduan, J., and Niiler, P. P. (**2000**). "Surface currents in the Canary Basin from drifter observations." *Journal of Geophysical Research*, 105(C9): 21 893–21 911. URL http://europa.agu.org/?view=article&uri=/journals/jc/2000JC900096.xml&t=jc,2000,Zhou.